



<https://theses.gla.ac.uk/>

Theses Digitisation:

<https://www.gla.ac.uk/myglasgow/research/enlighten/theses/digitisation/>

This is a digitised version of the original print thesis.

Copyright and moral rights for this work are retained by the author

A copy can be downloaded for personal non-commercial research or study,
without prior permission or charge

This work cannot be reproduced or quoted extensively from without first
obtaining permission in writing from the author

The content must not be changed in any way or sold commercially in any
format or medium without the formal permission of the author

When referring to this work, full bibliographic details including the author,
title, awarding institution and date of the thesis must be given

Enlighten: Theses

<https://theses.gla.ac.uk/>
research-enlighten@glasgow.ac.uk

WEATHERING AND IRON OXIDE MINERALOGY

OF HONG KONG GRANITE

by

OLUMUYIWA ADEBAYO AWOLEYE

(B.Eng; M.Eng; University of Benin)

Thesis Submitted for the degree of

DOCTOR OF PHILOSOPHY

in the University of Glasgow

April, 1991

ProQuest Number: 11007981

All rights reserved

INFORMATION TO ALL USERS

The quality of this reproduction is dependent upon the quality of the copy submitted.

In the unlikely event that the author did not send a complete manuscript and there are missing pages, these will be noted. Also, if material had to be removed, a note will indicate the deletion.



ProQuest 11007981

Published by ProQuest LLC (2018). Copyright of the Dissertation is held by the Author.

All rights reserved.

This work is protected against unauthorized copying under Title 17, United States Code
Microform Edition © ProQuest LLC.

ProQuest LLC.
789 East Eisenhower Parkway
P.O. Box 1346
Ann Arbor, MI 48106 – 1346

DECLARATION

To the memory of my grandmother, Mrs. M. Awoleye,
who passed away whilst this study was in progress.

DECLARATION

I hereby declare that this work is my own and that I have not copied any part of it from any other source.

I also declare that I have not used any other person's work without their permission.

I further declare that I have not used any other person's work without their permission.

I also declare that I have not used any other person's work without their permission.

I further declare that I have not used any other person's work without their permission.

I also declare that I have not used any other person's work without their permission.

TABLE OF CONTENTS

	Page
Acknowledgements	ix
Summary	xi
CHAPTER 1 <u>INTRODUCTION</u>	1
1.1 <u>GENERAL</u>	1
1.2 <u>AIMS OF THE PRESENT STUDY</u>	2
1.3 <u>METHOD OF STUDY</u>	3
CHAPTER 2 <u>LITERATURE REVIEW</u>	5
2.1 <u>INTRODUCTION</u>	5
2.2 <u>STRUCTURE OF THE IRON OXIDES AND OXYHYDROXIDES</u>	5
2.2.1 Wüstite, FeO (Cubic)	6
2.2.2 Hematite, α -Fe ₂ O ₃ (Trigonal)	6
2.2.3 Ilmenite, FeTiO ₃ (Hexagonal)	7
2.2.4 Magnetite, Fe ₃ O ₄ (Cubic)	8
2.2.5 Maghemite, γ -Fe ₂ O ₃ (Spinel, cubic or tetragonal)	8
2.2.6 Goethite, α -FeOOH (Orthorhombic)	9

2.2.7	Lepidocrocite, γ -FeOOH (Orthorhombic)	10
2.2.8	Akaganeite, β -FeOOH (Tetragonal)	11
2.2.9	Ferrihydrite and Ferroxhyte (δ -FeOOH), (Hexagonal)	12
2.3	<u>IRON OXIDES IN THE SOIL ENVIRONMENT</u>	14
2.3.1	Occurrence	15
2.3.2	Formation	20
2.3.3	Interaction of Iron Oxides with other Minerals and Elements	33
CHAPTER 3	<u>MATERIALS</u>	63
3.1	<u>INTRODUCTION</u>	63
3.2	<u>ROCK AND SOIL</u>	63
3.2.1	Description of Sampling Site	64
3.2.2	Engineering Geology of the Site	64
3.2.3	Weathering and Alteration	66
3.2.4	Soil Sampling	67
3.2.5	Sample Handling and Storage	68
3.2.6	Sample Numbers, Field and Laboratory Description of Samples.	69
3.4	<u>INITIAL SAMPLE PREPARATIONS</u>	73
3.4.1	Rock Samples	73

3.4.2	Soil Samples	73
3.5	<u>PARTICLES SIZE ANALYSIS AND SOIL MICROFABRIC</u>	75
3.6	<u>SYNTHETIC IRON OXIDES</u>	79
3.6.1	Ferrihydrite	79
3.6.2	Goethite	79
3.6.3	Hematite	80
3.7	<u>SUMMARY</u>	80
CHAPTER 4	<u>CHEMICAL METHODS</u>	104
4.1	<u>INTRODUCTION</u>	104
4.2	<u>CONCENTRATION METHODS FOR IRON OXIDES</u>	105
4.2.1	Boiling 5 M Sodium Hydroxide (NaOH) Method of Concentration.	106
4.2.2	Hydrofluoric Acid (HF) Method of Concentration.	106
4.3	<u>SELECTIVE DISSOLUTION METHODS FOR IRON OXIDES</u>	107
4.3.1	Dithionite Citrate Bicarbonate Method of Dissolution.	108
4.3.2	Acid Ammonium Oxalate Method of Dissolution.	108

4.4	<u>ELEMENTAL CONCENTRATION</u>	109
4.4.1	X-ray Fluorescence.	110
4.4.2	Atomic Absorption Spectrophotometry.	111
4.5	<u>DETERMINATION OF pH</u>	112
4.6	<u>DETERMINATION OF SOIL CO₂</u>	112
4.7	<u>RESULTS</u>	113
4.7.1	Elemental Concentration.	
4.7.2	Chemical Concentration of Fe.	117
4.7.3	Selective Dissolution of Fe.	120
4.7.4	Soil pH.	121
4.7.5	Organic Matter Content	122
4.8	<u>SUMMARY</u>	124
CHAPTER 5	<u>ELECTRON MICROSCOPY</u>	134
5.1	<u>INTRODUCTION</u>	134
5.2	<u>GENERAL</u>	135
5.3	<u>PRINCIPLES OF THE ELECTRON MICROSCOPE</u>	136

5.4	<u>LENS DEFECTS</u>	138
5.4.1	Astigmatism	138
5.4.2	Chromatic Aberration	139
5.4.3	Spherical Aberration	140
5.5	<u>BEAM – SPECIMEN INTERACTION</u>	140
5.6	<u>RADIATION DAMAGE</u>	141
5.7	<u>ELECTRON DIFFRACTION</u>	143
5.8	<u>DIRECT RESOLUTION OF THE CRYSTAL LATTICE (HREM)</u>	146
5.9	<u>EXPERIMENTAL METHODS</u>	148
5.9.1	Transmission Electron Microscopy	148
5.9.2	Scanning Electron Microscopy	148
5.10	<u>RESULTS</u>	149
5.10.1	Clay Mineralogy	149
5.10.2	Iron Oxide Mineralogy of Untreated Soils	153
5.10.3	Electron Microscopy Study of 5 M Boiling NaOH Treated Residue	165
5.10.4	Electron Microscopy Study of HF Treated Residue	170
5.10.5	Beam Damage to Soil Iron Oxides.	170

5.11	<u>SUMMARY</u>	174
5.11.1	Clay Mineralogy	174
5.11.2	Iron Oxide Mineralogy	174
CHAPTER 6	<u>X - RAY DIFFRACTION</u>	219
6.1	<u>INTRODUCTION</u>	219
6.2	<u>GENERAL</u>	220
6.3	<u>PRINCIPLES OF X - RAY DIFFRACTION</u>	220
6.4	<u>CHOICE OF RADIATION, FILTERS AND MONOCHROMATORS</u>	224
6.5	<u>PROBLEM OF THE STUDY OF IRON OXIDE MINERALOGY OF SOILS USING X - RAY DIFFRACTION</u>	224
6.6	<u>EXPERIMENTAL METHODS</u>	226
6.6.1	Instrumentation	226
6.6.2	Sample Preparation	226
6.7	<u>RESULTS</u>	227
6.7.1	Clay Fraction	227
6.7.2	Residues from Iron Oxide Concentration Treatments	231

6.8	<u>SUMMARY</u>	238
6.8.1	Clay Mineralogy	238
6.8.2	Iron Oxide Mineralogy	239
CHAPTER 7	<u>INFRARED SPECTROSCOPY AND DIFFERENTIAL SCANNING CALORIMETRY</u>	255
7.1	<u>INTRODUCTION</u>	255
7.2	<u>GENERAL</u>	255
7.3	<u>EXPERIMENTAL METHODS</u>	257
7.3.1	Infrared Spectroscopy	257
7.3.2	Differential Scanning Calorimetry	257
7.4	<u>RESULTS</u>	258
7.4.1	Infrared Spectroscopy	258
7.4.2	Differential Scanning Calorimetry	266
7.5	<u>SUMMARY</u>	267
7.5.1	Clay Mineralogy	267
7.5.2	Iron Oxide Mineralogy	267

CHAPTER 8	<u>GENERAL DISCUSSION</u>	279
8.1	<u>INTRODUCTION</u>	279
8.2	<u>GENERAL DISCUSSION</u>	279
8.2.1	Soil Weathering and Clay Mineralogy	279
8.2.2	Engineering Properties	283
8.2.3	Iron Oxide Mineralogy of the Weathered Granites	287
8.2.4	Iron Oxide Formation in the Weathered Granites	290
8.2.5	Properties of the Iron Oxides	296
8.2.6	Interaction of Iron Oxides with Clay Minerals	299
REFERENCES		303
APPENDIX:	<u>EXAMPLE OF THE ESTIMATION OF Al</u> <u>SUBSTITUTION FOR Fe IN GOETHITE</u>	322

ACKNOWLEDGEMENTS

The work reported in this thesis was carried out in the Department of Civil Engineering and the Department of Chemistry at the University of Glasgow and the contributions of the staff members of both departments towards the final completion of the thesis is gratefully acknowledged.

I am deeply indebted to my supervisors, Dr. P. Smart (Civil Engineering) and Dr. J. R. Fryer (Chemistry), for their support and illuminating guidance during the duration of the project. Their selfless criticisms, advice and contributions based on their profound knowledge and years of experience have made the work a worthwhile experience. I also thank them for their kind contributions to my personal welfare.

I am very grateful to Dr. T. Baird for his advice and assistance and to Dr. I. McConnochie for his advice and for his help with sample impregnation and in arranging for thin sections for optical microscopy.

I thank Professor A. Coull, Professor D. Muir-Wood, Dr. D. R. Green, Dr. P. D. Arthur and Dr. L. Tetley for their interest.

My thanks also go to my fellow workers in the Electron Microscopy group for their useful discussions, and in particular Mr. D. Thom for his technical assistance.

I am grateful to Mr. J. Gallagher and Mr. P. Ainsworth of the Geology

Department, and W. Henderson (Civil Engineering) for their technical assistance.

This study was made possible by an award of a commonwealth scholarship by the British Government and a study leave granted me by the University of Benin, Benin City, Nigeria, and I am grateful to both bodies and to the staff of the British Council who administered the scholarship.

Some of the work reported in the thesis were performed at the Macaulay Land Use Research Institute, Aberdeen. I therefore thank the Institute for the use of their equipment and the staff for their hospitality. In particular, I am very grateful to Dr. M. J. Wilson, Dr. W. McHardy, Dr. J. Russell, T. Fraser, and D. Duthie for their very valuable advice and the use of their expertise.

I thank the Geotechnical Control Office, Hong Kong for providing the soils used in the Investigation, and especially Dr. J. Massey and Dr. T. Irfan for their particular interest.

My gratitude goes to all the members of my family for their support and encouragement.

Finally, I thank all my friends and colleagues such as Dr. Babs Oyenyin, Dr. Bayo Famiyesin, Joe and Airen Okungbowa, Dauda Oladepo, David and Yinka Kaye, John and Mel Seddon, Dr. M. Bouazza, Dr. H. Jasem, Dr. M. Wei, G. Frangopoulos, S. Gaderbough, X. Leng, X. Xue, X. Bai, Z. P. Wu, A. Khan, A. Bensalem, S. Djellab, Y. Zhou and Dr B. Zhang for their encouragement.

SUMMARY

This thesis describes the research work done on the mineralogy and properties of iron oxides in a weathered granite from Hong Kong Island. In general, after the initial introductory chapters, subsequent chapters present studies made using different techniques with one chapter discussing one technique.

Chapter 1 gives the Introduction to the research and presents a basis for the study as well as the aim of the research. The methodology used in accomplishing the aims is presented.

Chapter 2 reviews the past literature relating to the investigation. The structure of the different iron oxides as proposed by past workers as well as the occurrence, properties and characteristics of iron oxides in the soil environment are reviewed.

In Chapter 3 descriptions of the soil materials are given in order to provide a framework of reference for the main part of the work. The sampling methods and both the field and laboratory descriptions of the soils used in the study are provided together with a brief geology of the sampling site. The initial sample preparation done prior to testing the soils has been outlined and results of preliminary tests such as particle size analysis and scanning electron microscopy presented.

Chapter 4 presents the aspect of the investigation where wet chemistry was used to provide additional information which helped in explaining some of the observation of the main techniques used. The chemical tests performed included concentration methods for the iron oxides using the 5 M boiling NaOH and HF methods, selective dissolution using dithionite citrate bicarbonate and acid ammonium oxalate methods, and determination of the chemical contents of the

untreated soils and residues obtained from the different treatments. pH and organic content determination of the soils were also performed.

Chapter 5 presents the electron microscopy study on the different fractions of the soils. The method has the advantage of allowing direct observation of the particles being studied. The theories explaining the acquisition of images in the transmission electron microscope are included. The experimental methods used for transmission and scanning electron microscopy are also presented. Complementary results of scanning electron microscopy are also given. The clay minerals and iron oxide minerals were identified on the basis of data provided by electron diffraction and lattice images, and the morphology of the different minerals is described.

Chapter 6 presents X-ray diffraction analysis on the samples. The technique complements electron microscopy in the identification of the mineralogy of the various soil components. Furthermore X-ray diffraction made it possible to estimate Al substitution for Fe in the iron oxide structure, a property that helped in explaining the formation and occurrence of the iron oxides in the soils. The experimental technique and testing procedures are given and the results presented and discussed.

Chapter 7 gives the details of the infrared spectroscopy and differential scanning calorimetry study of the soils. Both methods allowed a study of the mineralogy of the clays and iron oxides in the soils, thereby complementing the work done using electron microscopy and X-ray diffraction. Some additional information on particle size of some of the clay minerals was also obtained. The characteristics of the infrared vibrations and DSC traces of the iron oxides have been explained on the basis of some peculiar properties of the oxides.

Chapter 8 presents a general discussion on the basis of the collective

results obtained from using the different analytical techniques. The chapter also serves as a summary for some of the results presented earlier in the different chapters. Important conclusions drawn from these results are presented and discussed.

Iron oxides are the important components of soils and have to influence various soil properties. The existence of iron soils and presence of iron oxides in the soil is the other and these values are the important factors. Although several researchers have been studying the iron oxides in the soil, the present work is a review in the field of iron oxides in the soil. The present work is a review of the iron oxides in the soil and its properties and the relationship between the iron oxides and the soil properties. The present work is a review of the iron oxides in the soil and its properties and the relationship between the iron oxides and the soil properties. The present work is a review of the iron oxides in the soil and its properties and the relationship between the iron oxides and the soil properties. The present work is a review of the iron oxides in the soil and its properties and the relationship between the iron oxides and the soil properties.

In the present research different analytical techniques like X-ray fluorescence and X-ray diffraction are used to study the iron oxides in the soil. The present work is a review of the iron oxides in the soil and its properties and the relationship between the iron oxides and the soil properties. The present work is a review of the iron oxides in the soil and its properties and the relationship between the iron oxides and the soil properties. The present work is a review of the iron oxides in the soil and its properties and the relationship between the iron oxides and the soil properties.

CHAPTER 1

INTRODUCTION

1.1 GENERAL

Iron oxides are very important constituents of soils and have been known to influence various soil properties. The colours of many soils are due to the presence of iron oxides in one form or the other, and these colours are used in many soil classification systems. Although several researches have been conducted into the properties of iron oxides (some of these are reviewed in Chapter 2) there are still uncertainties about various aspects involving the occurrence and properties of these oxides in the soil environment. Also, due to the ease of controlling the environmental conditions in a synthetic system many researches into the properties and behaviour of iron oxides have been conducted using synthetic systems, and it is desirable to conduct more tests on natural iron oxides in order to determine if the relationships obtained from the synthetic systems apply to the natural environment.

In the present research different analytical techniques comprising low magnification and high resolution electron microscopy and electron diffraction and scanning electron microscopy, X-ray diffraction, infrared spectroscopy, differential scanning calorimetry and various chemical methods have been employed on a granitic weathering profile from a subtropical site in Hong Kong in order to elucidate the mineralogy and properties of the iron oxides in the soil. The sampling of the various iron oxide fractions (e.g mottles and dispersed forms) in

the soil and application of the techniques listed above have revealed some new evidence about the occurrence and properties of iron oxides in the soil environment. Direct observation under the electron microscope has allowed a study of the morphology and crystal sizes of the soil iron oxide particles. Results from chemical tests have allowed postulations on the formation and occurrence of the different iron oxide minerals and their interrelationship with various other soil components. Al substitution for Fe in the iron oxide structure was determined by X-ray diffraction and some structural aspects of the minerals determined.

In addition to the work on iron oxides, some aspects of clay mineralogy and engineering properties of the weathered granites have been studied. This study has enabled the mineralogy of the soils at the different weathering states to be obtained and, based on this, a probable weathering path for the different primary minerals in the original fresh rock has been postulated. Information on some engineering properties such as soil structure and particle size has been obtained from transmission and scanning electron microscopy observations.

1.2 AIMS OF THE PRESENT STUDY

The overall objective of the investigation was to conduct a study that will lead to a better understanding of the role of iron oxides in soils. It was thought that a systematic study that included the mineralogy and character of the iron oxide minerals and their arrangements relative to one another as well as other minerals from the early stages of their formation to the late stages in the residual soils was desirable. The present study has concentrated on determining the mineralogy and character of the iron oxides in the soils by using several modern techniques and opened the way to further studies that would lead to the fulfilment of the overall objective. Incidental to this immediate objective, the

clay mineralogy and micromorphology of the soils were studied in order to relate the findings to some of their engineering properties.

1.3 METHOD OF STUDY

In order to accomplish the objectives stated above, a young, weathered granitic profile was obtained from subtropical Hong Kong through the Geotechnical Control Office, Hong Kong. The profile is described in Section 3.2. The main techniques used to determine the mineralogy and character of the iron oxides were transmission electron microscopy, high resolution electron microscopy, electron diffraction, X-ray diffraction techniques and differential thermal analysis. Some wet-chemical methods, scanning electron microscopy and petrographic methods were done to complement the main techniques. A summary of the experimental programme that led to the conclusions of the study is given in the flow chart in Figure 1.1.

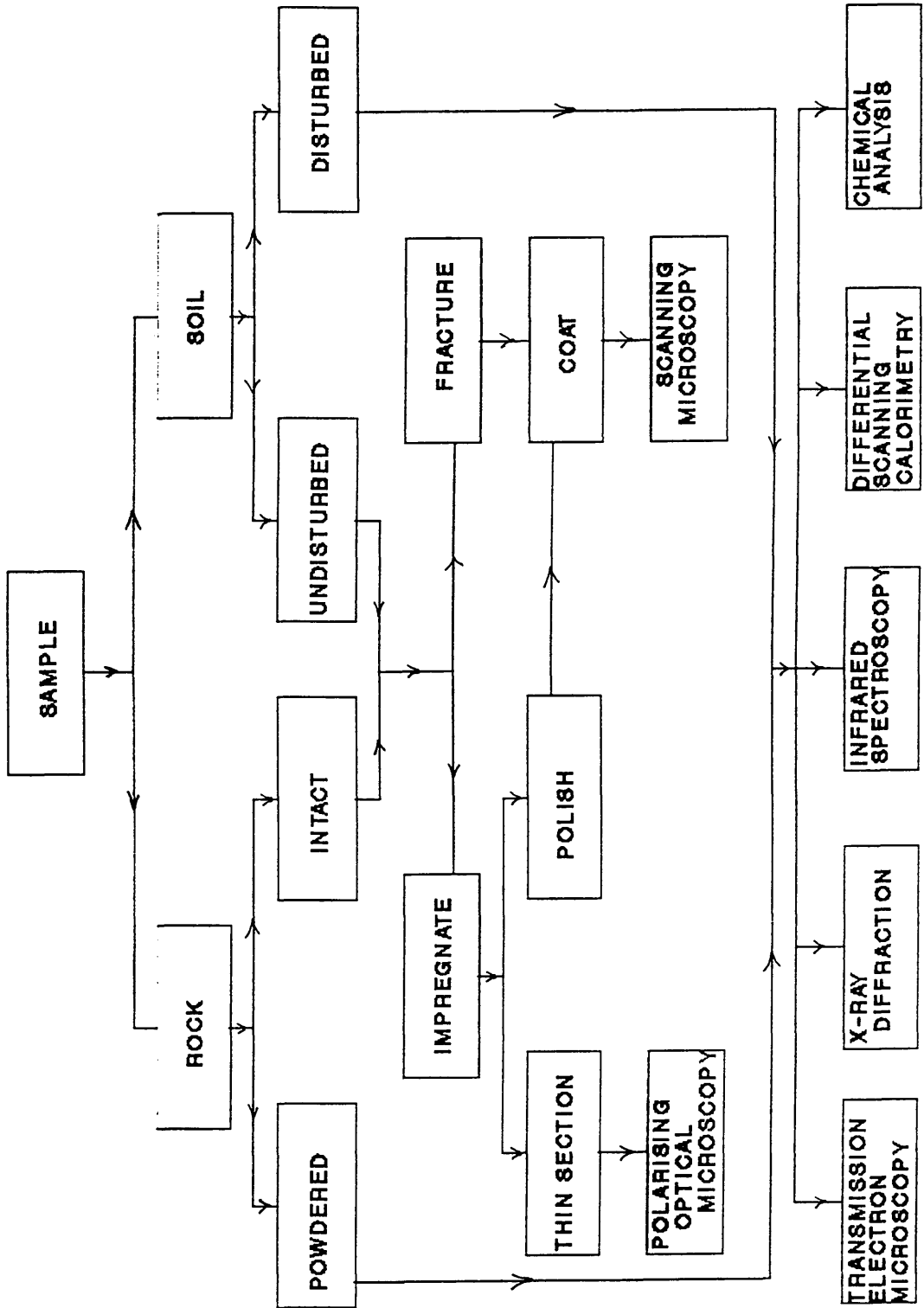


Figure 1.1: Flow chart of methodology used for investigation.

CHAPTER 2

LITERATURE REVIEW

2.1 INTRODUCTION

This chapter reviews the literature of some past work that are related to the present investigation. The structural aspects of the iron oxides and oxyhydroxides are discussed in Section 2.2, and the crystal structures of the different forms of iron oxides and oxyhydroxides as determined from previous investigations are given. Section 2.3 discusses iron oxides in the soil environment, and highlights the formation and stability as well as the character of the different phases of iron oxide in the pedogenic environment. Phase transformation under different soil conditions and cation substitution of the Fe in the iron oxide structure are also discussed.

2.2 STRUCTURE OF THE IRON OXIDES AND OXYHYDROXIDES

The structure of most of the Fe oxide minerals can be described in terms of hexagonal close packed planes of O atoms stacked one on top of the other with Fe occupying the interstitial octahedral and, in some cases, tetrahedral sites. Table 2.1 gives the crystallographic data and occurrence of some of the major iron oxide minerals, while Table 2.2 gives the powder diffraction data for some of these oxides. The stacking of the hexagonal close packed O planes in the third dimension can be either hexagonal (ABABAB...) or cubic (ABCABC...), see Table 2.1 (Fasiska, 1967; Eggleton et al; 1987). Often hexagonal and cubic

polymorphs exist. Lindsley (1976) has reviewed the structure of the Fe and Ti oxide minerals and the structures of some of the iron oxides and oxyhydroxides are given below:

2.2.1 Wüstite, FeO (Cubic)

Wüstite ideally has the NaCl structure with four Fe^{2+} and four O^{2-} ions per unit cell, but it is always deficient in iron (Jette and Foote, 1933; Willis and Rooksby, 1953; Roth, 1960; Kassim, 1982). The structure may be described as a stacking of close-packed planes with an (ABCABC...) sequence along the [111] direction. The structure may be regarded as two interpenetrating f.c.c. lattices, one of oxygen and the other of iron (Fasiska, 1967). FeO is a defect structure, consisting of both cation vacancies in octahedral sites and interstitial cation (Fe^{3+}) in tetrahedral sites. The composition may be described by Fe_xO where x lies in the range 0.83 to 0.98, depending on the method of preparation (Fasiska, 1967; Wells, 1962). This variable composition produces a range of a_0 varying from 0.428 to 0.431nm (Table 2.1). X-ray powder data (Table 2.2) for $\text{Fe}_{0.95}\text{O}$, indicated that Wüstite has a cubic structure with unit cell dimension $a_0 = 0.430\text{nm}$ (Rooksby, 1972).

2.2.2 Hematite, $\alpha\text{-Fe}_2\text{O}_3$ (Trigonal)

The structure of hematite ($\alpha\text{-Fe}_2\text{O}_3$) was determined using the technique of X-ray diffraction by Bragg and Bragg (1918). The structure was confirmed by Pauling and Hendricks (1925) who determined the crystal structure to be trigonal or rhombohedral with space group $R3C$. This structure was later confirmed by Blake et. al. (1966) who gave the trigonal unit cell dimension of $a_0 = 0.5038 \pm 0.0002\text{nm}$, and $c_0 = 1.3772 \pm 0.0012\text{nm}$.

Hematite consists of hexagonal close packed planes of O atoms stacked in an ABAB... sequence along [0001] with Fe(III) ions occupying octahedral sites.

Only 2/3 of the possible octahedral sites are occupied (Figures 2.1a,b), giving a dioctahedral arrangement (Eggleton et al; 1987). Each Fe(III) is surrounded by 6 O atoms and each O is shared by 4 Fe(III) ions. Planes of Fe atoms are shifted by one octahedral site in each successive layer along [0001] as illustrated in Figure 2.1b. Each FeO_6 octahedron shares 3 edges with three neighbouring octahedra in the [0001] plane and shares a face with an FeO_6 octahedron in the adjacent layer. Hematite belongs to the hexagonal unit cell system (Table 2.1), but it can also be indexed in the equivalent rhombohedral system (Eggleton et al; 1987). Tallman and Gulbransen (1967) calculated that the corresponding rhombohedral structure had a unit cell dimension of $a_0 = 0.5469\text{nm}$ and $\alpha = 55^\circ 13.9'$.

Both the O and Fe sublattices of the hematite structure are distorted from the ideal arrangement shown in Figure 2.1a,b. Iron atoms in octahedra which share faces are repelled from one another so that the Fe atoms lie closer to the unshared faces of the octahedra than the shared faces. Figure 2.1c best illustrates the distortion of the Fe sublattice. The distortion of the O sublattice is illustrated by the 5 shaded circles and is best seen when the structure is projected onto the (0001) plane (Figure 2.1d). The circles representing the O atoms are drawn just large enough so that the 3 spheres defining the shared face just touch one another. When this is the case, the three spheres defining the unshared face of the adjacent octahedron are separated from one another, illustrating the larger size of the unshared face (Eggleton et al; 1987).

2.2.3 Ilmenite, FeTiO_3 (Hexagonal)

The structure of ilmenite was reviewed by Lindsley (1976). It has essentially the same structure as hematite except that one-half of the Fe ions are replaced by Ti. The Fe and Ti are ordered such that along [0001] (the c-axis) there are alternating layers of Fe and Ti. The Fe is present in the

structure as Fe^{2+} while Ti is present as Ti^{4+} (Eggleton et al; 1987).

2.2.4 Magnetite, Fe_3O_4 (Cubic)

The structures of magnetite (Fe_3O_4) and maghemite (Fe_2O_3) are closely related. Both belong to the spinel group of minerals. Magnetite has the inverse spinel structure, with 8 Fe^{2+} ions distributed in octahedral sites and 16 Fe^{3+} ions, in which 8 are in octahedral sites and 8 in tetrahedral sites. Fe_3O_4 , therefore, is better known as $(\text{Fe}^{3+})_{\text{tet}}[\text{Fe}^{2+}\text{Fe}^{3+}]_{\text{oct}}\text{O}_4$ (Wells, 1962; Greenwood, 1970). The structure may be described as a stacking of close packed oxygens with an ABCABC... sequence along the [111] direction (Figure 2.2) (Fasiska, 1967). Magnetite is also a defect structure with a narrow range of composition, the Fe:O ratio varying from 0.750 to 0.744, depending on the cation impurities and methods of preparation (Wells, 1962; Greenwood, 1970). This variation in composition produces a range of a_0 from 0.8397 to 0.8394 nm. X-ray diffraction data obtained by Basta (1957) for magnetite, indicated that it has a face-centred-cubic structure with unit cell dimension $a_0 = 0.83963 \pm 0.00005$ nm.

2.2.5 Maghemite, $\gamma\text{-Fe}_2\text{O}_3$ (Spinel, cubic or tetragonal)

The structure of maghemite is more variable than that of the other Fe oxides. X-ray diffraction studies, indicated that $\gamma\text{-Fe}_2\text{O}_3$ had a spinel-like structure (Verwey, 1935; Haul and Schoon, 1939). The spinel structure essentially consists of a face-centred cubic lattice of oxygen ions plus cations in interstitial positions, of which there are two types. In one, the cation is surrounded by four oxygen ions located at the corner of a tetrahedron and in the other six oxygen ions located at the vertices of an octahedron surround the cation (see Figure 2.3). $\gamma\text{-Fe}_2\text{O}_3$ is a defect structure with the Fe:O ratio varying from 0.67 to 0.72 depending on the cation impurities in the lattices, including the

possible presence of hydrogen ions (protons) and of ferrous ions (Bloom and Goldberg, 1965; Fasiska, 1967; Morrish, 1980).

In γ - Fe_2O_3 there are $21\frac{2}{3}$ Fe(III) ions distributed amongst the 8 tetrahedral and 16 octahedral sites; $2\frac{2}{3}$ sites per unit cell are vacant. The distribution of the vacancies are still controversial (Eggleton et al; 1987). The vacancies could occur in either octahedral sites, tetrahedral sites or both. They are generally considered to occur in the octahedral sites (Verwey, 1935; Coey, 1987). According to Eggleton et al. (1987) both cubic and tetragonal structures of maghemite may be possible depending on whether the vacancies are ordered or not. Random arrangement of vacancies gives rise to the cubic structure, while the tetragonal structure requires the ordered arrangement of vacancies.

The unit cell a_0 parameter ranges from 0.830 to 0.835nm which Lindsley (1976) attributes to a continuous solid solution series between magnetite ($a_0 = 0.8396\text{nm}$) and maghemite. The higher a_0 values are probably from maghemites which contain some Fe(II) (Eggleton, et al; 1987).

2.2.6 Goethite, α -FeOOH (Orthorhombic)

The structure of goethite was described by Hoppe (1941, 1942), and later refined by Forsyth et al. (1968) and Szytula et al. (1968). Goethite is isostructural with diaspore (α - AlOOH) and consists of hexagonally close packed planes of O atoms stacked in an ABAB... sequence along the [100] direction (Eggleton et al; 1987). The Fe(III) ions occupy octahedral sites and are arranged in double rows which run along [001] (Figure 2.4a,b). Adjacent double rows within a layer are separated by a double row of empty octahedral sites. Occupied and unoccupied octahedral sites alternate in successive layers to give the pattern illustrated in Figure 2.4a. The structure can be double chains of octahedra along the c-axis which are joined to other double chains by sharing corners (Figures 2.4, 2.5, and 2.6). There are two kinds of O sites (Fig. 2.5): O_I sites where O atoms are

shared between octahedra in two different double chains, and O_{II} where O is shared by octahedra in the same chain (Eggleton et al; 1987).

The real structure is distorted from the idealized structure such that the $O_{II}-O_{II}$ distances are shorter than the other O-O distances (Figure 2.5). The effect is that of pinching in the middle of each double chain together. The double chains are also twisted slightly relative to each other, effectively shortening the O_I-O_{II} distance (Eggleton et al; 1987). This shortened O_I-O_{II} distance has been shown (Busing and Levy, 1958; Forsyth et al; 1968) to be the site of the H bond postulated by Ewing (1935b) for the isostructural mineral diaspore (α - $AlOOH$). The O_I-O_{II} distance is 0.276nm and the $O_{II}-H$ distance is 0.099nm (calculated from the data of Forsyth et al; 1968) (Eggleton et al; 1987). The H atom does not lie on a line joining the the O_I-O_{II} atoms, but lies on a line making an angle of about 11.6 degrees with the O_I-O_{II} vector. The H atoms spend most of their time near the O_{II} atoms so that the O_{II} sites can be considered the hydroxyl sites. All H bond sites are structurally equivalent, but the H bonds point in two different directions in the crystal.

2.2.7 Lepidocrocite, γ -FeOOH (Orthorhombic)

Lepidocrocite is the second common polymorph of FeOOH. Its crystal structure was determined by Ewing (1935a) using X-ray diffraction methods. The structure was later reexamined by Oles et al. (1970) using neutron diffraction methods and also by Christensen and Christensen (1978). The planes of O atoms are stacked in an ABCABC... sequence (cubic stacking) along [150]. The Fe^{3+} atoms occupy octahedral sites and are arranged in double rows along [001] as in goethite (Figure 2.7a,b) (Eggleton et al; 1987). The double rows in successive layers are arranged as illustrated in Fig. 2.7a. Like goethite, the lepidocrocite structure is described as having double chains of octahedra along the c-axis. The octahedra chains in lepidocrocite share edges instead of corners as in goethite

(Eggleton et al; 1987). Thus, the chains in lepidocrocite are joined to form corrugated layers as illustrated in Figures 2.7, 2.8 and 2.9. The H atoms are located in these layers and H bonds hold the layers together. These H bonds are represented as tubes in Figure 2.8.

There are two kinds of O sites: the O_I sites lie within the corrugated octahedral layer, while the O_{II} sites define the outer planes of the octahedral layer (Figure 2.8). Ewing (1935a) postulated that the H⁺ ions lie centred between adjacent O_{II} ions, an arrangement confirmed by Oles et al. (1970). Christensen and Christensen (1978), however, re-examined the structure also using neutron diffraction and concluded that the H⁺ ion is more likely to be closer to one of the O_{II} sites than the other. This arrangement is illustrated in Figure 2.8. For an O_{II}-H...O_{II} distance of 0.268nm, the O-H distance is 0.093nm and the H...O distance is 0.175nm. This is general agreement with H-bond lengths in goethite. The H⁺ ion lies on a line joining the two O_{II} sites and is not bent as it is in goethite (Eggleton et al; 1987).

2.2.8 Akaganeite, β -FeOOH (Tetragonal)

The structure of akaganeite was discussed in detail by Burns and Burns (1977, 1981) and Murray (1979). Other works on the crystal structure and morphology of the mineral include those by Watson et al. (1962), Gallagher (1970) and Galbraith et al. (1979). X-ray powder diffraction studies by Mackay (1960) showed that β -FeOOH is isostructural with the Mn mineral hollandite (BaMn₈O₁₆), with a tetragonal unit cell $a_0 = 1.048\text{nm}$, $c_0 = 0.3023\text{nm}$ and space group I_4/m . More recently refined Mossbauer and X-ray data obtained by Murad (1979) gave unit cell dimensions $a_0 = 1.0535 \pm 0.0002\text{nm}$ and $c_0 = 0.3030 \pm 0.0002\text{nm}$. The structure projection on the (001) face, (Figure 2.10), indicates that the Fe(III) ions are octahedrally surrounded by six oxygen or hydroxyl ions. These octahedra are linked to form double strings parallel to the

c – axis and each octahedron shares two edges with octahedra in the neighbouring string. The double strings are joined by sharing corners (Mackay, 1960).

2.2.9 Ferrihydrite and Ferroxhyte (δ -FeOOH), (Hexagonal)

The structures of ferrihydrite and ferroxhyte are not as well understood as those of the other Fe oxide minerals (Eggleton et al; 1987). Three different formulae were earlier proposed for ferrihydrite: $\text{HFe}_5\text{O}_8 \cdot 4\text{H}_2\text{O}$ for a synthetic product (Towe and Brandley, 1967), $\text{Fe}_5(\text{O}_4\text{H}_3)_3$ for a natural one (Chukrov et al; 1972) and $\text{Fe}_2\text{O}_3 \cdot 2\text{FeOOH} \cdot 2.6\text{H}_2\text{O}$ again for a synthetic product (Russell, 1979). Van der Giessen (1966) proposed a cubic unit cell for 6-line ferrihydrite but did not suggest a structure. Towe and Bradley (1966), using X-ray diffraction methods, suggested a pseudohexagonal unit cell ($a = 0.508\text{nm}$, $c = 0.940\text{nm}$) and a crystal structure, based on that of hematite, where Fe^{3+} ions occupy octahedral positions of a hexagonal close packing in such a way, that in 4 successive repeat layers the portions of occupied positions are 2/3, 1/3, 1/3, 1/3. It was believed that the corners of octahedra was occupied by O atoms and molecules of H_2O (Figure 2.11). Thus the structure is described by the formula $\text{HFe}_5\text{O}_8 \cdot 4\text{H}_2\text{O}$ (Chukrov et al; 1972). Chukrov et al. (1972) expressed reservations about this proposed structure and postulated some other possibilities based on the observations of the previous authors. Towe and Bradley (1967) reported general agreement between calculated and observed XRD intensities, but gave no atomic coordinates. They found no evidence for structural OH and concluded that the nine hydrogens in the formula were all present as water (Eggleton and Fitzpatrick, 1988). Russell (1979), using infrared methods, has since shown that about half the hydrogen is present as OH; he therefore suggested the formula $\text{Fe}_2\text{O}_3 \cdot 2\text{FeOOH} \cdot 2.6\text{H}_2\text{O}$ for ferrihydrite.

Simultaneously with the publication of the Towe and Bradley model,

Harrison et al. (1967) presented a model for the ferric oxyhydroxide core of ferritin (a metallo-protein) based on XRD evidence and a composition of $\text{FeO}(\text{OH})$. Their model has $a = 0.296\text{nm}$ and $c = 0.940\text{nm}$, a cell similar to that of Towe and Bradley but with 'a' of Towe and Bradley = $\sqrt{3}a$ of Harrison et al. The structure they proposed is based on double hexagonal closest packing of oxygens (a stacking sequence ABAC), with iron distributed randomly among all the octahedral and tetrahedral sites of the close-packed array. Brady et al. (1968) reported a third model from radial distribution function analysis of ferrihydrite formed by hydrolysis of ferric nitrate. They concluded that all the iron was in tetrahedral coordination with an Fe-O distance of 0.210nm . By contrast, Gray (1971) used electronic adsorption spectroscopy to rule out tetrahedrally coordinated iron. Eggleton and Fitzpatrick (1988) proposed a model derived largely from consideration of X-ray powder diffraction data. The model proposed is based on double-hexagonal close packing of oxygens and hydroxyls (ABAC), as in the Harrison et al. structure. Two sheets of mixed octahedrally coordinated iron are connected by two sheets of mixed octahedral and tetrahedral iron in the ratio 5 tetrahedral : 2 octahedral similar to that in spinels and in so called β -alumina (Eggleton and Fitzpatrick, 1988). They proposed a trigonal unit cell with $a = 0.508\text{nm}$, $c = 0.940\text{nm}$, but that a smaller unit cell, $a = 0.296\text{nm}$ equally well described the XRD data. The authors also reported that absorption edge spectrum suggested a similar tetrahedral iron content to that of maghemite (i.e 37.5% Fe). The model, derived from XRD intensities, had 36% tetrahedral iron. Cardile (1988) using Mossbauer spectroscopy and ferrihydrite synthesised by the same method as Eggleton and Fitzpatrick however reported that Mossbauer spectral data could not confidently differentiate between octahedral and tetrahedral iron in ferrihydrite nor demonstrate conclusively that tetrahedral iron was present in the sample, and Manceau et al. (1990) criticised some of the methods used by Eggleton and Fitzpatrick (1988) in arriving at their conclusion.

In reply Eggleton and Fitzpatrick (1990) defended their techniques and interpretations, but stressed that their proposed model should be regarded as tentative. In conclusion, all the structures proposed so far for ferrihydrite are speculative and none has yet been proven. There is therefore a need for further work in the determination of the structure of ferrihydrite.

Ferroxihite also consists of hexagonal-close-packed layers of O^{2-} , OH^- , and H_2O with Fe(III) occupying octahedral positions and has a structure similar to hematite. The Fe in ferroxihite is almost completely randomly distributed and the repeat is only 2 planes of O atoms ($c = 0.460\text{nm}$). In the ferroxihite the a dimension is taken as 0.293nm (Eggleton et al; 1987).

2.3 IRON OXIDES IN THE SOIL ENVIRONMENT

Because Fe is amongst the most stable elements formed by nuclear fusion, it has a high cosmic and terrestrial abundance. Iron is the most abundant element in the earth as a whole and the fourth most-abundant element in the earth's crust (Murad and Fischer, 1987). The average Fe concentration in the earth's crust is 5.09 mass % (Ronov and Yaroshevsky, 1969), corresponding to 1.87 atom %. The relative amounts of iron in the different rock types has been discussed by Turekian and Wedepohl (1961); Ronov and Yaroshevsky (1969); Garrels and Mackenzie (1971) and Sibley and Wilbrand (1977) while concentrations in the aquatic environment have been discussed by Lewis and Goldberg (1954) and Livingstone (1963). Iron is a major constituent in soils and is reported to range from 0.7 to 55% mass with a selected average of 3.8% (Lindsay, 1979). In primary soil minerals Fe occurs largely as ferromagnesium silicates in which Fe is present as reduced Fe(II). Weathering of these minerals releases Fe which oxidizes and precipitates largely as Fe(III) oxides and oxyhydroxides (Lindsay, 1987). Iron oxides in soils significantly influences both

the physical and chemical properties of the soils. The colour of many soils is due to the presence of iron oxide and this has been used extensively in soil classification (Schwertmann, 1985). Also, the abundance of iron oxides in some tropical soils may be responsible for their unique engineering properties. The occurrence, formation and interaction of iron oxides with other minerals in the soil environment are discussed below.

2.3.1 Occurrence

The crystal structure of the different forms of iron oxides was discussed in Section 2.2. Although all of these forms can be synthesised in the laboratory, some of them have not been identified in the pedogenic environment and some occur more frequently than others. The different forms of iron oxides that occur in the soil environment are indicated in Table 2.1 and the usual Munsell colours of the common iron oxides are given in Table 2.3. The iron oxide forms that have been found in soils include:

(a) Goethite

Goethite (α -FeOOH) is the most frequently occurring form of iron oxide in soils. Thermodynamically it has the greatest stability under most soil conditions (Schwertmann, 1977). Goethite occurs in almost every soil type and climate region and is responsible for the yellowish-brown colour of many soils. It may be dispersed evenly throughout the soil, or as with all the oxides be concentrated in certain horizons or structural forms, nodules, pipe-stems etc. This concentration may occur in initial development of the soil, or may proceed from a uniformly dispersed system due to a change in soil forming factors. The high concentrations of goethite may assume dark brown and even black colours, but they generally give the yellow-brown streak typical of the mineral (Schwertmann and Taylor, 1977).

Synthetic goethite is always acicular with the Z-axis crystal direction lying along the needle axis (van Oosterhout, 1960). This acicular morphology is also found in soils, although the needles are usually poorly developed. However, scanning electron micrographs show that the needle-like crystals are more prevalent where they have been able to develop in a void (Eswaran and Raghu Mohan, 1973), possibly due to reduced interference from the immediate environment (Schwertmann and Taylor, 1977).

(b) Hematite

Hematite (α -Fe₂O₃) which is the second most frequent form of iron oxide in soils is associated with goethite in many reddish soils. Unlike goethite, which is apparently not restricted to any climatic region, hematite appears to be absent in soils recently formed under a humid temperate climate such as in northern and mid-Europe and the northern part of the American continent (Schwertmann and Taylor, 1977). According to Schwertmann (1987), the influence of temperature and moisture partly explains the climatic distribution of hematitic (reddish) and non-hematitic, i.e. goethitic (yellowish-brown) soils. Accordingly, a tentative boundary can be drawn in the Northern Hemisphere, at approximately 40°N, latitude separating recent non-hematitic soils from hematitic soils (Schwertmann, 1987). A similar line was defined for the Southern Hemisphere (Fitzpatrick, 1987).

Hematite colours the soil red and has a greater pigmenting effect than goethite so that even low concentrations of it in goethitic soils change the hue to redder than 5YR. The pigmenting effect of hematite is particularly high when it occurs in a finely dispersed form. In denser accumulations, it generally appears much darker. As with goethite, typical crystal shapes of hematite are only weakly expressed, and isodimensional particles much less than 0.1 μm in diameter prevail. These particles sometimes show a hexagonal outline whereas hexagonal

plates at various stages of development are common for synthetic hematites (Schwertmann and Taylor, 1977).

(c) Lepidocrocite

Lepidocrocite (γ -FeOOH) occurs in soils less frequently than goethite or hematite (van der Marel, 1951; Brown, 1953; Schwertmann, 1959b). It is metastable with regard to goethite ($\Delta G_f = -114$ kcal/mol as against -117 kcal/mol for goethite). However, if kinetically favoured it will easily form in pedogenic environments and due to sluggish kinetics it may be stable even for pedogenic times. This can be deduced from its occurrence in many soils all over the world where it often can be recognised by its orange colour (7.5YR) (Schwertmann, 1985). It is often associated with its polymorph goethite, sometimes with ferrihydrite, but rarely with hematite. It occurs in mottles, bands, pipestems (hollow, tubular Fe accumulations around roots), and concretions just like the other Fe oxides, but in contrast to these it is rarely evenly dispersed over the whole soil matrix (Schwertmann, 1987b). This local concentration of lepidocrocite indicates that it characteristically occurs in soils mainly in the temperate and subtropic regions in which Fe is heterogeneously distributed due to reductomorphic processes (Van der Marrel, 1951; Brown, 1953; Schwertmann, 1959; Schwertmann and Fitzpatrick, 1977; Fitzpatrick et al; 1985).

Lepidocrocite forms from the oxidation of precipitated Fe^{2+} hydroxy compounds and appears to be restricted to hydromorphic soils where the presence of Fe^{2+} is generated due to oxygen deficiency. In fact the occurrence of lepidocrocite is indicative of hydromorphic conditions. It is commonly found in gleys and pseudogleys (surface water gleys), particularly those high in clay, but it has not been reported in calcareous hydromorphic soils where goethite forms instead (Schwertmann and Taylor, 1977).

Macroscopically, lepidocrocite occurs as bright orange mottles or bands.

Under the electron microscope the crystals resemble those formed synthetically by oxidation of Fe^{2+} salt solutions at pH 5–7 and ambient temperature. They appear as highly serrated elongated plates, 0.1–0.7 μm in length and of variable thickness or as laths or starlike twins (Schwertmann, 1973). The lath axis is the crystallographic Z–axis direction (van Oosterhout, 1960). In contrast to goethite, lepidocrocite in soils are usually reasonably well crystallized (corrected width at half–height of the (020) line at 6.27Å is around $0.2\text{--}0.3^\circ, 2\theta$). Lepidocrocite of much lower crystallinity does form, however, if the rate of oxidation and thus the rate of crystallisation is high. A higher rate of Fe^{2+} supply and a faster oxidation are most likely to occur in the air–conducting coarse pores whereas within the aggregates the rate may be much lower (Schwertmann, 1985). Even lower crystallinities of lepidocrocites were found in ochreous deposits which form by rapid oxidation of Fe^{2+} –bearing waters as they appeared at the surface (Schwertmann and Taylor, 1977; Schwertmann and Kämpf, 1983). Thus, according to Schwertmann (1985), the crystal size of lepidocrocite may function as an indicator of rate of aeration in pedogenic environments although other factors such as pH (the lower the pH, the less well crystallised, Schwertmann and Thalmann, 1976) will also be of significance.

(d) Ferrihydrite

Several occurrences of ferrihydrite in soils and other natural surface environments have been described, such as in ochreous precipitates from Fe^{2+} –containing cold and thermal waters (Chukrov et al; 1974; Henmi et al; 1980; Carlson and Schwertmann, 1981; Childs et al; 1982; Murad 1982), drainage precipitates (Susser and Schwertmann, 1983), hydromorphic soils (Schwertmann et al; 1982), podzols (McIntosh et al; 1983; Campbell and Schwertmann, 1984; Kassim et al; 1984), and pelagic clay sediments (Johnson and Glasby, 1982). According to Schwertmann (1985) ferrihydrite appears to be an indicator of

pedogenic environments in cool or temperate, moist climates characterised by young Fe oxide formations and soil solutions relatively rich in compounds (organics, Si, etc.) hindering the immediate formation of goethite and lepidocrocite. It occurs in nature either as the sole Fe oxide or in close association with goethite or lepidocrocite. Although it is considered a necessary precursor for hematite it has not been positively identified with this mineral so far. The reason for this is probably that the transformation of ferrihydrite, once formed, to the much more stable hematite is much faster than the formation of ferrihydrite itself (Schwertmann, 1985).

The mineral appears as a rusty, voluminous precipitate rich in adsorbed water and often rich in adsorbed inorganic ions and organic matter. It forms very small (50–100 Å diameter) spherical particles with a high surface area (200–350 m²/g) (Schwertmann and Taylor, 1977). These particles are generally highly aggregated and are 90–100% soluble in ammonium oxalate (Schwertmann and Fischer, 1973).

(e) Maghemite

Maghemite is the cubic, ferrimagnetic form of Fe₂O₃ (γ -Fe₂O₃). It occurs frequently in tropical and subtropical soils (Bonifas and Legoux, 1957; Adetoye, 1970; Taylor and Schwertmann, 1974; Fitzpatrick, 1978; and Coventry et al; 1983), but has occasionally been identified in the soils of the humid temperate areas as well (Van der Marel, 1951; Schwertmann and Heinemann, 1959; Schwertmann, 1987b). It is especially common in highly weathered soils of tropical and sub-tropical soils of Hawaii, Australia, India, Africa, and Lebanon. In temperate regions the mineral has been found in soils in Holland, Germany, Japan, Russia, and Canada. Occurrences in soils formed from basic igneous rocks seem to prevail in all these regions. The mineral is reddish-brown (see Table 2.3 for Munsell hue) and ferromagnetic. It may be finely dispersed or in

concretions frequently in association with hematite. Highly opaque isodimensional particles similar to synthetic maghemite can be observed under the microscope (Schwertmann and Taylor, 1977). A detailed review of the occurrence and formation of maghemite is given in Taylor and Schwertmann (1974) and Schwertmann (1987b).

(f) Akaganeite

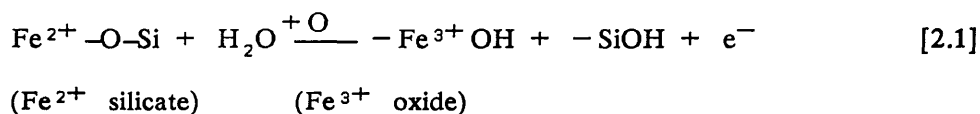
Akaganeite (β -FeOOH) has the same composition as goethite and lepidocrocite, but is structurally different. It has been identified in mineral deposits (Mackay, 1962), but not as yet in soils (Schwertmann, 1977).

(g) Magnetite

Magnetite (Fe_3O_4) in soils usually is considered lithogenic, and no pedogenic magnetite has yet been detected (Schwertmann, 1987b). However, magnetite has been identified in bacteria and other organisms (Loewenstam, 1962; Blakemore, 1975; Towe and Moench, 1981).

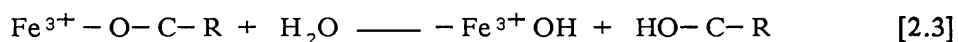
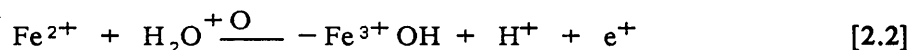
2.3.2 Formation

The primary reaction through which Fe^{3+} oxides are formed is the hydrolytic and oxidative decomposition of Fe^{2+} -containing primary minerals (mainly Fe^{2+} silicates) through the reaction:



The degree to which this irreversible reaction has taken place varies widely between weakly and strongly developed soils and is useful for characterising the degree of weathering (Schwertmann, 1985). Once formed, the Fe^{3+} oxides can be dissolved either through (microbial) reduction to Fe^{2+} or through

complexation by organic ligands. Both, Fe^{2+} and Fe-organic complexes may again be the source for Fe^{3+} through re-oxidation (Eq. 2.2) or hydrolytic decomposition (Eq. 2.3), respectively:



Just like every chemical reaction all these Fe^{3+} oxide-forming reactions are governed by the reaction conditions which, in this sense, are pedogenic factors (Schwertmann, 1985). An understanding of the conditions and modes leading to the formation of the various iron oxides may indicate present and/or past conditions prevailing in a particular soil environment (Schwertmann and Taylor, 1977). Although the different forms of iron oxides have been synthesised successfully in the laboratory (Towe and Bradley, 1967; Fischer and Schwertmann, 1975; Baird et al; 1977; Schwertman, 1987a), the conditions do not exactly correspond to those obtained in the soil environment. Synthesis and thermodynamic considerations can be used to deduce the formation of iron oxides in soils. A diagram for the formation of some of the iron oxides based on the results of synthesis experiments was given by Schwertmann and Taylor, 1977 (see Figure 2.12). Under equilibrium conditions, compounds will form which are thermodynamically most stable. However, conclusions deduced from stability diagrams constructed from known thermodynamic data often disagree with what actually happens in a soil. This may be due either to differences in free energy data arising from particle size or impurity effects in soil phases, or to the non-attainment of equilibrium between these phases and the environmental solution due to slow reaction rates (Schwertmann and Taylor, 1977). The later effect often occurs when soil minerals are inherited from an earlier weathering cycle where conditions differed from the present, for example, the subjection of a

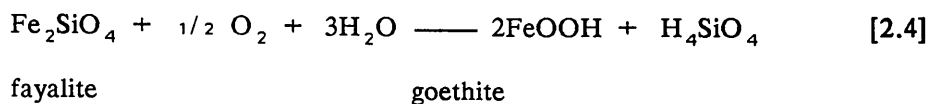
highly weathered tropical soil to drier conditions as has occurred in many parts of Australia (Veen, 1973). Furthermore, transformation of kinetically favoured metastable phases to more stable ones may be extremely slow (Schwertmann and Taylor, 1977). The formation of some of the iron oxide forms are discussed below.

(a) Goethite

Goethite (α -FeOOH) is the most stable of iron oxides. It is synthesised from Fe^{2+} compounds under conditions that rule out precipitation of other Fe^{3+} minerals from the solutions: (1) at very slow rate of Fe^{2+} oxidation, and (2) at very low or very high pH values (Chukrov et al; 1975). Although the actual conditions that lead to the formation of goethite in soils are still not well known, available data appear to suggest that, depending on further system parameters and climatic factors, goethite in soils may be formed from:

- (i) oxidation of Fe^{2+} ions produced from weathering of lithogenic Fe^{2+} – containing primary minerals (mainly Fe^{2+} silicates) (Chukhrov et al; 1975, Schwertmann, 1987b).
- (ii) formation from ferrihydrite (Schwertmann, 1987b)
- (iii) transformation of hematite (Schwertmann, 1985)

The oxidation of Fe^{2+} ions proceeds as given earlier in Equation 2.1. The specific equations for the formation of goethite from a weathering silicate may be given as



(Schwertmann, 1987b)

For example, the formation of goethite from the weathering of olivine was discussed by Delvigne et al. (1979), Eggleton (1983) and Eggleton (1987) and formation from weathered biotite was discussed by Banfield (1985).

The mechanism for the formation of goethite and hematite from ferrihydrite was discussed by Schwertmann (1987b) and is summarised in Figure 2.13. Goethite forms from solution, i.e; after dissolution of ferrihydrite under suitable conditions, whereas hematite forms through an internal rearrangement and dehydration within the ferrihydrite aggregates.

Hematite in sediments and palaeosols exposed to a subsequent cooler and wetter climate, can frequently transform to goethite as evidenced by a yellow colour penetration from the top into the redder subsoil (Schwertmann, 1971). Here the hematite is dissolved by reduction and/or complex formation, and subsequent oxidation and/or precipitation under the new environmental climate causes the neo-formation of goethite (or lepidocrocite), but never hematite. The active participation of organic matter in this process is demonstrated by the occurrence of a yellow zone adjacent to recent roots in a red soil, where under the influence of organic matter supplied from the roots, hematite is transformed to goethite (Schwertmann and Taylor, 1977).

Since goethite and hematite are often found together in most soils, the relative quantities of one compared to the other has often been used as an indication of the conditions that are more favourable for the formation of the larger quantity phase. As deduced from numerous observations, important factors which influence the quantitative relationship between goethite and hematite are

soil temperature, activity of soil water, soil pH, soil organic matter, and possibly the release rate of Fe during weathering (Schwertmann, 1985). The influence of these factors on the formation of the different phases were discussed in Schwertmann (1985, 1987b).

(b) Hematite

Current understanding of the formation of hematite ($\alpha\text{-Fe}_2\text{O}_3$) in soils indicates that it is only formed through ferrihydrite, i.e. ferrihydrite is a necessary precursor for the formation of hematite (Feitknecht and Michaelis, 1962; Schwertmann, 1966; Chukhrov et al; 1973, 1975; Schwertmann, 1985; and Schwertmann, 1987b), hence the conditions necessary for the formation of ferrihydrite (discussed below) are the initial conditions necessary for the formation of hematite. Hematite forms from ferrihydrite through an internal rearrangement and dehydration within the ferrihydrite aggregate. This dehydration can take place even in the presence of liquid water (Schwertmann, 1985). However, since hematite forms from ferrihydrite in competition with the formation of goethite from ferrihydrite (as discussed above) the formation of hematite in the soil even after ferrihydrite had been formed will depend on other pedogenic conditions (see Figure 2.13).

According to Schwertmann (1985, 1987b), soil temperature and soil water activity, soil pH, soil organic matter, Al in the system and possibly release rate of Fe during weathering are some of the important deciding factors. All experiments in which ferrihydrite was converted to hematite and goethite have shown that hematite is favoured as the temperature increases (Schwertmann, 1985). (Schwertmann, 1987b) presented a graph (see Figure 2.14) showing the variation of Hm/Hm+Gt (Hm = hematite, Gt = goethite) ratio within a temperature range of 4 to 25°C and at varying pH and showed that the ratio increases even within this temperature range. In the case of water activity,

Chapter 2: Literature Review

depending on further system parameters (e.g; pH) hematite may be kinetically favoured over goethite even in the presence of liquid water (i.e water activity = 1) free of electrolytes. The water activity in soils of warmer regions may drop below 1 (Schwertmann 1987b). Torrent et al. (1982) investigated the effect of relative humidity (RH) on the crystallisation of goethite and hematite from ferrihydrite at 45°C. They found that with increasing relative humidity relatively more hematite was formed, but at the same time the rate of transformation decreased rapidly. At 28°C the rate of transformation was 1/50th that at 45°C. From these results it was concluded that for hematite formation in soils, the variation of soil temperature may be as important as that of water activity. The influence of temperature and moisture partly explains why cool humid areas are usually free of hematitic soils, whereas in warmer areas hematite-containing soils are widespread (Schwertmann, 1987b).

Generally, organic matter has an "anti-hematitic" effect. This is often demonstrated by a radial zonation of Fe in root channels in reddish palaeosols, where a bleached zone immediately around the root is followed by a yellow goethitic zone free of hematite, beyond which is the unaffected reddish (hematitic) bulk soil (Schwertmann, 1971). Analogously, in soils formed in cool or temperate climates from hematitic parent materials such as red Mesozoic sandstones or on colluvial red soil material in depressions, hematite disappears, and goethite, lepidocrocite, and/or ferrihydrite are the Fe oxides formed (Campbell and Schwertmann, 1984), also, in the tropics and sub tropics, soils which have a yellow A over a red B horizon are widespread (Fitzpatrick, 1978; Kämpf and Schwertmann, 1982) and red mottles or hematitic concretions in tropical and subtropical soils often show yellow goethitic rims free of hematite (Coventry et al; 1983). The anti-hematitic effect of soil organic matter has not yet been explained satisfactorily, nor has it been reproduced in the laboratory (Schwertmann, 1987b). The effect of pH in an Fe^{3+} system on the formation

of goethite and hematite from ferrihydrite was demonstrated with laboratory experiments by Knight and Sylva (1974) and Schwertmann and Murad (1983). The later found that at 25°C as the pH drops from 8 to 4, the Hm/(Hm+Gt) ratio decreased from 0.7 to 0.04; whereas below pH 4 hematite again increased, and above pH 8 goethite increased. According to Schwertmann (1987b), the proportion of goethite formed thus parallels the concentration of monovalent Fe^{3+} ions in solution: as $\text{Fe}(\text{OH})_2^+$ increases between pH 8 and pH 4 and $\text{Fe}(\text{OH})_4^-$ increases above pH 8, more goethite and less hematite is formed. It was therefore suggested that these monomeric, monovalent species are the most suitable for nucleation and growth of goethite crystals in solution. Although the relevance of this result to soil environments is yet to be seen, Kämpf and Schwertmann (1982) found that within the pH range of 4–6 the proportion goethite relative to hematite increased with decreasing pH for A-horizon soils from southern Brazil. The effect of aluminium on the formation of hematite from ferrihydrite was discussed by Schwertmann (1987b). Results of laboratory experiments show that aluminium strongly suppresses the formation of goethite in favour of that of hematite.

Although the formation of hematite through the dehydration of goethite has since been found impossible in the normal pedogenic environment, due to the high temperature needed for this conversion, the conversion of goethite to hematite is still a possibility during forest/grass fires which commonly occur in the tropical and subtropical areas (Fitzpatrick, 1980, 1987).

(c) Lepidocrocite

Although the exact nature of the process of formation of lepidocrocite ($\gamma\text{-FeOOH}$) in soils is still not fully understood (Schwertmann, 1987b), there is an agreement amongst researchers that the mineral is formed from Fe^{2+} compounds (Schwertmann and Taylor, 1972; Chukhrov et al; 1975 and Fitzpatrick,

1987). This concept is supported by the findings of various synthesis experiments which have shown that lepidocrocite is often formed from oxidation of Fe^{2+} solutions (Schwertmann, 1959; Schwertmann, 1973 and Taylor, 1980), although synthesis from Fe^{3+} systems were reported in a few cases (Feitknecht and Michaelis, 1962; Murphy et al; 1976 and Cornell et al; 1989), and the fact that lepidocrocite is of common occurrence in soils, mainly from the temperate and subtropic regions, in which Fe is heterogeneously distributed due to reductomorphic processes i.e in gleyed soils (Van der Marrel, 1951; Brown 1953; Schwertmann, 1959b, Schwertmann and Fitzpatrick, 1977, Adams and Kassim, 1984 and Fitzpatrick et al; 1985). In such soils, oxygen deficiency leads to a reduction of Fe^{3+} oxides, and Fe^{2+} will be formed. Fe^{2+} will then move to zones of higher redox potential where it is reoxidised and lepidocrocite may be formed (Schwertmann, 1987b). This view follows the findings of synthesis experiments in which oxidation of Fe^{2+} solutions with air at ambient conditions with pH controlled between 5 and 7 yielded pure lepidocrocite of crystal morphology identical to soil lepidocrocite (Schwertmann, 1959a; 1973 and 1987b).

Chukrov et al; (1975) stated that the mineral was synthesised by a process involving moderately quick oxidation of Fe^{2+} and the forming of intermediate products with Fe^{2+} and Fe^{3+} , which were named green rusts. The formation of $\text{Fe}^{2+} - \text{Al}^{3+}$ hydroxy anion compounds isostructural with $\text{Fe}^{2+} - \text{Fe}^{3+}$ (so-called green rust) compounds with Al essentially substituting for Fe^{3+} was also reported by Taylor and McKenzie (1980). Where CO_3^{2-} was the only anion in the system, an $\text{Fe}^{2+} - \text{Al}^{3+}$ compound hydrotalcite was formed. These products were found to be unstable in air due to oxidation of Fe^{2+} . Oxidation of the dried sample in air yielded akaganeite (β - FeOOH), whereas, if the sample was maintained in a moist condition and oxidised by air under water, lepidocrocite or aluminous goethites were formed along with small amounts of ferrihydrite. They likened this product to the dark green-blue compounds

associated with gleyed horizons and suggested that a similar path for the formation of iron oxides in soils was likely. It is not, however, known if these compounds are necessary precursors in the formation of lepidocrocite.

(d) Ferrihydrite and Feroxihyte

The high degree of disorder and/or extremely small particle size of ferrihydrite as compared to other iron oxide minerals indicates that disorder is caused either by rapid formation and/or hindrance to crystallisation. The first mechanism is supported by the observation that ferrihydrite forms when waters containing Fe^{2+} are oxidised very quickly for example in bog ores (Schwertmann, 1959b and Evans et al; 1978) and lake ores (Schwertmann et al; 1987) both of which are temporarily anaerobic environments in which Fe^{2+} is produced, or into which it is laterally transported. Chukrov et al. (1972) also reported the finding of ferrihydrite in the mines of some Altay localities where they said it was precipitated from solutions percolating through sulphide ores and containing Fe^{2+} iron. The participation of microorganisms in the formation of ferrihydrite in some of these localities and other environments through the oxidation of Fe^{2+} had been discussed by various authors (Spencer et al; 1983; Ottow, 1969; Schwertmann and Fischer, 1973; Chukhrov et al; 1972; Carlson and Schwertmann, 1981 and Fischer, 1987). Some of these organisms need Fe as a source of energy or as a sink for electrons whereas the influence which other microbes have on these reactions seems to be a "by-product" of their metabolism (Fischer, 1987). According to Chukhrov et al. (1972) ferrihydrite is formed in some geological recent precipitates by rapid oxidation in connection with the vital functions of iron bacteria, first of all by *Gallionella*, *Lepthotrix* and *Toxothrix*. The relicts of such bacteria composed of ferrihydrite or protoferrihydrite were found in all iron oxides deposited in all cold iron springs with pH of water near 7 in different parts of the U.S.S.R (Chukhrov et al; 1972). However, according

to Fischer (1987) the participation of microorganisms in the oxidation of Fe^{2+} is well established in the very acid range (*Thiobacillus*), but questionable in the pH range of 5–7 (*Lephotrix*, *Gallionella*) because in this range "chemical" oxidation is usually rapid. Mossbauer spectroscopy, as well as x-ray diffraction, showed an Fe^{3+} oxide precipitate from an artesian fountain to be a poorly crystalline ferrihydrite. These particles contained structures of the bacteria *Gallionella* (Murad, 1982). Such a globular morphology has often been described for bacterial precipitates (Fischer, 1987). Fitzpatrick (1987) also reported the finding of minute spherical particles of ferrihydrite embedded or encrusted in sheath-like structures of Fe-oxidising bacteria composed mainly of *Sphaerotilus* in South Africa. Bacterial action has also been found responsible for the formation of other phases of iron oxides, such as, goethite, lepidocrocite, hematite and magnetite (Loewenstam, 1962; Blakemore, 1975; Huggins et al; 1980; Towe and Moench, 1981 and Tazaki et al; 1989). It is however not clear whether these oxides were formed during the precipitation itself or by subsequent recrystallisation. Ferrihydrite is also produced when groundwater containing Fe^{2+} ions exits at ground surface leading to a rapid oxidation of the Fe^{2+} ions (Carlson and Schwertmann, 1981).

As shown in laboratory experiments, organics, silicates or phosphates even at low concentrations can impede crystallisation of iron oxides thereby favouring the precipitation of ferrihydrite in favour of the more crystalline phases (Schwertmann et al; 1984). These compounds have in common a high affinity for the iron oxide surface, and therefore may block the surface of the growing crystal. Parfitt et al. (1977) discussed the adsorption of fulvic and humic acids on goethite, gibbsite and imogolite while Parfitt and Russell (1977) and Tipping (1981) have discussed the mechanisms involved. The inhibiting effect of organics was demonstrated by Schwertmann et al. (1984) on aerial aeration of a stimulated ground water in the presence of varying concentration of soil organic. They

found that the formation of lepidocrocite was inhibited in favour of the formation of ferrihydrite with increasing concentrations of soil organic matter. A similar inhibiting effect of organic matter was found in podzol B horizons and placic horizons (Campbell and Schwertmann, 1984), and also in ochreous deposits from drain pipes or drain ditches (Susser and Schwertmann, 1983). Ferrihydrite was also detected in lake waters containing about 1.5 mg/L of humics (Tipping et al; 1981). Model experiments found that among simple organic acids the carboxyl–hydroxyl acids such as citric acid are particularly strong inhibitors of crystallisation (Schwertmann et al; 1968; Kodama and Schnitzer, 1977; Cornell and Schwertmann, 1979; and Schwertmann et al; 1986).

Another important constituent inhibiting crystallisation and thereby favouring ferrihydrite formation over more crystalline phases is silicate. Poorly crystalline ferrihydrite which precipitated on aeration of ground waters in Finland were found to contain 2–6% mass percent Si strongly adsorbed at the ferrihydrite surface as indicated by IR bands at $930\text{--}960\text{cm}^{-1}$ assigned to Si–O–Fe bonds (Carlson and Schwertmann, 1981; and Wilson and Russell, 1983). Ferrihydrite from silicon rich waters was also reported in New Zealand by Henmi et al. (1980) and by Childs et al. (1982). The crystallinity of ferrihydrite apparently is related to the amount of oxalate–soluble Si (Carlson and Schwertmann, 1981). In contrast, where the Si concentration of ferriferous waters is probably low, such as in a highly desilicified Oxisol landscape of central Brazil, Ochreous precipitates in a creek were found to consist of lepidocrocite and goethite rather than ferrihydrite (Schwertmann and Kämpf, 1983). Laboratory simulation of the effect of Si on crystallisation of iron oxides have shown that silicate and phosphate strongly inhibit the crystallisation (Schellmann, 1959; Schwertmann and Thalmann, 1976; Karim, 1984 and Quin et al; 1988). Quin et al. (1988) carried out tests using synthetic goethite with silicon (Si) or phosphorous (P) as dopants. They found that the Si and P did not substitute for

Fe in the crystal structure of goethite, but were adsorbed on growth sites where they caused restriction in crystallite size and forced irregularities in crystal growth. Very low levels of incorporation produced poorly crystalline materials while at higher levels poorly crystalline goethite was formed as well as ferrihydrite. Ultimately, adsorbed Si and P prevented the formation of goethite altogether. Synthetic ferrihydrite has been prepared by neutralising a ferric salt solution (e.g; Murphy et al; 1976), by dialling a ferric nitrate solution with distilled water (Towe and Bradley, 1967), and by oxidising a ferrous salt (Schwertmann and Taylor, 1972). Neutralising a ferric salt generally produces 2-line ferrihydrite, whereas dialysis produces the more crystalline 6-line ferrihydrite.

Chukhrov et al. (1977) postulated that ferroxihyite forms in nature by a rapid abiotic oxidation of Fe at neutral to slightly acid pH. Carlson and Schwertmann (1980) on studying the characteristics and genesis of a natural occurring ferroxihyite identified in Holocene iron oxides precipitated from ferriferous groundwaters in glaciofluvial sands and gravels of Finland concluded that the mineral was formed from rapid oxidation of Fe^{2+} compounds. According to them, this requires that the Fe^{2+} be in an easily oxidisable form and that the rate of air supply be high. This appears to be the case where ferriferous waters run through highly porous, sandy sediments close to the surface, similar to the situation where ferroxihyite was located by the authors in Finland. In contrast, ferrihydrite is commonly formed where groundwater discharges onto the surface (Carlson and Schwertmann, 1980). Since very few accumulations of ferroxihyite has so far been identified in nature, the possible modes of formation in the natural environment are still open to question.

δ -FeOOH, a compound similar to ferroxihyite has been synthesised by the oxidation of $Fe(OH)_2$ (Glemser and Gwinner, 1939; Feitknecht et al; 1969; and Povitskii et al; 1976), from soluble Fe^{2+} hydroxy complexes (Misawa et al; 1970) and by oxidising $FeCl_2$ solutions with 30% H_2O_2 at pHs between 5 and 8

(Carlson and Schwertmann, 1980).

(e) Maghemite and Magnetite

Three main possible pathways have been postulated for the formation of maghemite ($\gamma\text{-Fe}_2\text{O}_3$) in soils. The oxidation of magnetite is one realistic possibility. This may be particularly important in soils formed on basic igneous rocks initially rich in magnetite. Bonifas and Legoux (1957) for example, have shown that massive maghemite in lateritic weathering products arose from the oxidation of the high concentrations of magnetite in the basic dunite rock. However, this does not explain the occurrence of maghemite in soils whose parent rocks are very low in magnetite nor its concentration near the soil surface as is the case in some of its occurrences (e.g; Fitzpatrick, 1980, 1987). Moreover, although fine-grained magnetites are known to oxidise at low temperatures (Farrell, 1972), coarse grained samples, as could be expected from residual primary minerals, alter on thermal oxidation to hematite rather than maghemite (Farrell, 1972 and Feitknecht, 1965). Thus, oxidation of magnetite may not be a common pathway for maghemite formation in soils and can not account for some occurrences of maghemite.

Oades and Townsend (1963) suggested that maghemite in soils is formed by a pedogenic process from the iron oxides present through the action of organic matter at normal temperatures. They further stated that the presence of Fe^{2+} is a necessary initial requirement. Similarly, Taylor and Schwertmann (1974) and Taylor (1980) have shown by laboratory experiments that maghemite can be produced by oxidation of green rust (an iron oxide mineral limited to strong reducing conditions) at pH around 7–8. These conditions, however, will limit maghemite to only reductomorphic soils and would not account for its occurrence in other soils.

A third possibility is the transformation of other pedogenic iron oxides by

heating to approximately 300 – 500°C in the presence of organic matter. This may happen during fires, which frequently occur in subtropical and tropical areas partly due to very high summer temperature, and may likely account for the concentration of maghemite in the surface soil in some tropical and subtropical areas (Fitzpatrick, 1980, 1987). For example, in Southern Africa and Australia where forest and/or grass–fire field trials have been conducted, the magnetic susceptibility of bulk surface soils (0 – 5cm depth) are much higher in the burnt sites than in adjacent, unburned soils or at depths below 10cm (Fitzpatrick, 1987). This is due to the formation of maghemite (and hematite) from the goethite in the various types of ferruginous accumulations (e.g; glaeboles, clay fractions, etc.) by heating in relatively high–temperature fires ranging from 200 to 800°C in the presence of organic matter (Fitzpatrick, 1980, 1987). Also, according to Schwertmann (1987), where maghemite has been found in temperate regions, occurrences are limited to small areas containing charcoal; and, since it is concentrated at the surface, fire undoubtedly caused its formation.

Hence, it is possible that known occurrences of maghemite in soils may have been due to formation by some or all of the possibilities outlined above depending on the dominating conditions in the soil.

As discussed earlier in Section 2.3.1(g) no pedogenic magnetite (Fe_3O_4) has yet been identified and the mineral is still considered to be lithogenic. It has, however, been synthesised by various means (e.g; Schwertmann and Taylor, 1973; Tamaura et al; 1983 and Taylor, 1985).

2.3.3 Interaction of Iron Oxides with other Minerals and Elements

The interaction of iron oxides with other materials in the soil environment is a common occurrence. While knowledge of some of these interactions is fairly well established, some are still not well understood. In addition, most of the available knowledge is based on results from experiments on synthetic systems in

laboratory environments which may not reflect actual soil environments. Some of the well discussed interactions of iron oxides with other substances include the adsorption of organic substances and various anions and cations on the surface of the iron oxide crystals, isomorphous substitution of Fe in the iron oxide structure by other elements and interaction with clay silicates. These are discussed below.

(a) Adsorption of Anions and Cations

The surface of iron oxides are hydroxylated, as a result of which the surface charge and potential of iron oxides are determined by the concentration of H^+ and OH^- ions in solution. The surface charge is created by an adsorption or desorption of H^+ (or desorption or adsorption of OH^- , respectively) in the potential determining layer consisting of O, OH, and OH_2 groups. Hence the charge of iron oxides is pH dependent (in contrast to those layer silicates that have permanent charge from isomorphous substitution). The pH-dependent charge of iron oxides had been discussed by Parks (1965), Onoda and de Bruyn (1966), Atkinson et al. (1967), Breeuwsmma (1973) and Taylor (1987). This charge on the oxides can be balanced by an equivalent amount of anions or cations (counter ions), electrostatically held in the outer diffuse electric double layer. This type of adsorption which treats the counter ion as a point charge is termed nonspecific. Examples of those ions which are adsorbed in this way are the anions Cl^- , NO_3^- , ClO_4^- and most of the alkali and alkaline earth cations. In contrast, other anions and cations may be held more strongly by the oxide surface because these ions penetrate the coordinating shell of the Fe atom, exchange their OH and OH_2 ligands and are bound by covalent bonds directly via their O and OH groups to the structural cation. This type of adsorption has been termed chemisorption or specific adsorption. It is further characterised by the ion adsorbing on neutral surfaces and surfaces with a charge of the same sign as the ion. These ions will reverse the sign of the surface

charge which nonspecifically adsorbed ions do not (Schwertmann and Taylor, 1977). For further details see Gast (1977), Parfitt (1978) and Mott (1981). Ions such as phosphate, silicate, molybdate, arsenate, selenate, sulphate and organic anions are some important anions specifically adsorbed by iron oxides while cations such as Zn, Cd, Cu, Pb, Li and Mg can be specifically adsorbed.

The different reactions of organic matter with iron oxides and other soil minerals had been discussed by previous authors such as Moshi et al. (1974), Harter (1977), Karim (1977), Schnitzer and Kodama (1977), Parfitt et al; (1977), Parfitt (1978), Tipping (1981) and Goodman (1987) amongst others while the adsorption of other ions such as Si and P was discussed by Schwertmann (1977), Borggaard (1984), Goldberg and Sposito (1984), Schwertmann et al. (1986), Schwertmann (1987a), Quin et al; (1988) etc. Generally, ion adsorption on the surface of the iron oxides has the effect of altering the crystallinity and surface properties such as size and growth of the iron oxide crystals. Organic matter has been found to retard or inhibit crystallisation of non-crystalline iron oxide to the crystalline form (Cornell and Schwertmann, 1979, and Adams and Kassim, 1984) and silicon and phosphorous have been found to have the same effect (Schwertmann and Thallmann, 1976, Saleh and Jones, 1984, Koch et al; 1986, and Quin et al; 1988).

(b) Isomorphous Substitution

Apart from adsorption of anions and cations by iron oxides, the replacement of Fe in the iron oxide structure by other cations, termed isomorphous substitution had been discussed by various authors. In this respect the isomorphous substitution of Fe by Al in which Al substitutes directly for Fe in octahedral sites has been the most researched. This substitution is made possible by the fact that the ionic radius of Al^{3+} (0.53Å) (Shannon and Prewitt, 1969) is similar to that of Fe^{3+} (0.645Å).

It had been shown that soil goethites (Norrish and Taylor, 1961), hematites and maghemites (Schwertmann and Fechter, 1984; Schwertmann and Kämpf, 1985) contained aluminium substituted isomorphously for some of the iron in these iron oxide structures. Beneslavsky (1956) and Jonas and Solymar (1970) also reported that goethite and hematite associated with bauxite deposits contain aluminium in their structures. Aluminium substituted iron in natural lepidocrocite was reported by De Villiers and van Rooyen (1967). The authors presented indirect evidence for the existence of aluminous lepidocrocites in soils. This mineral was not detected by X-ray, probably due to the limited crystal development and the consequent reduction in diffracted intensities resulting from aluminium incorporation, an effect they demonstrated in synthetic samples. Aluminium substitution was inferred on the basis of the higher temperatures required for dehydration to maghemite, a behaviour also exhibited by their aluminium substituted synthetic lepidocrocites. Moreover, the resultant maghemites from their heated soil sample and synthetic material required higher temperatures for their transformation to hematite, an observation consistent with aluminium incorporation (Taylor, 1980). However, according to Taylor (1980), based on the results of van der Marrel (1951) and unpublished data by himself, both normal and aluminium substituted goethites will transform to maghemite when heated in the presence of organic materials, e.g; humic acids, and this possibility was not apparently considered by De Villiers and van Rooyen (1967). In any case, the occurrence of aluminous lepidocrocite appears to be less common in soils. According to Schwertmann (1987b) this is probably because, under most conditions, aluminium in the soil solution suppresses lepidocrocite formation in favour of goethite.

Norrish and Taylor (1961) found that some soil goethites contained up to 30 mole per cent and some other investigators have shown that natural goethites may exhibit up to 33 per cent aluminium substitution, the actual amount

depending on the conditions of formation (Fitzpatrick and Schwertmann, 1982). The extent of aluminium substitution in goethites appears to be limited to 1/3 and in hematite to 1/6 of the possible octahedral positions (Schwertmann, 1987b). Changes to properties of iron oxides due to isomorphous substitution have been discussed by various authors (e.g; Taylor and Schwertmann, 1980; Fey and Dixon, 1981; Schulze, 1984; Schulze and Schwertmann, 1984; Mann et al; 1985; and Eggleton, 1987). Some of the major changes that have been pointed include a change to the size of the unit cell of the iron oxide. The fact that the size of the Al cation is about 16% smaller compared to the Fe leads to a smaller unit cell size of the aluminous iron oxide compared to those of the pure iron oxides. Changes in other properties such as crystal size, surface area and changes in X-ray diffraction, thermal behaviour, magnetic properties, phosphate adsorption, dissolution behaviour in HCl have been observed.

Attempts have been made by several authors (Norrish and Taylor, 1961; Thiel, 1963; Jonas and Solymar, 1970; Taylor and Schwertmann, 1978; and Schwertmann et al; 1979) to estimate aluminium substitution and unit cell dimension of aluminous iron oxides from X-ray diffraction. Norrish and Taylor (1961) obtained an inverse relationship between the d(111) spacings of soil goethites and mole per cent. aluminium. Thiel (1963) studied Al - substituted goethites synthesized under hydrothermal conditions at high pH and found that the d(111) spacings and the cell dimension decreased linearly with aluminium substitution. Jonas and Solymar (1970) attempted to duplicate the relationship found by Thiel, but on a plot of d(111) vs mole % aluminium, their data deviated considerably from those of Thiel. They attributed the deviation to extra aluminium present as "amorphous free aluminium hydroxide" which they believed could not be completely washed out of their samples before analysis, but they gave no additional evidence for the existence of extra aluminium. Schulze (1984) has, however, found that the a-dimensions of aluminium substituted synthetic

goethites varied widely for goethites with the same aluminium substitution (this was not the case with the b and c dimensions). Since goethite has an orthorhombic unit cell, the d-value for a given line with Miller indices hkl is related to the cell dimensions a,b,c as follows:

$$d(hkl) = [(h/a)^2 + (k/b)^2 + (l/c)^2]^{-1/2} \quad [2.5]$$

Thus the large amount of scatter in the a- dimension is reflected in the d- value of diffraction lines with $h \neq 0$ and the differences in the d(111) vs mole % Al substitution noted by Jonas and Solymar (1970) are accounted for by the variability of the a- dimension. This also explains the reason for the much larger scatter in d(111) or d(130) in the data obtained by Taylor and Schwertmann (1978, their Figure 9). Hence Al substitution based on regression lines obtained by using the d(111) of goethite, like those given by Norrish and Taylor (1961) and Thiel (1963) could be in error if d(111) is influenced by factors other than aluminium substitution. According to Schulze (1984) the large amount of scatter in the a- dimension is probably caused by structural defects in the structure of goethite due to aluminium substitution. High resolution electron microscopy may be able to reveal such defects, but such studies are rare (e.g Mann et al; 1985) and have been done mainly on synthetic samples. Gerth (1990) reported evidence for structural defect in the a dimension of synthetic goethites based on high resolution microscopy, but comprehensive results were not given. The ideal reflections to be used for obtaining regression lines will be the 0kl or 00l reflections, but these goethite reflections are often too weak or coincide with reflections from other minerals e.g clays and so cannot be determined accurately. Schulze (1984) has proposed a procedure for estimating Al substitution in goethites based on the c dimension. He gave the regression equation as:

$$\text{mole \% Al} = 1730 - 572.0 \cdot c \quad [2.6]$$

c can be calculated from the position of the 110 and 111 diffraction line using the formula:

$$c = [(1/d(111))^2 - (1/d(110))^2]^{1/2} \quad [2.7]$$

However the values of d(111) and d(110) have to be corrected for line shifts arising from structure factor especially in broad diffraction lines. Correction curves relating diffraction line shifts to width at half height (WHH) calculated assuming goethite particles with the same finite number of unit cells along the a and b axes but infinitely many unit cells along the c-axis were given by Schulze (1984) and shown on Figure 2.15. Values from Figure 2.15 are given in tabular form in Table 2.4.

A confidence interval of 2.5 mole % Al was obtained for the regression in Equation 2.6 compared to the ± 4.0 mole % obtained for the regression got from using the d(111) and given by the formula:

$$\text{mole \% Al} = 2086 - 850.7 d(111) \quad [2.8]$$

(Norrish and Taylor, 1961).

However, Schwertmann et al. (1987) reported finding, for natural goethites from two Finnish lakes, that using the Equation 2.6 given by Schulze (1984), the values of Al substitution estimated were significantly greater than those obtained chemically from Al_D (Al dissolved by dithionite extraction). Since this deviation cannot be explained by the extraction of Al from sources other than goethite, an over-estimation of Al substitution by using Equation 2.6 appeared to be inferred.

An examination of their (Schwertmann et al; 1987) Table 3 however appeared to indicate the contrary for Lake Eno, and infact suggested higher values of up to 2.1% of estimation from chemical method over those from X-ray diffraction, and if this is true, then estimation of Al from other sources (e.g free oxides and hydroxides of Al) by the chemical treatment is possible. The authors also reported that the goethites from Lake Murto (in particular) which contained essentially no Al_d , had c values which were significantly lower than those for pure goethites, and stated that "...the measured reduction in c therefore cannot be due to Al substitution, as is usual for goethites". According to the authors, "...because of this variability on one side and the rigid nature of the structure on the other side, a minute increase in a (or b) may be compensated by a corresponding decrease in c, which then in itself no longer indicates the degree of Al substitution. Thus, the cell volume seems to be a better indicator of the contracting effect of Al-for-Fe substitution than does the value of c ". The authors gave a relation between unit-cell volume and Al substitution based on results from synthetic goethites prepared under different conditions (Figure 2.16). An average value of Al substitution obtained from using cell volume for goethites from Lake Eno was given as 7.9 mole %, which compared well with 7.88 mole % (obtained by me from the authors' Table 3) obtained from Al_d (chemical analysis). However, an average value of 6.88 mole % (obtained by me from the authors' Table 3) obtained for the same goethites using Equation 2.6 appeared close to those obtained from using cell volume. Also, since due to interference from other silicates and/or poor crystallinity of natural goethite particles from many sites, it may not be possible to obtain all the lines required for the estimation of all unit cell constants (hence cell volume), and estimation of Al substitution using the c dimension (Equation 2.6) would continue to have wide application.

Aluminium substitution for hematite based on the relationship obtained for

Chapter 2: Literature Review

seven synthetic Al substituted hematites synthesized at 70°C was given by Schwertmann et al. (1979) as:

$$\text{mole \% Al} = 3109 - 617.1 \cdot a \quad [2.9]$$

where a is the a - dimension of hematite.

Substitution of Fe by Mn in the iron oxide structure has also been reported (Stiers and Schwertmann, 1985, and Cornell and Giovanoli, 1987). These authors have shown manganese to replace as much as 15 mole % of the Fe in the structure of synthetic goethite while Mn-hematite containing as much as 5 mole % Mn was formed by Cornell and Giovanoli (1987). Although Mn substituted goethites are rare in natural systems and only one reference to such goethites appears to exist (Thiry and Sornein, 1983) the possibility of manganese and iron precipitates coexisting in marine and terrestrial environments (Cornell and Giovanoli, 1987) is a valid reason for further research in this area. Gerth (1990) has studied the effect on goethite of isomorphous substitution of trace metals Co^{3+} , Ni^{2+} , Cu^{2+} , Zn^{2+} , Cd^{2+} , and Pb^{4+} . According to him, evidence for an isomorphous substitution of these metals is a systematic variability of the unit cell b -parameter of goethite. The Changes in the b dimension per unit mole % incorporation can be linearly related to the ionic radii of the foreign metals which were incorporated into the goethite structure.

(c) Interaction with Clay Silicates.

The association of iron oxides with clay minerals has been a subject of interest amongst researchers due, mainly, to the implications on agricultural and engineering properties of soils especially in the tropical and subtropical areas where the iron oxide content of some of the soils (e.g lateritic soils) is relatively high. Some review of previous works in this area was done by Taylor (1987) and

Schwertmann (1987b).

One of the earlier understanding of iron oxide – clay interaction was that the iron oxides in tropical (lateritic) soils caused aggregation of the soil through cementation of the individual clay particles by the iron oxide minerals which formed a thin coating on the surfaces of the kaolinite particles (Coleman et al; 1964). Presently, however, there are opposing views on the ability of iron oxide to promote aggregation purely by interaction with clay minerals. Deshpande et al. (1964) working with highly weathered soils with total iron oxide contents from 2 to 15%, found that iron oxide was generally present as discrete mineral particles and did not influence the stability of the aggregates by cementation. This discrete nature of the iron oxide minerals, even when they were present on the surface of clay minerals has also been noted by Fripiat and Gastuche (1952), Greenland et al. (1968) and Schwertmann and Kämpf (1985). Smart (1973) using electron microscopy to observe ultra–thin sections of a red tropical clay from Kenya noted that the iron oxide particles in the soil were often widely spaced and often self–aggregated (although some iron oxide particles appearing singly and in irregular groups appeared to be in contact with the metahalloysite clay plates), whereas the clay particles in the soil often approached and touched directly. According to him, at first sight the iron oxide particles appeared to be in the wrong positions to act as cement. On the other hand, Kemper (1966) obtained a correlation between iron content and the water stability of aggregates, thus indicating the role of iron oxide in the formation of soil aggregates. Blackmore (1973) and Schalabi and Schwertmann (1970) found that freshly precipitated ferrihydrite promoted aggregate stability more than more crystalline iron oxides, and Greenland and Oades (1968) found that hydrolysis of a FeCl_3 solution at pH 3 bonded kaolin particles into larger masses. The interaction between kaolinite and synthetic ferrihydrite at various pH was studied by Saleh and Jones (1984) using electron microscopy methods. They reported no,

Chapter 2: Literature Review

attraction between the ferrihydrite and kaolinite surfaces at pH 9, when the surfaces of both clay and ferrihydrite will be negatively charged, nor was there any attraction between the ferrihydrite and the edge surfaces of kaolinite at any pH since the charges on the edge surface of kaolinite is similar to that of ferrihydrite, being pH-dependent with similar pzc (point of zero charge). However, they found that the positively charged ferrihydrite particles were attracted to any permanent negative charges on the basal surfaces of kaolinite and coated them. In general, for synthetic systems, very small Fe-hydroxy-polycations with a high positive charge at low pH are particularly effective (Rengasamy and Oades, 1977; Robert et al; 1982).

In summary, the role of iron oxides in promoting aggregation in soils remains somewhat controversial and seems to vary in different soils. This is probably due to variations in the amount and nature of iron oxides and other components in soils. There is therefore a strong need for further studies on the process of aggregation in soils and the possible role of iron oxides.

Table 2.1: Some Crystallographic Data and Occurrence of the major Fe Oxide Minerals.
(modified from Eggleton et al; 1987)

Mineral	Formula	Crystal System	Cell Dimension [†] (nm)	Stacking of Hexagonal Close-Packed O Layers		Occurrence
				Sequence	Direction	
Hematite	α -Fe ₂ O ₃	hexagonal (or rhombohedral)	a=0.5034 c=1.3752	ABABAB...	[0001]	Common in soil and fired clays
Ilmenite	FeTiO ₃	hexagonal	a=0.5884	ABABAB...	[0001]	Common in soil
Magnetite	Fe ₃ O ₄	cubic	a=0.83967	ABCABC...	[111]	Lithogenic
Maghemite	γ -Fe ₂ O ₃	cubic or tetragonal	a=0.8350 or a=0.834 c=2.502	ABCABC...	[111]	Occurs in soil
Goethite	α -FeOOH	orthorhombic	a=0.4608 b=0.9956 c=0.30215	ABABAB...	[100]	Common in soil
Lepidocrocite	γ -FeOOH	orthorhombic	a=0.388 b=1.254 c=0.307	ABCABC...	[150]	Occurs in soil
Akaganeite	β -FeOOH	tetragonal	a=1.048 b=0.3023			Identified in mineral deposits

Table 2.1 (contd).

Mineral	Formula	Crystal System	Cell Dimension [†] (nm)	Stacking of Hexagonal Close-Packed O Layers		Occurrence
				Sequence	Direction	
Ferrihydrite*	$\text{Fe}_5\text{O}_7(\text{OH}) \cdot 4\text{H}_2\text{O}$	hexagonal	a=0.508 c=0.940	ABABAB...	[0001]	Occurs in soil
Ferroxyhite	δ' -FeOOH	hexagonal	a=0.293 c=0.460	ABABAB...	[0001]	Occurs in soil

[†]Data from JCPDS card numbers: 13-354 (hematite), 29-733 (ilmenite), 24-81 and 25-1402 (maghemite),

19-629 (magnetite), 29-712 (goethite), 13-157 (akaganeite), 29-712 (ferrihydrite). Lepidocrocite data from Christensen and Christensen (1978). Ferroxyhite data from Carlson and Schwertmann (1980).

*Formula from Towe and Bradley (1967). Other proposed formulae include:

$\text{Fe}_5(\text{O}_4\text{H}_3)_3$ (Chukhrov et al; 1973) and $\text{Fe}_2\text{O}_3 \cdot 2\text{FeOOH} \cdot 2.6\text{H}_2\text{O}$ (Russell, 1979).

Table 2.2: Powder diffraction data for some iron oxides.

Compound	1 FeO (Wüstite)		2 Fe ₃ O ₄ (Magnetite)		3 (Tetragonal) γ-Fe ₂ O ₃ (Maghemite)		4 (Cubic spinel) γ-Fe ₂ O ₃ (Maghemite)		5 α-Fe ₂ O ₃ (Hematite)	
	d	I/I ₀ hkℓ	d	I/I ₀ hkℓ	d	I/I ₀ hkℓ	d	I/I ₀ hkℓ	d	I/I ₀ hkℓ
	0.2475	50 111	0.485	40 111	0.82	8 101	0.5815	2 110	0.3685	30 012
	0.2145	100 200	0.2966	70 220	0.74	18 102	0.479	5 111	0.2703	100 104
	0.1515	65 200	0.2530	100 311	0.635	8 004	0.4115	1 200	0.2519	71 110
	0.1292	25 311	0.2419	10 222	0.595	60 103, 110	0.3700	5 210	0.2295	2 006
	0.1237	25 222	0.2096	70 ¹ 400	0.575	4 111	0.3381	2 211	0.2208	23 113, 021
	0.1072	10 400	0.1712	60 422	0.537	8 112	0.2937	34 220	0.2080	2 202
	0.0982	7 331	0.1614	85 333, 511	0.500	8 104, 005	0.2502	100 311	0.1843	39 024
	0.0960	25 420	0.1483	85 440	0.484	40 113	0.2397	1 222	0.1697	48 116
			0.1327	20 620	0.432	25 105, 114	0.2215	0.5 321	0.1637	0.5 211
			0.1279	30 533	0.413	2 200, 006	0.2079	24 400	0.1604	2 122
			0.1264	10 622	0.386	12 115	0.1861	0.5 420	0.1601	9 018
			0.1211	20 444	0.375	100 106, 203	0.1688	0.5 422	0.1487	32 214
			0.1121	30 642	0.350	12 204	0.1599	33 511, 333	0.1454	32 300
			0.1092	60 553, 751	0.342	65 213, 116	0.1547	0.5 432, 520	0.1351	3 208
			0.1049	40 800	0.3216	25 214, 205	0.1513	1 521	0.1313	12 1, 0, 10
			0.0989	10 660, 822	0.3077	2 117	0.1470	53 440	0.1308	2 119
			0.0969	40 555, 751	0.2950	100 ⁺ 206, 220	0.1423	1 433, 530	0.1260	8 220
			0.0939	30 840	0.2871	<1 222	0.1314	7 620	0.1229	3 306
			0.0879	40 931	0.2799	18 009, 300	0.1270	11 533	0.1215	1 223
			0.0857	50 844	0.2642	25 310, 303	0.1257	3 622	0.1192	2 312
			0.0811	40 951	0.2521	100 ⁺ 119, 313	0.1208	5 44	0.1191	5 128
					0.2451	<1 305, 314	0.1113	7 642	0.1165	6 0, 2, 10

Table 2.2 (contd.)

Compound	γ -FeOOH (Lepidocrocite) 6			α -FeOOH (Goethite) 7			β -FeOOH (Akaganeite) 8			δ -FeOOH 9			Ferrihydrite 10		
	d	I/I ₀	hk ℓ	d	I/I ₀	hk ℓ	d	I/I ₀	hk ℓ	d	I/I ₀	hk ℓ	d	I/I ₀	hk ℓ
		0.6267	100	020	0.4976	12	020	0.7467	40	110	0.461	1	001	(0.62)	4
	0.3295	66	021	0.4179	100	110	0.5276	30	200	0.2545	10	100	(0.42)	4	G
	0.2984	3	110	0.3380	10	120	0.3728	5	220	0.2255	10B	101	(0.332)	7	A.L
	0.2475	55	130	0.2692	45	130	0.3333	100	310	0.1685	10VB	102	(0.269)	3	G
	0.2436	7	041	0.2582	23	021	0.2634	25	400	0.1471	10	110	0.254	100	100
	0.2364	14	111	0.2526	6	101	0.2550	55	211	0.1271	2	200	0.246	25	111
	0.2089	4	060	0.2488	16	040	0.2483	2	330	0.1223	2	112	0.224	90S	112
	0.2086	3	131	0.2448	80	111	0.2356	9	420	0.1104	2VB	202	0.1977	40MS	113
	0.1942	23	150	0.2303	3	200	0.2295	35	301	0.0965	2B	210	0.1727	20MS	114
	0.1937	18	002	0.2252	13	121	0.2104	7	321	0.0943	2B	211	0.1512	50MS	115
	0.1850	6	022	0.2243	3	210	0.2067	7	510				0.1469	80S	300, 213
	0.1736	17	9J1	0.2189	20	140	0.1954	20	411				0.127	<1	220, 206
	0.1625	1	112	0.2090	1	220	0.1862	4	440				0.1228	2	222, 304, 215
	0.1567	5	080	0.2010	4	131	0.1807	<1	530				0.1177	4	223, 008, 312
	0.1536	7	200	0.1920	8	041	0.1756	15	600				0.1166	1VB	224
	0.1525	18	132	0.1801	12	211	0.1730	3	431, 501				0.1053	5	225
	0.1492	3	220	0.1773	3	141	0.1686	<1	620				0.0996	2	119, 316

Table 2.2 (contd.)

0.1453	1	0.1719	40	221	0.1643	35	521		
0.1437	10	0.1690	12	240	0.1516	9	002		
0.1420	2	0.1659	4	060	0.1503	5	611		
0.1392	7	0.1603	9	231	0.1490	3	710,550		
0.1372	11	0.1563	27	151	0.1485	3	112		
0.1299	2	0.1511	12	002	0.1458	1	202		
0.1265	2	0.1506	5	250	0.1446	15	541		
0.1238	1	0.1450	4	241					
0.1218	3	0.1467	6	320					
0.1204	5	202							
0.1193	4	0,10,1							

Note:

VB = very broad
B = broad

Note:
L = probably from γ -FeOOH
G = probably from α -FeOOH
A = probably from β -FeOOH
S = sharp
MS = medium sharp
VB = very broad

1. Wüstite, FeO. Data of Rooksby (1961).
2. Magnetite Fe₃O₄. Data of Rooksby (1961).
3. Maghemite, γ -Fe₂O₃ (Tetragonal). Ref.: Von Schrader, R. and Büttner, G. Z (1963). Z. anorg. allg. Chem; 320, 209.
4. Maghemite, γ -Fe₂O₃ (Cubic spinel). Ref.: Haul, R. and Schoon, T. (1939). Phys. Chem; 44, 216.
5. Hematite, α -Fe₂O₃. Calculated diffractometer pattern. Brown, G. (1980). In Brindley, G.W and Brown, G. (eds.). "Crystal Structures of Clay Minerals and their X-ray Identification"; 371.
6. Lepidocrocite, γ -FeOOH. Powder data of Rooksby (1961).
7. Goethite, α -FeOOH. Calculated diffraction pattern. Brown G. (1980). (see 5).
8. Akaganeite, β -FeOOH. Ref.: Murad, E. (1979). Clay Miner; 14. 273.
9. Delta-FeOOH. Ref.: (same as 5).
10. Ferrihydrite Ref.: (same as 5).

Chapter 2: Literature Review

Table 2.3: Frequent Munsell hues of Fe-oxides in soils.
(after Schwertmann, 1987a).

Mineral	Munsell hue
Hematite	5R - 2.5YR
Goethite	2.5Y - 7.5YR
Lepidocrocite	5YR - 7.5YR
Ferrihydrite	5YR - 7.5YR
Maghemite	2.5YR - 5YR

Table 2.4: Corrections to observed 110, 111, and 130 line positions for line shifts caused by diffraction from small crystallites. The corrections are calculated for $\text{CoK}\alpha$ radiation. (after Schulze; 1984).

WHH_{corr} ($^{\circ}2\theta$) ¹	Correction ($^{\circ}2\theta$)		
	110	111	130
0.1	0	0	0
0.2	0	0	0
0.3	0	0	0
0.4	0	0.01	0
0.5	0	0.01	0
0.6	0	0.02	0
0.7	-0.01	0.02	0
0.8	-0.01	0.03	0.01
0.9	-0.01	0.04	0.01
1.0	-0.01	0.05	0.01
1.1	-0.01	0.06	0.01
1.2	-0.02	0.07	0.01
1.3	-0.02	0.08	0.02
1.4	-0.02	0.09	0.02
1.5	-0.03	0.10	0.02

¹WHH corrected for instrumental line broadening.

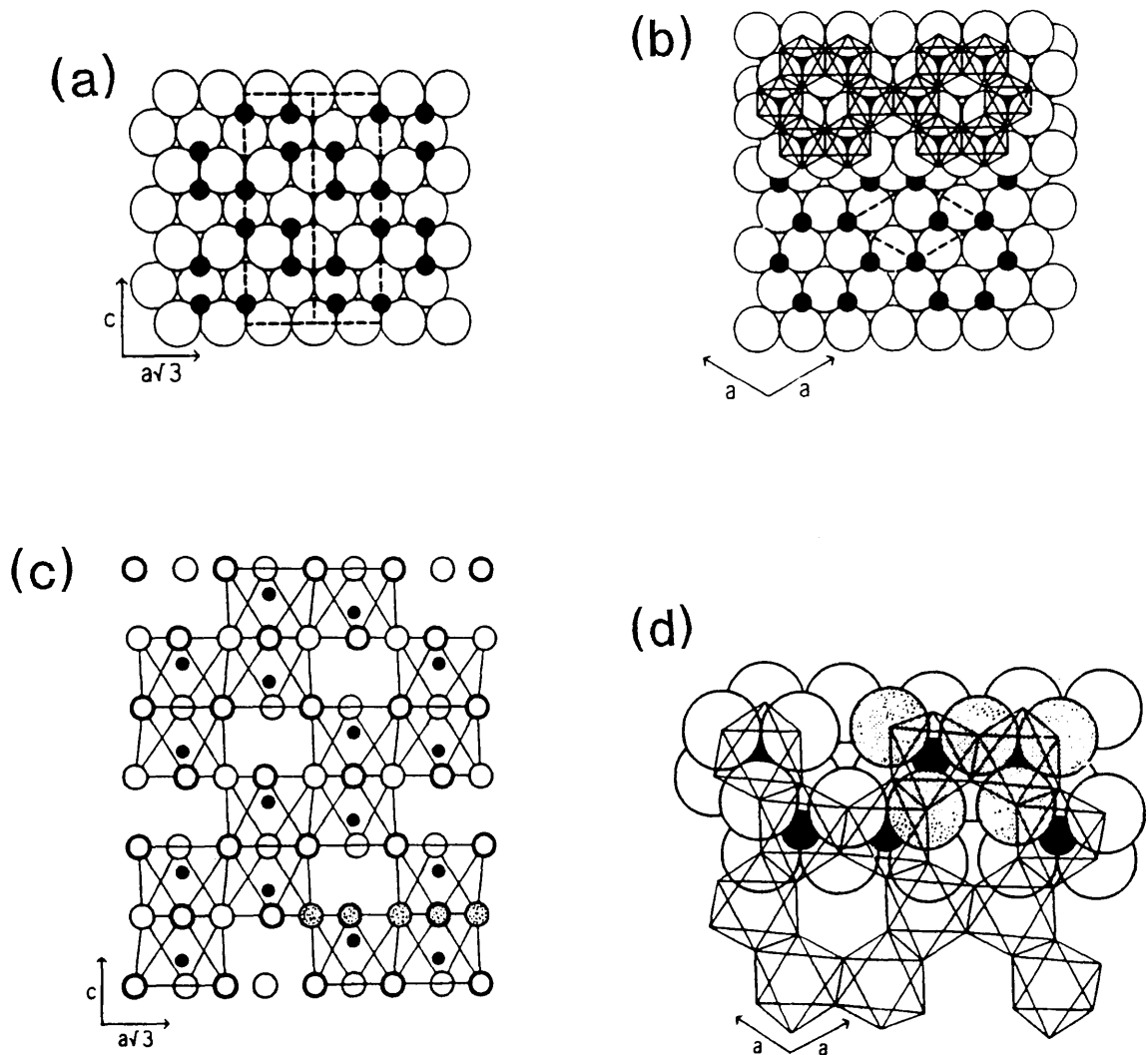


Figure 2.1: (a) & (b) Close-packed models of the ideal hematite. Large open circles are O atoms, small black circles are Fe atoms. Selected octahedra are outlined with thin solid lines, unit cells are outlined with dashed lines.

(c) The hematite structure projected onto $[1120]$. Solid circles are in the plane, thin open circles are below the plane, and thick open circles are above the plane of the paper.

(d) The hematite structure projected onto $[0001]$. The same five O atoms are shaded in (c) & (d).

(after Eggleton et al; 1987).

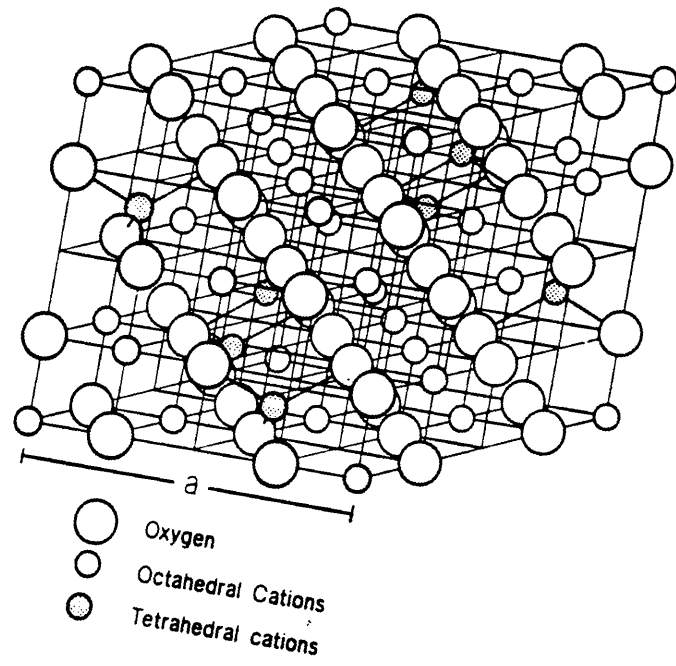


Figure 2.2: The spinel unit cell oriented to emphasise the [111] planes.
(after Eggleton et al; 1987).

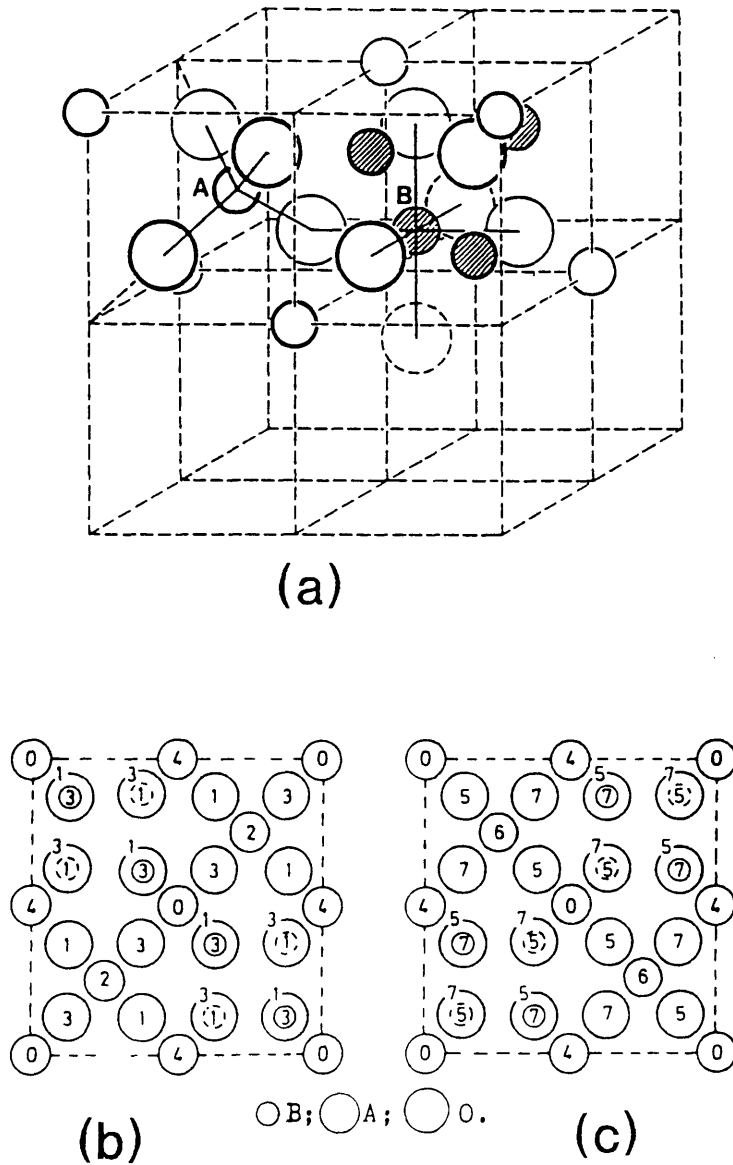


Figure 2.3: The unit cell of the spinel structure. The small unshaded and shaded spheres in 2(a) represent cations in tetrahedral (A) and octahedral (B) sites respectively. The larger spheres represent oxygen atoms. For clarity the upper, 2(b), and lower, 2(c), halves of the cell are shown separately as the structure projected from the top of the cell. The height of the atoms are indicated in units of $1/8 a_0$.

(after Kassim, 1982)

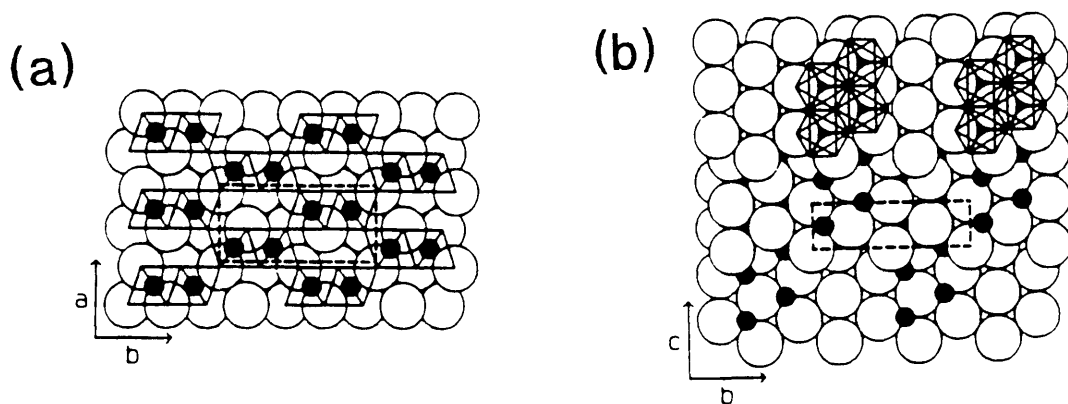


Figure 2.4(a) & (b): Close-packed models of the ideal goethite structure.

Large open circles are O atoms, small black circles are Fe atoms. Selected octahedra are outlined with thin solid lines, unit cells are outlined with dashed lines. (after Eggleton et al; 1987).

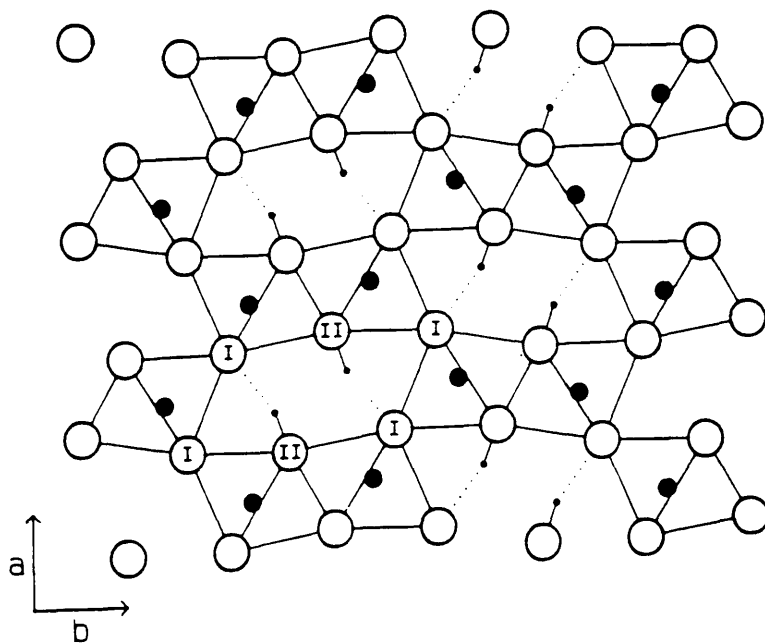


Figure 2.5: The goethite structure projected onto [001]. Oxygen atoms are represented by large open circles, Fe atoms by medium solid circles, and H atoms by small solid circles. Octahedra are outlined by solid lines. Hydrogen bonds are indicated by solid and dotted lines. (after Eggleton et al; 1987).

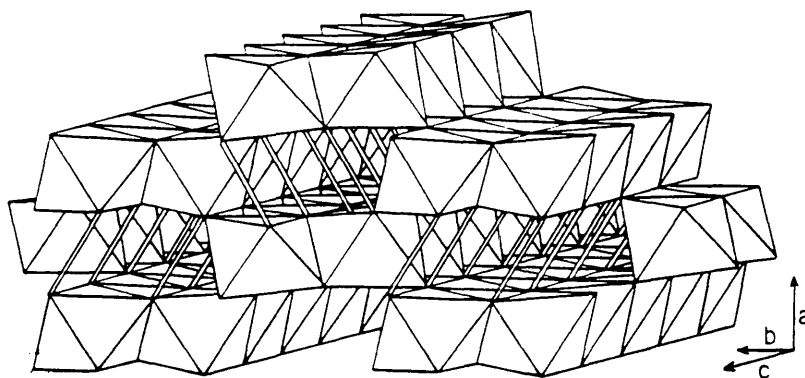


Figure 2.6: An octahedra model of the goethite structure. Hydrogen bonds are represented by small bars. (after Eggleton et al; 1987).

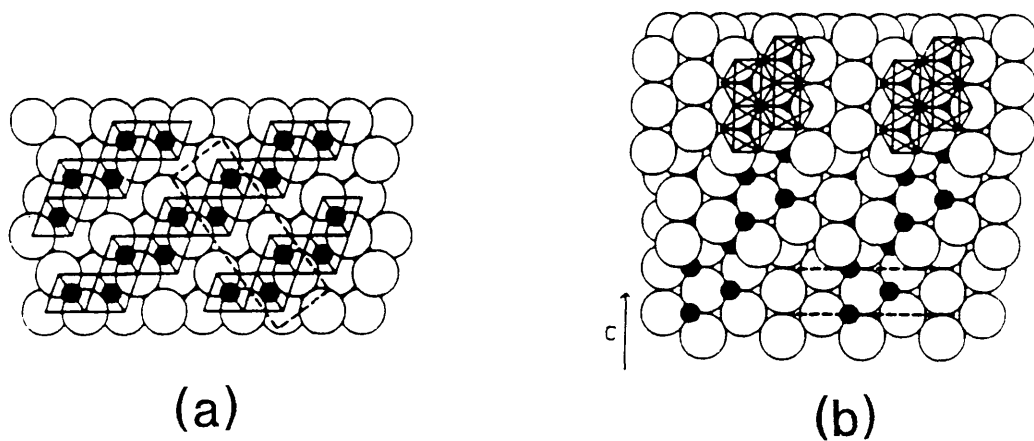


Figure 2.7 (a) & (b): Close-packed model of the ideal lepidocrocite structure. Large open circles are O atoms, small black circles are Fe atoms. Selected octahedra are outlined with thin solid lines, unit cells are outlined with dashed lines. (after Eggleton et al; 1987).

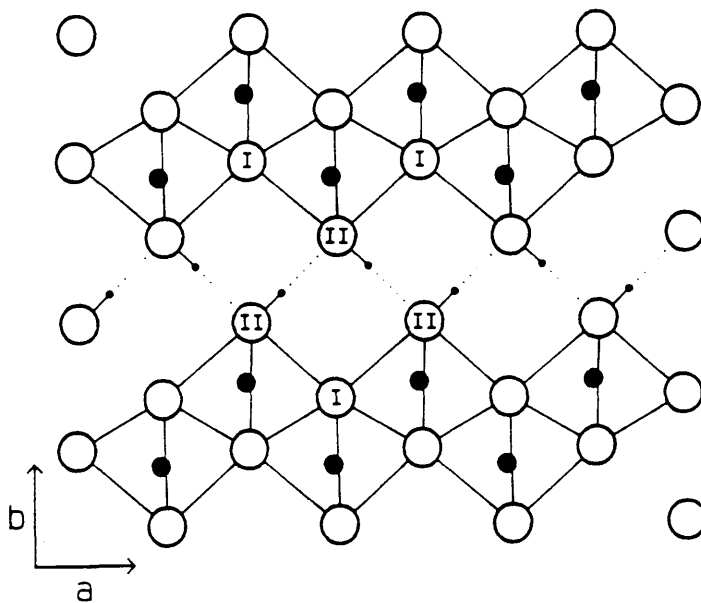


Figure 2.8: The lepidocrocite structure projected onto [001]. Oxygen atoms are represented by large open circles, Fe atoms by medium solid circles, and H atoms by small solid circles. Octahedra are outlined by solid lines. Hydrogen bonds are indicated by solid and dotted lines. (after Eggleton et al; 1987).

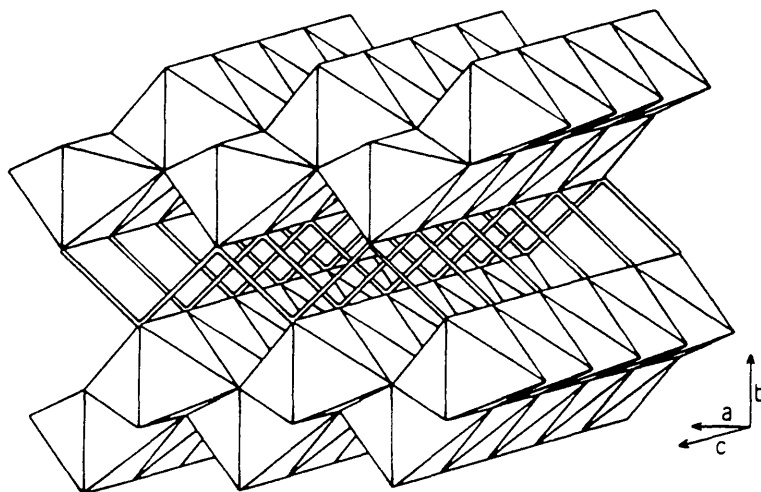


Figure 2.9: An octahedra model of the lepidocrocite structure. Hydrogen bonds are represented by small bars. (after Eggleton et al; 1987).

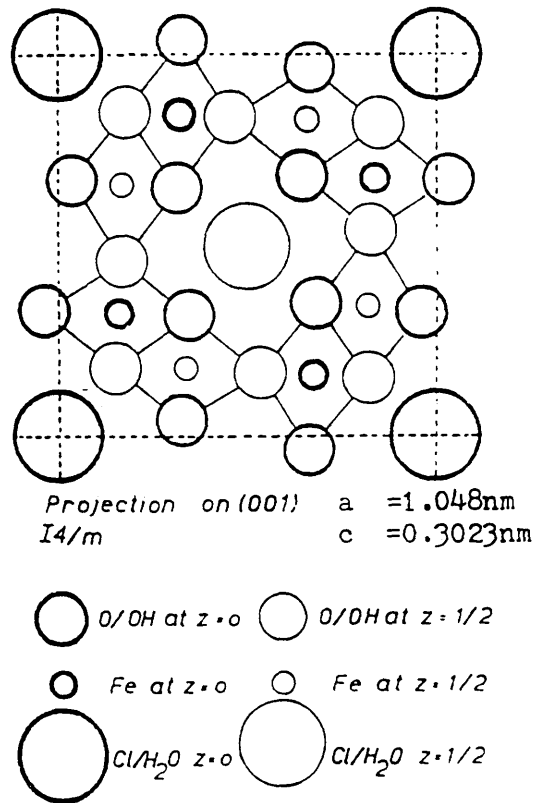


Figure 2.10: The crystal structure of akaganeite, projected on the [001] face. (after MacKay, 1960).

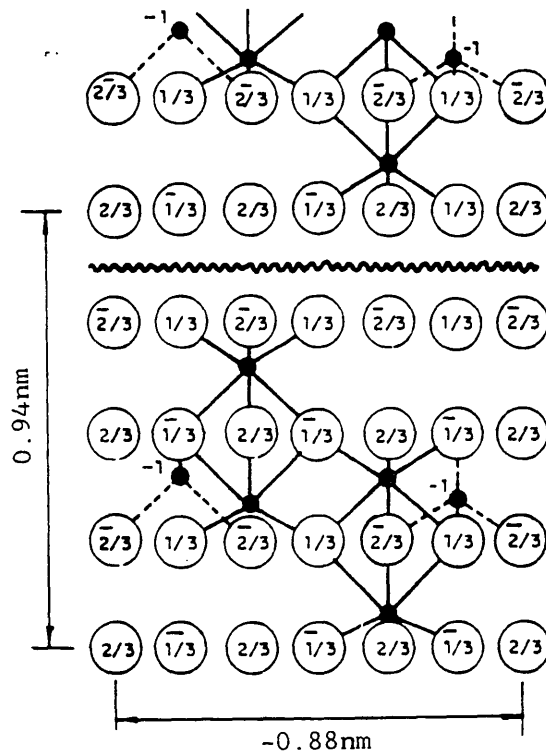


Figure 2.11: The structural scheme of ferrihydrite according to Towe and Bradley (1967). Open circles are O, solid circles are Fe. Wavy line indicates a level at which the lateral displacements are optional. (after Chukhrov et al; 1972).

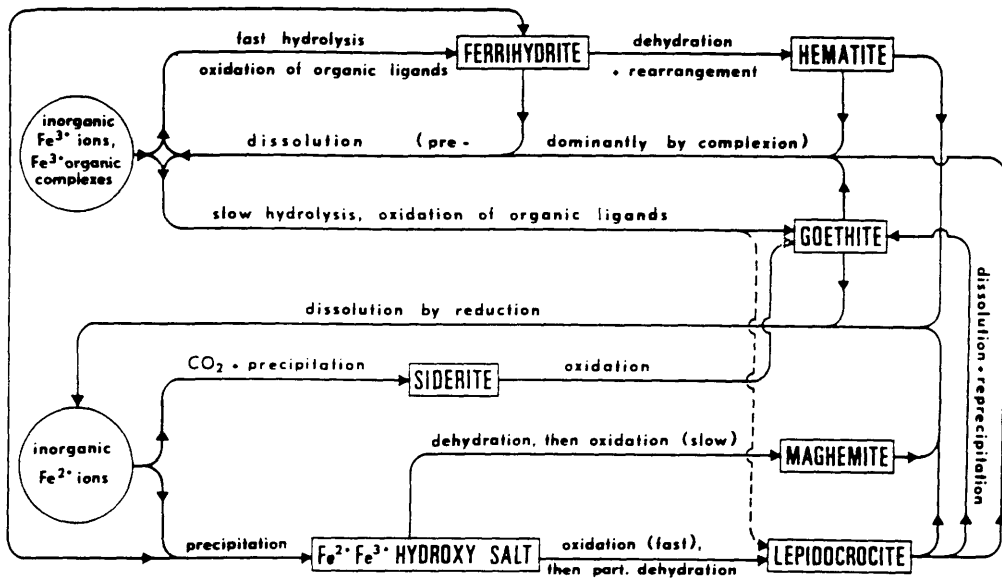


Figure 2.12: Possible pathways of iron oxide formation under near pedogenic conditions.

(after Schwertmann and Taylor, 1977).

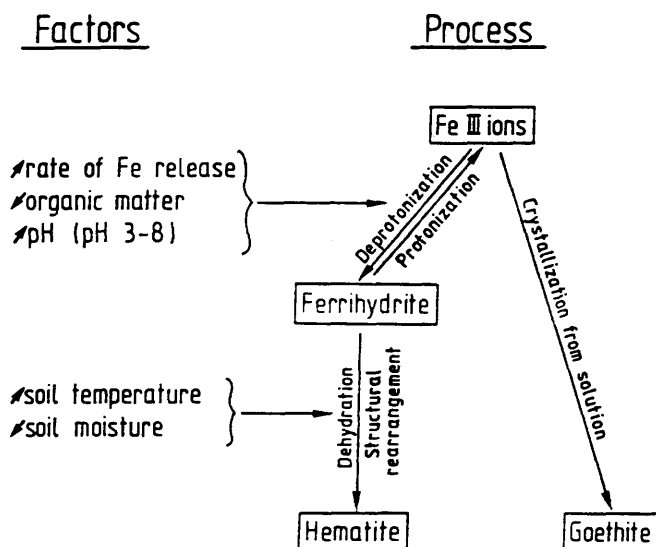


Figure 2.13: Hematite and goethite: schematic representation of their competitive processes of formation and factors influencing them in soil environments. Small arrows indicate that increasing or decreasing expression of the factor favours hematite formation with the opposite effect for goethite. One factor can also bring about two different processes. Higher soil temperature may not only induce dehydration of ferrihydrite and thereby reinforce hematite formation directly, but may also accelerate Fe release and organic matter decomposition and thereby favour hematite formation indirectly.

(after Schwertmann, 1987b).

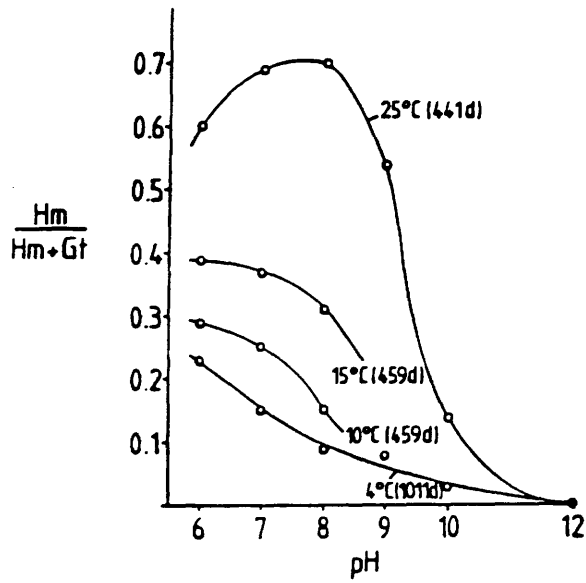


Figure 2.14: The ratio of hematite to hematite + goethite ($Hm/Hm+Gt$) formed from ferrihydrite increases with increasing storing temperature between 4 and 25°C. Besides temperature, pH also has a strong effect. (after Schwertmann, 1987b).

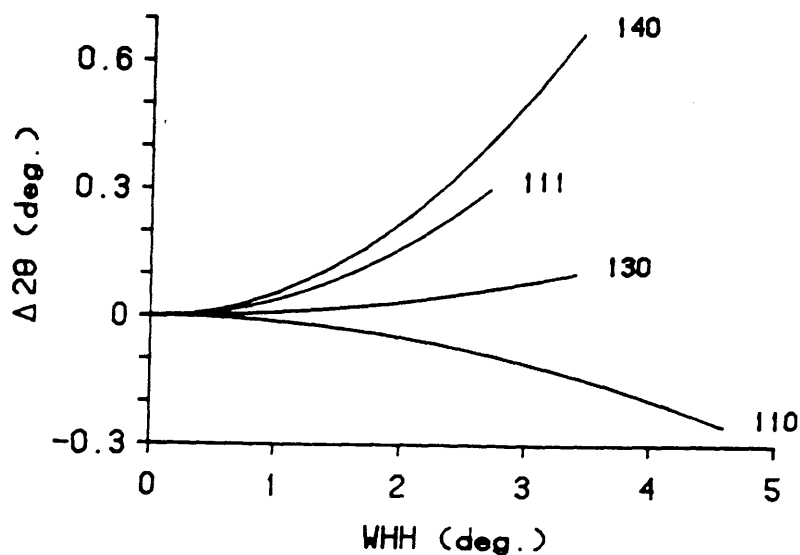


Figure 2.15: Curves relating the shift due to diffraction from small particles for selected goethite lines. These curves were calculated assuming crystallites with the same number of unit cells along the a and b axes but infinitely many along the c axis. (after Schulze, 1984).

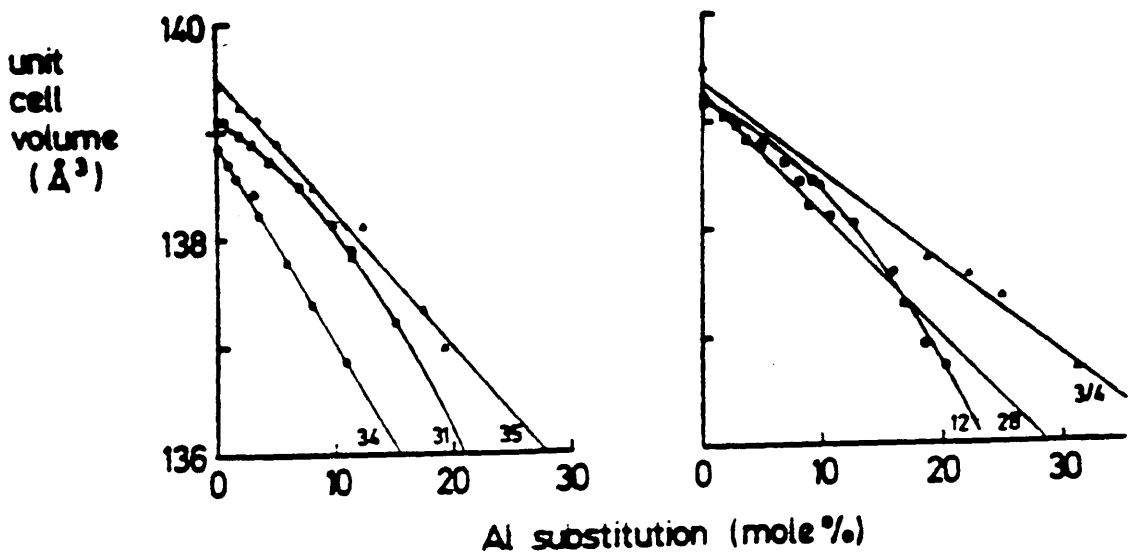


Figure 2.16: Relation between unit-cell volume and Al substitution for synthetic goethites. The goethites were prepared from ferrihydrite containing different amounts of Al in 0.3 M KOH at 70°C (series 28, 31, 34; Schulze, 1984); in 0.3 M KOH at 25°C (series 35; Schulze and Schwertmann, 1987) in 2 M KOH at 70°C (series 12; Schulze, 1984), and by oxidation of $\text{FeCl}_2\text{-AlCl}_3$ solutions at pH 6-7 and 25°C (series 3/4; Schulze, 1983). (after Schwertmann, 1987b).

CHAPTER 3

MATERIALS

3.1 INTRODUCTION

This chapter presents a preliminary description of the series of samples used in the investigation in order to provide a framework of reference for the main part of the work. Some of the experimental methods which were used in the initial preparation of the samples are outlined and the results of some of the preliminary classification tests on the samples presented. The earlier sections of the chapter summarise soil sampling, sample handling and storage and initial sample preparations prior to tests being conducted on the soils. The procedures used in separating the soil into the different fractions on the basis of mineralogy, colour and particle size are then presented. The preparation of the synthetic iron oxide particles which were used as controls for the experiments are outlined in the later sections.

3.2 ROCK AND SOIL

The rock and soil samples used for the investigation were supplied by the Geotechnical Control Office (GCO) in Hong Kong., soil sampling and some initial tests were also done by the staff of the GCO who also arranged transportation to Glasgow University, Scotland. A Special Project Report detailing the description of the site, geology and sampling procedures was supplied (Irfan, 1986), and extracts from the report are summarised in parts of the next sections.

3.2.1 Description of the Sampling Site

The samples were collected from recently excavated cut slopes in Shouson Hill, Hong Kong Island. The sampling site is situated on top of a hill (125m above Principal Datum, which is approximately at sea level) at the junction between Deep Water Bay Road and Shouson Hill Road West. Figure 3.1 shows a generalised solid geological map of Hong Kong Island. The location of the Shouson Hill site is marked on the figure. It could be seen from Figure 3.1 that, in general, Hong Kong Island is composed of granitic as well as volcanic rocks. Although the sample site indicated in the figure overlaps between the two types of rocks, the samples used in this investigation had been selected from the granitic rock area. The topography of the site at the time of block sampling is shown in Figure 3.2. As a result of recent road widening to provide easy access to a building site below the hill, the site has since been reduced in size by cutting into the hill both from the east and north. Cut slopes 10 to 20 metres high have now been formed on the eastern, northern and western sides of the hill (Irfan, 1986).

GCO's preliminary inspection of the sampling site indicated that there was horizontal as well as vertical variation in degree of decomposition and disintegration of the granite over the site (Irfan, 1986).

3.2.2 Engineering Geology of the Site

Detailed descriptions of the geology of Hong Kong can be found in Davis (1953) and Allen and Stephens (1971) amongst others. The site was composed of weathered granite. The rock in the area was mapped by Allen and Stephen (1971) as medium-grained facies of Hong Kong granite. The new Geological Survey of Hong Kong re-defined the granite on site as belonging to the fine-to medium-grained granite type, i.e. average grain size of 1 to 4mm. Individual grains as large as 8 to 10mm could be found, however (Irfan, 1986).

Chapter 3: Materials

In the fresh state the granite was grey coloured, equigranular and non-porphyritic. The main constituents of Hong Kong granite as given by Allen and Stephens (1971) are:

Quartz	23% to 42%
Potassium feldspar	31% to 42%
Plagioclases.....	16% to 35%
and Muscovite	unspecified

Davis (1953) also gave the composition of what he described as a typical Hong Kong granite (from Kowloon Peninsula) as:

Quartz	30.54%
Orthoclase (Potassium feldspar).....	30.02%
Albite (Sodium plagioclase).....	27.77%
Anorthite (Calcium plagioclase)	5.00%
Diopside	0.71%
Hypersthene	3.77%
Magnetite	0.70%
Ilmenite	0.46%
and Pyrite	0.20%

There is a close agreement in the broad mineralogy of the granite as given by both authors.

A fine grained granitic dyke (aplite) of varying width, 1 to 3m, cuts the granite in a NE - SW direction at the southern end of the site (see Plate 2 of Irfan, 1986). A number of quartz veins were present striking approximately

WNW – ESE. Two nearly vertical joint sets and gently dipping sheeting joints formed the three dominant discontinuity sets in the granite. Joint spacing is 0.5 to 1m for vertical sets and 0.2 to 0.6m for the subhorizontal set (Irfan, 1986).

3.2.3 Weathering and Alteration

A report on the weathering and alteration of the soils at the time of sampling was given in Irfan (1986) and is summarised below.

The granite on site was completely weathered to a considerable depth with a thin residual soil layer on top. A few corestones of less weathered granite, up to 1m in diameter, occurred mainly towards the top of the completely weathered zone. Although the rock was weathered to soil-like material and could be generally described as 'completely decomposed granite (CDG)' or 'grade V decomposed granite' according to the commonly used classification in Hong Kong (GCO, 1984; also see Table 3.1), variations in degree of weathering both in terms of chemical decomposition and physical disintegration, occurred vertically as well as laterally throughout the site. A general classification of the soils formed from the weathering of granite at Shouson Hill is given in Table 3.2. Figure 3.3 gives a sketch of one of the newly formed slopes illustrating the variability of weathering characteristics found on the site. In addition, the granite was hydrothermally altered (kaolinised) mainly around the quartz veins (see Plate 4 of Irfan, 1986). The degree of chemical alteration was intense in these hydrothermally altered areas, with all the feldspars altered to kaolin pseudomorphs, and the granitic soil in these locations is clayey silt with some sand (Irfan, 1986). The intensity of alteration decreased away from the quartz veins. It is considered that hydrothermal alteration, i.e. alteration of rock as a result of breakdown by heated water, played a significant role in the chemical altering of the granite during the late stages of intrusive activity. Weathering effects under a hot and humid sub-tropical climate were then superimposed at a

later time when the rock was exposed to atmospheric agents (Irfan, 1986).

The degree of weathering away from the hydrothermally weathered zones was not as intense, although the plagioclase feldspars were weathered to gritty- to- soft grains. The potash feldspars were generally less decomposed but highly fractured. Within this general matrix of chemically decomposed granite, there were "corestones" and/or areas where feldspars showed very little decomposition but the rock was weathered to the condition of friable granitic soil (gravelly sand) as a result of mechanical disintegration.

The transition from completely weathered granite to residual soil was gradual (see Figure 3.3). Nearer to the ground surface the original granitic fabric was completely destroyed and soil was somewhat compact due to collapse (see Irfan's Plate 5). The intensity of decomposition of feldspar increased upwards in the weathering sequence, with a related increase in the silt-clay content of the soil. The final product was a clayey-silty sand. No feldspars were recognisable near the surface.

The sub-horizontal sheeting joints near the surface contained dark yellowish-brown clayey-silt infills presumably washed in by infiltrating surface water and/or formed as a result of more intense weathering along joints.

3.2.4 Soil Sampling

Soil sampling was done by the staff of the Geotechnical Control Office (GCO) in Hong Kong based on the specifications supplied by us at Glasgow University, to provide undisturbed samples at various degree of weathering from fresh rock to the most weathered soil.

Undisturbed block samples of weathered soil measuring 450 x 450 x 300 mm were taken at various depths from trial pits excavated on top of the hill. Fresh (unweathered) rock fragments were broken from corestones. The field description of the samples were made by the sampling team and these are

summarised in Table 3.3. The weathered soil samples were trimmed with a knife, covered with aluminium foil and wax, to prevent drying out, and placed in a pre-fabricated wooden box before being carefully transported to the GCO's Public Works Central Laboratory at North Point in Hong Kong. Sub-samples were obtained from the main samples, with minimum disturbance, for direct shear tests, sieve analysis, atterberg limits and other preliminary tests. Undisturbed sub-samples were covered with aluminium foil and wax, wrapped in air-bubble polyethylene sheets, placed in well padded cardboard boxes and sealed for shipping to Glasgow University.

3.2.5 Sample Handling and Storage

On arrival at Glasgow University each package was examined carefully for signs that may indicate whether the package had been roughly handled while in transit. Each package was found to have notes posted on them advising the customs officials of the contents of the package and on the need for careful handling of the sample and avoidance of scanning with rays that may be detrimental to the integrity of the samples. Warning that the aluminium foil may trigger off metal detectors were also given. A copy of the same note was also found in each package. The packages were carefully opened, and notes made of the observations on packaging and conditions and size of each sample. The samples were checked against the field descriptions that were made earlier and additional descriptions of the state of the sample on arrival in the laboratory at Glasgow University, size, colour and other features of interest were made and these will be discussed later. Photographs of features of interest were obtained, and sub-sampling done as necessary. The remaining samples were covered with aluminium foil and wax, wrapped in polythene and stored in a refrigerator set at 9°C.

3.2.6 Sample Numbers, Field and Laboratory Description of Samples

All the samples from the present site have been numbered with a common prefix of 404 to differentiate them from other soils from other sites that are being investigated within the Glasgow University, Fundamental Geotechnical Engineering Research Group. This prefix is then followed by a number which identifies the particular sample from other samples from the same site. The number normally begins from 01 for the deepest soil and progresses upwards to the shallowest soil. In the present case the samples have sample numbers beginning from 404.01 for a fresh rock sample to 404.08 for the residual soil (i.e. 8 samples in all). Duplicate samples, where available, were numbered from 11 after the main samples, e.g. 404.11 for the duplicate sample of 404.01 and 404.12 for the duplicate of 404.02 etc.

Table 3.3 gives the decomposition grade, location and field descriptions of the samples. The decomposition grades used are according to the GCO classification and described in Table 3.1. The description of block samples was carried out in standard engineering geological terms based on the scheme proposed by the Geological Society Working Committee (1972) and adopted in BS 5930 (BSI, 1981). In turn, Table 3.4 explains the terms on which the description of the degree of weathering of the rock materials are based and Table 3.5 defines the simple manual index tests used to determine the degree of chemical alteration of feldspar.

The laboratory descriptions made in Glasgow are summarised below and expressed in tabular form in Table 3.6. The identification of the minerals were based on petrographic investigations done both in Hong Kong and at Glasgow. Most of the photographs shown were taken using a single oblique flash-gun. Each side of each small square of the scale mark represents 2mm.

Sample 404.01 is fresh rock obtained from a corestone from a deeper section of the site. A photograph of a typical section of the sample is shown in

Plate 3.1. The granite could be seen to be non-porphyritic with equigranular texture. The light pink (K-feldspar) and white (plagioclase), transparent or dulled (quartz) and black (biotite) grains could be distinguished easily. The white patch (labelled A) was very rare. It was composed of powdery material (probably kaolin) and appears to signify the weathering of some of the original granite components to a clay pseudomorph.

Sample 404.02 is another rock sample taken from a corestone in a completely weathered zone and the texture of the grains bear a close resemblance to those described for the fresher rock (sample 404.01). The feldspars in this case, however, showed a slight decomposition signifying a slightly more advanced stage of weathering compared to Sample 404.01. In addition, the sample had an outer shell (3 to 15mm depth) which formed an iron stained rim around a fresher inner core. A photograph of the sample is shown in Plate 3.2 and both the fresh inner core and outer iron-stained shell (e.g top left of photograph) described for the sample could be distinguished in the photograph. Plate 3.3 shows a photograph of a section through the sample revealing the two distinct zones of stained (top part of sample) and unstained rock. The iron staining may have been from iron released from the minerals (e.g biotite) within the granite itself ("self-staining") or from an external source.

Sample 404.03 was similar to sample 404.02 in most respects as far as decomposition of the primary minerals was concerned. A characteristic of the sample, however, was the staining of iron oxide (reddish brown) around the fresh biotite grains, which tended to give the indication that the staining in this case was from iron oxide formed from the iron released from the biotite particles within the sample. Plate 3.4 shows a photograph of the sample. A coating of yellowish-brown dust, different from the iron oxide staining in sample 404.02), on the outer part of the rock could be seen in the photograph. It was possible to brush-off the dust coating in this case, and seems more likely to be from an

external source.

Sample 404.04 was slightly more weathered than Samples 404.01 to 404.03. In this case the plagioclase feldspars showed more decomposition, although the K-feldspars were still generally fresh indicating that the plagioclase feldspars weathered faster than the K-feldspars. The black biotite had also lost some of its lustre. The rock at this stage had become weak and characterised by microfractures within the rock mass. Plate 3.5 shows part of the sample and the presence of microfracture is evident on the photograph. A yellowish-brown colouring of the rock was also apparent. The dull colour of the biotite particles also contrasted with those of the biotite particles of the Sample 404.01 shown in Plate 3.1. A close examination of the microfractures in the sample itself showed them not to strictly follow the boundaries of the mineral grains as they could be seen sometimes to pass through individual minerals of feldspar, biotite and quartz.

Sample 404.05 was the first soil in the series. At this stage, the rock had become extremely weak, fractured and fragile, and the fine particle content (discussed later under particle size analysis) had increased as a result of increased weathering of the primary minerals. The K-feldspars showed more decomposition than in the previous sample, but were still less altered than the plagioclase which now showed a moderate to high degree of decomposition. The photograph (same scale as in Plate 3.7) of the sample (Plate 3.6) showed a yellowish-brown staining (perhaps of iron oxide) of most of the soil particles. Very occasional red coloured mottles like that surrounding the biotite particle in the middle of the particle shown could be seen. These mottles were often found surrounding the biotite particles thus giving an indication of having been formed from iron released from the biotite. Some white, powdery materials (e.g below the red mottle in the photograph) were also sometimes seen and could be kaolin that has not been stained by iron oxide.

Sample 404.06 showed a more intense chemical decomposition of the

Chapter 3: Materials

primary minerals than 404.05, and the plagioclase feldspars showed extreme decomposition although the K-feldspars were still less weathered. The quartz grains also showed some loss of lustre. Apart from a general yellowish-brown colouring of most of the soil, larger and more wide-spread patches of red mottles than was the case with Sample 404.05 could be seen. As was the case with Sample 404.05 most of the red mottles were found surrounding the biotite grains and gave the indication of having been formed from iron released from the biotite. The photograph of a fragment of the sample is shown on Plate 3.7 and shows red coloured mottle around a biotite grain. White patches of powdery, unstained material (perhaps kaolin) could also be seen on the photograph.

Laboratory examination of Sample 404.07 showed the primary minerals to be more intensely weathered than the previous samples. The sample was more homogeneous, than the previous soils, and friable. The colour was mainly strong yellowish-brown with patches of black derived from decomposed biotite. The granitic fabric was almost lost, and the grain boundaries were no longer distinct. Most of the plagioclases were soft to powdery, K-feldspars were gritty and quartz grains were prominent. The photograph of a typical section of the sample (Plate 3.8) showed black patches of decomposed biotite, and the main yellowish-brown stained area of soil. Small particles of white feldspars (most <2mm across) could also be seen on the photograph. One crumb of the soil showing atypical patch of red-stained particles (see Plate 3.9) was also seen.

Sample 404.08 was residual soil. The granitic fabric was totally lost leaving a uniform, strong yellowish-brown to strong orange-brown coloured soil. Plate 3.10 shows a photograph of the sample. The soil could be seen to be composed of dulled quartz grains (\approx 30%), some as large as 8mm, in a silty matrix. Plant roots, similar to those seen in the photograph, were also common. Occasional, tiny, root holes could be seen in the sample. Although the soil was the most highly weathered in the series, it was also the most firm. It is thought

that the firmness of the soil may have been occasioned by collapse and possibly by the presence of a higher clay content which helped to bind the soil particles together.

3.4 INITIAL SAMPLE PREPARATIONS

3.4.1 Rock Samples

Typical areas of rock samples were sectioned and identical pieces obtained for impregnation (for subsequent thin sectioning), grinding for the various mineralogical analysis, scanning electron microscopy, etc. Some atypical areas were treated in the same manner. Powder or dust on the rock samples where available was carefully brushed off and stored in separate sample bottles for relevant testing.

3.4.2 Soil Samples

Generally, soil samples were required in either the disturbed or undisturbed states. Undisturbed lumps were obtained from required areas for impregnation and subsequent thin sectioning for polarised light microscopy and for making polished sections for scanning electron microscopy. Sub-samples for disturbed soil testing were obtained from typical areas of the samples, lightly crushed between the fingers and passed through a riffle box. Successive riffling of the sub-sample was done to obtain representative samples for all the tests that were to be carried out. Sub-samples were stored in the refrigerator when not immediately used. Where possible, sub-samples were obtained from the main samples on the basis of mineralogy, colour and particle size and the procedures used in achieving these are given below.

(a) Separation on Basis of Mineralogy

For investigation of some of the intact (unweathered or weathered but recognisable) primary minerals of the soil such as feldspars, micas, quartz, etc., the minerals were hand-picked and kept in separate, labelled sample bottles and stored in a refrigerator until needed.

(b) Separation on Basis of Colour

In soils where distinct colouring of some of the weathered minerals occurred in the form of patches, mottles or concretions, such as the red and yellow coloured mottles of iron oxide minerals, samples were obtained from these areas using clean spatulas and tested immediately.

Because the mottles were diffuse, it was not always possible to obtain absolutely pure samples in—as far as colour of samples was concerned and the colours of the samples stated refer only to the main colour of most of the particles.

(c) Separation on Basis of Particle Size

Samples were separated on the basis of particle size in order to obtain the mineralogical distribution in the different size fractions of the sample and for concentration of the iron oxide minerals in certain fractions of the soil. About 10g of the soil was mixed with 50ml of distilled water and crushed lightly with a rubber pestle and mortar. The soil/water mixture was then sieved through a 63 μ m sieve. The pH of the soil solution passing the 63 μ m sieve was adjusted to \approx 9.5 using sodium hydroxide, and the soil ultrasonically dispersed for about 10 minutes. Sedimentation was carried out in a standard 1000ml cylinder with the soil solution constantly maintained at a pH of \approx 9.5. For the fraction <2 μ m the soil solution in suspension above the upper 5ml mark was decanted (using a

pipette) after 8 hours. This was done repeatedly on different batches of soil until sufficient sample was obtained for the required tests. For the fraction $<20\mu\text{m}$ the soil solution in suspension was decanted after 2 hours and sufficient sample obtained by repeated sedimentation of different batches of soils. The pH of the decanted soil solution was neutralised to ≈ 7.0 using hydrochloric acid and the clay fraction recovered by centrifuging at 4000 rpm for 15 minutes, air-dried, crushed lightly and stored in sample bottles.

3.5 PARTICLE SIZE ANALYSIS AND SOIL MICROFABRIC

Particle size and plasticity characteristics have been used to classify engineering soils, e.g. British Soil Classification System (see BS 5930: 1981), Unified Soil Classification System and AASHTO system. This is particularly true of transported soils. The relationships which have been successfully developed for transported soils relating the results of soil classification tests and various engineering properties (e.g. Terzaghi, 1958), seem not to hold for tropical residual soils (Mitchell and Sitar, 1982). This partly stems from the difficulty of determining the exact grain size of engineering soils formed from the weathering of rocks under mainly tropical conditions. Particle size distribution of such soils is sensitive to the procedures used, e.g. use of pestle and mortar to crush the soil, type of dispersing agent, amount of agitation, oven drying, etc. Another factor to be considered is that besides the variations within very short distances related to micro-environment of weathering, variations in grain size also result from variability in the initial mineral size and composition of the the original rock. Lumb (1962) reported that considerable variation in grading and void ratio of the decomposed granite can occur in small volumes of soil, and this variations seemed haphazard and quite unpredictable even within a single trial pit of borehole.

Various procedures have been recommended for the preparation of tropical and sub-tropical residual soils for particle size analysis (a brief review of some of the proposed methods was given by Irfan, 1986). While some of the methods proposed have discouraged the use of pestle and mortar for crushing the soil prior to particle size analysis, others have argued that the variability of the grain size due to non-use of pestle and mortar is insignificant. Oven drying may change the composition of clay minerals in lateritic soils (Mitchell and Sitar, 1982), and Irfan (1986) also reported experiences with less weathered soils typically present in Hong Kong. According to him, samples which were oven dried before treatment gave lower clay and silt contents when compared with air-dried samples. The current practice at the Public Works Central Laboratory (PWCL) of the Geotechnical Control Office in Hong Kong for particle size determination involves oven drying at 110°C on occasion followed by breaking down using a porcelain pestle and mortar. The soil is then dispersed using sodium hexametaphosphate (Irfan, 1986).

For the benefit of comparison between results of particle size analysis performed on samples from the same site by the GCO, the samples were treated in a similar way to those used by the PWCL. The samples were dried, overnight, in an oven at 110°C, then crushed under distilled water using a porcelain pestle and mortar. The soil was then dispersed using sodium hexametaphosphate before sieve analysis and hydrometer tests were performed. Both sieve analysis and sedimentation, by hydrometer test, were done in accordance with the provisions of BS 1377 of 1975. Due to the small amount of samples available only one determination of particle size was done for each soil. This reason, combined with the low silt and clay content of samples 404.05 and 404.06, made it impracticable to perform hydrometer tests on these samples.

The summary of particle size distribution (psd) results is given in Table 3.7, and the associated grading curves are given in Figure 3.4. Table 3.8 gives

the summary of psd results obtained by Irfan (1986) for samples from the same site. From Table 3.7, the combined silt and clay contents could be seen to increase from Sample 404.05 to 404.08 signifying the direction of increase in weathering of the primary granite minerals as observed by visual examination (Section 3.2.6). Although it was not possible to determine the separate silt and clay contents for Samples 404.05 and 404.06, due to sample shortage, a comparison of the values obtained for samples 404.07 and 404.08 showed that the content of the clay size fragment had increased from about 9% in Sample 404.07 to about 18% in the Sample 404.08. Also, almost all the clay in Sample 404.08 (17% of the 18% total clay content of the soil) was found to have particle size smaller than $0.25\mu\text{m}$. Suspension of the dispersed silt and clay fractions of the other soils also showed particles that remained in suspension for upward of 3 days, signifying the presence of clays of very small particle size in all the soil samples. Results of infrared analysis, reported in Chapter 7, also showed the kaolinite particles in the soils to be of very small particle size.

The microfabrics of the soils were investigated by scanning electron microscopy (SEM). The procedures for SEM are discussed in Chapter 5, under electron microscopy, and additional SEM micrographs are shown in the Chapter. Figure 3.5 shows a representative SEM micrograph of fractured surfaces from Samples 404.05 and 404.06. The micrographs were dominated by fibrous particles (which were identified to be halloysite tubes by transmission electron microscopy) which appeared to be growing out from a primary mineral (probably a feldspar). As discussed later in Section 5.10.1, both silt and clay size tubes could be seen (see also Figure 5.10). An examination of the soil sections also indicated a high void ratio signified by a generally porous structure of the soils. Three main types of voids could be identified and included:

(1) Etch-pits in the feldspar grains. These were few, perhaps due to the

advanced weathering stage of some of the feldspars.

(2) Voids with rounded edges similar to those seen in Figure 5.10. These were fairly common, and could be seen to go through the piles of halloysite tubes with some having diameters of up to $5\mu\text{m}$. The dark centre of the holes gives the impression of good depth, and the rounded edges appeared to indicate formation by infiltrating fluid. Although these may have been formed *insitu*, there is also the possibility that some of them were formed during sample preparation by critical point drying. In any case, the presence of the voids is an indication that the halloysite particles were loosely packed in large, deep voids within the soil fabric.

(3) 'Channels' or 'troughs' between ridges of remnant feldspars from which halloysite particles were growing out (see Figure 3.5). In optical microscopy of thin sections, these were seen as clay-filled channels and were the most common of the voids.

As weathering progressed, the mineralogy of the soils changed slightly (as discussed in Section 5.10.1) and a more compact structure of the soil was indicated (e.g see Figure 5.14 for SEM of Sample 404.08). It is possible that the small size of some of the clay particles in the soils contributed to their ease of being leached out of the soil, leading to an increase in void ratio and subsequent collapse of the soil fabric. Irfan (1986) had stated, for the Shouson Hill soils, that "...the low clay contents may have resulted either from leaching out of fine clay minerals and colloids as they are formed during the course of weathering, or from extensive etch-pit solution of feldspars without forming clay minerals. Those samples are hence likely to show metastable behaviour (collapse) and densification, during deformation under load, due to their high void ratios

and clay deficient microfabrics". The findings of the present study supports this statement.

3.6 SYNTHETIC IRON OXIDES

Experiments on synthetic iron oxide particles were used as controls for the main experiments on the soil samples. Ferrihydrite, goethite and hematite being the most common forms of iron oxides present in soils were used as controls pending the outcome of initial tests on the soils. Further tests on the soils did not reveal the presence of other forms of iron oxide which may necessitate using their synthetic forms as control. The procedures used in the preparation of the synthetic forms are outlined below. Analar quality reagents were used.

3.6.1 Ferrihydrite

Six-line ferrihydrite was prepared by the method of Eggleton and Fitzpatrick (1988). 5 g of $\text{Fe}(\text{NO}_3)_3 \cdot 9\text{H}_2\text{O}$ was dissolved in 500ml of deionised H_2O at 75°C with vigorous stirring and left for 13 minutes before rapid cooling in ice water. The solution was dialysed for 3 weeks with daily replacement of deionised water. The precipitate was then centrifuge-washed three times with deionised water before being dried with acetone and ether. Some properties of similarly prepared six-line ferrihydrite were given by Eggleton and Fitzpatrick (1988).

3.6.2 Goethite

The synthetic goethite used in the studies was kindly supplied by Mr. E. Paterson of the Macaulay Land Use Research Institute (MLURI), Aberdeen. Preparation of the goethite was done using the method described by Atkinson et al. (1968). A partially neutralised, aqueous solution of iron (III) nitrate was aged

at room temperature for 50 hours, then adjusted to pH 11.5 with aqueous sodium hydroxide (NaOH) solution. The resulting suspension was then maintained at 60°C for 5 days in order to promote crystal growth. Some properties of similarly prepared goethites were given by Atkinson et al. (1968) and by Paterson and Swaffield (1980).

3.6.3 Hematite

The synthetic hematite used was provided by Blythe Colours of Stoke-on-Trent, England and has been named ALH 27 by the company. The hematite was prepared from a mixture of FeSO_4 and Na_2CO_3 . The product was precipitated and oxidised in air at 17°C and pH 7.4 and then fired at 400°C for 40 minutes.

3.7 SUMMARY

The following summarise some of the findings of the study presented in this chapter:

- (1) The clay contents of the weathered granite and residual soil were generally low with the maximum clay content of 18% indicated for the most weathered, residual soil.
- (2) As expected, the combined silt and clay contents of the soils increased from the least weathered soil to the most weathered soil.
- (3) An indication of a very small particle size ($<0.25\mu\text{m}$) of some of the clay particles in the less weathered soils and most of the clay particles in the most weathered

soil was given by particle size analysis. . .

- (4) Scanning electron microscopy indicated a porous structure for the less weathered soils. The structure became more compact as weathering progressed.

- (5) It is possible that the small size of some of the clay particles contributed to their ease of being leached out of the soil, leading to an increase in void ratio and subsequent collapse and densification of the soil fabric.

Table 3.1: Classification of Rock Material Decomposition Grades (after GCO, 1988)

Descriptive Term	Grade Symbol	General Characteristics for Granitic & Volcanic Rocks & Other Rocks of Equivalent Strength in the Fresh State	Additional Typical Characteristics for Specific Rock Types			
			Granite	Granodiorite	Coarse Ash Crystal/Lithic Tuff	
Residual Soil	VI	Original rock texture completely destroyed. Can be crumbled by hand and finger pressure into constituent grains.	Reddish brown. Feldspars completely destroyed. Quartz is only remaining primary mineral; usually dull, etched or pitted and reduced in size compared with fresh condition.	Dark reddish brown. Feldspars completely destroyed. Quartz only remaining primary mineral; grains reduced in size compared with fresh condition.	Brown or reddish brown. Quartz only remaining primary mineral.	Fine Ash Vitric Tuff Yellowish brown
Completely Decomposed	V	Original rock texture preserved. Can be crumbled by hand and finger pressure into constituent grains. Easily indented by point of geological pick. Slakes when immersed in water. Completely discoloured compared with fresh rock.	Yellowish brown to reddish brown. Feldspars powder to soft. Hand penetrometer shear strength index < 250 kPa. Zero rebound from N Schmidt hammer.	Yellowish brown to reddish brown. Plagioclase feldspars powder to soft, very easily grooved by pin. Orthoclase feldspars gritty, less easily grooved. Zero rebound from N Schmidt hammer.	Brown to reddish brown. Slakes slowly in water. Mafic minerals soft, dull, dark green to brown, difficult to distinguish.	Yellowish brown. Slakes readily in water.
Highly Decomposed	IV	Can be broken by hand into smaller pieces. Makes a dull sound when struck by geological hammer. Not easily indented by point of geological pick. Does not slake when immersed in water. Completely discoloured compared with fresh rock.	Yellowish brown to yellowish orange/brown. Feldspars powder. Hand penetrometer shear strength index 30-50. N Schmidt rebound value < 25.	Yellowish brown to yellowish orange/brown. Plagioclase feldspars powder to gritty. N Schmidt rebound value 15-30.	Yellowish brown. Mafic minerals soft, dull, dark green.	Yellowish grey. Surface can be scratched by knife.
Moderately Decomposed	III	Cannot usually be broken by hand, easily broken by geological hammer. Makes a dull or slight ringing sound when struck by geological hammer. Completely stained throughout.	Yellowish brown. Feldspars gritty. Biotite not shiny. N Schmidt rebound value 25-45.	Yellowish brown. Plagioclase feldspars partly decomposed to gritty small pieces. N Schmidt rebound value 25-50.	Yellowish grey. Mafic minerals generally not shiny, soft, black or stained dark brown.	White or light grey. Surface cannot be scratched by knife.
Slightly Decomposed	II	Not broken easily by geological hammer. Makes a ringing sound when struck by geological hammer. Fresh rock colours generally retained but stained near joint surfaces.	Feldspars hard to slightly gritty. Orthoclase feldspars often pink. Biotite slightly stained and dull around edges. N Schmidt rebound value > 45.	Plagioclase feldspars slightly gritty. Biotite and hornblende slightly stained and dull. N Schmidt rebound value 45-70.	Light grey or greenish grey. Mafic minerals shiny, hard, black, may be slightly stained and dull around edges.	Grey, light grey or greenish grey. Cloudy appearance.
Fresh	I	Not broken easily by geological hammer. Makes a ringing sound when struck by geological hammer. No visible signs of decomposition (i.e. no discolouration).	Overall rock colour grey/white. Feldspars hard and shiny. Biotite shiny, not stained. Quartz colourless or grey, glassy.	Overall rock colour grey. Feldspars hard and shiny. Biotite and hornblende shiny, not stained. Quartz colourless or grey, glassy. N Schmidt rebound value > 60.	Overall rock colour ranges from light greenish grey (JSM) to grey (JSM, JYT). Feldspars hard and shiny. Mafic minerals shiny, hard, black. Quartz colourless or grey, glassy.	Overall rock colour black. Glassy appearance.
General Notes		(1) Not all these general characteristics are applicable to rocks whose strength in the fresh state is moderately strong or less (see Table 2). Alternative classifications may be more appropriate for such materials (see Section 2.3.4). (2) Use of geological hammer applicable mainly to materials confined in a field exposure.	(3) Based on Moye (1955), Hatcher & Martin (1982) and unpublished work by the GCO. (4) Assessments of minerals applicable to medium and coarse-grained granite, may be difficult or impossible to assess in fine-grained granites.	(5) Based on Irton & Powell (1985a,b).	(6) Based on unpublished work by the GCO. (7) JYT: Yim Tin Tsai Formation (see HKGS maps and memoirs). (8) Mafic minerals referred to are biotite and hornblende.	(9) Based on unpublished work by the GCO.
Notes on Index Tests		(10) Slake test: samples already close to saturation moisture content are less likely to slake. (11) Feldspar alteration test: Hard: cannot be cut by knife or grooved by pin; Gritty: can be cut by knife or grooved by pin, can be moulded very easily to clay in fingers. (12) N Schmidt hammer test: rebound values are for hammer held perpendicular to rock face take initial 'sealing' blows to ensure good contact and record average value from a minimum of five consecutive impacts, ignoring unusually low readings. (13) Hand penetrometer test: press instrument head slowly and smoothly into sample, take an average of ten values and divide by two to give shear strength index, test may be impractical on very small samples. (14) Test results in general may be affected by sample moisture content and degree of microfracturing.				

Table 3.2: Classification of Engineering Soils Formed From Weathering of Granite at Shouson Hill (after Irfan, 1986).

Material Type	Material Weathering Grade (UCC, 1984)	Degree of Decomposition/ Disintegration (*)	State of Decomposition/Disintegration of Major Mineral Constituents			Original Rock Fabric	Colour	Grain Size of Soil	Other Properties
			Feldspars (**)	Quartz	Micas				
1. Residual Granitic Soil	VI	Extreme decomposition	Extremely to completely decomposed; feldspar pseudomorphs unrecognisable	Reduced in size; loss of lustre	Biotite is completely decomposed to colourless hydrous mica	Not present	Light yellowish grey to reddish brown (leached)	Clayey silty sand	Slakes readily
2. Transition Granitic Soil	V/VI	Extreme to high decomposition	Extremely decomposed to powdery-to-soft grains	Fractured; some loss of lustre	Biotite is extremely decomposed to yellowish grey flakes	Partly lost	Light yellowish grey to reddish brown (leached)	Clayey silty sand to silty gravelly sand	Slakes readily
3. Decomposed Granitic Soil	V	High to extreme decomposition; complete disintegration	Highly to extremely decomposed to gritty-to-soft grains	Fractured; slight loss of lustre	Biotite is highly decomposed to yellowish grey flakes	Present	Light yellowish grey (May be leached)	Silty gravelly sand with little clay	Slakes readily
4. Altered Granitic Soil	V	Extreme to complete alteration	Extremely to completely decomposed (altered) to soft clayey kaolinitic pseudomorphs	Greatly reduced in size and amount due to solution	Biotite is completely altered to muscovite & chlorite(?)	Changed	Mottled light pink and creamy white	Clayey sandy silt	Slakes after agitation
5. Disintegrated Granitic Soil	V	Complete disintegration, slight to moderate decomposition	Slightly to highly decomposed to hard to powdery grains	Fractured; slight loss of lustre	Biotite is slightly to moderately decomposed to greenish black - yellowish green flakes	Present	Light yellowish grey	Sandy gravel to gravelly sand	Slakes readily
6. Highly Decomposed Granite	IV	Moderate to high decomposition; partial disintegration	Slightly to moderately decomposed to hard-to-gritty grains	Slight loss of lustre	Biotite is slightly decomposed to greenish yellowish brown staining around grains	Present	Yellowish grey	Gravelly sand to sandy gravel	Slakes very little very weak rock - dense soil; a series of very closely spaced macrocracks may be present
Fresh Granite	I	None	Plagioclase and potash feldspars are hard and sound	Lustrous; high quartz content (35-40%)	Biotite is black, no muscovite	Equigranular; granitic	Light pinkish grey to light grey	Medium-to coarse-grained (1 to 4 mm)	

Table 3.3 . Weathered Granite Samples from Shouson Hill, Hong Kong Island

Description of Weathered Granite Samples Collected from Shouson Hill
for Mineralogical and Chemical Analysis by Dr. P. Smart of Glasgow University.

All samples were collected from recently excavated cut slopes.

Sample No.	Decomposition Grade	Location (see Map)	Description of Hand Specimen
404.08	VI (type 1 - see report)	Top of hill, just below ground surface. (Residual soil is 1-2 m thick on the hill top).	Yellowish brown. No granitic fabric left quartz grains (~30%) in a silty matrix. Contains roots and voids.
404.07	V (type 5 - see report)	Sample taken from the crest of 4 m high road cutting in completely weathered granite zone; adjacent to a grade III/IV corestone.	No hand specimen available for description.
404.06	V (type 4 - see report)	Sample taken from 2.5 m below crest of 4 m high road cutting, adjacent to a quartz-kaolin vein.	Chemical decomposition is intenser than sample No. 5. K-feldspars are gritty, some hard. Most plagioclases are soft to powdery. Quartz show some loss of lustre.
404.05	V (type 3 - see report)	Sample taken from 2 m below crest of 4 m high road cutting in completely weathered granite.	Extremely weak, yellowish grey, normally weathered grade V granite (as opposed to altered grade V granite - sample No. 6). Plagioclases are gritty to powdery (i.e. moderate to high degree of decomposition - see attached report, Table 3). K-feldspars are hard to slightly gritty (i.e. fresh to slightly decomposed) but microfractured. Biotite is softened, black to greenish black to silvery grey.

cont.

Table 3.3 contd.

Sample No.	Decomposition Grade	Location (see Map)	Description of Hand Specimen
404.04	IV (Stronger end-type 6 see report) (Weaker grade IV not collected)	Sample taken from a 0.4 m diameter boulder (corestone) excavated from the new slope, in completely weathered zone.	Weak to very weak; completely discoloured (yellowish brown), microfractured throughout. Some plagioclases are hard, some gritty, occasionally powdery (i.e. slight to moderate decomposition). K-feldspar generally fresh or very slightly decomposed but fractured. Biotite is still black but has lost some its lustre. The rock is chemically little altered but physically disintegrated.
404.14	IV	Second portion of original Sample No. 4, see above.	
404.03	III	Sample taken from a 0.5 m diameter boulder (corestone) excavated from the new slope in completely weathered zone.	Moderately strong, completely discoloured, light yellowish grey in colour. Plagioclases are generally hard, but occasional grains are slightly gritty (slight decomposition). K-feldspars are very hard (fresh), some are microfractured. Biotite is still shiny black but with reddish brown staining around grains. Grain boundaries have tendency to open up.
404.13	III	Second portion of original Sample No. 3, see above.	
404.02	II	Sample taken from a grade II corestone, approx. 0.5 m in diameter, in completely weathered zone.	Yellowish brown stained rim (5 to 25 mm wide) fresher core. Greenish grey to milky grey plagioclase feldspars in the fresher core indicate slight decomposition. In the iron oxide stained rim some plagioclases are gritty to hard. K-feldspars are fresh.

cont.

Chapter 3: Materials

Table 3.3 contd.

Sample No.	Decomposition Grade	Location (see Map)	Description of Hand Specimen
404.01	I	Approx. 20 m below crest of cut slope from a 4 m diameter grade I/II corestone in moderately weathered Granite zone.	Very strong, light pinkish grey, fresh, medium-grained (2 to 6 mm) GRANITE. Equigranular texture but with occasional feldspars up to 10 mm in diameter Biotite < 5%.
404.11	I	Second portion of original Sample No. 1, see above.	

Retyped from the original signed by Dr.T.Y.Irfan, 27.11.87, with the following changes: re-ordered; series number 404 prefixed to sample numbers; samples 1, 3, and 4, subdivided.

The report referred to is: T.Y.Irfan. (1986). Description and classification of granitic soils from Shouson Hill. Special Project Report SPR 4/86. Geotechnical Control Office, Civil Engineering Services Department, Hong Kong.

Table 3.4 Terms for the Description of the Degree of Weathering of Rock Material (based on IAEG*, 1981)

Term	Degree of Change (Per cent)
Fresh	0
Slightly	Over 0 - 10
Moderately	10 - 35
Highly	35 - 75
Extremely	Over 75
Completely	100

* International Association for Engineering Geology

Table 3.5 Simple Manual Index Tests to Determine the Degree of Chemical Alteration (Weathering and Hydrothermal Alteration) of Feldspar (after Irfan, 1986)

Scale	Term	Degree of Alteration	Field Recognition
1	Hard	Fresh to Slightly	Cannot be cut by knife; cannot be grooved with a pin
2	Gritty	Moderately	Can be cut by knife or grooved with a pin under heavy pressure
3	Powdery	Highly to Extremely	Can be crushed to silt size fragments by finger pressure
4	Soft	Completely	Can be moulded very easily with finger pressure, to clay size fragments

Table 3.6 Summary of the Laboratory Description of Samples.

Sample No.	Decomposition Grade	Sample Description
404.08	VI (type 1 - see report)	Total sample size was 203 x 178 x 102 mm. Intact lump with small cracks. Homogeneous, firm, but somewhat friable (not stiff) with roots and tiny root holes. Structure of soil appeared to be massive and no large voids were noticed. Sub-angular, dulled, quartz grains ($\pm 30\%$) in a matrix of fine material. Quartz size ranged between 2 to 5 mm. Colour was uniform: Munsell* 10 YR 8/6 (Light yellowish orange).
404.07	V (type 5 - see report)	Total sample size was 190 x 140 x 70 mm. Weathered GRANITE composed mainly of highly weathered feldspars, decomposed biotite and quartz. Granitic fabric almost lost and grain boundaries no longer distinct. Homogeneous, and friable. Very fine roots (rare). No large voids were noticed, but generally voids were larger than in sample 404.08. Grain size of largest particle was about 3 mm. Most quartz grains were dulled but occasional transparent particles could be seen. Colour was mottled: Mainly Munsell 10 YR 6/6 (Strong yellowish-brown) with patches of 7.5 YR 1/1 (Black) from decomposed biotite.
404.06	V (type 4 - see report)	Total sample size was 230 x 170 x 60 mm. Weathered GRANITE composed mainly of weathered feldspars, biotite and dulled quartz grains. Very friable with traces of very fine roots. Because the sample was badly broken on arrival it was difficult to estimate the size and distribution of the voids, but generally voids appeared to be larger and

Sample No.	Decomposition	Sample Description
404.05	V (type 3 - see report)	<p>more wide-spread than in samples 404.07 and 404.08. Red patches were common and occurred mainly around black grains of biotite.</p> <p>Colour: Fine particles stained mainly Munsell 2.5 Y 8/8 (Yellow). Red patches: From 7.5 R 7/8 (Bright red) to 7.5 R 5/8 (Red).</p> <p>Total sample size was 150 x 100 x 60 mm. Sample already broken into lumps on arrival. Weathered GRANITE composed mainly of weathered feldspars, relatively fresh biotite, and quartz (some dulled and some transparent) Highly friable, no roots found. Voids were similar in size and distribution to those in sample 404.06.</p> <p>Main staining of yellow and patches of unstained, white clay. Occasional red mottles around some of the biotite grains.</p> <p>Colour: Mainly Munsell 2.5 Y 8/8 (Yellow). Unstained area ($\pm 3\%$) 2.5 Y 8/0 (Gray white). Red mottles ($< 0.5\%$) 7.5R 7/8 to 7.5 R 5/8</p>
404.04	IV (Stronger end - type 6 - see report)	<p>Sample size was 190 x 90 x 90 mm. Slightly weathered GRANITE. Weak to very weak with fractures. Fractured surfaces composed of dulled quartz grains (up to 10 mm), black grains of biotite (up to 5 mm) and some white powdery patches, perhaps kaolinite, (up to 2 mm). Surface stained with patches of Munsell 7.5 YR 8/4 (Light orange) and 2.5 YR 6/6 (Strong orange). Some darker stained grains, Munsell 2.5 R 2/2 (Black reddish brown), occurred at one end of the sample. The darker stained area looked like a slightly more weathered rim of about 25 mm deep. The opposite end was flatter and had a fairly uniform but thin powdery coating of Munsell</p>

Sample No.	Decomposition Grade	Sample Description
404.03	III	<p>7.5 Y 7/2 (Light yellowish grey).</p> <p>Moderately strong, but completely discoloured GRANITE. The interior composed mainly of prominent grains of quartz (mostly transparent), feldspars (generally hard, some slightly decomposed) and black biotite (fresh). Reddish-brown staining occurred around most of the biotite grains. The interior seemed more weathered than sample 404.02, but what was taken to be an external (fracture) surface was less weathered than sample 404.02 and more weathered than sample 404.01.</p>
404.02	II	<p>GRANITE. Sample composed of an inner zone of strong GRANITE and an outer zone of strongly weathered GRANITE. The inner zone was of a non-porphyritic, equigranular texture and feldspars showed only slight decomposition while biotite particles were still fresh and quartz were mostly transparent.</p> <p>The outer zone formed an outer strongly weathered, iron stained, weak shell around the fresher inner rock. Depth of the shell varied from 3 to 15 mm. The colour of the shell was Munsell</p>
404.01	I	<p>Fresh GRANITE. Non-porphyritic and equigranular texture. Composed of plagioclase (mostly white), K - feldspars (mostly pink), biotite (mostly black) and quartz (mostly transparent). Primary minerals were almost unweathered apart from 4 white powdery patches (probably kaolinitised areas). Slight yellowing seen on one surface.</p>

Table 3.7 Summary of Particle Size Analysis

Sample No.	Particle Size Fraction (%)				
	Gravel	Sand	Silt	Clay	Silt & Clay
404.08	53.0	16.0	13.0	18.0	31.0
404.07	48.0	34.1	8.8	9.0	17.8
404.06	37.7	50.7	n.d	n.d	11.6
404.05	46.6	47.4	n.d	n.d	6.0

Table 3.8: Result of Particle Size Analysis on some Shouson Hill Soils (after Irfan, 1986)

Sample No.	Particle Size Analysis (%) PWCL method ¹				Particle Size Analysis (%) Ultimate Grain Size ²					
	Gravel	Sand	Silt	Clay	Silt & Clay	Gravel	Sand	Silt	Clay	Silt & Clay
HS 5	57	34	6	3	9	n.d				
HS 4	55	41	3	1	4	50	43	5	2	7
TP7-2	38	47	12	3	15	38	44	13	5	18
TP6	42	40	14	4	18	40	42	14	4	18
TP7-1	40	45	11	4	15	24	38	26	12	38
TP3	31	42	18	9	27	31	39	20	10	30
TP5 (W)	36	38	20	6	26	26	38	30	6	36
TP5 (a)	34	35	25	6	31	26	31	34	9	43
TP1	41	35	17	7	24	n.d				
TP2	41	31	18	9	27	n.d				
HS 3	6	30	56	8	64	5	26	60	9	69

¹ see page 76

² Involving finger crushing of soft feldspar in addition to PWCL.
n.d - not determined.

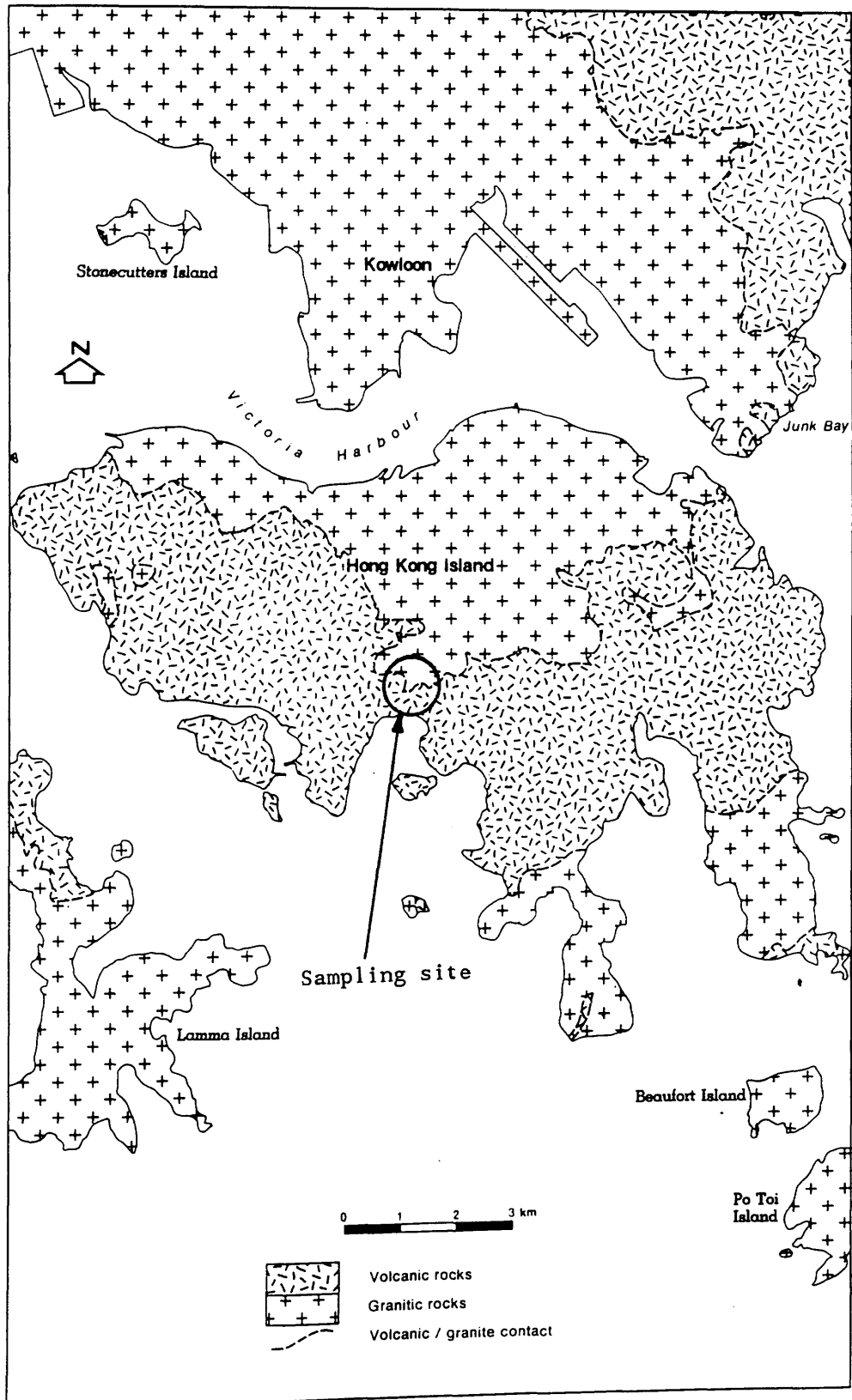


Figure 3.1: Generalised solid geology of Hong Kong Island showing the sampling site (circled). (modified from Irfan, 1986).

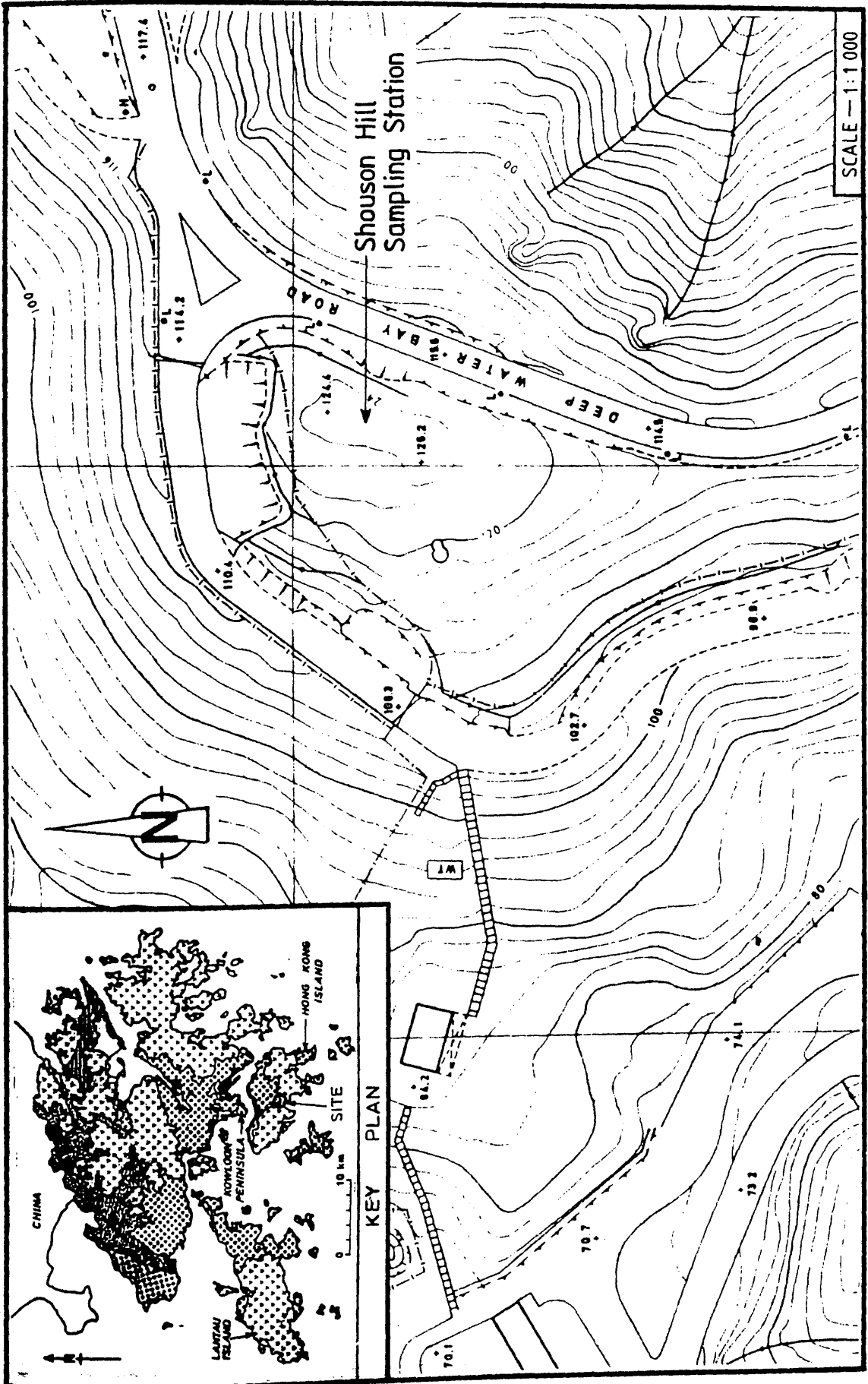


Figure 3.2: Topography of sampling site (after Irfan, 1986).

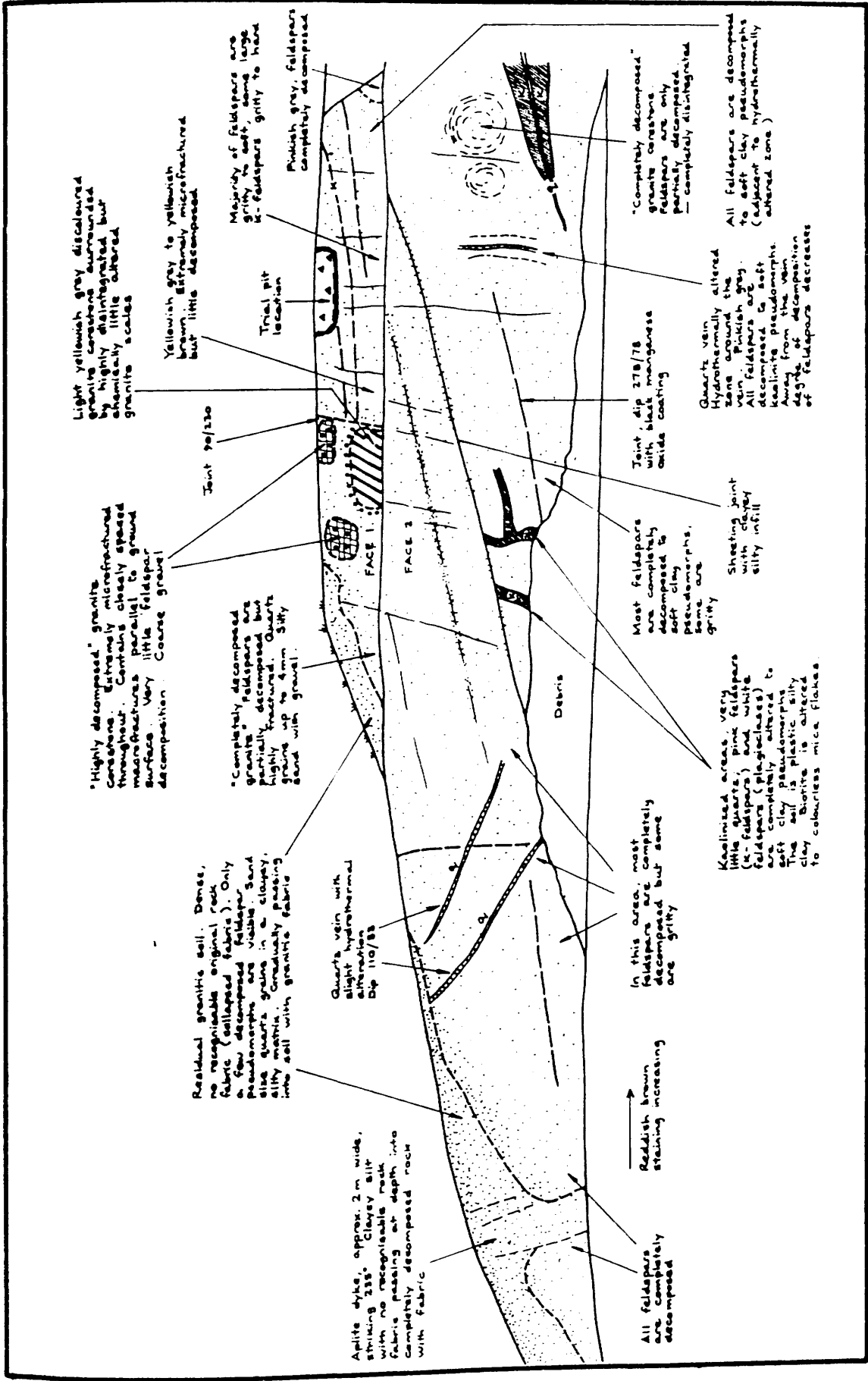


Figure 3.3: A sketch of newly formed slope showing the variability of weathering characteristics of completely weathered granite on site. A trial pit is marked in red. (after Irfan, 1986).

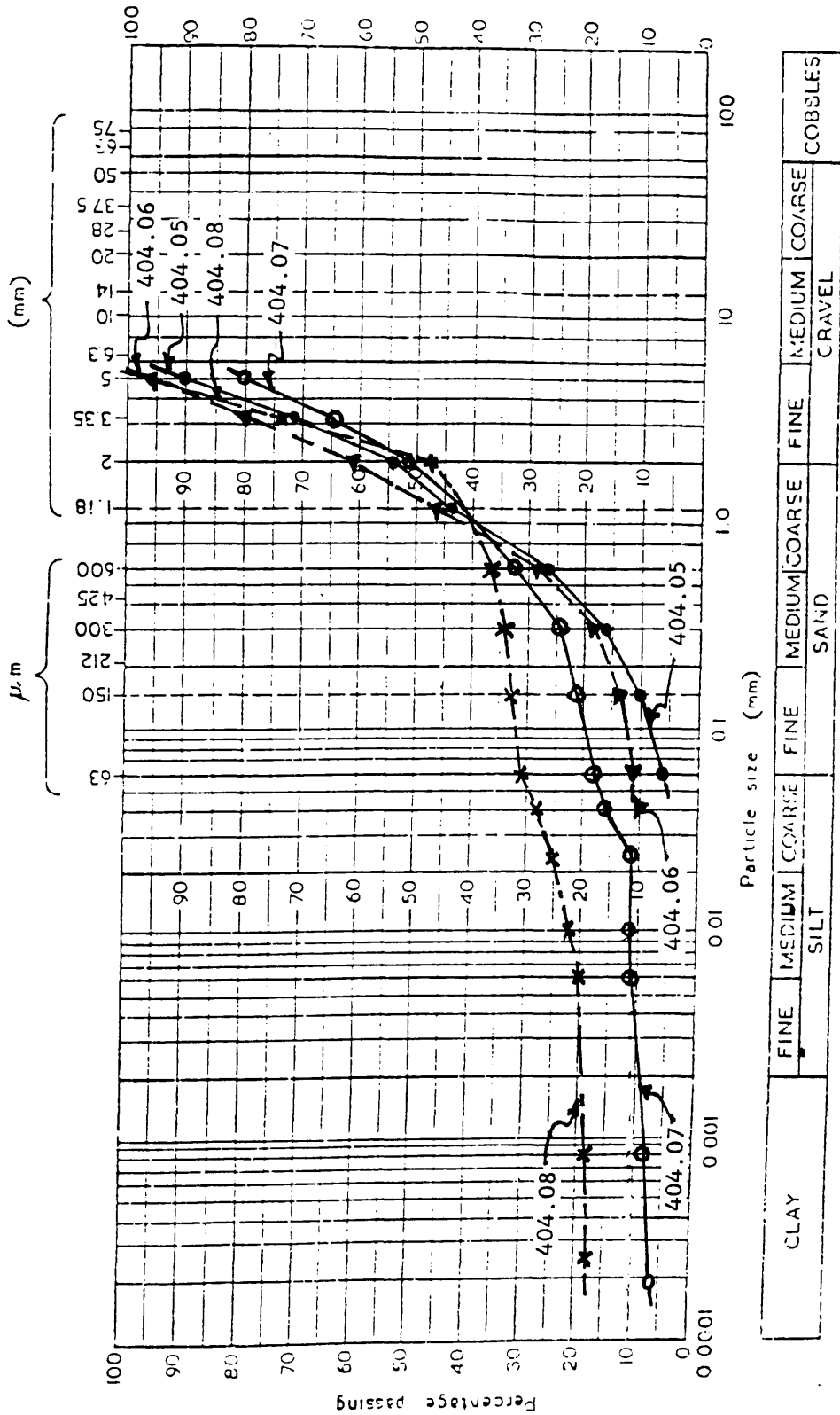


Figure 3.4: Particle size distribution curves

Figure 3.5: Typical SEM of Samples 404.05 and 404.06 showing clay fibres (halloysite) and 'channel' voids.



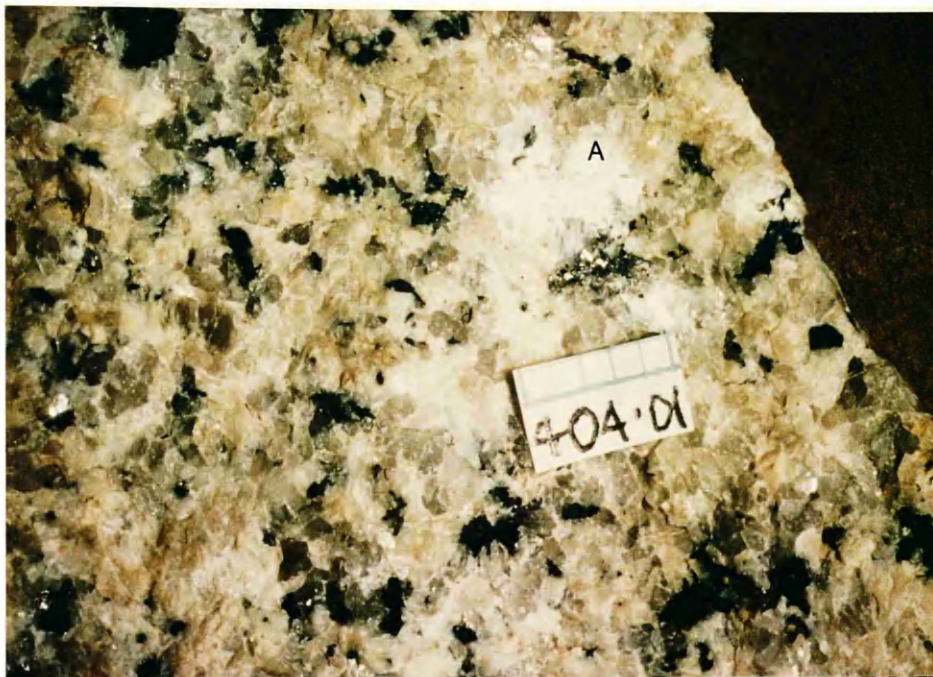


Plate 3.1: Sample 404.01: Fresh Granite.



Plate 3.2: Sample 404.02: Granitic rock with outer iron-syained rim and a fresher inner core.



Plate 3.3: Sample 404.02: Section of rock showing stained (top of photograph) and unstained rock.

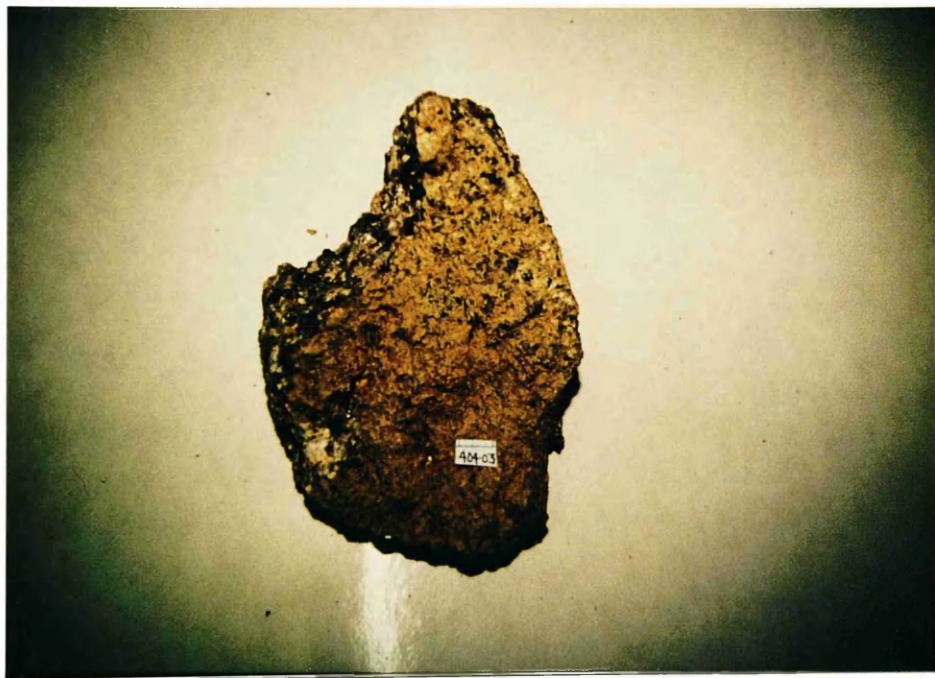


Plate 3.4: Sample 404.03: The sample is coated with a yellowish-brown coloured dust.



Plate 3.5: Sample 404.04 showing microfractures and yellowish-brown colouring of rock.



Plate 3.6: Sample 404.05: Yellowish-brown coloured soil particles and red mottle around biotite grain. Scale is same as in Plate 3.7.



Plate 3.7: Sample 404.06: Red mottles and white (unstained) clay.



Plate 3.8: Sample 404.07: Yellowish-brown soil with black patches from decomposed biotite.



Plate 3.9: Sample 404.07 showing atypical patch of red-stained particles.

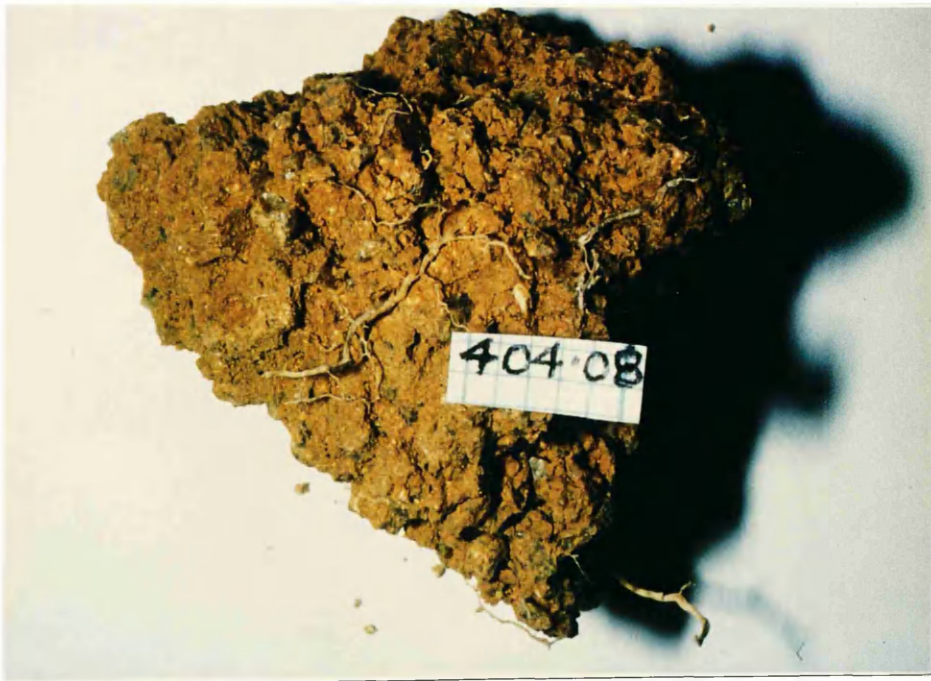


Plate 3.10: Sample 404.08: Residual soil with plant roots and quartz grains.

CHAPTER 4

CHEMICAL METHODS

4.1 INTRODUCTION

All the methods that involved the use of wet chemistry have been termed chemical methods in the present investigation. Some of the work reported in this chapter was made necessary by the need to prepare the soil samples for investigation using the main techniques reported later. This work includes concentration of the iron oxides in the soils and selective dissolution methods for the iron oxide minerals. In other cases, chemical methods such as X-ray fluorescence and atomic absorption spectroscopy were used to determine the elemental concentrations of untreated soils and of products obtained from the concentration and dissolution methods. In general, these tests provided additional information which helped in explaining some of the observations of the main techniques.

This chapter presents the procedures and results for the chemical methods in this investigation. Section 4.2 discusses the methods used to concentrate the iron oxides in the soils in order to make them easier to study by the main techniques, while section 4.3 presents the selective dissolution methods used to estimate the different phases of iron oxides in the soils. Section 4.4 gives the methods which were used for the determination of the elemental concentrations of the samples, and pH and organic content of the soils are given in Sections 4.5 and 4.6 respectively. The results of the chemical tests are presented in Section 4.7. Analar grade reagents were used throughout.

4.2 CONCENTRATION METHODS FOR IRON OXIDES

Due to the low concentration of iron oxides in the soils in relation to other minerals, it was difficult to study them by the major techniques used in this investigation. After consideration of other options, it was decided to concentrate the iron oxides in the soils by dissolving some of the clay minerals in the soils. One common method of concentrating iron oxides in kaolinitic soils by dissolution of the clay minerals is the boiling 5 M NaOH method. This method was first proposed by Norrish and Taylor (1961) and has subsequently been used by other workers (e.g. Davey et al., 1975., Bigham et al., 1978., Kitagawa and Moller, 1979; Torrent et al., 1980 and Kämpf and Schwertmann, 1982). A brief review of the method was given by Kämpf and Schwertmann (1982) who also carried out a detailed examination of the method and have concluded that no significant changes to crystal morphology and Al substitution were induced by this treatment if the Si concentration in the boiling NaOH was sufficiently high. According to these authors, this is usually guaranteed by the kaolinite that dissolves in 5 M NaOH.

Dissolution of silicate materials with hydrofluoric acid is a well known method (Loveland, 1987) which has often been used to dissolve silicate materials for the purpose of analysing them for their elemental concentration (Langmyhr and Paus, 1968; Jeffery and Hutchinson, 1981; and Hannaker and Lie, 1984). A review of the method was given by Loveland (1987). Norrish (1968) used HF to concentrate soil phosphates and found that while kaolin minerals were effectively dissolved by the hydrofluoric acid, phosphate as well as accessory minerals such as titanium oxide, iron oxides and hydroxides, ilmenite and quartz were not attacked by the treatment. Illite was also found to be resistant to attack by HF. Hence it would appear that under favourable conditions, such as in the absence of large amounts of other minerals that may resist attack by hydrofluoric acid, the method

could be used to concentrate iron oxide minerals, especially in soils where kaolin is the main clay mineral. So far, however, very few authors have used the method for concentrating iron oxides in soils.

4.2.1 Boiling 5 M Sodium Hydroxide (NaOH) Method of Concentration

The procedure used in this investigation was described by Kämpf and Schwertmann (1982) after the method used by Norrish and Taylor (1961). 100 ml of 5 M NaOH was added to a 1 g clay in a covered 150 ml beaker. The mixture was boiled for 60 minutes on a sand bath and transferred to centrifuge tubes after cooling. The sample was spun down, the clear liquid was discarded, and the sample was washed once with 5 M NaOH, once with 0.5 M HCl for 15–20 minutes to dissolve sodalite, twice with 1 N $(\text{NH}_4)_2\text{CO}_3$ to remove NaCl, and twice with distilled water to remove excess NH_4 and CO_3 . The sample was then transferred to a glass beaker and dried at 60°C overnight to volatilize the remaining $(\text{NH}_4)_2\text{CO}_3$. The $(\text{NH}_4)_2\text{CO}_3$ step was preferred over ethanol or acetone washing because it was supposed to give better flocculation (Kämpf and Schwertmann, 1982); and drying was done at 60°C instead of the 100°C recommended by Kämpf and Schwertmann (1982) so as not to effect any change in phase to ferrihydrite, if present. The residue was lightly crushed and stored in a glass sample bottle prior to testing.

4.2.2 Hydrofluoric Acid (HF) Method of Concentration

A review of the use of HF for decomposition of clay minerals was given by Loveland (1987). The procedure outlined by Norrish (1968) was used in this investigation for its simplicity. 2 g of clay was suspended (by mixing thoroughly with a plastic spatula) in 80 ml of distilled water in a 1000 ml plastic beaker. 80 ml of $\approx 40\%$ HF m/v was added, and the attack allowed to proceed for two minutes. (Where only a very small amount of sample was available it was found

possible to scale down the quantities of soil, water and HF used accordingly). The reaction was then stopped by rapid diluting to 1000 ml with distilled water, the residue was recovered as quickly as possible (usually within 10 to 30 minutes in this investigation) by centrifuging at 4000 rpm for 15 minutes, and it was then washed once with 1 N NaOH, once with 1 N HCl and three times with distilled water or until all the NaCl had been washed out. The residue was then dried overnight in an oven at 60°C, lightly crushed and stored in a glass bottle prior to testing.

4.3 SELECTIVE DISSOLUTION METHODS FOR IRON OXIDES

As opposed to concentration of the iron oxides in the soil by dissolution of clay silicates and other oxides, selective dissolution in this investigation refers to dissolution of either the total or a fraction of the iron oxides in the soil leaving mainly clay silicates and sometimes silicates with a fraction of the iron oxides as residue. A review of dissolution techniques for iron oxides was given by Borggaard (1987).

Two methods of selective dissolution which had been used by various authors were used in the present investigation. These are the dithionite citrate bicarbonate method and the acid ammonium oxalate methods. The dithionite citrate bicarbonate method is a reduction procedure commonly used to determine the free iron present in a soil sample. The total iron present in soil includes the fraction of iron present in the structures of other minerals, such as in ferromagnesian silicates, biotite mica, illite clay minerals, nontronite, etc and the amount of free iron oxides, the crystalline and amorphous forms of iron oxides and iron associated with organic matter collectively constitute the free iron in soil.

It is now clear that several soil materials can be extracted with oxalate

and, although the method needs to be used with caution it is possible to get useful indications of the type of short-range-order minerals which are present in a soil. Acid-ammonium oxalate is known to dissolve, or partly dissolve allophane, imogolite, ferrihydrite, Al associated with humus, lepidocrocite, maghemite, magnetite and Al from chloritised vermiculite (Parfitt and Childs, 1988).

The procedures employed for the dithionite citrate bicarbonate and the acid ammonium oxalate methods are outlined below.

4.3.1 Dithionite Citrate Bicarbonate Method of Dissolution

The dithionite citrate bicarbonate method of dissolution was done using the procedure of Mehra and Jackson (1960). 100 mg of the clay fraction of the soil was weighed into a 100 ml polypropylene tube and 5 ml of 1 M sodium bicarbonate (NaHCO_3) solution was added. 40 ml of 0.3 M sodium citrate was then added to the mixture. The tube was placed in a water bath of boiling water and the contents brought to a temperature of 80°C. 0.5 g of sodium dithionite ($\text{Na}_2\text{S}_2\text{O}_4$) powder was added to the mixture and stirred continuously for 1 minute. The mixture was maintained at a temperature of 80°C and stirred occasionally for 15 minutes. 10 ml of saturated sodium chloride (NaCl) solution was then added to the mixture (to promote flocculation) and left to cool. After cooling the residue was recovered by centrifuging and the procedure repeated to make three extractions in all. The residue was then washed with 50 ml of 0.05 M HCl to dissolve pyrite (FeS), and washed with distilled water until freed of salt. The residue was dried overnight in an oven at 60°C, lightly crushed and stored in a glass sample bottle prior to testing.

4.3.2 Acid Ammonium Oxalate Method of Dissolution

A review of the various procedures for dissolution with acid ammonium

oxalate was given by Parfitt and Childs (1988). In this investigation the procedure outlined by Schwertmann (1964) was adopted with slight modifications. A 0.2 M ammonium oxalate solution was adjusted to pH 3 using oxalic acid. 40 ml of the solution was added to 100 mg of the clay fraction of the soil sample in a polypropylene tube, which was then stoppered and shaken continuously in the dark (shaking in the dark prevents re-precipitation of the dissolved iron oxide) for 4 hours. The procedure was repeated to make two extractions on each sample in order to allow complete extraction of ferrihydrite, if present, from the sample. After each extraction the aliquot was decanted in the dark and kept in dark coloured bottles which were excluded from sunlight until tested for its Fe and Al contents using atomic absorption spectroscopy. The residues obtained were washed with distilled water using a centrifuge, dried at 110°C, and stored in the dark until examined by X-ray analysis. Both atomic absorption spectroscopy and X-ray analysis were done in rooms excluded from direct sunlight.

4.4 ELEMENTAL CONCENTRATION

Elemental concentrations were determined both for untreated soils and for residues and aliquots from the concentration and selective dissolution methods described above. The aims were, principally, to know the chemical contents and concentration of the elements in the samples, estimate the effectiveness of the concentration methods, and identification of the iron oxide phase following selective dissolution. Two methods were used depending on the type and amount of sample available. Although X-ray fluorescence (XRF) could be used to determine the concentration of several elements in one preparation, it is only useful for powdered samples available in large quantities. Atomic absorption spectroscopy was used for samples available in very small quantities and aliquots. Hence, both methods were used, sometimes complementarily, and the procedures

used are presented below.

4.4.1 X-ray Fluorescence

The principles and methods of X-ray fluorescence spectroscopy was adequately covered in Vanden Heuvel (1965). The elements were analysed from fused discs prepared as outlined below.

(a) Initial Sample Preparations

For the rock and whole-soil, the samples were ground in an agate mortar to at least 100 mesh, and dried in an oven at 110°C for 24 hours to remove water. Clay-fraction samples were obtained by sedimentation as outlined earlier in chapter 3 and dried in an oven at 110°C for 24 hours.

(b) Preparation of Fused Discs

0.375 g of oven-dry soil was mixed with 2.0 g of flux (SPECTROFLUX 105 containing lithium carbonate, lithium tetraborate and lanthanum oxide) in a platinum crucible. The crucible was then covered and placed in a furnace set at 1000°C for 15 minutes, to free the sample of organic matter and water after which it was brought out, placed on a clean aluminium surface and allowed to cool. The soil-flux mixture was then melted on a blast burner and swirled (while holding the crucible with platinum-tipped crucible tongs) to ensure a uniform mix, until the melt was at dull red heat. The disc was formed by carefully pouring the melt onto a platten placed on a hot plate maintained at 225°C, and under a plunger assembly, and lowering the plunger firmly over the melt for a few seconds. The disc and platten were then placed between two asbestos blocks and transferred onto a hot plate maintained at 200°C and left to stand for 30 minutes after which the platten and disc were allowed to cool, still enclosed within the asbestos blocks. When cooled, the disc was carefully removed

and labelled, ready for analysis.

(c) Instrumentation

Analysis was carried out using a Philips PW1450/20 automatic X-ray fluorescence spectrometer equipped with a 60 position sample changer and on-line "SuperBrain" microcomputer for data processing. The major elements were analysed from fused glass discs using influence factors to correct for the remaining absorption – enhancement effects (Jenkins and De Vries, 1969). The calibration coefficients were established routinely from internal Glasgow University standards with periodic checks of accuracy against international standards. The processing of data was done automatically through the microcomputer, and the results were expressed in percentage proportions by weight of the oxides of the different elements obtained. A summary of statistics obtained for determination of some major elements using the system is given in Table 4.1. The figures are within the acceptable limits for the present investigation.

4.4.2 Atomic Absorption Spectrophotometry

The soil samples were digested with HCl prior to elemental analysis using the method of Schulze (1984). 10 mg of the clay fraction of the sample was dissolved on 2 ml of concentrated HCl in a 25 ml volumetric flask. The flask was heated to about 150°C on a sand bath until the sample dissolved, and allowed to cool before being filled to 25 ml with distilled water. Al and Fe were determined using a Perkin-Elmer Model 1100B atomic absorption spectrophotometer. The instrument was calibrated with appropriate standards prior to elemental analysis, and the values of the concentrations of the elements were printed out by an on-line microcomputer connected to the instrument.

4.5 DETERMINATION OF pH

The pH of the soil was measured in both water and 1 M KCl solution according to the methods of Jackson (1958). The pH in 1 M KCl was done because it had been found to be less variable with experimental procedure, probably due to the presence of salts (Jackson, 1958). 10 g of the soil passing the 2 mm aperture sieve was placed in a glass bottle, and 25 ml of distilled water (or 1 M KCl) was added. The mixture was shaken end-to-end in a mechanical shaker for 30 minutes and allowed to settle. The pH of the suspension was measured using a Calomel Reference Electrode connected to a pH meter. The average of two different determinations was taken for each soil.

4.6 DETERMINATION OF SOIL CO₂

Carbon occurs in soils in four mineral or organic forms viz: Carbonate mineral forms (chiefly CaCO₃); organic carbon (e.g. charcoal, graphite, coal); humus, and little altered organic residues of plants and animals (Jackson, 1958). Each of these fractions, if present, contributes to the total soil carbon. In the case of the soils used in the present investigation, tests for the presence of carbonates using 4N HCl (Allison, 1965) were negative, indicating that the contribution from carbonates to the carbon content of the soils was minimal. The carbon content of the soils was determined by dry combustion using the method outlined by Allison et al. (1965). After drying the soil at 110°C, to remove surface water, a furnace running at 1100°C was employed for oxidising the soil carbon to CO₂ which was then removed, together with the water produced, with a current of nitrogen, absorbed in a tube which was packed with soda asbestos with a small amount of anhydrous magnesium perchlorate and determined gravimetrically.

4.7 RESULTS

4.7.1 Elemental Concentration

Based on site observations and results of mineralogical analysis which showed possible mineralogical connections between the fresh rocks obtained from the site and the weathered soils it was assumed that the soils were derived from granite rocks that were similar to those obtained from the site and that all the soils were derived from similar parent material. Comparison of the chemical composition of the fresh granite obtained in this investigation with those obtained for other "Hong Kong granites", from different sites, by other authors (e.g Davis, 1953) showed similarities which appeared to indicate that the granite may not be significantly variable over the area. The discussions in the following paragraphs are based on these assumptions. The samples in the Tables are arranged in order of decreasing weathering (downwards) as shown in Table 3.1. As noted earlier, the elements have been expressed in the form of their oxides, although some of them were not necessarily present in these forms.

The summary of chemical contents of the untreated whole sample and clay fraction of the soils are shown in Tables 4.2 and 4.3 respectively. Changes in the concentration of the various elements in a soil sometimes reflect the weathering behaviour of the primary minerals in the rock. The concentrations of Mn and P in the samples were very low, as could be seen from Tables 4.2 and 4.3, thus suggesting that minerals which contain these elements, e.g oxides of manganese, and apatite (a P bearing mineral found in some igneous rocks) may be of very minor proportion in the samples. The Ti content of the whole soil and clay fractions was also found to be of very minor quantity and did not vary significantly between samples, thus signifying the absence of any appreciable amount of titanium minerals in the samples.

From Table 4.2, the CaO and Na₂O contents of the samples could be

seen to be fairly constant in the rock samples (404.01 to 404.04), but Ca was absent in the soil samples (404.05 to 404.08) while Na was sharply depleted in samples 404.05 to 404.07 and absent in the residual soil (404.08). Since the Ca and Na in the soil were likely to be mainly from plagioclase (Ca and Na feldspars), the sharp depletion of the elements in the sample 404.05 suggested that most of the plagioclase was already weathered at this stage. This view is in line with observations made during petrographic studies of the samples in the course of this investigation and by Irfan (1986). SEM observations of fractured surfaces of Sample 404.05 showed a predominant presence of fibrous minerals which were later identified to be halloysites by electron diffraction (see Chapters 3 and 5). Since petrographic studies and determination of elemental concentration (discussed below) appeared to suggest that the other main primary minerals namely quartz, biotite, and K-feldspar were still mostly intact in this sample, it would appear that the plagioclase feldspar was the first mineral to weather in the soil and that it weathered into halloysite tubes.

A slight difference in the K_2O content of the fresh rock (404.01) and the slightly weathered rocks (404.02 to 404.04) was indicated in Table 4.2, but this difference was not large enough to constitute a significant depletion of the element in the slightly weathered rocks and could also have occurred from slight variations in the distribution of K bearing minerals within each rock. Hence, the K content would appear to remain almost constant from the fresh rock to sample 404.07, but the concentration dropped from over 5 % in these samples to 0.76 % in the residual soil (404.08). Melfi et al. (1983) reported an upward enrichment of K for weathering granites from two sites having semi-arid and sub-humid climates in Brazil. They, however, reported an upward leaching of K for a third site having humid, sub-tropical climate. In the present case, since K, in the whole soils was mainly from K-feldspar, and interlayer K in biotite the constant K content of samples 404.01 to 404.07 suggested that either

K-feldspar or biotite or both minerals weathered at a slower rate than the plagioclase. Petrographic studies also showed that the plagioclase feldspars in the soils weathered faster than both the K-feldspar and biotite. It would thus appear that the behaviour of K in a profile is complex and may depend on several factors such as initial primary minerals, climate, terrain etc.

MgO was found to be of constant concentration in all the samples and the slight depletion indicated in samples 404.07 and 404.08 may not be of much significance considering the accuracy of measurement of Mg given in Table 4.1. It is possible that most of the Mg was present as octahedral cation in the biotite and was later incorporated into the structures of the chlorite and clay mica identified in the soils by X-ray diffraction, with very little loss. The higher concentration of Mg in the clay fractions of the soils (Table 4.3) also supports this suggestion, although the possibility of some fine biotite particles getting into the clay fraction may not be completely ruled out.

Silicon was the most abundant element in all the samples. From Table 4.2, the SiO_2 content of the samples, which contains contributions from all silicates (e.g. quartz, clay minerals, feldspars, mica etc.), showed no significant variation within the profile although a very small depletion of the element in the soils compared to the rocks is indicated. The upward increase in silica content which is sometimes an indication of the residual accumulation of quartz as a result of washout of fine materials (e.g. Melfi et al; 1983) or weathering of other less resistant minerals (e.g. Gilkes et al; 1980) was absent in this case although this observation does not necessarily preclude any of these possibilities.

Since quartz dissolution in the soils was found to be minimal from petrographic studies, the behaviour of Si in the profile may have been largely due to the weathering of the primary minerals. Hence, the constant proportion of quartz through the profile may be an indication that, at least initially, most of the primary aluminosilicates were weathered into other aluminosilicates with

very little loss of silicon. Hence, as noted earlier, most of the plagioclase which was weathered earlier may have been converted into halloysite with very little loss of the plagioclase due to dissolution.

The Al_2O_3 content of the samples (Table 4.2) showed an overall upward increase from the fresher rocks to the residual soil. The presence of a minor amount of gibbsite in the residual soil (404.08), indicated by X-ray and infrared spectroscopy may be contributory to the higher Al content of this soil. The ratio of the total SiO_2 to Al_2O_3 is given for the soils in Tables 4.2 and 4.3. A slight upward decrease in the ratio from the rock samples to the soil samples is indicated. The decrease in the $\text{SiO}_2/\text{Al}_2\text{O}_3$ ratio coincides with the path of increased weathering in the soils, and appeared to suggest the leaching of silicon relative to aluminium in the primary and/or secondary minerals in the soils with the formation of oxides of aluminium, such as gibbsite. The fact that Sample 404.08 which had the lowest $\text{SiO}_2/\text{Al}_2\text{O}_3$ ratio also had the highest Al content and was the only soil in which gibbsite was identified supports this suggestion.

Fe was measured as total Fe (i.e. $\text{Fe}_2\text{O}_3 + \text{FeO}$), recorded in the tables as Fe_2O_3 . The Fe content of the whole soil and rock samples ranged from 1.27% to 2.41% (Table 4.2) with the lower values being obtained for the relatively unweathered rock samples. The values are within the limit expected for granitic material. The Fe content of the whole soil is probably a contribution from both the 'free' iron oxide and octahedral Fe in biotite.

The chemical composition of the clay fraction of the soils (Table 4.3) showed similar trends in most respects to those of the whole soil samples. SiO_2 contents of the soils showed no significant variation from soil to soil and a slight enrichment of the Al_2O_3 content in the residual soil was indicated. The $\text{SiO}_2/\text{Al}_2\text{O}_3$ ratio of about unity obtained for the clays is an indication that most of the minerals in the clay fraction were 1:1 minerals (mostly kaolin, as suggested by X-ray diffraction).

Most of the K in the clay fraction is likely to be from clay mica identified in all the soils by electron microscopy, X-ray diffraction and infrared spectroscopy, and the relative concentration of Mg in the clays compared to the whole soils appeared to show Mg to be mainly from the chlorite in this fraction, as mentioned earlier in the discussion for the whole soils.

The Fe content of the clay fraction of the soils showed no significant variation between the soils, but concentration of the Fe was achieved due to particle separation. Table 4.4 shows the concentration factor, $\frac{Fe_{clay}}{Fe_{whole\ soil}}$, achieved for the Fe in the soils as a result of particle separation to be over two-fold for all the soils. Since the concentration of chlorite (a possible Fe bearing mineral) in the soil was very low, free iron oxides would be responsible for most of the Fe in the clay fraction.

4.7.2 Chemical Concentration of Fe

In order to determine the efficiency of the NaOH and HF concentration methods for Fe in the clays, the Fe content of the residues obtained from both treatments (see section 4.2) were compared with those obtained for the untreated soils and discussed below.

The Fe content of the residues obtained from the NaOH and HF treated soils was determined by atomic absorption spectrophotometry, and the values obtained are given in Table 4.5. Values obtained for the untreated whole soils and clay fractions (see Tables 4.2 and 4.3 respectively) have been included in Table 4.5 for comparison. The exact agreement in the Fe contents of the residues from NaOH and HF treatments for sample 404.08 and the residue from the NaOH treatment of sample 404.07 is, presumably, fortuitous. From Table 4.5, except for sample 404.08 where similar values were obtained for both the NaOH and HF residues, the Fe content of the residues from HF treatment of the other clays gave significantly lower values than those obtained for residues

from the NaOH treatment of the same soils. In all cases, for these other clays, the Fe content for the residues from the NaOH treatment were about twice that for the residues from HF treatment. Two explanations may be possible for this observation. Firstly, it is possible that the HF treatment was less successful in dissolving the 2:1 minerals (clay mica) and chlorite, discussed later, which were found to be of higher quantity in the deeper soils than in the residual soil. Although quantitative X-ray diffraction was not carried out on the residues obtained from the concentration treatments, a study of the diffraction peaks did not indicate a significant difference in the proportion of 2:1 minerals in the residues from both methods, thus ruling out the likelihood of the first possibility. Secondly, a fraction of the iron oxide in the soils may have been dissolved by HF. Control tests were carried out (during this investigation) with synthetic iron oxides using 5% of the oxide to 95% of synthetic kaolinite and subjecting them to the same treatments as the clays. The results of the tests supported this second suggestion. The tests showed that synthetic goethite and hematite were not affected by the HF treatment, but the synthetic ferrihydrite dissolved immediately and completely on contact with HF, thus indicating that the reduction in Fe content in the HF residues compared to the NaOH residues for Samples 404.05, 404.06 and 404.07 may have been due to ferrihydrite or similar poorly crystalline Fe mineral in the soils being dissolved by HF. Electron microscopy (discussed in Chapter 5) revealed the presence of ferrihydrite in the red fraction of Sample 404.05 while selective dissolution using acid ammonium oxalate (discussed below) showed that ferrihydrite may be present Samples 404.05, 404.06 and 404.07 but absent in Sample 404.08.

The concentration factors achieved, as a result of the treatments, with respect to the whole soil and clay fraction values (Table 4.6) gave values of 4.43 to 7.45 with respect to the whole soil values (i.e Fe content of residue divided by Fe content of whole soil from Table 4.2) and 1.87 to 3.2 with respect to the

clay fraction values (i.e Fe content of residue divided by Fe content of clay fraction from Table 4.3) for the NaOH treated samples. Torrent et al. (1980) and Schwertmann et al. (1982) had earlier reported that the NaOH method of concentration was less effective in concentrating iron oxide in soils dominated by 2:1 minerals. In this investigation the lower concentration factors were obtained for samples 404.05 and 404.06 which were found, by X-ray diffraction and electron microscopy, to contain more 2:1 minerals (e.g biotite and clay mica) than the 404.07 and 404.08 soils. An examination of the NaOH-treated soil residues obtained in this investigation by X-ray diffraction and electron microscopy showed the 2:1 minerals and chlorite to be resistant to attack by boiling NaOH. Fe concentration factors of 3 to 20 had been reported for kaolinitic soils (Schulze, 1987) while concentration factors from 2.5 to 3 were obtained for illitic-smectitic soil clays from Germany (Schwertmann et al; 1982), and Torrent et al (1980) obtained concentration factors from 1.5 to 5.2 for some soil clays from Spain.

The HF treatment gave Fe concentration factors from 2.39 to 6.74 with respect to the whole soil and 1.01 to 3.20 with respect to the clay fractions with the lower factors being obtained for samples 404.05 and 404.06 which contained more 2:1 minerals than the other samples. Norrish (1968) reported that illite (a 2:1 mineral) was not dissolved as quickly as kaolin by the HF treatment. X-ray diffraction and electron microscopy on the residues done in the course of this investigation also revealed that the 2:1 clay minerals (clay mica) and chlorite in the samples were more resistant than kaolin to attack by HF.

Thus, both the NaOH and HF treatments appeared to be very useful in concentrating iron oxide in clays provided the main clay mineral is kaolin. HF, however, appears to be unsuitable for concentration of iron oxide minerals where the iron oxide mineral to be concentrated included ferrihydrite or similarly poorly crystalline iron oxide mineral. However, since HF was found to dissolve

ferrihydrate and not goethite or hematite, the method may be further investigated for use as a selective dissolution method for iron oxide phase determination.

4.7.3 Selective Dissolution of Fe

In order to identify the poorly crystalline iron oxide phases in the samples, selective dissolution of these phases using acid ammonium oxalate treatment (as outlined in section 4.2) was carried out on the clay fractions of the samples and the Fe content of aliquots obtained from the method determined by atomic absorption spectrophotometry. Table 4.7 gives the Fe content in aliquots obtained from ammonium oxalate treatment of the clay fraction of the soils. The ratio of oxalate soluble iron (Fe_O) to that of the total Fe (Fe_t) in the clay fraction of the untreated soils is also shown in the Table. Synthetic ferrihydrate, goethite and hematite were also subjected to the same treatment as the natural samples as controls. The ratio of the oxalate soluble Fe to that of the total Fe or dithionite extractable Fe had been used as a measure of the amount of poorly crystalline iron oxide, mainly ferrihydrate, in soil samples (e.g. McKeague and Day, 1965; McKeague, 1966; Schwertmann et al; 1987; Carlson and Schwertmann, 1987 and Parfitt and Childs, 1988). For pure, very poorly crystalline ferrihydrate samples an Fe_O/Fe_d or Fe_O/Fe_t of ≈ 1 is expected. Values of Fe_O/Fe_t for the soils in this study suggested a higher amount of poorly crystalline iron oxide in the deeper soils than in the residual soil with samples 404.05 and 404.06 having equal proportions, while sample 404.07 had a slightly lower proportion. Sample 404.08 had the lowest proportion of all the samples. This observations support those made in respect of HF treatment (discussed above) of the possible presence of ferrihydrate in samples 404.05, 404.06 and 404.07. Childs (1985) proposed estimating ferrihydrate concentration (Fh_{est}) from Fe_O using the equation:

$$Fh_{est} = 1.7 \times Fe_O\% \quad (4.1)$$

Using Equation 4.1 the values of ferrihydrite concentration obtained for the soils in this investigation (Table 4.7) were found to vary from about 0.01 for sample 404.08 to 0.31% for sample 404.05. A value of 105.64% obtained for the synthetic ferrihydrite may be an indication of the possibility of a fair estimation of ferrihydrite in soil samples from Fe_2O_3 using Childs' equation. The values of ferrihydrite concentration obtained for the soils indicated a general decrease in the amount of ferrihydrite in the soils with increased weathering. Since goethite was the only other iron oxide identified in the soils it would appear that the ferrihydrite in the younger soils was later converted to goethite with time.

4.7.4 Soil pH

Before applying the results of pH tests obtained in this investigation, certain facts have been considered. Because pH was not measured until the samples arrived at Glasgow university, changes to the pH caused by drying, packaging and storage environments cannot be eliminated, and these factors may affect the samples differently. However, due to the fact that the insitu moisture content of the soils may have been low, and since precautions were taken to prevent excessive drying—out of the samples (see Chapter 3), the effect of drying on pH may not be drastic. Care was also taken to store the samples away from chemicals which may effect changes to the pH.

The pH of the soils (given in Table 4.8) varied between 5.01 and 6.81 in water and between 4.14 and 6.08 in 1 M KCl. This result gave an indication that the soils were slightly acidic. The lowest value of pH was obtained for the most highly weathered soil (404.08), most probably due to the presence of organic substances in the form of roots in this soil, while Samples 404.07 and 404.05 gave almost equal values, and Sample 404.06 gave the highest value of all. In a general sense, it could be said that the pH of the soils which gave an indication

of the presence of ferrihydrite (Samples 404.05 404.06 and 404.07) were higher than that of Sample 404.08 where only goethite was indicated. It would appear that the pH range of 5.01 to 6.81 obtained for the soils, may favour the formation of goethite, from ferrihydrite, over the other forms of iron oxides. Tests on synthetic oxides to demonstrate the effect of pH on the formation of goethite and hematite from ferrihydrite, at 25°C (Schwertmann and Murad, 1983) also showed that the proportion of goethite increased relative to hematite as the pH of the system dropped from 8 to 4. According to these authors, goethite formation is strongly favoured where the concentration of monovalent Fe^{3+} ions, either $\text{Fe}(\text{OH})_2^+$ or $\text{Fe}(\text{OH})_4^-$, is at maximum. The maximum for $\text{Fe}(\text{OH})_2^+$ activity is at $\text{pH} \approx 4$ and the minimum at around pH 8. Although the results obtained in this present study is in line with the findings reported for the synthetic oxides, it is not known if the explanation given above by Schwertmann and Murad (1983) is relevant to soil environments.

4.7.5 Organic Matter Content

The organic matter content of the whole soil and clay fraction, measured in terms of CO_2 , are given in Table 4.9. Values of organic matter content of less than 2% was indicated for all the soils. This is in agreement with the findings of infrared spectroscopy (Chapter 7) where the traces showed no reflection for organic matter thereby signifying a low percentage of organic matter in the soils. An indication of a decrease in organic matter content with weathering was given for the whole soil samples with the organic matter content increasing from 0.18% in Sample 404.08 to 0.45% in Sample 404.05. However, no such indication was apparent in the results for the clay fraction samples. Although visual observation of the soils revealed significantly more roots in Sample 404.08 than in the other samples, the presence of these roots did not appear to lead to a higher organic content in this soil, perhaps due to the fact

that most of the roots were large and easily separated from the soil. It is also possible that some other forms of organic matter, present in higher proportions in the deeper soils, are responsible for the higher organic matter content of these soils.

The presence of organic matter, even in low quantity, had been reported to promote the formation of ferrihydrite in soils and other environments by impeding the crystallisation of the iron oxide into more crystalline forms (see review in 2.3.2(b) and 2.3.2(d), for a detailed review see Schwertmann et al; 1986). Also, increased organic matter content has been found to favour the formation of goethite over hematite in soils (see review in Schwertmann, 1987b) although this "anti-hematitic" effect has not been explained satisfactorily, nor has it been reproduced in the laboratory (Schwertmann, 1987b). In the present investigation, the sole role of organic matter in the formation of iron oxides in the soils is not easily determined especially as other materials such as silicates (which were also found in the soils) have similar inhibiting effects as organic matter on iron oxide crystallisation (Saleh and Jones, 1984; and Schwertmann, 1987b). However, the fact that Samples 404.05, 404.06 and 404.07 which were indicated to contain ferrihydrite also contained more organic matter (in the whole soil, Table 4.9) appeared to support the findings of earlier authors. Moreover, the absence of hematite in the soils may be an indication that there was enough organic matter in the soils to prevent the formation of hematite even though ferrihydrite, which is a precursor for the formation of hematite, was present in some cases. Thus, the effect of organic matter in the soils may be to lead to the formation of ferrihydrite in the soils as well as prevent the subsequent formation of hematite from the ferrihydrite.

Hence, for the soils under investigation the presence of organic matter appeared to have favoured the formation of ferrihydrite in the deeper soils while the combination of organic matter and pH conditions favoured the formation of

goethite rather than hematite in all the soils.

4.8 SUMMARY

Some of the important findings of the study done in this chapter are summarised below:

- (1) In line with detailed observations of hand specimens and results of petrographic studies, chemical determination indicated that the plagioclase feldspar was the first mineral to weather and the mineral appeared to have weathered into the halloysite tubes identified in the soils by SEM and TEM.
- (2) Comparison of the behaviour of potassium in the soils compared with earlier studies suggested that the depletion or concentration of potassium in a profile, as weathering progresses, may depend on a complex interplay of several factors such as initial primary minerals, climate, terrain etc.
- (3) Silicon was the most abundant element in all the samples, and its proportion in the rocks and soils was more or less constant, thus indicating an overall minimal loss of silicon with increased weathering.
- (4) A slight leaching of silicon relative to aluminium in the primary/secondary minerals was indicated by a decrease in

SiO_2 : Al_2O_3 ratio with increased weathering and supported by the identification of gibbsite in the residual soil.

- (5) Low values of Fe content ranging from about 1.3% to 2.4% obtained for the whole soils were within the limit expected for granitic soils.
- (6) Both the boiling NaOH and HF treatments were effective in concentrating iron oxides in soils. However, HF was found to dissolve ferrihydrite and would not be suitable for concentration of ferrihydrite or other poorly crystalline iron oxides.
- (7) Selective dissolution using acid ammonium oxalate indicated ferrihydrite in Samples 404.05, 404.06 and 404.07.
- (8) The pH of the soils varied between 5.01 and 6.81 in water and between 4.14 and 6.08 in molar KCl.
- (9) The organic matter content of the whole soil samples was found to decrease with increased weathering. It is possible that the presence of organic matter favoured the formation of ferrihydrite in some of the soils, and this together with a favourable pH promoted the subsequent formation of goethite, rather than hematite, from the ferrihydrite.

TABLE 4.1: Summary Statistics of Major Elements

Element	SiO ₂	TiO ₂	Al ₂ O ₃	Fe ₂ O ₃	MnO	MgO	CaO	Na ₂ O	K ₂ O	P ₂ O ₅
Count rate error (%)	0.6	0.8	1.0	1.0	3.0	1.5	0.6	0.7	0.6	1.6
Std. error of estimate (wt.%)	0.54	0.03	0.52	0.15	0.01	0.30	0.09	0.20	0.07	0.01
Calibration range: lower	8.00	0.00	0.00	0.00	0.00	0.00	0.00	0.00	0.00	0.00
: Upper	80.00	3.20	23.00	14.80	0.20	50.00	32.50	5.40	5.00	0.60
Detection limit (wt.%)	0.086	0.018	0.087	0.045	0.012	0.165	0.006	0.155	0.002	0.018
Accuracy (± wt%) (avg. deviations of 11 standards)	0.46	0.11	0.36	0.10	0.008	0.13	0.17	0.26	0.09	0.02
Precision c% : G-SL	0.76	1.55	0.75	1.45	11.10	6.47	1.34	4.35	1.03	4.35

Table 4.2: Chemical Content of Whole Soil and Rock Samples

SAMPLE No.	ELEMENTS (%)										
	SiO ₂	TiO ₂	Al ₂ O ₃	Fe ₂ O ₃	MnO	MgO	CaO	Na ₂ O	K ₂ O	P ₂ O ₅	SiO ₂ /Al ₂ O ₃
404.08	75.24	0.18	20.86	2.41	0.02	0.18	0.00	0.00	0.76	0.03	3.61
404.07	75.18	0.15	16.16	2.18	0.08	0.18	0.00	0.40	5.32	0.01	4.65
404.06	75.16	0.13	16.12	2.20	0.06	0.25	0.00	0.44	5.45	0.01	4.66
404.05	75.44	0.12	15.58	2.28	0.06	0.28	0.00	0.66	5.54	0.02	4.84
404.04	77.60	0.12	11.78	1.32	0.08	0.23	0.63	2.95	5.10	0.02	6.58
404.03	77.61	0.12	11.98	1.41	0.08	0.23	0.63	2.98	5.07	0.02	6.48
404.02	77.70	0.12	11.85	1.27	0.03	0.28	0.67	2.92	5.05	0.02	6.56
404.01	76.85	0.13	11.74	1.59	0.08	0.28	0.85	3.08	5.53	0.02	6.55

Table 4.3: Chemical Content of Clay Fraction (<2 μ m) of Soil Samples

SAMPLE No. ↓	ELEMENTS (%)										
	SiO ₂	TiO ₂	Al ₂ O ₃	Fe ₂ O ₃	MnO	MgO	CaO	Na ₂ O	K ₂ O	P ₂ O ₅	SiO ₂ /Al ₂ O ₃
404.08	49.03	0.20	43.98	5.08	0.00	0.39	0.00	0.00	0.50	0.03	1.11
404.07	48.78	0.21	41.21	5.29	0.15	0.39	0.00	0.00	0.72	0.04	1.18
404.06	50.55	0.14	42.09	5.22	0.01	0.24	0.00	0.00	0.79	0.03	1.20
404.05	50.83	0.17	41.43	5.09	0.05	0.40	0.00	0.00	0.96	0.05	1.23

Table 4.4: Fe Concentration Factor Between Whole Soil and Clay Fractions

Sample No. ↓	Concentration Factor = $\frac{\text{Fe}_{\text{clay}} \text{ (from Table 4.3)}}{\text{Fe}_{\text{whole soil}} \text{ (from Table 4.2)}}$
404.08	2.11
404.07	2.43
404.06	2.37
404.05	2.23

Table 4.5: Fe Content of Untreated and Treated Soils

SAMPLE No. ↓	IRON OXIDE CONTENT (%)			
	*Whole Soil	**Clay Fraction	NaOH Residue	HF Residue
404.08	2.41	5.08	†16.25	†16.25
404.07	2.18	5.29	†16.25	8.50
404.06	2.20	5.22	9.75	5.25
404.05	2.28	5.09	10.25	6.35

* From Table 4.2.

** From Table 4.3

† This agreement is presumably fortuitous.

Table 4.6: Fe Concentration Factor Following Chemical Concentration Using NaOH and HF

SAMPLE No. ↓	CONCENTRATION FACTORS			
	NaOH TREATMENT		HF TREATMENT	
	*Whole Soil	**Clay Fraction	†Whole Soil	††Clay Fraction
404.08	6.74	3.20	6.74	3.20
404.07	7.45	3.07	3.90	1.61
404.06	4.43	1.87	2.39	1.01
404.05	4.49	2.01	2.78	1.25

* $\frac{\text{Fe NaOH residue (see Table 4.5)}}{\text{Fe whole soil (from Table 4.2)}}$	** $\frac{\text{Fe NaOH residue (see Table 4.5)}}{\text{Fe clay (from Table 4.3)}}$
† $\frac{\text{Fe HF residue (see Table 4.5)}}{\text{Fe whole soil (from Table 4.2)}}$	†† $\frac{\text{Fe HF residue (see Table 4.5)}}{\text{Fe clay (from Table 4.3)}}$

Table 4.7: Fe Content of Ammonium Oxalate Dissolved Clay Fraction

Sample No.	Fe _o (%)	*Fe _t	Fe _o /Fe _t	**Fhest (= 1.7 x Fe _o %)
404.08	0.04	5.08	0.008	0.068
404.07	0.12	5.29	0.023	0.204
404.06	0.16	5.22	0.031	0.272
404.05	0.18	5.09	0.031	0.306
Synthetic Ferrihydrite	62.14	n.d	n.d	105.64
Synthetic Goethite	none	n.d	-	-
Synthetic Hematite	none	n.d	-	-

* Values from Table 4.3.

** Estimated ferrihydrite concentration from Fe_o (after Childs, 1985).

Table 4.8: pH of the Soil Samples

Sample No.	pH(H ₂ O)	pH(KCl)
404.08	5.010	4.140
404.07	5.900	4.795
404.06	6.805	6.075
404.05	5.765	4.385

Table 4.9: Organic CO₂ Content of the Soil Samples

Sample No.	Organic CO ₂ %	
	Whole Soil	Clay Fraction
404.08	0.18	0.98
404.07	0.31	1.49
404.06	0.43	0.95
404.05	0.45	1.49

CHAPTER 5

ELECTRON MICROSCOPY

5.1 INTRODUCTION

This chapter discusses all the aspects of electron microscopy that are related to the present investigation. Electron microscopy is a major technique used in the present investigation for the identification and characterisation of the clay and iron oxide minerals. Both transmission and scanning electron microscopy have been used by soil mineralogist for some time, but the initial inavailability of the equipment put considerable constraint on their wide usage. The method has the advantage of allowing a direct observation of the various soil particles and identification of the particles can sometimes be made on the basis of morphology. For the transmission electron microscopy, the possibility of electron diffraction which can be applied to a single crystal or a group of particles is an added advantage in mineral identification and characterisation. Although both transmission and scanning electron microscopes were used in the investigation, only the transmission microscope was used to a great detail while the scanning microscope was used mainly as support. Hence, only the transmission microscopy will be discussed in detail, and, where necessary, the results of scanning electron microscopy will be presented alongside those of transmission electron microscopy.

A brief general review of electron microscopy is given in Section 5.2. Section 5.3 discusses the principles of the electron microscope, Section 5.4 discusses the lens defects which may be hindrances to the succesful retrieval of

Chapter 5: Electron Microscopy

vital information from electron microscopy, while the interactions that occur between the beam and the specimen are given in Section 5.5. Section 5.6 discusses radiation damage, Section 5.7 discusses electron diffraction and Section 5.8 discusses the direct resolution of the crystal lattice (high resolution electron microscopy). The experimental methods used are given in Section 5.9 and the results of electron microscopy investigation on the samples are presented in Section 5.10. A summary of some of the important findings of the study in this chapter is presented in Section 5.11.

5.2 GENERAL

The transmission electron microscope (TEM) was developed in the 1930's and 40's (Ruska, 1934; von Borries and Ruska, 1939; Burton et al; 1939; Hillier and Vance, 1941; von Ardenne, 1944; Hillier and Ramberg, 1947) and has been commercially available since then. The first commercial scanning electron microscope was made available by the Cambridge Scientific Instrument Company in 1965. The principles and practice of transmission electron microscopy are covered in many texts, including Kay (1965), Hirsch et al. (1965), Beeston et al. (1972), Edington (1976), Wenk (1976), Fryer (1979), Smart and Tovey (1981, 1982), and Nadeau and Tait (1987) while those of scanning electron microscopy are adequately presented in Smart and Tovey (1981, 1982), and McHardy and Birnie (1987). One of the first notable works on electron microscopy of clay minerals was by Ardenne et al; (1940) who showed the electron microscope to be another powerful tool (apart from the optical microscope and X-ray diffractometer that were already in use at the time) for the investigation of clay minerals. It provided precise information on the shape and morphology of the extremely small particles making up these materials (Grim, 1988).

More recently, with improvement in resolution of modern electron

microscopes, electron microscopy has been extended to the study of the mineral structure of soil components. It offers the advantage of allowing the direct observation of individual particles of the soil components and the initial optimism of the likelihood of identifying clay minerals on the basis of their shape was only abandoned when it was found that clay particle shape changes with condition of formation and degree of weathering (Kittrick, 1965). However, the later possibility of obtaining electron diffraction of the individual particles further enhanced the study of clay mineralogy by electron microscopy methods.

Iron oxide mineralogy of soils has especially benefited from electron microscopy techniques. The low concentration and crystallinity of iron oxides in most soils compared to the clay minerals often limit their study by methods such as X-ray diffraction, while the small size of the particles puts them beyond the limit of the resolution of the light microscope. Transmission electron microscopy studies of soil iron oxides have been used in the determination of mineralogy (e.g. Schwertmann and Kampf, 1985), crystal morphology and size (e.g. Greenland et al; 1968; Smith and Eggleton, 1980; Schwertmann and Latham, 1986; Eggleton, 1987 and Schwertmann, 1987(a)), and association with other soil minerals (e.g. Greenland et al; 1968, Smart, 1973 and Schwertmann, 1987(a)). More extensive studies of synthetic iron oxide minerals have been done by electron microscopy techniques and brief reviews of some of these studies are available in Eggleton, (1987) and Schwertmann, (1987a).

5.3 PRINCIPLES OF THE ELECTRON MICROSCOPE

The main features of a modern transmission electron microscope are shown in Figure 5.1. The microscope uses a series of magnetic lenses to focus an electron beam that is accelerated, by a high potential, through the specimen. Electrons are greatly influenced by the medium through which they pass and have

Chapter 5: Electron Microscopy

almost no penetrating power. They can only travel for any reasonable distance in a vacuum. Accordingly, the pressure in the column must be maintained at 10^{-3} Pa or less and the specimen must be very thin. An electrically heated cathode at selected negative potential emits electrons. A tungsten hair-pin filament is usually employed (Haine and Cosslet, 1961; Hall, 1966). However, better brightness can be obtained using a special pointed tungsten filament (Wolf and Joy, 1971) or from a lanthanum hexaboride cathode (Ahmed, 1971; Batson et al; 1976, Yonezawa et al; 1977). The use of a field emission gun (Crewe et al; 1968) as an alternative to electrical heating derives similar benefits.

The electrons are accelerated by the electrical potential difference between the filament and anode and are focussed, via a double condenser lens system with field-limiting aperture, unto the specimen. An image or diffraction pattern from the specimen is obtained on a fluorescent screen via a three- or four- lens magnification system and can be recorded on a photographic plate. Image contrast may be enhanced by the use of an objective aperture, and the area for diffraction may be selected by a selected area aperture. The image is focussed with the objective lens, and magnification is controlled by the excitation of the intermediate and/or diffraction lens.

The resolution of a microscope is an important parameter to be considered in electron microscopy work. The instrument resolution of a microscope can be defined as the smallest distance that can exist between two separate objects before they appear as one under the microscope (Kittrick, 1965). In light microscopy the resolution is limited by the nature of light. The way in which radiation and matter interact limits resolution to about one-half the wavelength of the light used. Many light microscopes can use light with wavelength of about 400nm (4000Å); which will give a resolution limit of about 200nm (2000Å); i.e; if two objects are 200nm (2000Å) apart, they will appear to be only one object. In the electron microscope, it is possible to use electrons that have a wavelength of less

than 0.005nm (0.05Å), depending on the accelerating voltage, which gives a theoretical resolution limit of about 0.0025nm (0.025Å). However, lens defects such as astigmatism, chromatic and spherical aberrations (and other aberrations), which are discussed Sections 5.4, set a practical limit to the performance of the electron microscope and limit the resolution. Nevertheless, in general, the accuracy of operation and calibration of the instrument control the quality of electron micrographs, and the precision with which they can be analysed quantitatively.

In the case of the JEOL JEM 1200EX electron microscope used in this study, either a pointed tungsten filament or a lanthanum hexaboride cathode was used as a source for electrons. The image forming lenses number six; namely, an objective lens, an objective mini-lens, three stage intermediate lenses and a projection lens. Using this configuration the magnification may be altered from 50 to 1,000,000. The whole optical column is maintained at a vacuum of 10^{-5} Pa. This microscope has an accelerating voltage of 120kV and as such an electron beam wavelength of 0.003nm.

5.4 LENS DEFECTS

Like glass lenses, all electromagnetic lenses suffer from defects such as coma, barrel or pincushion distortion, astigmatism, chromatic and spherical aberration. From the operator's standpoint the last three are the most important in relation to the objective lens because they determine the resolution of the electron microscope (Edington, 1974).

5.4.1 Astigmatism

This is caused by a defect in the magnetic field due to asymmetry of the lens, resulting in differing lens strength in two directions at right angles. The

defect arises from lack of perfection in manufacture, in particular lack of circularity in the bores and flatness of the pole-pieces or inhomogenities in the material of the lens itself. In addition, astigmatism may be due to contamination within the microscope column which builds up a charge and distorts the field. The result is that a point object is imaged as two mutually perpendicular lines at different levels in image space, causing a directional structure in the image.

Astigmatism of the condenser lens system is important because it reduces the coherence of the beam, while that of the objective lens is important because it can cause a serious loss in image resolution. Condenser astigmatism is manifested by an elliptical illumination spot when the condenser 2 is defocussed. The astigmator is adjusted to make the defocussed spot circular. Objective astigmatism is manifested by streakings in one direction of fine detail of the image (Edington, 1974). The defect may be corrected by using compensating cylindrical lens fields which affect each other at right angles.

5.4.2 Chromatic aberration

Chromatic aberration arises because of the energy, and therefore wavelength, spread of the electron beam. Instabilities in accelerating voltage or lens current could be contributory factors, but both are negligible because of the high stability of modern power supplies (Edington, 1974). Although there is a small energy spread, 3 eV, in the electron beam leaving the tungsten filament in the electron gun, the major factor is the large energy loss $\Delta E = 5$ to 50 eV suffered by many electrons on passing through the specimen (Edington, 1974). In effect the focal length of the lens varies with the electron energy and a disc of confusion, radius Δr_c , is produced given by

$$\Delta r_c = \frac{C_c \beta \Delta E}{E} \quad [5.1]$$

where C_c is the chromatic aberration constant of the lens and is approximately equal to its focal length, β is the lens aperture, E is the energy of the electrons (without loss) and ΔE is the energy loss. The effect of chromatic aberration is negligible at low resolution, but at high resolution it sets a limit to the resolution of the microscope.

5.4.3 Spherical Aberration

Spherical aberration is the inability of a lens to focus all incident electron beam from a point source to a point focus. The outer zones of the lens have a greater strength so the off-axis beams are always bent more and brought to a focus before those close to the axis. Therefore, a point in the object is imaged by the objective lens as a disc, known as the disc of least confusion; the disc diameter, d_s , is given by:

$$d_s = \frac{1}{2C_s\alpha^3} \quad [5.2]$$

where C_s is the spherical aberration coefficient and α the semi-angular aperture of the lens.

Spherical aberration cannot be compensated for, but can be minimised to some extent by reducing the angular aperture, by insertion of a limiting aperture in the back focal plane of the objective lens. Unfortunately, insertion of this aperture will give rise to interference effects or diffraction as well as loss of information of the image transfer properties of the beam, due to removal of scattered electrons.

5.5 BEAM – SPECIMEN INTERACTION

The interaction of a high-energy electron beam with a solid specimen

generates a variety of signals all of which yield information on the nature of the solid. The events of interest to transmission electron microscopy, where very thin films of solid are studied are shown in Figure 5.2. When interacting with the atoms of a solid, impinging electrons may suffer two types of scattering processes:

(a) elastic scattering, due to interaction with the nuclei in the specimen – this does not involve transfer of energy to the atoms.

(b) inelastic scattering, due to interaction with the orbital electrons in the specimen thus involving energy transfer and absorption.

Although TEM will make use of both elastically and inelastically scattered electrons, the major imaging techniques are based on the elastic processes. More detailed presentation can be seen in Hirsch et al. (1965) and Humphreys (1979). The ratio of directly transmitted electrons to that of elastically scattered is related to the contrast of the images in TEM. Images of crystalline specimens are largely influenced by Bragg reflections. Inelastically scattered electrons may cause chromatic aberration in the image formation process. The absorbed energy, i.e. the energy which scattered electrons have lost while passing through the specimen, results in excitation of the atoms and atomic nuclei in the specimen. This causes heating, magnetism, ionisation etc.

5.6 RADIATION DAMAGE

Most materials undergo some form of alteration during examination in the electron microscope. To the extent that such alterations affect the integrity of the information sought from the specimen, they are referred to as 'radiation damage', but, when the effects prove incidental to this information, they are largely ignored.

Radiation damage frequently occurs in minerals and other inorganic materials (Burton et al; 1947; Dahmen et al; 1978; Fryer, 1979; Hobbs, 1979, 1984, 1987; Csencsits and Gronskey, 1987; Sharma et al; 1987 and Smith et al;

1987). As the present work is concerned with inorganic materials, it would be useful to consider here the various ways in which electron microscopical examination of the materials can be hampered by their radiation sensitivity and to mention some of the the methods that may be employed to alleviate the problem. Since this project is not concerned with a study of the process involved in radiation damage, only an introduction to the problem will be provided in this section.

There are basically two avenues for electron beam damage in the TEM:

(a) "Knock-on displacement from the bulk (Mckinley and Feshbach, 1948; Seitz and Koehler, 1956) which involves the interaction of the incident electron with the cores of atoms in the specimen and occurs above the critical energy thresholds.

(b) Radiolytic mechanisms which involve the transfer of energy from the incident electrons to the electrons in the specimen leading to bond breakage and consequently to the possible alteration of the structure (Hobbs, 1987).

Many attempts have been made to minimise radiation damage. Encapsulation of organic crystals by carbon films proved to be extremely successful (Fryer and Holland, 1984; Holland, 1984) and image intensifiers have been used to aid focus adjustment when low beam doses are used (Reynolds, 1968; English and Venables, 1971, 1972; Hart and Yoshiyama, 1975). A system that permits photography of beam sensitive specimens with a minimum dose in the high resolution region has been developed (Williams and Fisher, 1970; Fujiyoshi et al; 1980). This system was named the Minimum Dose System (MDS) and has been used effectively in taking HREM photographs of beam sensitive specimens without sacrificing the resolving power of the electron microscope (Fujiyoshi et al; 1980; Uyeda et al; 1980; Fryer, 1983). The additional use of either nuclear track emission (Kuo and Glaeser, 1975) or x-ray films for image recording, have also been reported as providing further useful

gains (Fryer, 1978; Fryer et al; 1980).

Although sample heating which may occur due to beam-sample interaction in the electron microscope was initially thought of as a possibility that could lead to phase changes in iron oxide minerals, initial tests did not reveal any need for the use of any special sample preparation procedure or microscopy technique in this study.

5.7 ELECTRON DIFFRACTION

A crystalline specimen will diffract the electron beam strongly through certain angles, according to the Bragg law (see Eqn. 5.4). The diffracted beams, along with the undeviated incident beam are brought to a focus at the back focal plane of the objective lens, to form an electron diffraction pattern (EDP). Electron diffraction patterns and microscope images are closely related by the fact that electrons scattered by a specimen provide EDP at the back-focal plane of the objective lens and images are formed from this through a Fourier transform operation. Thus the EDP and the intermediate image are always present in the electron microscope and the intermediate lens setting determines which is projected onto the image plane. In normal imaging mode, the intermediate lens is focussed on the first intermediate image (see Figure 5.3a), whilst for electron diffraction, the intermediate lens is focussed on the back focal plane of the objective lens producing a magnified image of the diffraction pattern which is further magnified by projector lenses and displayed on the screen (Figure 5.3b). Since the electron beam is diffracted by the electrons and nuclei in the atoms of the particle, the electron diffraction pattern contains information about the structure of the specimen under examination. The theory and principle of electron diffraction has been discussed in details by Beeston (1972), Edington (1974), Andrews et al. (1971) and Nadeau and Tait (1987) amongst others.

In order to be able to correlate between features observed in the specimen and its crystallography, it is essential to be able to form a diffraction pattern from a specific region of the specimen. This process is known as selected area diffraction (SAD) and the principle is illustrated in Figure 5.4. Here there is an incident beam covering the specimen, and all transmitted and diffracted rays contribute to the diffraction pattern formed in the back focal plane of the objective lens. If an aperture of diameter D is inserted coplanar with the image, only the transmitted and diffracted rays that originate within the region given by D/M (where M is the magnification of the objective) can reach the final screen. The apertures inserted in the plane can typically be as small as $20\mu\text{m}$. With an objective magnification of 50 times a selected area of only $0.4\mu\text{m}$ in diameter can be analysed. The procedure for performing SAD has been described by Agar (1960) and Phillips (1960) based on the technique developed by Le Poole (1947).

Typical electron diffraction patterns are composed of a simple array of bright spots for a single crystal diffraction and concentric rings for polycrystalline specimens, where the specimen consists of a large amount of crystals at different orientations from each other.

The formation of the electron diffraction pattern is shown diagrammatically in Figure 5.5 for a set of lattice planes, spacing d , at an angle θ to the electric beam. If R is the distance between the incident and the diffracted beam at the plane of the photographic plate and L the camera length, which is dependent upon the lens excitation, then:

$$\tan 2\theta = R/L \quad [5.3]$$

Now the Bragg law states that

$$\lambda = 2d \sin \theta \quad [5.4]$$

and since the angle θ , through which the electrons are diffracted are very small, only $1^\circ - 2^\circ$ (Beeston, 1972), the approximation

$$\tan 2\theta = 2 \sin \theta, \quad [5.5]$$

can be made with very little error. Then,

$$R/L = \lambda/d, \quad [5.6]$$

$$\text{or } Rd = \lambda L, \quad [5.7]$$

So if values of R , L and λ for a particular diffraction spot or ring can be measured, then the d -spacing of the set of lattice plains giving rise to that spot or ring can be determined. This procedure can be repeated for all the spots or rings in the diffraction pattern, and a list of d -spacings can be compiled for all the sets of planes in the specimen which are reflecting. These d -spacings can then be used to determine a number of important pieces of information about the specimen (Beeston, 1972).

In practice, a standard specimen of known diffraction spacings (e.g. graphite, thallos chloride or gold) is used as a calibrating standard so that λL is obtained and the unknown is studied under the same microscope conditions. The d -spacing of the unknown is obtained using the equation:

$$d_{(\text{unknown})} = \frac{\lambda L_{(\text{from standard})}}{R_{(\text{measured})}} \quad [5.8]$$

The accuracy of the calibration depends upon the experiment, but an error of $\pm 2\%$ should be achieved reasonably easily and further improvements are possible,

down to $\pm 1\%$, with considerable care both in operation of the microscope and in measurement and corrections of the plate (Edington, 1974). In this study, graphite evaporated on the carbon film on which the specimen was placed for microscopy was used as a standard. Errors of the order of 0.05% were obtained for measurement of the d - spacings of the graphite standard.

Generally, the identification of a substance from an electron diffraction pattern is accomplished by comparing electron diffraction data with the available X-ray diffraction data published by the Joint committee on Powder Diffraction Standards (Philadelphia, USA).

5.8 DIRECT RESOLUTION OF THE CRYSTAL LATTICE (HREM)

With present high - resolution microscopes it is possible to resolve the individual lattice planes in suitably chosen thin crystals. In this method, referred to as direct (or high) resolution microscopy and first applied to platinum phthalocyanine by Menter (1956), two, or possibly more of the diffracted waves are allowed to contribute to the final image (details can be seen in Amelinckx, 1964 and Howie, 1965). The interference between these waves results in the formation of fringe pattern of average spacing equal to the lattice spacing d (or possibly to some submultiple of d). Small local variations in fringe spacings can result from changing thickness or orientation of the crystal. These effects have been discussed by Hashimoto et al; (1960). The fringe patterns are located not only at the exit surface of the crystal but also at a number of other planes, the so-called Fourier image planes (Cowley and Moodie, 1957), and hence the details of the observed image depend on where the microscope is focussed. A number of other factors such as lens aberrations and inelastic scattering effects in the specimen are also of importance in determining the fringe profile (Howie, 1965). The main advantage of the method is that lattice structure and any imperfections

in it are directly resolved. The presence of dislocations, for instance, may be indicated as extra half planes in the fringe structure; although their Burgers vector cannot be assigned from a simple two beam image.

For the direct resolution method more stringent requirements for specimen preparation and microscope resolution and operation are often demanded compared to those required for lower resolution electron microscopy. The specimen has to be sufficiently thin and all lens aberrations such as astigmatism of the condenser and objective lenses have to be eliminated as much as possible in order to obtain lattice images and for accurate interpretation of the micrographs. Also, because specimen drift (see Agar, 1965) is more pronounced at high resolution microscopy, it is often required that photographs are taken at as short time as possible. This demands that the electron beam intensity be turned sufficiently high to obtain adequate illumination of the object for photography within a short time. Such high electron beam intensity may, subsequently, lead to electron beam damage in some highly electron beam sensitive materials and high resolution microscopy may have to be combined with other techniques (see Section 5.6) such as the minimum dose technique or use of special X-ray films for these materials (see Fryer, 1979).

Most modern TEMs can be expected to resolve to 0.3nm, and at this resolution are suited to lattice imaging. The JEOL JEM 1200EX used in this study has a point resolution of 0.3nm but could resolve lattices at 0.2nm. Operated at about 200,000 to 300,000 magnification, lattice fringes of about 0.3nm spacing were easily observed. Since iron oxide particles are subject to phase and, hence, structural changes following heating which may be caused by interaction of the particles with the electron beam, during high resolution microscopy, adequate precaution was taken to avoid long exposure of the samples to the electron beam by carrying out microscope adjustments such as rough focussing and correction of objective lens astigmatism on a sample on a different

grid square from that to be photographed and exposure time was limited to between 2 and 3 seconds during photography. Initial tests conducted on the iron oxides showed them to be stable for the period required for high resolution microscopy using this precautionary measures. A series of photographs at different adjustments of focus were taken of each area in order to ensure correct interpretation of the micrographs.

5.9 EXPERIMENTAL METHODS

The sample preparations for electron microscopy were done as follows:

5.9.1 Transmission Electron Microscopy

The sample was crushed lightly, under distilled water, with an agate mortar and pestle. The soil-water mixture was then dispersed ultrasonically by placing a test tube containing the mixture in an ultrasonic bath. After dispersion, some of the mixture was withdrawn with a finely drawn disposable pipette and a drop placed on a carbon coated copper grid and allowed to dry in air. This procedure produced dispersed samples ready for electron microscopy observation.

5.9.2 Scanning Electron Microscopy

Fractured surfaces were prepared for scanning microscopy by first saturating the soil pieces with distilled water. The water was gradually replaced by acetone, by successively passing through 1:4, 1:1, 3:1 acetone-water mixtures, and finally into 100% acetone. The acetone was changed daily for 7 days (this time was found adequate for $\pm 20 \times 20 \times 20$ mm samples) to allow all the water in the pores to be replaced by acetone. The samples were then dried by critical point drying using CO_2 (see Smart and Tovey, 1982 and McHardy and Birnie, 1987). The critical drying apparatus used was a Polaron Model E3000 equipped with a liquid transfer boat with integral drain valve.

The dried specimens were mounted on aluminium support stubs using silver paint and coated with gold-palladium alloy before observation. Either a Phillips SEM 500 or a Cambridge Instruments STEREOSCAN 360 was used for scanning electron microscopy observations.

5.10 RESULTS

5.10.1 Clay Mineralogy

Some aspects of the clay mineralogy of the soils have been presented under X-ray diffraction (Chapter 6) and infrared spectroscopy (Chapter 7), and it is advised that these be read in conjunction with the results presented in this section. An advantage of electron microscopy is that the soil particles can be observed directly and the morphology of the clay particles determined.

The transmission electron micrograph of a section of the ultrasonically dispersed, but whole soil Sample 404.05 is shown in Figure 5.6. The predominant soil minerals were in the form of long "rolled-up" tubes. Some of the tubes were found to be up to $9\mu\text{m}$ long and many were up to $4 - 5\mu\text{m}$ long even after ultrasonic dispersion. The selected area diffraction of a tube (Figure 5.7) showed the typical streaked pattern indicative of a tubular morphology (Nadeau and Tait, 1987). The pattern showed reflections with d -spacings of 0.739nm, 0.445nm, 0.421nm, 0.358nm, 0.254nm, 0.224nm, 0.151nm and 0.149nm. Comparison of these reflections with standard tables suggested the tubes to be halloysite (7A) and the 0.739nm and 0.358nm reflections could be assigned to the basal (001) and (002) reflections respectively. Measurement of the space between the rows of streaks, which represents the b -axis elongation of the halloysite particles (Nadeau and Tait, 1987), gave a value of $b = 8.915\text{\AA}$ and compares well with that given for halloysite ($b = 8.92\text{\AA}$) in the Powder Diffraction File. In addition to the halloysite tubes, very few, large irregular

plates could be seen in the micrographs. The electron diffraction of one of the plates is shown in Figure 5.8 and reflections at 0.445nm, 0.257nm, 0.225nm, 0.170nm and 0.149nm amongst others indicated the plates to be clay. The characteristic of the diffraction pattern and tracings is however typical of many clays and it is difficult to identify the clay on the basis of electron microscopy alone. However, X-ray diffraction (discussed in Chapter 6) suggested the clay to be mica (most probably muscovite, which was present in the unweathered rock). The electron micrograph of the clay fraction of the same sample (404.05) shown in Figure 5.9 revealed a similar mineralogy, with tubular halloysite particles accounting for over 90% (visual estimation from several micrographs) of the clay minerals, while platy clay muscovite could also be seen on the micrographs. In this case however, most of the halloysite particles are shorter (1 to 3 μ m long) than those seen in the whole soil but gave similar reflections and structural properties. It thus appeared that halloysite tubes were present as silt size and clay size minerals in the soil. The results of complementary scanning electron microscopy on fractured surfaces of the soil (Figure 5.10) also confirms this finding. In Figure 5.10 fibrous particles which are similar to the halloysite tubes seen in the transmission electron micrographs could be seen. Some of the fibres, which appeared to be forming from a primary mineral (probably a plagioclase feldspar, as discussed in Chapter 4, although no detailed investigation of the formation of halloysite from the primary minerals was done) could be seen to be up to 8 μ m long, while smaller particles could also be seen in the figure. It is possible that some of the halloysite particles in the clay fraction were produced directly from the primary minerals while others were derived from a mechanical break down of the larger particles. This possibility may be partly responsible for some of the earlier findings on the particle size distributions of these soils (Irfan, 1986) and similar soils from Hong Kong (Lumb, 1962). Lumb (1962) reported that considerable variation in grading

and voids ratio of the decomposed granite can occur in small volumes of soil and these variations seemed haphazard and quite unpredictable even within a single trial pit and bore hole. Irfan (1986) did particle size analysis for the soils used in this investigation using two methods: one which involved drying the soil and breaking it down with a porcelain pestle and mortar and another which involved, in addition to this, finger crushing of the soft feldspar grains which were not dispersed during pretreatment. The author found that for a soil, the clay content increased from 4% (using the first method) to 12% (using the second method). Apart from other likely causes such as the effectiveness of dispersive agents etc, it is clear from the results of this investigation that a breakdown of silt size halloysite to clay size fractions due to mechanical treatments such as finger crushing or crushing in a mortar, shaking, ultrasonic dispersion etc; is highly likely. A variation in the method of treatment and amount of mechanical treatment given to the soil before particle size determination may lead to haphazard results.

The results obtained for the shallower Sample 404.06 were similar to those presented above for Sample 404.05. Figure 5.11 shows a section of the dispersed clay fraction of the soil. Halloysite tubes were predominant, and muscovite plates were the other clay minerals identified in the soil.

Sample 404.07 showed a slight variation in mineralogy from Samples 404.05 and 404.06. Figure 5.12 shows a section of the dispersed soil. As was the case with the previous samples halloysite tubes as well as clay plates could be seen on the micrograph. In this case however, the proportion of halloysite had decreased while that of the clay plates had increased. In most of the micrographs, an almost equal proportion of halloysite tubes and clay plates was indicated. Also, most of the clay plates in the clay fraction of the soil could be seen to be smaller (most less than $1\mu\text{m}$) than those seen in the deeper soils. An

electron diffraction study showed the smaller clay plates to be kaolinite (see inset in Figure 5.12). Similar results were obtained for the soils in X-ray diffraction (Chapter 6).

Electron microscopy observation of the residual Sample 404.08 (Figure 5.13) showed a continuation of the trend noted above. The halloysite tubes had decreased further relative to the clay plates (observation from Figure 5.13 and several other micrographs), and more plates than tubes could be seen in the micrographs. The majority of the clay plates were kaolinites (from electron diffraction, see inset in Figure 5.13) and the size could be seen to be less than $1\mu\text{m}$ in most cases, thus confirming the results obtained from infrared spectroscopy (Chapter 7). The length of the halloysite tubes was also shorter (many, about $1\mu\text{m}$ or less). Scanning electron microscopy of the soil (Figure 5.14) also confirmed the results obtained from transmission microscopy. In Figure 5.14, small clay plates and short tubes are indicated. Hence, in this soil, kaolinite has replaced halloysite as the major clay mineral in contrast to Sample 404.05. The general trend appeared to be a gradual replacement of halloysite by kaolinite in the soils as weathering increased. It is possible that the kaolinite was produced directly from one or more of the primary minerals (feldspars or biotite) or from the halloysite, although this aspect was not investigated in this study. Hydrothermal alteration which was reported to have taken place in some parts of the site is also a possible source for kaolinite (Irfan, 1986).

Halloysite tubes had previously been reported in weathered granites from Hong Kong by Parham (1969a,b) and Lumb and Lee (1975). From electron microscopy Parham (1969a,b) concluded that neither halloysite nor kaolinite were produced by direct decomposition of the feldspars but that some intermediate produce (allophane) was involved, formed at points of structural weakness on the feldspar surfaces, which subsequently changed to a kaolin mineral. The author inferred that under humid tropical conditions of weathering where good drainage

exists, a general sequence of mineral alteration occurs in which feldspars alters first to allophane, then allophane to halloysite and finally with sufficient time, halloysite to kaolinite. In the present investigation, Figure 5.10 and several other SEM micrographs of the soils appeared to indicate that the halloysite tubes "grew" out singly and directly from the primary mineral, and no indication of formation from an intermediate product was observed. In addition, no indication of the presence of allophane was given in any of the soils investigated by any of the identification methods used. Allophane, if present in any appreciable quantity should have been indicated by a large endothermic peak in the differential scanning calorimetry (reported in Chapter 7) at about 180 to 200°C.

5.10.2 Iron Oxide Mineralogy of Untreated Soils

Due to the low concentration of iron oxide in the soils, about 5% (see Chapter 4, Table 4.3), each grid of dispersed particles did not always produce iron oxide particles and a large number of grids were examined to allow enough observations to give a statistical significance. Concentrating the iron oxide in the soil by fractionating, to obtain the $<2\mu\text{m}$ fraction, increased the concentration of iron oxide in the soil two-fold (see Chapter 4 Table 4.4) and increased the chances of obtaining iron oxide particles from the grids while concentrating to obtain the $<1\mu\text{m}$ fraction was also helpful. Over 100 aggregates of iron oxide particles were examined for each soil.

Transmission electron microscopy of the general sections of the dispersed soil often showed the iron oxide minerals to be strongly self-aggregated in all the soils. The size of the aggregates were varied and ranged from less than $1\mu\text{m}$ to over $3\mu\text{m}$ although these may be fractions of larger aggregates which had been broken down by ultrasonic dispersion. The results of transmission and high resolution electron microscopy on the different soils are presented below:

(a) Sample (404.05)

A full description of this sample was given in Chapter 3. The soil was mottled, and separate areas of predominantly red and yellow staining could be seen. These areas were suspected to be iron oxide concentrated areas and were separated on the basis of colour, as outlined in Section 3.4.2(b), and each fraction examined by electron microscopy.

(i) Red mottles (Munsell 7.5R 7/8 to 7.5R 5/8)

As noted earlier, most of this red fraction was found around biotite particles, thus appearing to indicate formation from interlayer iron released from biotite. Electron microscope studies of the red mottles in this soil revealed the fraction to be composed of mainly halloysite (rolled-up tubes) particles with some iron oxide particles. As expected, electron microscopy indicated a higher concentration of iron oxide in these mottles than was the case when either the whole sample or the clay fraction of the soil were examined.

Figure 5.15 shows a typical aggregate of iron oxide particles seen in the mottles. Electron diffraction obtained from the particles is shown in Figure 5.16. The diffraction showed a very weak and diffused ring pattern and gave a reflection with spacing of 0.254nm. The diffused and broad nature of the electron diffraction ring in Figure 5.16 is an indication of the low crystalline nature of the particles. Due to the sub tropical origin of the soils, ferrihydrite was not expected as ferrihydrite had been found to be characteristic of cool or temperate, moist climates (Schwertmann, 1985). However, other aggregates of iron oxide particles seen in the red mottles such as that shown in Figure 5.17 gave similar reflections which suggested them to be ferrihydrite particles. Also, comparison of these particles and the electron diffraction patterns with those of goethite particles which were later identified in the soil showed them to differ in particle morphology and diffraction pattern. In most cases, for the ferrihydrite

particles, electron diffraction patterns showed very weak reflections and only the 0.254nm(100) reflection, which is the strongest ferrihydrite reflection, was clearly visible.

Although aggregation of the particles hindered the morphology of the individual ferrihydrite particles from being ascertained in most cases it could be seen from Figures 5.15 and 5.17 that the particles have rounded edges and appeared likely to be spherical. Figure 5.18 shows another micrograph of ferrihydrite particles. In this case the particles are better dispersed and individual particles of ferrihydrite, could be seen to have rounded edges (similar to those observed in previous micrographs). Measurement of the distances across each particle from different points on the particle showed very little variation thus indicating the spherical nature of the particles since there was no variation in contrast within the particles that would indicate them to be discs. Measurement of the diameter of 90 particles obtained from available micrographs showed the size of the particles to vary within the narrow range of 5.1nm and 5.6nm with an average size of about 5.5nm. Since some earlier studies (e.g Parham, 1969a,b and Lumb and Lee, 1975) had suggested the possibility of allophane occurring in the Hong Kong weathered granites and considering the similarities in some properties of allophane and ferrihydrite, e.g spherical morphology and low crystallinity (Henmi and Wada, 1976 and Wada, 1977), the possibility of the particles being allophane rather than ferrihydrite was investigated. The absence of the 0.33nm reflection, which is the strongest allophane reflection (Wada, 1977), in any of the diffraction patterns obtained distinguished these particles from allophane.

In order to verify some of the properties obtained for the soil ferrihydrite, electron microscopy was performed on a synthetic ferrihydrite prepared as outlined in Section 3.7.1. A high resolution image of a typical view of synthetic ferrihydrite particles is shown in Figure 5.19. Electron diffraction pattern of the

ferrihydrate particles contained 6 broad rings with the diffraction spacings shown (Figure 5.20). The shape of the particles could be seen to be similar to those of the soil ferrihydrate shown in Figure 5.18. The diameter of the particles, obtained from several micrographs, ranged between 3.2nm and 5.3nm with an average size of about 4.6nm making them of comparable size to the soil ferrihydrate. The spherical morphology of most natural and synthetic ferrihydrate particles is well documented (e.g. Carlson and Schwertmann, 1981; Eggleton and Fitzpatrick, 1988)

Due to the trace amount percentage of the red mottles compared to the whole soil, it was only possible to examine a limited amount of iron oxide aggregates in the mottles. There was no indication of the presence of any other phase of iron oxides in all the aggregates examined in the red mottles and it would appear that ferrihydrate was the main form of iron oxide present in these mottles.

(ii) Whole soil and clay fraction

Due to the similarities in the results of electron microscopy observation on separate fractions of the whole soil and of the clay fractions ($< 2\mu\text{m}$), the results will be presented together in this section without differentiating between the two. Although it was desired to concentrate the iron oxide in the soil by fractionating, the effect of the dispersion agent (NaOH, in this case) was not known. It was therefore necessary to perform electron microscopy on both untreated sample and sample dispersed with NaOH prior to fractionating to check this effect. Similarities in the results of electron microscopy on the two samples suggested that no changes were effected on the iron oxide particles due to adjustment of the soil pH using NaOH and allowing the soil solution to stand for the time necessary for fractionating (8 hours). Fractionating caused a higher than two-fold concentration of the iron oxide content of the samples (as shown in

Table 4.4) and made electron microscopy easier thus making it possible to examine more particles.

Figure 5.21 shows a high resolution image of a typical aggregate of iron oxide particles seen in the sample. The 0.42nm lattice fringes corresponding to the (110) plane of the orthorhombic structure of goethite could be seen in the micrograph. The corresponding electron diffraction (Figure 5.22) shows ring patterns, which may be indicative of aggregation of the particles, with diffraction spacings which could be identified as goethite. The diffraction shows the 0.418nm (110) reflection to be the strongest reflection. Also, a high crystallinity of the goethite particles was often suggested from the sharpness of the diffraction rings.

Due to strong aggregation of most of the goethite particles it was not possible to determine the morphology of individual particles in most cases. In Figure 5.23, however, goethite particles which appeared to be laths were seen in the high resolution micrograph. The electron diffraction of the particles is shown as inset in the micrograph. Figure 5.24 shows some other aggregates of iron oxide particles found in the soil (particles labelled A, B, C, D and E in the figure are likely to be clay particles). Small laths as well as subrounded particles could be seen in the figure. The high resolution image of a group of laths labelled F in Figure 5.24 is shown in Figure 5.25. The 0.42nm lattice fringes evident on the laths indicated them to be goethite. Measurement of the width of ten laths in Figure 5.24 showed it to range from 3.1nm to 6.1nm with an average width of about 4.4nm. This measurement was done with the assumption that the particles were all lying on the same crystallographic axis and showing the (100) face. The morphology of this soil goethite can be compared with that of a synthetic goethite prepared as outlined in Section 3.7.2 (Figure 5.26). Goethite laths, with predominant (100) face, seen in the micrographs and those from several other micrographs have widths ranging from 16nm to 24nm with an

average width of about 20nm making them, generally, much larger than the soil goethites. The electron diffraction of the synthetic goethite particles is shown as inset in Figure 5.26 while the lattice image (also shown as inset in Figure 5.26) revealed the 0.50nm (020) and 0.42nm (110) lattice fringes.

Two diamond shaped particles labelled G and H in Figure 5.24 appeared to be goethite particles seen edge-on, i.e with the b -axis normal to the electron beam, and with visibility of the (110) face. Similarly shaped particles were reported for some impregnated and sectioned synthetic and natural goethite particles (Smith and Eggleton, 1980; Schwertmann, 1984; Schwertmann et al; 1985 and Mann et al; 1985). Clearly, the particle could be seen to have a single domain most probably running along the c direction. The dimensions of the particle were found to be 8.98nm by 20.32nm and compared well with the 10 by 20nm obtained by Smith and Eggleton (1980) for a soil goethite. A fault (arrowed on particle G) could be seen to run across the section and would appear to run along the crystallographic z -axis. The high resolution image of particle G (Figure 5.27) showed lattice fringes with spacings of 0.977nm which corresponded to the cell constant b_0 of the goethite particle. Lattice defects, perhaps caused by the fault mentioned earlier, could be seen on the particle. Mann et al. (1985) found that the morphology of synthetic goethite varied with Al substitution. According to them, crystals of goethite^e which consisted of many domains (multidomainic) parallel to the c axis, at zero substitution became less domainic with increasing Al substitution (see also Schulze and Schwertmann, 1984). Mann et al. (1985) stated that the interference of higher Al concentrations with crystal growth may be responsible for the decrease in domain number per crystal and the good visibility of the (110) faces of the acicular crystals (see Figure 5.28, below). Domains, or intergrowths, running parallel to the c axis and with a double chain of $\text{Fe}(\text{O}, \text{OH})_6$ in common are believed to form by secondary nucleation under conditions of high $[\text{OH}^-]$ and rapid growth.

Domain formation decreases with increasing Al substitution because the rate of growth is reduced. Ultimately, single crystals with a few well developed (110) faces form (Mann et al., 1985). In the present investigation, although it is not known how representative of the entire goethite particles the two particles (G and H) are, an Al substitution of 9.4 mole % found for Sample 404.05 (Chapter 6), with the single domain of the particles described above, appeared to agree well with the domain behaviour and Al substitution found by Mann et al. (1985) and the conditions that apply to the synthetic system may well apply in the soil system.

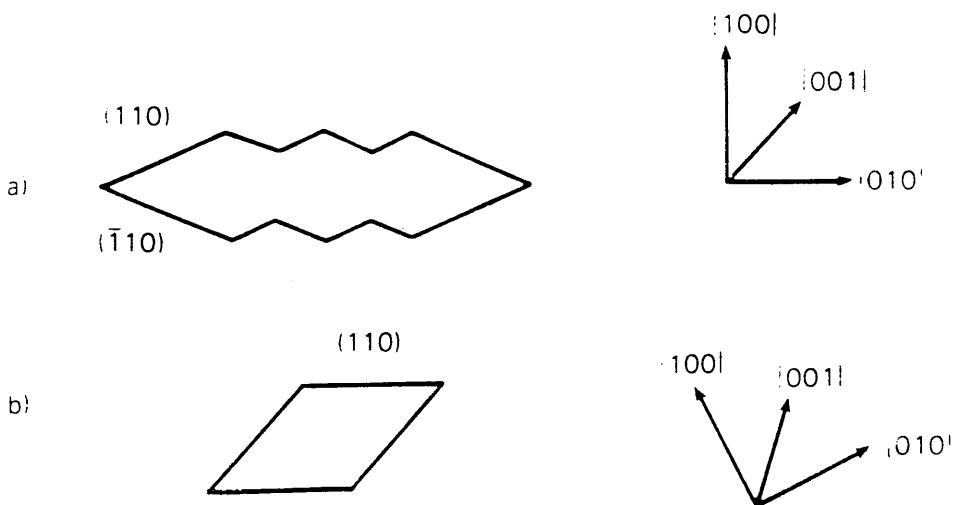


Figure 5.28: Schematic representation of goethites with domain structure. (a) Multidomain crystal with many (110) faces. (b) Single domain crystal with a few well-developed (110) faces lying in the $[110]$ zone. (After Mann et al, 1985).

The high resolution image of a group of spherical particles labelled J in Figure 5.24 is shown in Figure 5.29. Although no electron diffraction was available for the particles, their morphology was similar to those of ferrihydrite particles identified in the red mottles. An average size of 5.6nm obtained for 20

particles in the aggregate compares well with that obtained for ferrihydrite particles in the red mottles and discussed in 5.10.2a(i). It would thus appear that the aggregates of iron oxide particles in Figure 5.24 contained both goethite and ferrihydrite existing side by side.

Although no association of iron oxide with clay particles was obvious for most part of the investigation as iron oxide particles tended to be self-aggregating, it is not clear from Figure 5.24 if there was any specific association between iron oxide particles and the clay particles in the figure. In the figure, aggregated iron oxide would appear to be attached to the tips of the clay particles while goethite laths could be seen on the surface of particles B and C. A similar arrangement of goethite aggregates and clay particles could be seen in Figure 5.30 (electron diffraction of the goethite particles is shown as inset). These observations are, however, not conclusive on the association of iron oxide with clay particles.

(b) Sample (404.06)

(i) Red mottles (Munsell 7.5R 5/8 or 7.5R 6/8)

The red mottles in this soil was found by electron microscopy to be composed of clay particles and aggregates of iron oxide particles. As was the case with the red mottles of Sample 404.05, a higher concentration of iron oxides was indicated in the mottles than was the case when the dispersed whole soil was examined.

Figure 5.31 shows a low magnification image of aggregated iron oxide particles, and the associated electron diffraction (Figure 5.32) showed reflections with spacings that are typical of goethite. Due to aggregation of the particles, it was not possible to determine the morphology of the goethite particles. Figure 5.33 is a high resolution image obtained from a different iron oxide aggregate

from the red mottles. In this case also, the electron diffraction (shown as inset in Figure 5.33) revealed reflections that are characteristic of goethite. Some of the goethite particles appeared to be slightly elongated although definite laths were rare. Measurements of the lesser dimension across 15 particles in the available micrographs showed it to range between 7.87nm and 10.11nm. It was not possible to measure the longer length of most of the particles because this was more obscure in most cases. One lath-like particle labelled A in the figure could be seen amongst the other particles. A higher magnification micrograph of this lath-like particle is shown as inset in Figure 5.33 and lattice fringes with spacings of approximately 0.42nm which corresponds to the (110) plane of goethite could be seen on the particle. A breadth of about 9.74nm obtained for this particle makes it larger than the laths of goethite encountered in the red mottles in the deeper soil (Sample 404.05) whose breadth ranged from 3.1nm to 6.1nm (see Figure 5.24). Figure 5.34 shows a high resolution micrograph of another aggregate of iron oxide particles from the red fraction. The electron diffraction (shown as inset) gave reflections that identified the particles as goethite. The high resolution image of a lath-like particle labelled 'A' in Figure 5.34 is shown in Figure 5.35 and lattices with 0.42nm(110) spacings of goethite could be seen on this particle. The high resolution micrograph of another area, labelled 'B' in Figure 5.34 is shown in Figure 5.36 and particles with lattice fringes of 0.50nm(020) and 0.42nm(110) of goethite could be seen. Figures 5.33 and 5.34 are typical of the electron microscopy observations made on the iron oxides from the red mottles in this soil. Since electron diffraction of the aggregates gave the reflections of goethite, while the reflections that may indicate other phases of iron oxide were absent in all the diffraction patterns it would appear that the particles seen in the micrographs are goethite particles. Due to the red colour of the fraction which compared with the red mottles in Sample 404.05 ferrihydrite was also expected in the red fraction of the soil. It is

however possible that the weaker reflections of a less crystalline ferrihydrite were suppressed in a ferrihydrite/goethite mixture.

As in all other cases association of iron oxide particles with other soil minerals was rare in most of the cases encountered in this fraction. Figures 5.37a and 5.37b, however, show two sections of one particle and aggregates and individual particles of iron oxide appeared to be stuck to the edges as well as surfaces of the particle. Although no electron diffraction of the particle was available it was found to have similar morphological characteristics with the halloysite clay particles seen in the soil. It would thus appear from this case and that already described in the last section that the association of iron oxide particles with halloysite clay particles is a possibility though not a common occurrence in these soils.

(ii) Yellow fraction (Munsell 10YR 8/8 to 10YR 8/6)

Generally, the yellow coloured oxides were more dispersed throughout the soil and gave the soil its general colour. However, some areas of higher concentration of yellow coloured material could be identified in the soil, and these were separated as yellow fraction. As was the case with the red mottles, a higher concentration of iron oxide particles, than in the whole soil, was indicated in this fraction. Electron microscopy observations showed the morphology of some of the iron oxides particles in the fraction to be different from those encountered in the red fraction.

An aggregate of iron oxide particles from the yellow fraction of Sample 404.06 is shown in Figure 5.38. The electron diffraction of the particles, shown as inset in the figure gave the reflections of goethite. Most of the particles in this case have a definite lath-like (or acicular) morphology. Measurement of the width of five particles seen in the figure showed the width to range between 13.15nm and 20.16nm. Some of the particles seen in Figure 5.38 and labelled A

and B in the figure are shown in Figures 5.39 and 5.40 respectively. Lattice fringes with spacings of about 0.42nm which corresponds to the (110) plane of goethite could be seen on the particles. In general, the goethite particles in Figure 5.38 are different from those encountered and presented earlier for the red mottles as lath-like morphology of many of the goethite particles is apparent in this case and the particles are also larger. The particles are also larger than those encountered in the less weathered Sample 404.05. The fact that the goethites in the two different fractions from the same soil showed morphological differences may be an indication that the goethites were formed in different ways. It is possible that the goethite in the red fraction was formed from ferrihydrite under conditions (e.g the presence of organics, etc) that inhibited crystal growth while the larger goethite particles in the soil may have been formed directly from Fe^{3+} in the soil system (without going through the ferrihydrite route) and have been able to grow uninhibited. Alternatively, both goethites were produced in similar ways, but with the larger particles being formed earlier.

Another high resolution image of iron oxide particles is shown in Figure 5.41. Lattices with spacings of 0.42nm (110) of goethite could be seen on some particles. The particle labelled A on the micrograph would appear to be a goethite particle seen on-edge. A crystal fault similar to that observed on the particle in Figure 5.27 could be seen on this particle. Lattice spacing of 0.455nm seen running across the a-axis corresponds to the cell constant, a_0 , of the goethite crystal while the lattices running across the b-axis have spacing of 0.960nm and corresponds to the cell constant b_0 . The value of b_0 obtained in this case agrees well with the 0.977nm obtained for the particle in Figure 5.27. However, a size of 18.48nm x 30.24nm measured for this particle as against the 8.98nm x 20.32nm for the particle in Figure 5.27 further supports the observation of a larger size of the goethite particles in this soil compared to those in Sample 404.05. Although differences in Al substitution had been reported to be a

common factor responsible for differences in size and morphology between goethite particles with goethites with higher Al substitution being generally smaller (e.g. Schulze, 1982; Schwertmann, 1984), the fact that aluminium substitution for Sample 404.06 was found to be higher (see Chapter 6) than that for Sample 404.05 would appear to rule out aluminium substitution being responsible for the difference in the sizes of the soil goethites in this case. A more likely explanation may be that the goethites in the more weathered Sample 404.06 were produced earlier and have had more time to grow.

The presence of goethite as the iron oxide phase in this fraction was as expected based on the yellow hue of the fraction.

(iii) Whole soil and clay fraction

Results of electron microscopy of the dispersed whole soil and clay fraction showed particles that were similar to those already presented for the red and yellow fractions. Laths of goethite particles often showing lattices with spacing of 0.42nm (110) were often seen amongst aggregates of iron oxide particles. In most cases aggregation of the particles hindered an evaluation of the morphology of the individual particles.

(c) Sample 404.07

The sample description and Munsell colours for this soil were given in Chapter 3. Since there were very few concentrations of iron oxides (in form of mottles, concretions etc) in the soil, electron microscopy observations were performed only on the clay fraction ($<2\mu\text{m}$) of the soil. As was the case with the other soils, strong aggregation of the iron oxide particles was indicated by electron microscopy. Electron diffraction suggested all the iron oxide particles encountered in this soil in the course of the investigation to be goethite.

A typical aggregate of iron oxide particles seen in the soil is shown in

Figure 5.42 amidst clay particles. Electron diffraction of the particles (shown as inset) revealed reflections that identify the particles as goethite. Due to severe aggregation of the iron oxide particles in the soil it was not possible to study the morphology of the individual particles of iron oxide in detail.

(d) Sample 404.08

The sample description and Munsell colours for the sample were given in Chapter 3. No obvious concentrations of iron was found in the soil, hence electron microscopy was performed only on the clay fraction ($<2\mu\text{m}$).

Electron diffraction suggested all the iron oxide particles encountered during microscopy to be goethite. Figure 5.43 shows a high resolution image of an aggregate of iron oxide particles from the sample. Aggregation of the iron oxide particles in all the cases encountered hindered morphological studies of the individual iron oxide particles.

5.10.3 Electron Microscopy Study of 5 M Boiling NaOH Treated Residue

Due to the low concentration of iron oxides in the soils it was found necessary to concentrate the oxides and increase the percentage in the sample to enable their study by some of the techniques employed in the investigation. Concentration was achieved by the use of boiling 5M NaOH solution for 1 hour. Details of the procedure had been described in Chapter 4 and results of chemical tests on untreated and NaOH treated samples were given in Table 4.5. Electron microscopy study of the residues from the boiling NaOH treated samples was performed to obtain more information on the character of the iron oxides and assess the effect of the chemical treatment on the oxides, if any.

Generally, boiling NaOH treatment on the clay fraction ($<2\mu\text{m}$) of the soils concentrated the iron content by factors of between 2.1 and 3.2 on the clay fraction and between 4.3 and 7.5 on the whole soil (see Table 4.6). The higher

percentage of iron oxide in the residues following NaOH treatment made microscopic studies of the oxides easier than was the case with the untreated soil. All kaolinitic minerals (halloysite and kaolinite) were effectively dissolved by the boiling sodium hydroxide treatment leaving aggregates of iron oxide particles and muscovite. The results of electron microscopy studies on the residues obtained from NaOH treatment on the soils are presented below for each of the soils.

(a) Sample 404.05

A general section of the NaOH treated residue (Figure 5.44) showed aggregates of small particles and thin clay plates. Electron diffraction showed the aggregates to be iron oxide particles while the clay plates were muscovite. In contrast with the general section of the untreated soil virtually all the halloysite clay minerals in the soil was dissolved by the NaOH treatment while the muscovite particles were more resistant to the treatment.

Electron diffraction patterns of the aggregate studied revealed reflections of goethite. Figure 5.45 shows a high resolution image of an aggregate of iron oxide particles. The associated electron diffraction (shown as inset) gave reflections of goethite. Although the morphology of most of the individual particles could not be discerned due to aggregation some short lath-like particles could be seen amongst the particles in the aggregate shown in ^{Figure} 5.45. This was typical of most of the aggregates studied. Measurement of the width of 15 lath-like particles obtained from several micrographs showed it to range between 4.0nm and 5.0nm with an average width of about 4.5nm. This compares well with an average width of about 4.4nm obtained for lath-like goethite particles in the untreated soil (Section 5.10.2a). In general, no change to the morphology of the iron oxide particles was observed following treatment with 5M boiling NaOH. Similarly, no indication of improvement in crystallinity of the goethite particles was apparent from comparison of intensities of the electron diffraction of treated

and untreated soils.

Although ferrihydrite was identified mainly in the red mottles of the untreated soil, electron diffraction did not indicate the presence of ferrihydrite in the residue from NaOH treatment of the whole soil. This is most probably due to the fact that the proportion of ferrihydrite, and hence its detection, in the whole soil was much lower than that in the red mottles although the conversion of ferrihydrite into other products following NaOH treatment could not be ruled out (e.g Goodman et al, 1988).

(b) Sample 404.06

Electron diffraction of the iron oxide particles examined in this sample gave goethite reflections. A high resolution image of an aggregate of iron oxide particles encountered in the sample is shown in Figure 5.46. In agreement with observations made on the yellow fraction of the untreated soil, definite laths, some with lattice fringes of 0.42nm of goethite (see inset), were evident. The width of 20 laths measured from several micrographs ranged between 5.0nm and 12.3nm with an average of about 8.2nm thus making them generally larger than those observed in the shallower soil (404.05). A similar trend was observed for the untreated soils.

(c) Sample 404.07

Electron diffraction of the aggregates of iron oxide particles seen in the boiling 5M NaOH treated residue showed goethite reflections as was the case with the untreated soil. The high resolution image of the aggregates (e.g. Figure 5.47) often showed severely aggregated particles which made it difficult to determine the morphology of the particles. However, most individual goethite particles appeared to have a morphology that is more plate-like than acicular (or lath-like). This morphology is in contrast to those of the goethite particles in

the deeper soils where lath-like goethite particles were common.

(d) Sample 404.08

Because the content of the 2:1 clay minerals in this soil was lower and the kaolinite content higher compared to the deeper soils as revealed by X-ray diffraction (Chapter 6) and infrared spectroscopy (Chapter 7) of the clay fraction of the soils, fewer clay particles were found in the residue and better concentration of the iron oxides was indicated. Iron oxide particles could be seen as aggregates while clay particles (mostly muscovite) were present as thin, irregular plates. As was the case with the untreated soil, electron diffraction of the aggregates revealed reflections that were indicative of goethite. Figure 5.48 shows a high resolution image of some goethite in the NaOH-treated residue while Figures 5.49 and 5.50 show enlargements of some of the particles in Figure 5.48. The lattice fringes shown have spacings that are characteristic of goethite. Several of the particles that could be discerned in the available micrographs had the appearance of elongated plates and an estimation of the width of 17 particles obtained from the micrographs showed it to range between 8.0nm and 20.0nm with an average of about 12.2nm. Because it was not possible to obtain the morphology of the individual particles in the untreated soils no comparison in morphology of the iron oxide particles could be made between treated and untreated soils. Generally, the goethite particles seen in this soil appeared to have a platy morphology. Hence there is a general trend of a progressive change in the morphology of the goethite from lath-like in the deeper soils to plate-like in the more weathered soils.

(f) 5 M NaOH Treatment of Synthetic Iron Oxides

As control for the sodium hydroxide concentration experiment on the natural samples, synthetic samples of ferrihydrite and goethite were treated in the same way as the clay samples. The preparation of the synthetic forms were

discussed earlier in Chapter 3. Before treatment with sodium hydroxide the synthetic iron oxides were mixed with 50% well crystallized "Georgia kaolin" as recommended by Kämpf and Schwertmann (1982). Since, from X-ray analysis results, the amount of kaolin (present as mixture of halloysite and kaolinite) in all the clay samples was more than 50%, addition of 50% kaolinite to the synthetic samples should still make them comparable with the natural samples. Results of electron microscopy performed on both untreated and sodium hydroxide treated synthetic samples are presented below:

(i) Ferrihydrite

The micrograph showing the particles of untreated ferrihydrite is shown in Figure 5.19 and the electron diffraction is shown in Figure 5.20. Electron microscopy of the 5M boiling sodium hydroxide treated ferrihydrite showed particles of ferrihydrite that are similar in size and morphology to those of the untreated samples and the electron diffraction gave the same spacings as those for the untreated samples. No phase transformations or improvement of crystallinity of the ferrihydrite particles could be inferred from the electron diffraction results.

(ii) Goethite

Transmission electron microscopy and electron diffraction of synthetic goethite particles before and after treatment with 5M boiling NaOH did not indicate any transformations to the goethite particles. The high resolution image and electron diffraction of untreated goethite particles is shown in Figures 5.26. Electron microscopy results obtained for the NaOH treated sample showed them to be similar to those obtained for the untreated sample.

The results presented above for the control tests are in line with those presented by Kämpf and Schwertmann (1982) and appeared to indicate that the NaOH treatment did not affect the synthetic ferrihydrite and goethite particles

adversely, although the effect of the treatment on the soil oxides may be different and needed to be monitored.

5.10.4 Electron Microscopy Study of HF Treated Residue

Except for the synthetic ferrihydrite, the results of electron microscopy on residues obtained from HF treated soil and synthetic oxides (controls) were similar to those presented above for 5 M boiling NaOH treated oxides. In the case of the synthetic ferrihydrite, as discussed earlier in Chapter 4, the ferrihydrite particles were instantly dissolved on contact with the HF and no residue was obtained.

5.10.5 Beam Damage to Soil Iron Oxides

The soil iron oxides (ferrihydrite and goethite particles) were investigated for electron beam damage by exposure in the diffraction mode and high resolution microscopy mode. The diffraction pattern of the exposed particles was obtained immediately and at 3 minutes intervals of exposure. No change in phase or crystallinity of the soil ferrihydrite particles was observed from comparison of the diffraction patterns obtained at immediate diffraction and even after ten minutes, thus showing the ferrihydrite to be reasonably stable to the electron beam under diffraction conditions. However, comparison of electron diffractions done before and after exposure of the ferrihydrite to the electron beam at transmission mode (for high resolution microscopy) showed that the ferrihydrite was converted to hematite after about ten minutes exposure. The immediate diffraction (before exposure to the electron beam in transmission mode) pattern of an aggregate of soil ferrihydrite is shown in Figure 5.16 and Figure 5.51 shows the diffraction pattern after ten minutes of exposure to the electron beam at transmission (HREM) mode. The 0.184nm, 0.269nm, and 0.367nm reflections which are indicative of hematite are evident in Figure 5.51 thus

indicating that the ferrihydrite particles had been converted to hematite. Although a detailed study of beam damage to ferrihydrite was not done, no reflections of any other iron oxide mineral obtained at any time during the conversion of ferrihydrite to hematite in the electron beam thus suggesting that conversion of ferrihydrite to hematite was not through an intermediate phase.

Similar tests on the soil goethites showed that they were not affected by the electron beam in the diffraction mode for ten minutes, but the goethite particles were found to convert to hematite at ten minutes exposure to the electron beam in high resolution mode as illustrated by the diffraction patterns before and after exposure in HREM (Figures 5.52 and 5.53 respectively). Figure 5.52 shows the typical goethite reflections obtained from the particles before electron microscopy while Figure 5.53 shows typical hematite reflections after exposure to the electron beam. In both cases, for ferrihydrite and goethite, no change in morphology accompanied the change to hematite. Some of the results of beam damage obtained for the soil iron oxides in this investigation, however appeared to be in contrast to those obtained by some previous authors. Eggleton and Fitzpatrick (1988) reported, for synthetic 2-line and 6-line ferrihydrite, that "...the electron diffraction patterns of the ferrihydrite aggregates are similar to the XRD patterns and do not change after prolonged (10 min) electron-beam exposure" and that "...the crystals were quite stable under the electron beam, surviving for minutes with no apparent damage". Although it was not made quite clear by the authors, it would appear that the first statement refers to exposure in the diffraction mode while the second statement refers to exposure in bright field, transmission mode under high resolution microscopy. A similar result was obtained for the synthetic 6-line ferrihydrite (prepared in a similar way to Eggleton and Fitzpatrick's) used as control in this study. Considering these cases, the results obtained for the soil ferrihydrites in this study agreed with those for synthetic ferrihydrites reported by Eggleton and Fitzpatrick (1988) for exposure in

Chapter 5: Electron Microscopy

the diffraction mode, but the conversion of the soil ferrihydrites to hematite appeared contrary to what was reported for the synthetic ferrihydrites by these authors for exposure under high resolution microscopy. Also, Smith and Eggleton (1983) reported that no appreciable radiation damage was detected when some natural goethites were exposed (presumably in high resolution microscopy conditions) to the electron beam for long periods of \approx 20 minutes. This is contrary to what was obtained for the soil goethites particles in this study.

In the present case, the change from ferrihydrite and goethite to hematite is most likely to have been brought about by dehydration of the particles, caused by specimen heating, as a result of electron-specimen interactions already reviewed in Section 5.6. The conversion of ferrihydrite to hematite following dehydration caused by heating is well known (e.g Schwertmann, 1959; Schwertmann and Fischer, 1966; Fischer and Schwertmann, 1975). According to these authors hematite forms from ferrihydrite through an internal dehydration and rearrangement within the ferrihydrite aggregates. Similar conversion of goethite to hematite on dehydration is well documented and akaganeite has been shown to undergo structural changes during HREM observation (Galbraith et al; 1979).

Although the microscope operating conditions such as accelerating voltage used and exposure time have a role to play in causing electron beam damage, comparison of the results obtained for the synthetic ferrihydrite by Eggleton and Fitzpatrick (1988) with those obtained in this investigation may suggest that the synthetic ferrihydrites are more stable in the electron beam than the natural ferrihydrites and goethites encountered in the soils studied. Hence, there may be structural differences between some synthetic and natural ferrihydrites and applications of tests done on synthetic forms to natural forms have to take this into consideration. Alternatively, conversion of ferrihydrite and goethite to hematite may depend on some variable physical conditions such as the heating

Chapter 5: Electron Microscopy

rate and the initial physical state of the particles (e.g. initial moisture content etc). Indeed Eggleton and Fitzpatrick (1990) stated that thermal transformations between the various iron oxide phases are complex and may depend on the structure of the original phase, crystal size and heating rates (see also Mackenzie, 1970 and Rooksby, 1961).

An implication of these results is that it is possible to mis-identify soil ferrihydrite and/or goethite as hematite if electron diffraction is done after microscopy in the transmission mode, when the particles may have been subjected to change, due to exposure to electron beam. Hence necessary precautions must be taken not to over-expose the particles to the beam during microscopy. In the cause of this investigation the following procedure was followed to prevent mis-identification due to beam damage to iron oxide particles. The dispersed soil, on a carbon coated grid, was inspected to locate the iron oxide particles under a very low electron beam. Once the iron oxide particles were located, an electron diffraction pattern was obtained from the particles, followed by high resolution microscopy (this should be done as quickly as possible to prevent beam damage). It is advisable to do high resolution microscopy before low magnification microscopy because beam damage could be possible during low magnification microscopy and lattice images obtained from HREM thereafter would be that of a damaged structure, thereby leading to misinterpretation of the micrographs. Another diffraction pattern was then obtained after the series of high resolution microscopy in order to determine if beam damage occurred during HREM. Finally, the low magnification microscopy was done. A diffraction pattern after the low magnification microscopy may be desirable for further monitoring of beam damage.

5.11 SUMMARY

Some of the important findings of electron microscopy observations presented in this chapter are summarised below.

5.11.1 Clay Mineralogy

- (1) Transmission and scanning electron microscopy showed the main clay minerals in the deeper soils to be rolled-up tubes of halloysite while very few plates of muscovite were also identified.
- (2) Both silt and clay size tubes of halloysite could be identified by electron microscopy. It is possible that mechanical treatment to disperse the soil prior to particle size analysis may lead to a breakdown of the silt fraction tubes to clay fraction sizes and variations in the type and amount of treatment used may lead to variations in grading of the same soil.
- (3) As weathering increased, in the shallower soils, a variation in the mineralogy of the soils was indicated with small sized kaolinite plates progressively replacing halloysite as the predominant clay mineral in the soils. The particle size of the halloysite tubes also reduced.

5.11.2 Iron Oxide Mineralogy

- (1) Spherical ferrihydrite particles with diameter ranging between 5.1 and 5.6nm were identified in the red mottles of Sample 404.05. Goethite particles were identified as

- the only other iron oxide minerals in the soil. The goethite particles had lath-like (or acicular) morphology with an average width of about 4.4nm for crystals that were assumed to show the (100) plane.
- (2) Goethite crystals that appeared to show the (110) face showed single domains and XY dimensions of 8.98 x 20nm. The single domainic structure obtained for the goethites with Al substitution of 9.4mole % agreed well with observations made earlier for synthetic systems.
 - (3) A possible cell constant of $b_0 = 0.977\text{nm}$ was indicated for the goethite particles in Sample 404.05.
 - (4) Electron diffraction only revealed goethite particles in the red mottles of Sample 404.06 although the presence of a less crystalline ferrihydrite (as was found in Sample 404.05) could not be totally discounted.
 - (5) Only goethite particles, showing lath-like (or acicular) morphology were identified in the yellow fraction of Sample 404.06. The goethite particles were larger than those seen in the red mottles of the same soil and those seen in Sample 404.05.
 - (6) Cell constants of $a_0 \cong 0.455\text{nm}$ and $b_0 \cong 0.960$ was obtained for a goethite particle in Sample 404.06.
 - (7) Only goethite particles were identified in Samples 404.07 and 404.08. The acicularity of the goethite particles was lesser than in the deeper soils and the morphology of the particles was more plate-like.
 - (8) Evidence of iron oxide attached to the edge and surfaces of a few clay particles appeared to indicate that the

interaction of iron oxide with clay particles, in this way, is a possibility but it was not common enough to influence the properties of the clays in the soils studied.

- (9) Both soil ferrihydrite and goethite particles were found to be stable in the electron beam in the diffraction mode.
- (10) In contrast to some earlier reports, both soil ferrihydrite and goethite were found to be converted to hematite on exposure to the electron beam in high resolution mode. It was concluded that phase transformation on heating is complex and may depend on various factors.
- (11) Hints on electron microscopy on iron oxides in order to avoid mis-interpretation as a result of beam damage have been given.

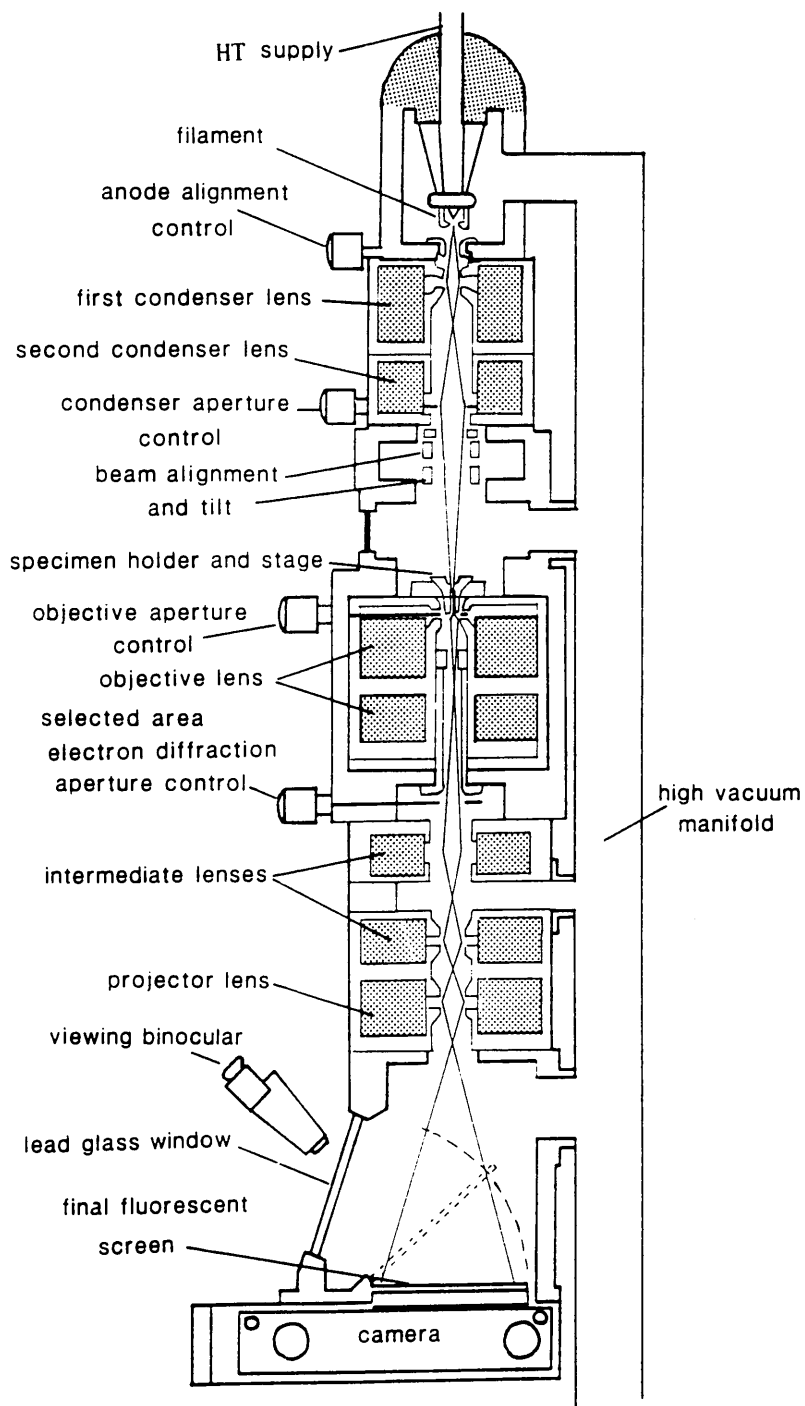


Figure 5.1: Schematic diagram of a high resolution transmission electron microscope

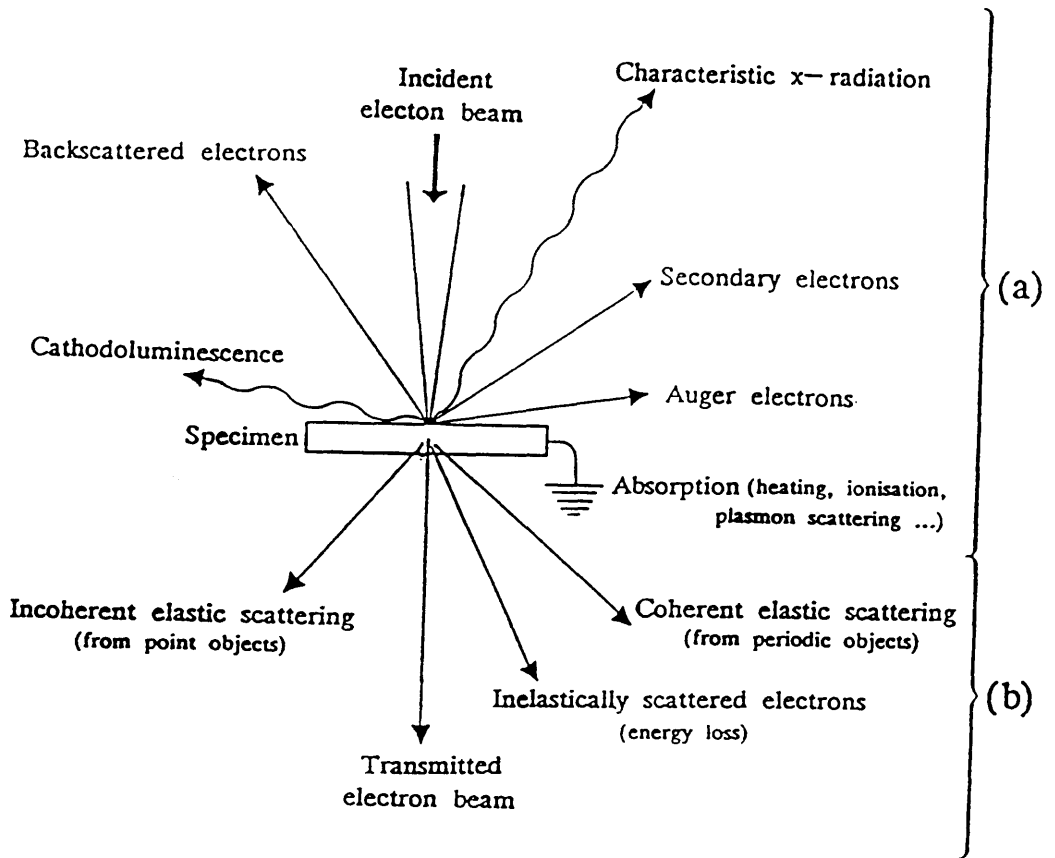


Figure 5.2: Schematic representation of the wealth of information resulting from the interaction between the electron beam and the specimen in:

- (a) scanning or analytical electron microscopy
- (b) conventional and scanning transmission electron microscopy.

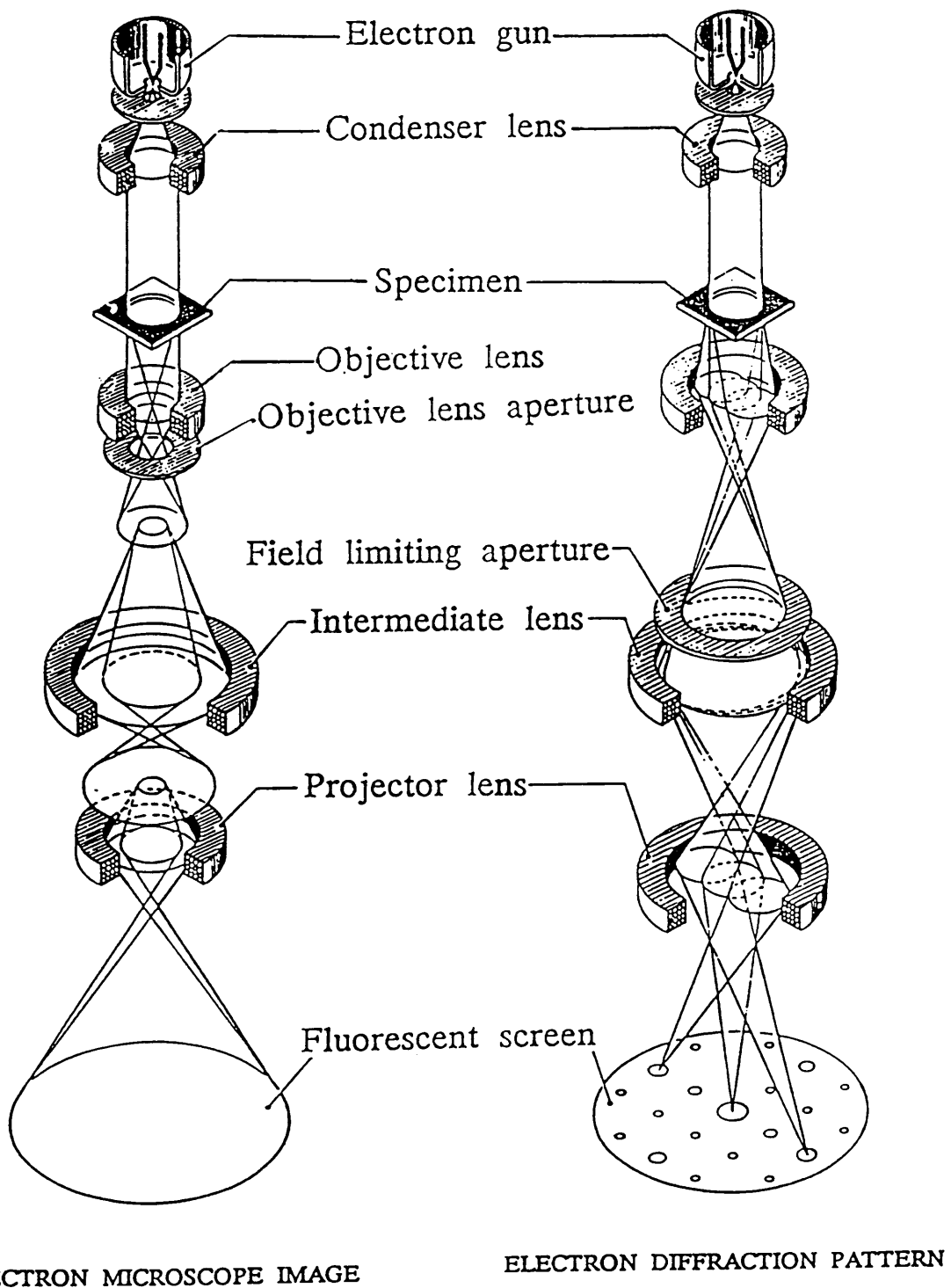


Figure 5.3: Comparison between image and electron diffraction pattern formation in the transmission electron microscope.

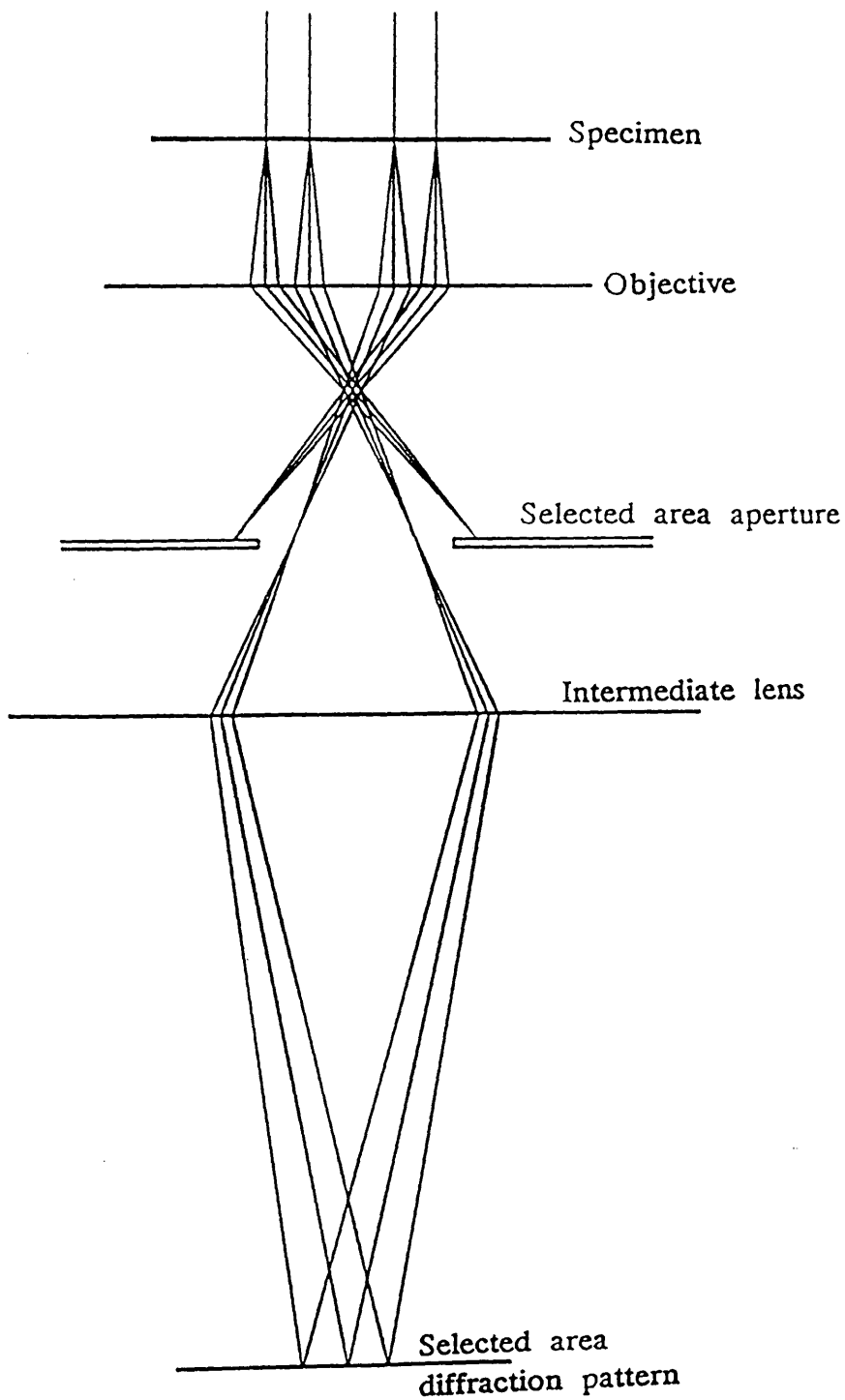


Figure 5.4: The selected-area aperture ensures that only electrons coming from a chosen region in the specimen contribute to the electron diffraction pattern.

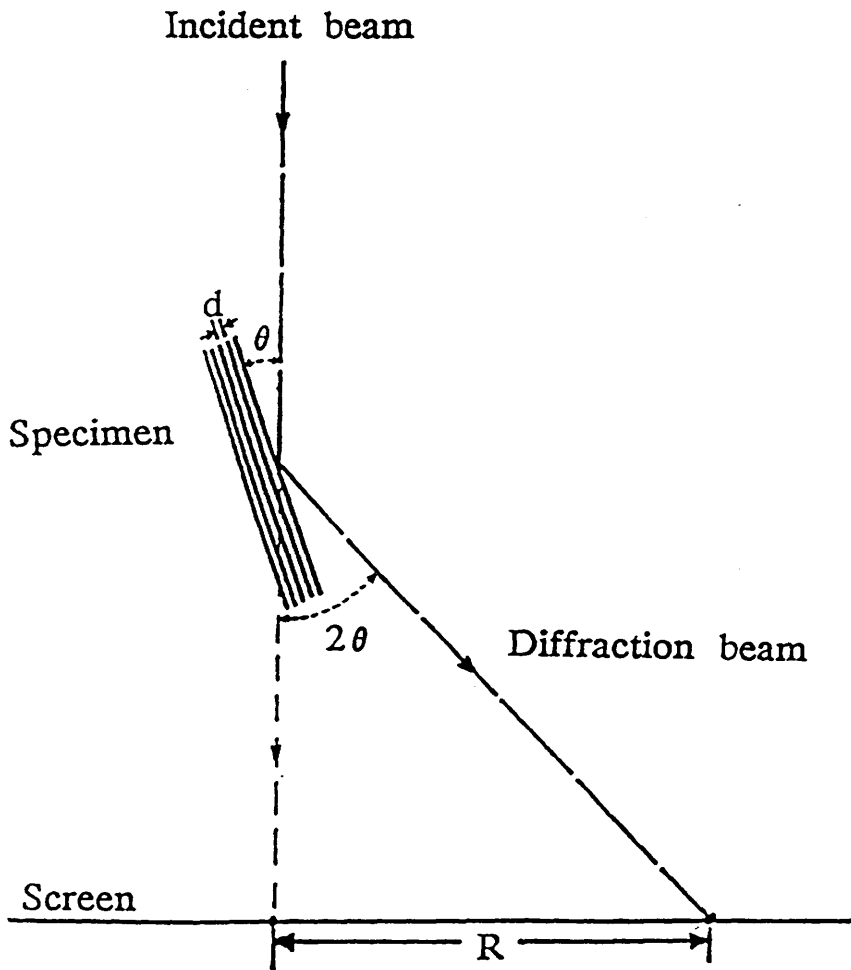


Figure 5.5: The transmission electron microscope as a simple diffraction camera.

NEXT PAGE

Figure 5.6: TEM micrograph of the whole soil Sample 404.05 showing long, rolled-up tubes of halloysite and some clay plates



NEXT PAGE

Figure 5.7: Single crystal diffraction pattern of a halloysite tube showing reflections at 0.739nm, 0.445nm, 0.42nm, 0.358nm, 0.254nm, 0.224nm, 0.151nm and 0.149nm. The streaked pattern is indicative of a tubular morphology.

Figure 5.8: Single crystal diffraction of a clay plate showing reflections at 0.445nm, 0.257nm, 0.225nm, 0.170nm and 0.149nm. The clay may be a mica.



NEXT PAGE

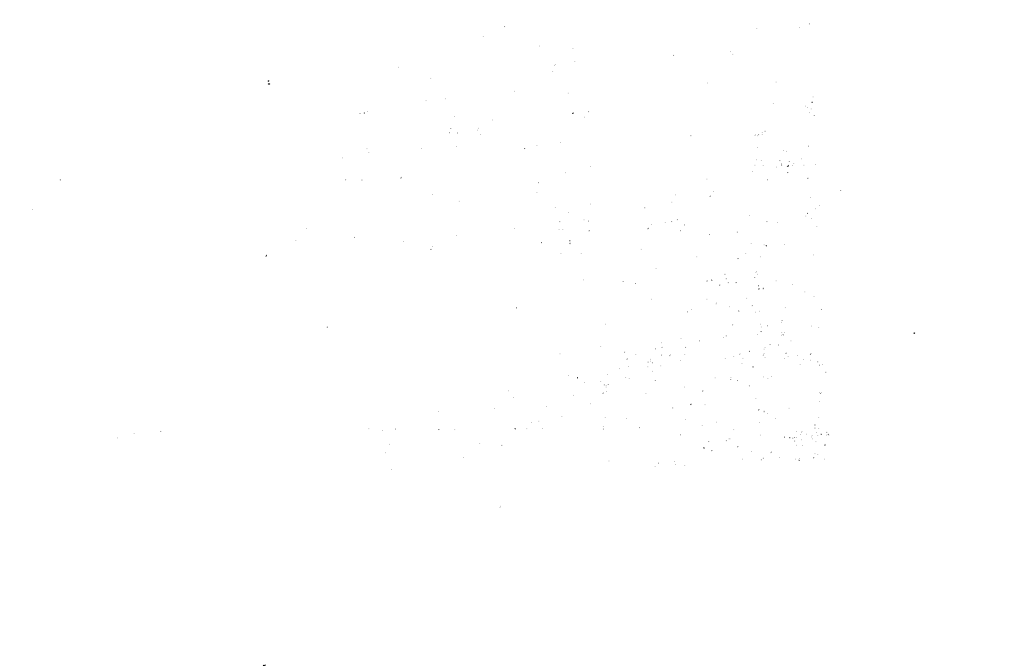
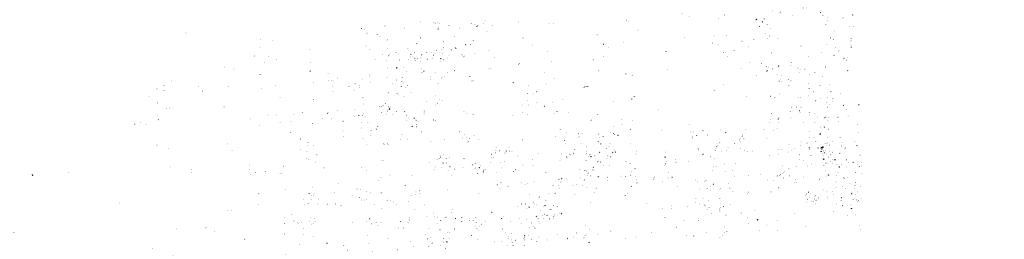
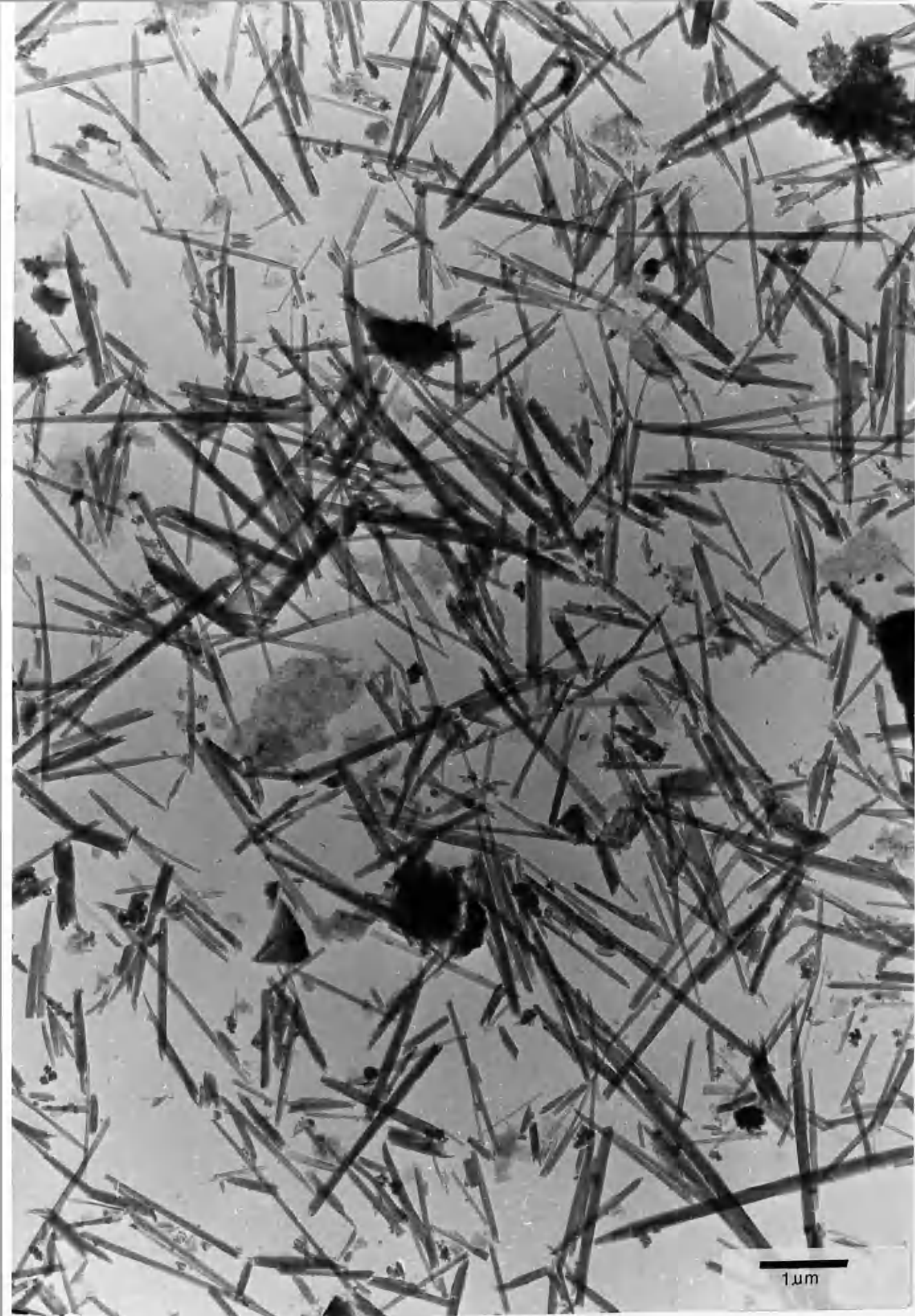


Figure 5.9: TEM micrograph of the clay fraction of Sample 404.05. The halloysite tubes are shorter than those shown for the whole soil in Figure 5.6.





NEXT PAGE



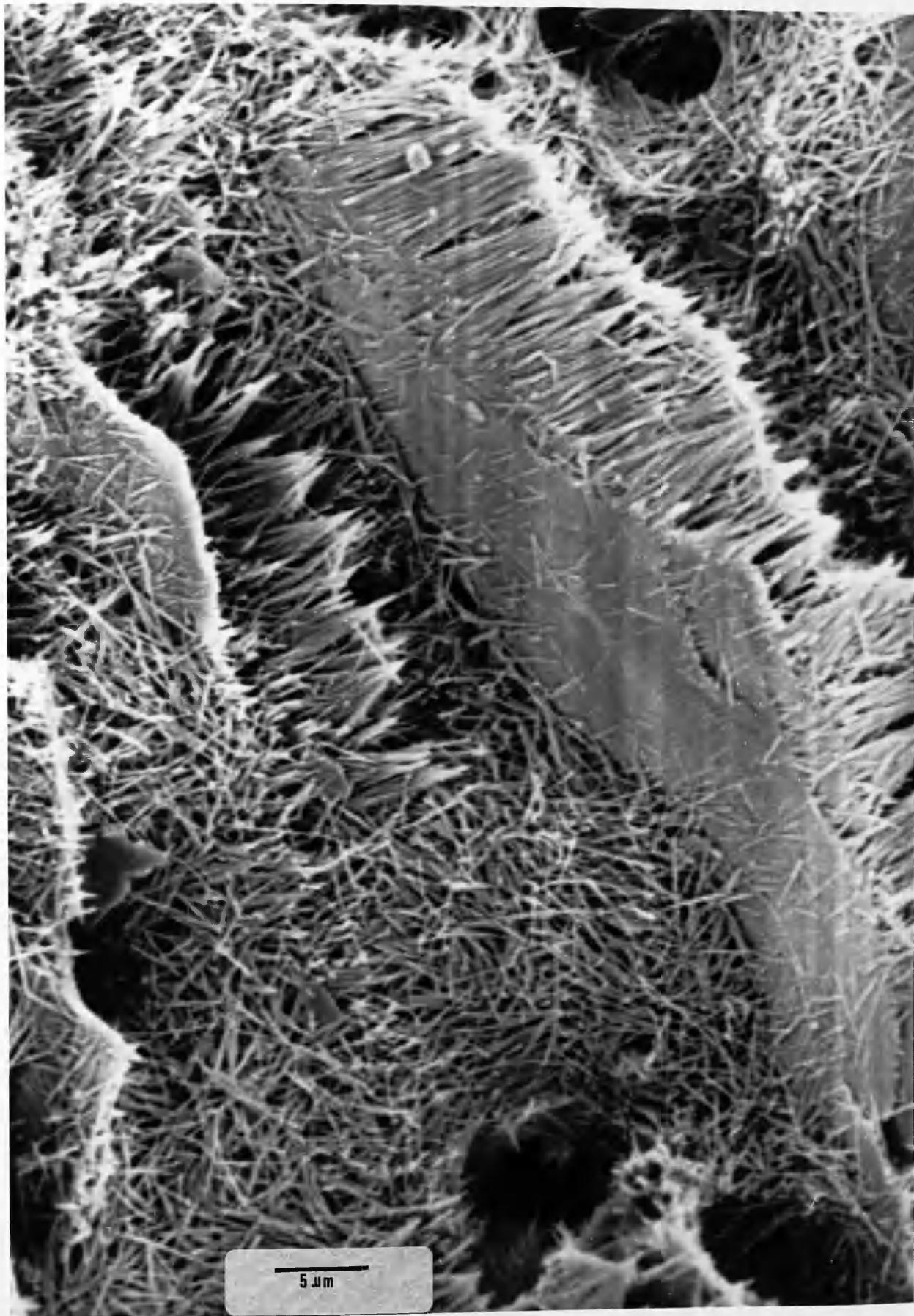


Figure 5.10: SEM micrograph of Sample 404.05 showing long fibres being formed from a primary mineral (most probably plagioclase). Voids with more or less circular cross section could be seen on the micrograph.



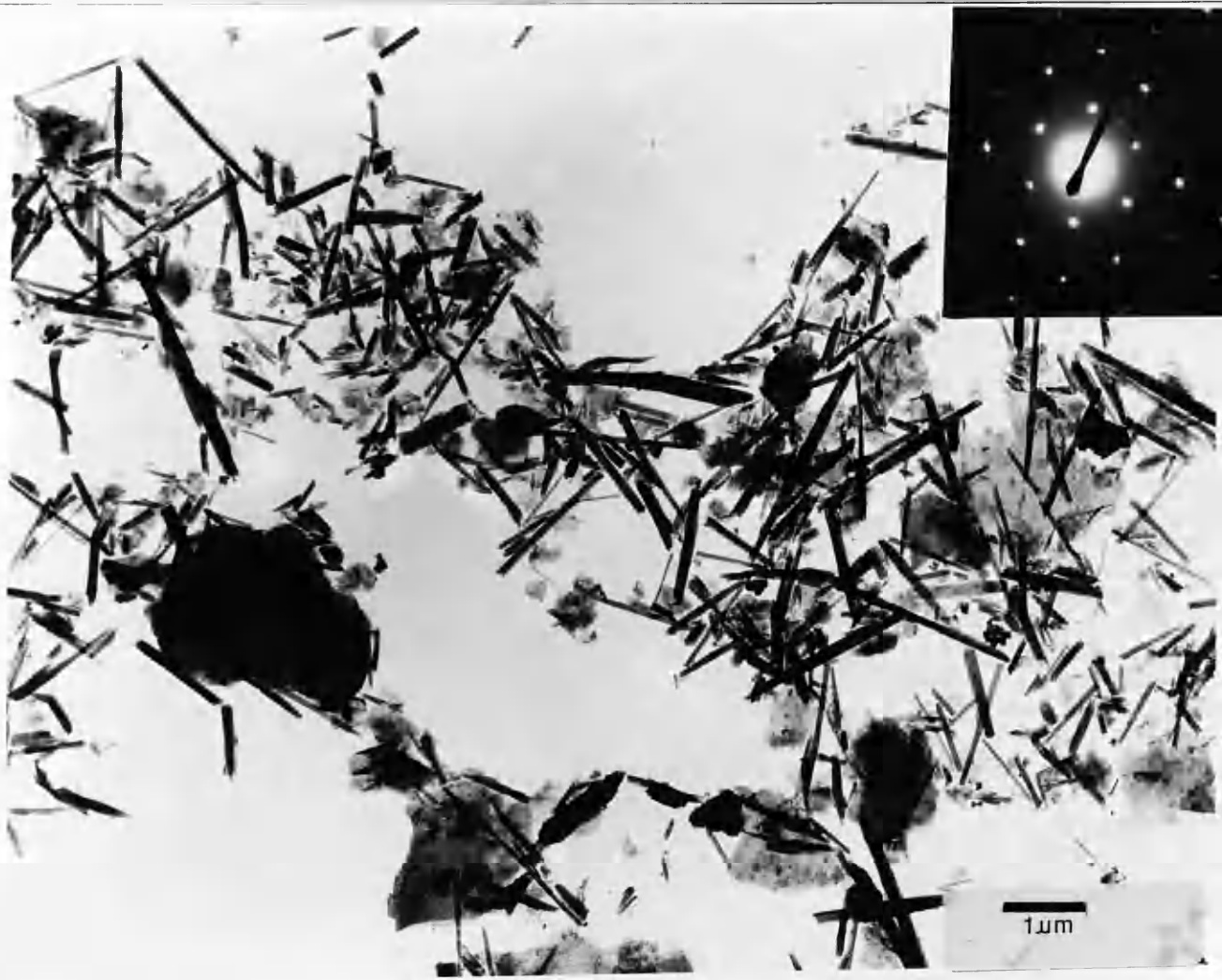


NEXT PAGE

Figure 5.11: TEM micrograph of the clay fraction of Sample 404.06 showing halloysite tubes and mica plates.



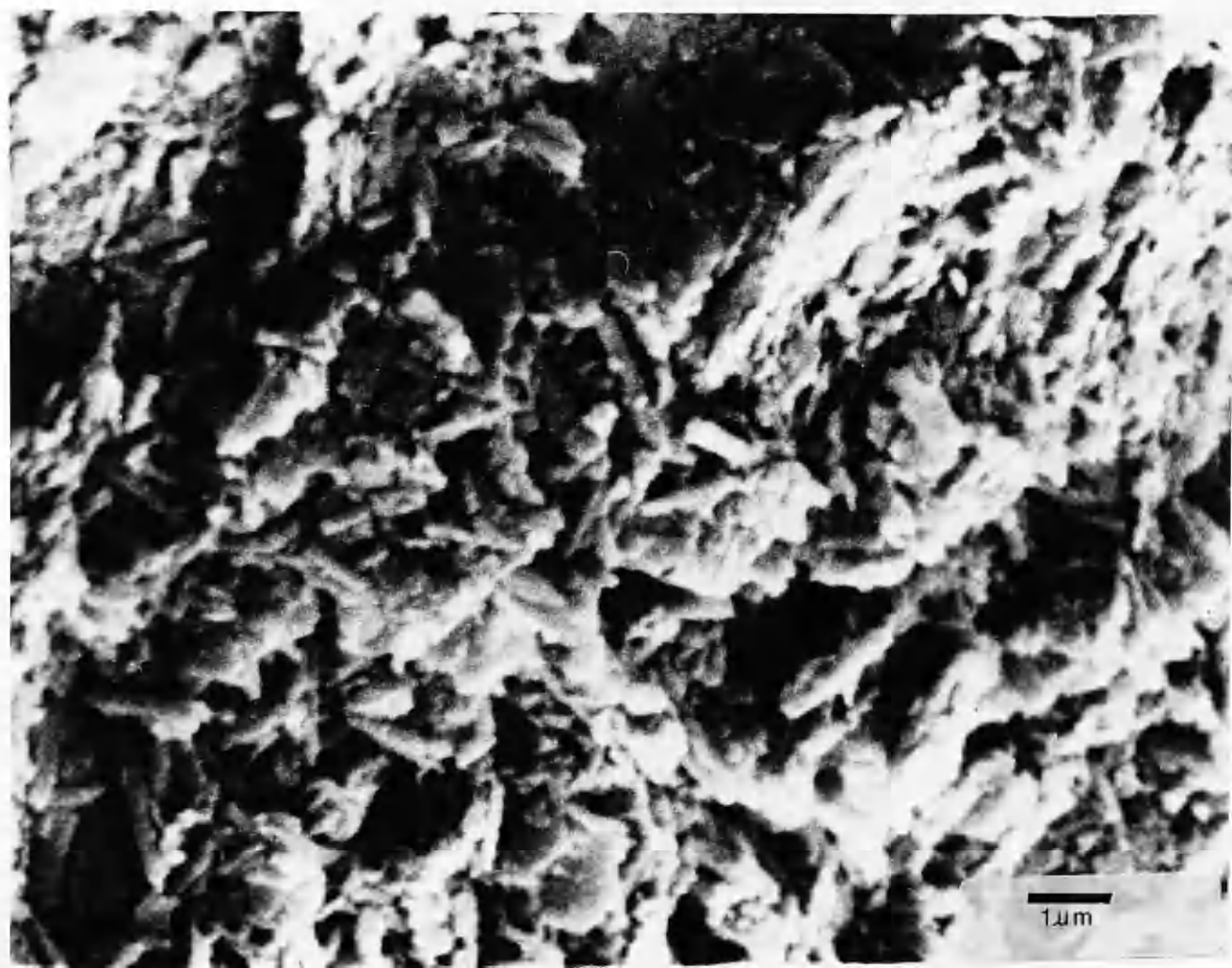
Figure 5.12: TEM micrograph of Sample 404.07 showing halloysite tubes and clay plates. The proportion of clay plates has increased compared to the previous samples.



NEXT PAGE

Figure 5.13: TEM of the clay fraction of Sample 404.08 showing short halloysite tubes and clay plates (mostly kaolinite).

Figure 5.14: SEM micrograph of Sample 404.08. A more compact structure of the soil than the previous soils is indicated.



NEXT PAGE


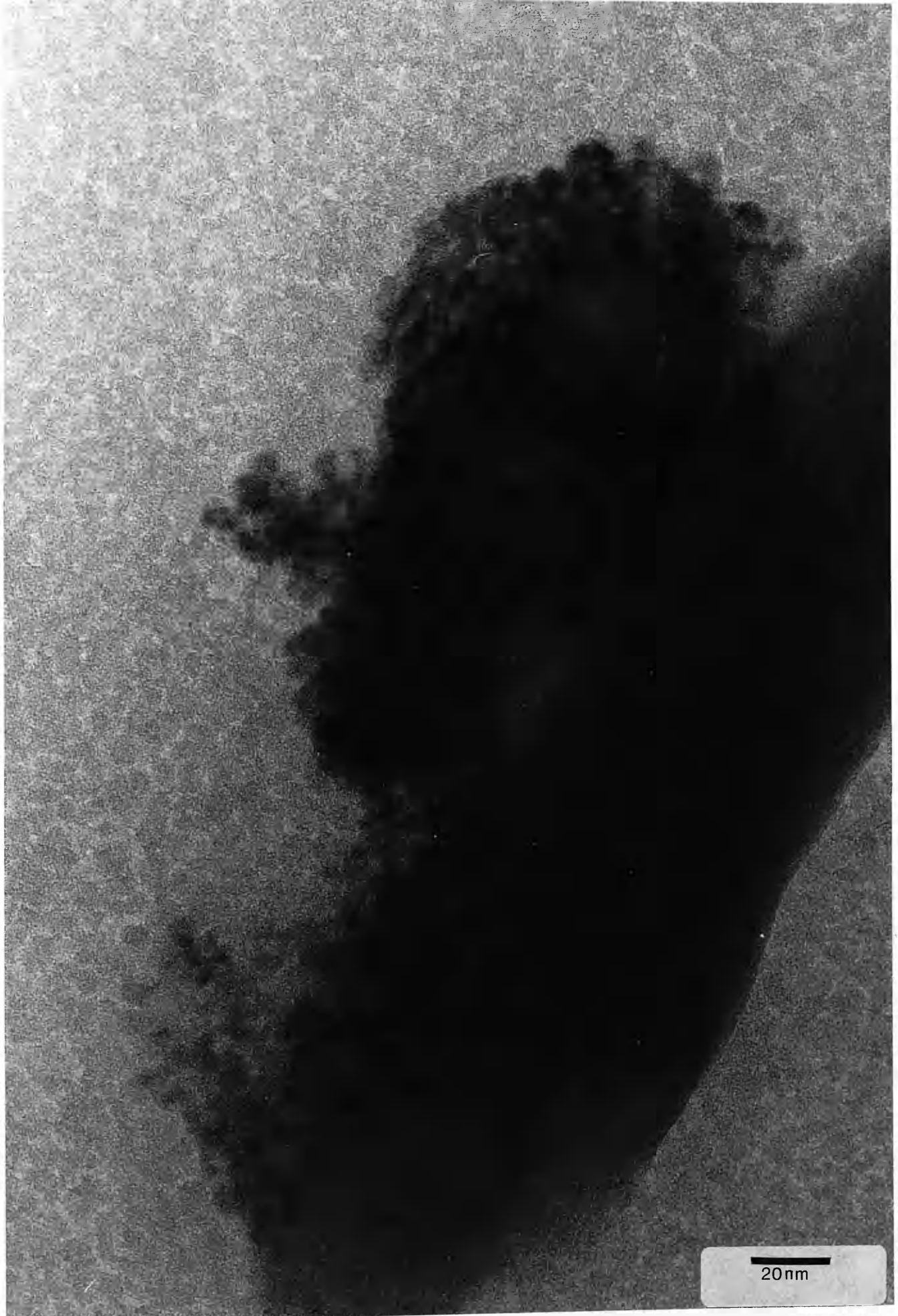


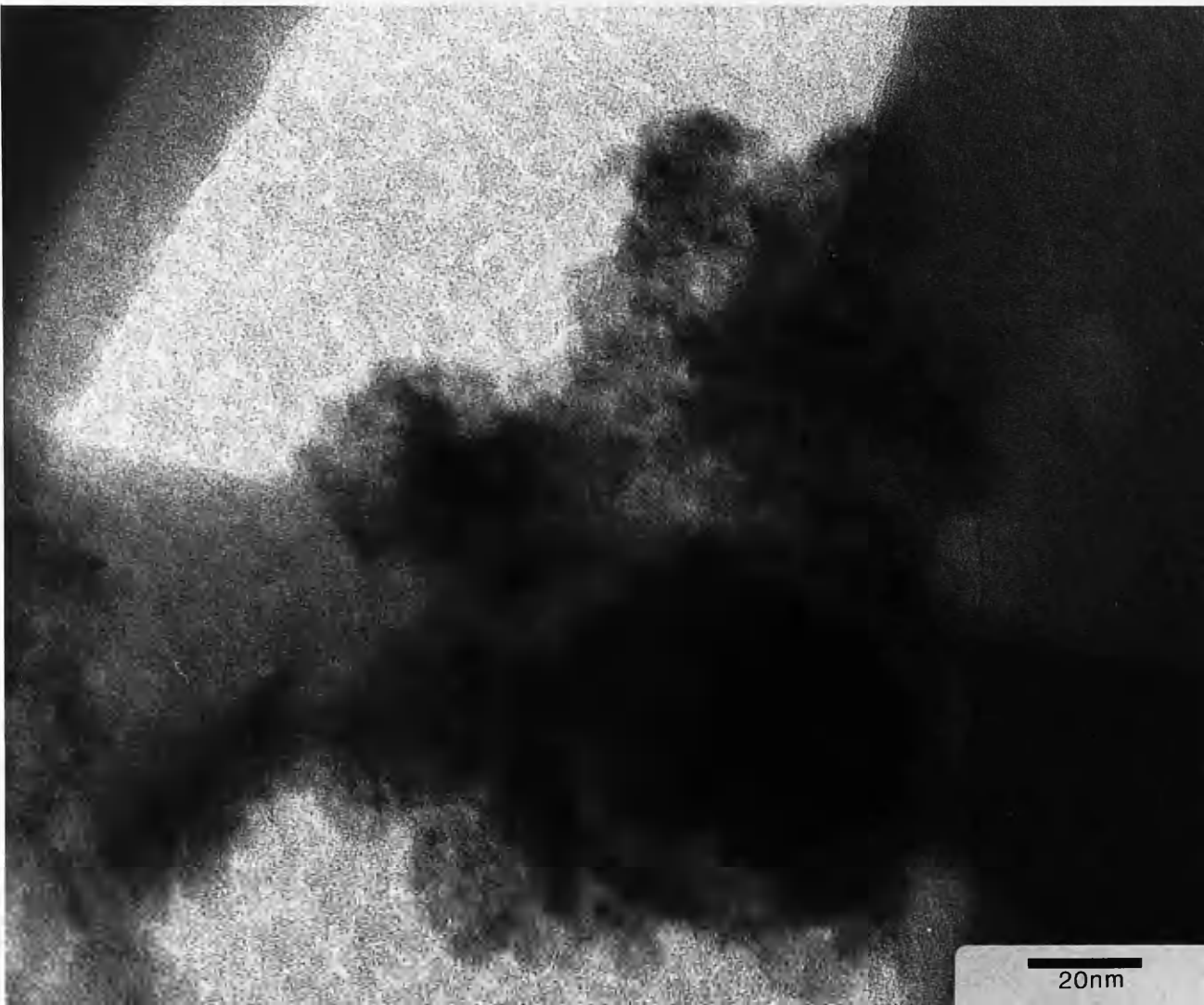
Figure 5.15: HREM Of spherical particles of ferrihydrite in the red fraction of Sample 404.05. The long lath-like particle is halloysite.



NEXT PAGE

Figure 5.16: Electron diffraction pattern of the ferrihydrite particles shown in Figure 5.15.

Figure 5.17: HREM of another aggregate of ferrihydrite particles in the red fraction of Sample 404.05. The lath-like particles are halloysite.



NEXT PAGE

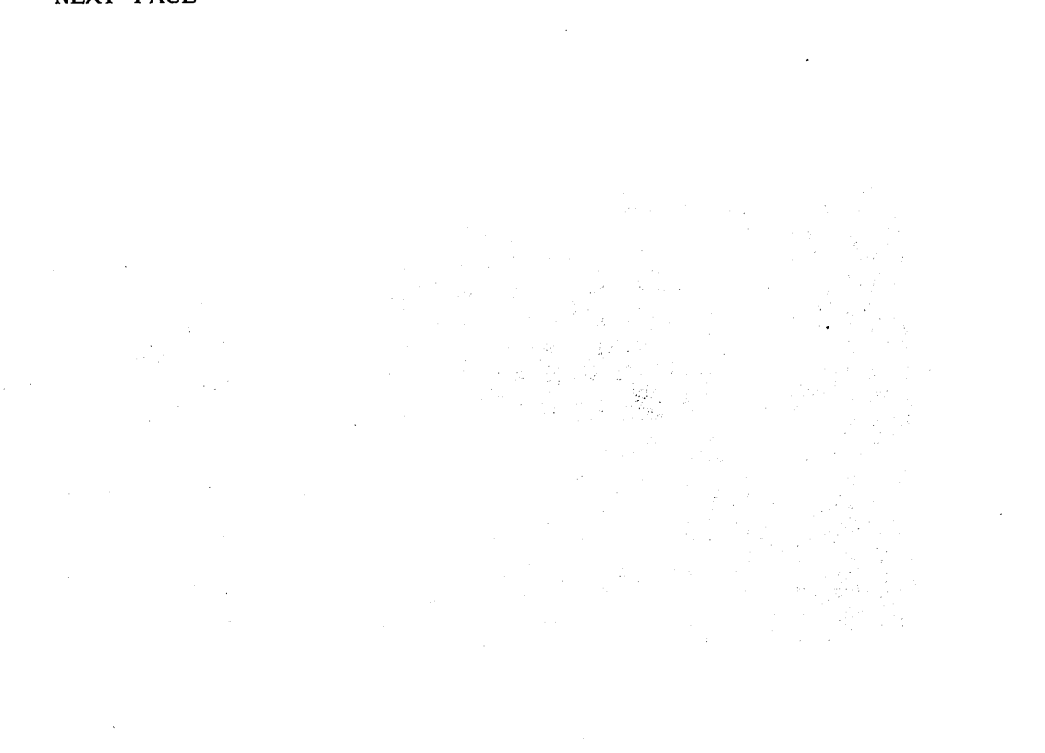

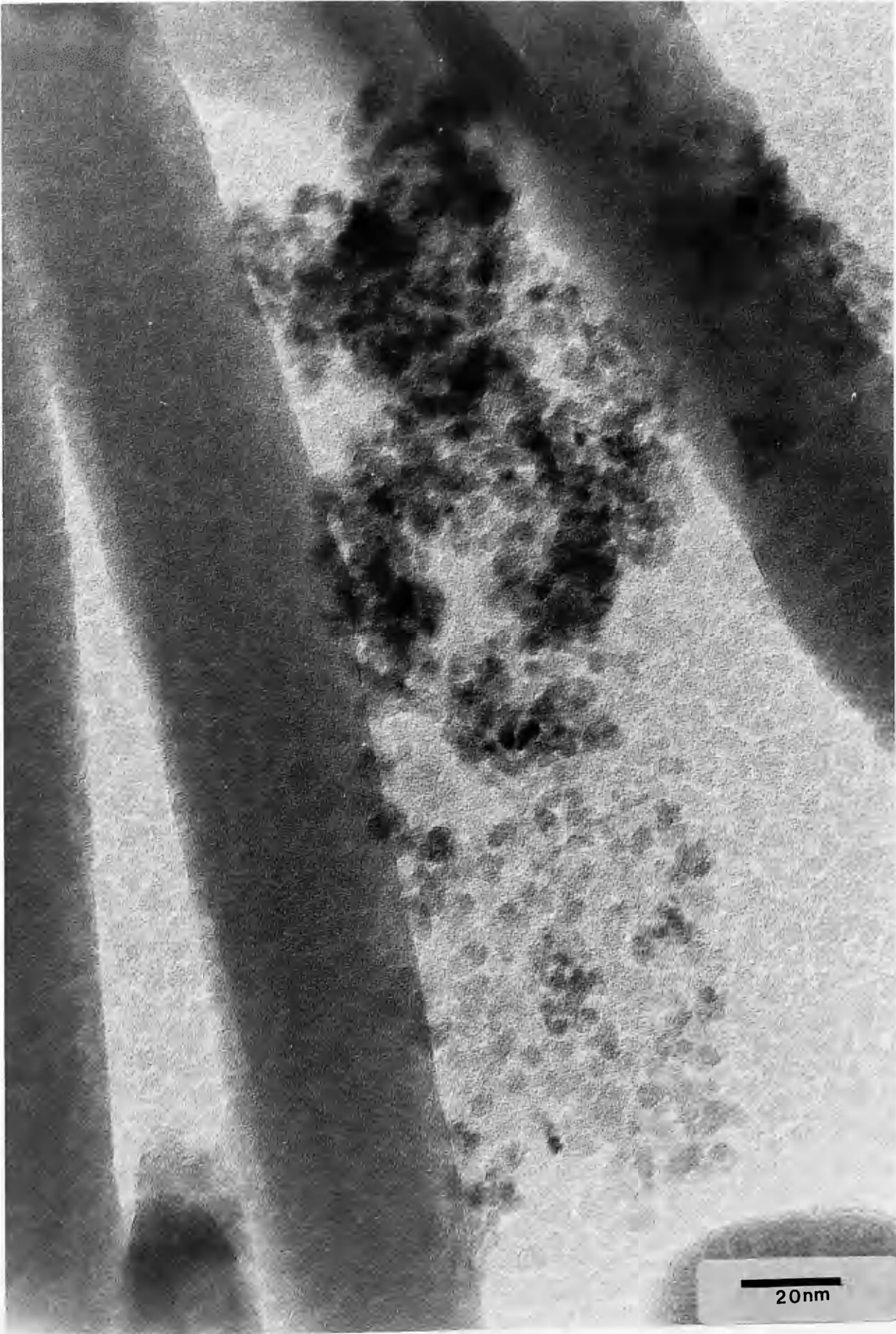


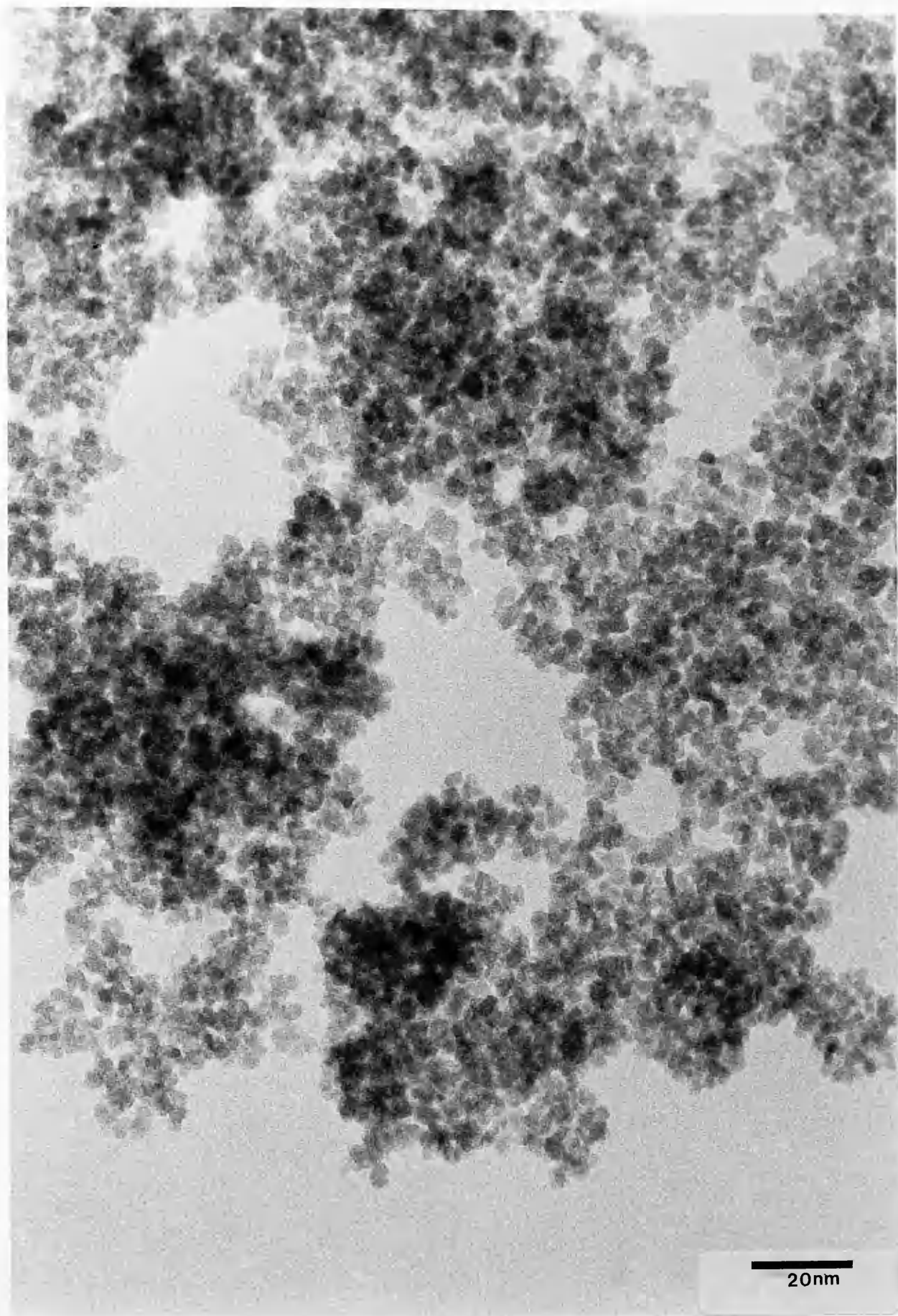
Figure 5.18: HREM of an aggregate of spherical ferrihydrite particles. Some individual particles suitable for particle size determination could be seen in the micrograph.





NEXT PAGE

Figure 5.19: HREM of synthetic ferrihydrite showing similarities in morphology and particle size to the soil ferrihydrite in Figure 5.18



NEXT PAGE

Figure 5.20: Electron diffraction pattern of the synthetic ferrihydrite shown in Figure 5.19.

O.147nm
O.151
O.173
O.198
O.224
O.254



NEXT PAGE

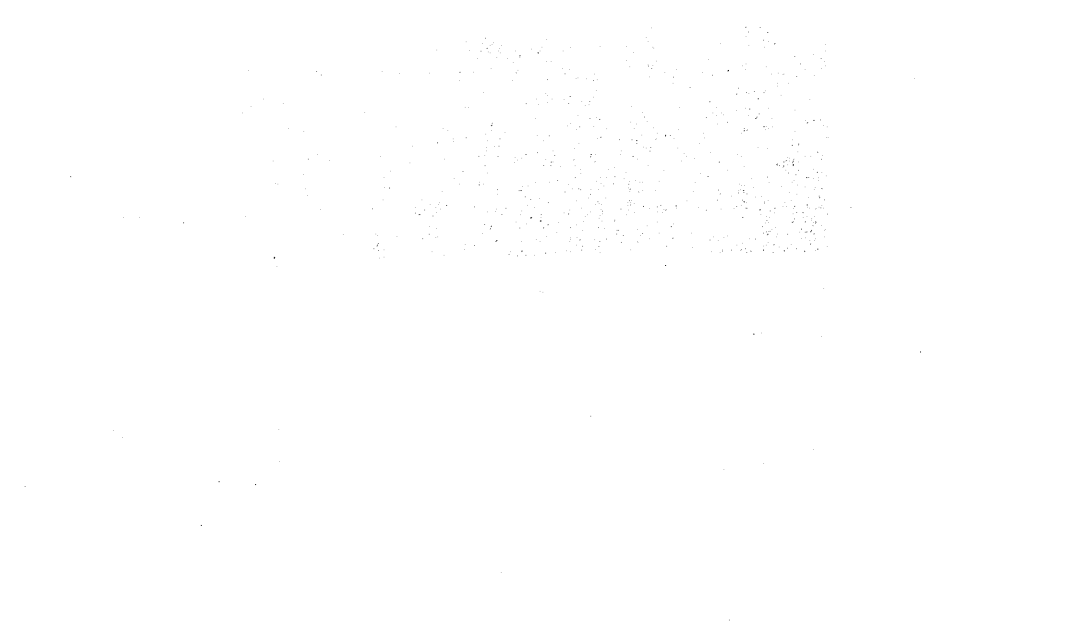
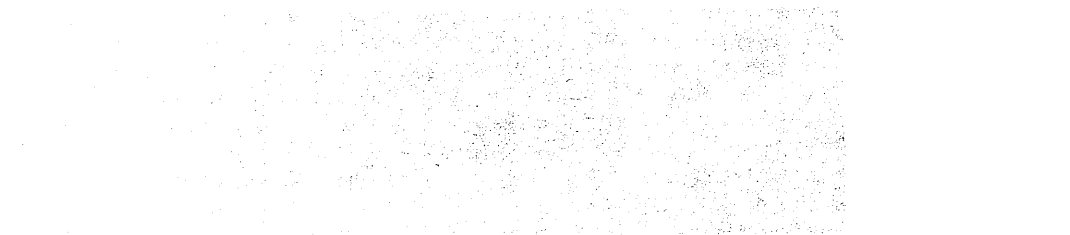
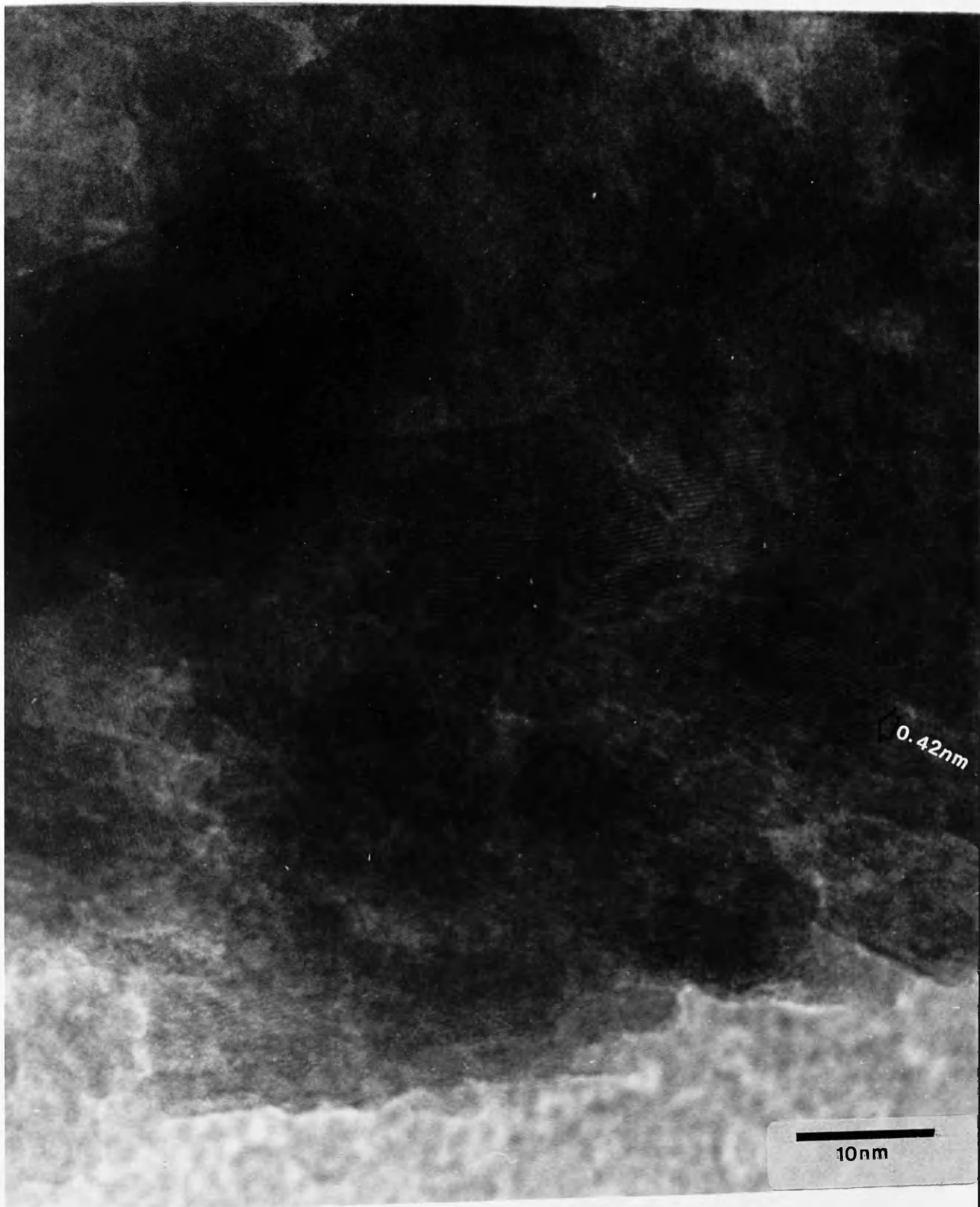


Figure 5.21: HREM of iron oxide particles in Sample 404.05. The 0.42nm(110) lattice fringes of goethite are in evidence





NEXT PAGE

Figure 5.22: Polycrystalline electron diffraction pattern of the goethite particles in Figure 5.21.

0.172nm

0.181

0.192

0.226

0.245

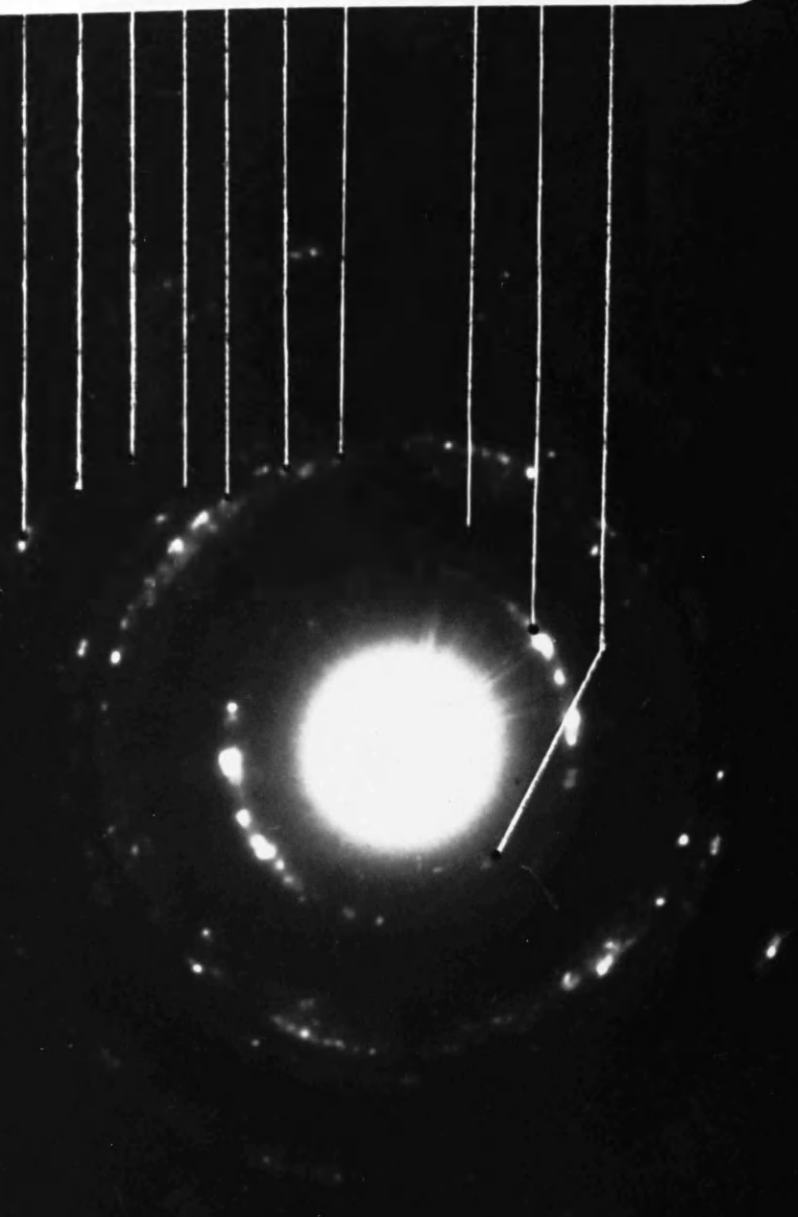
0.257

0.269

0.335

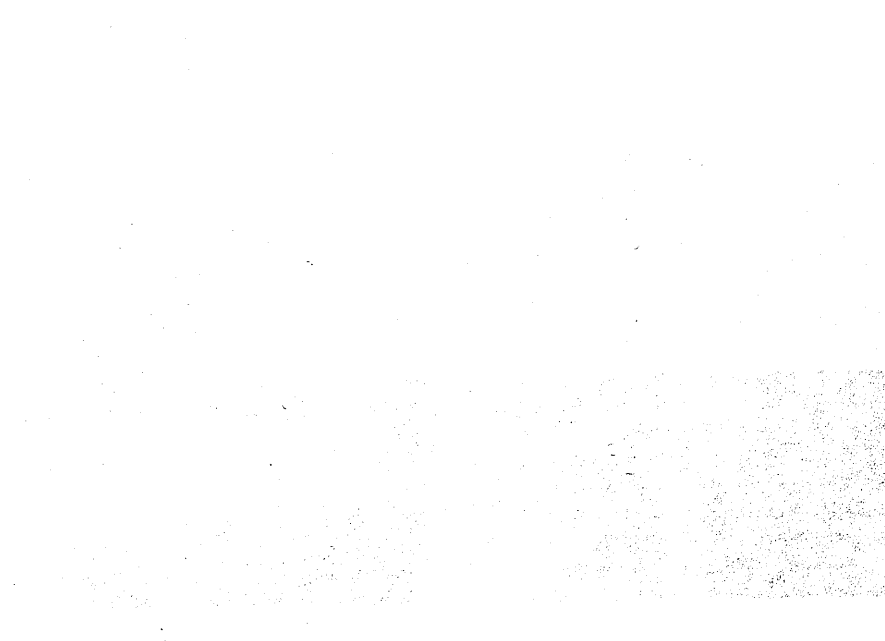
0.419

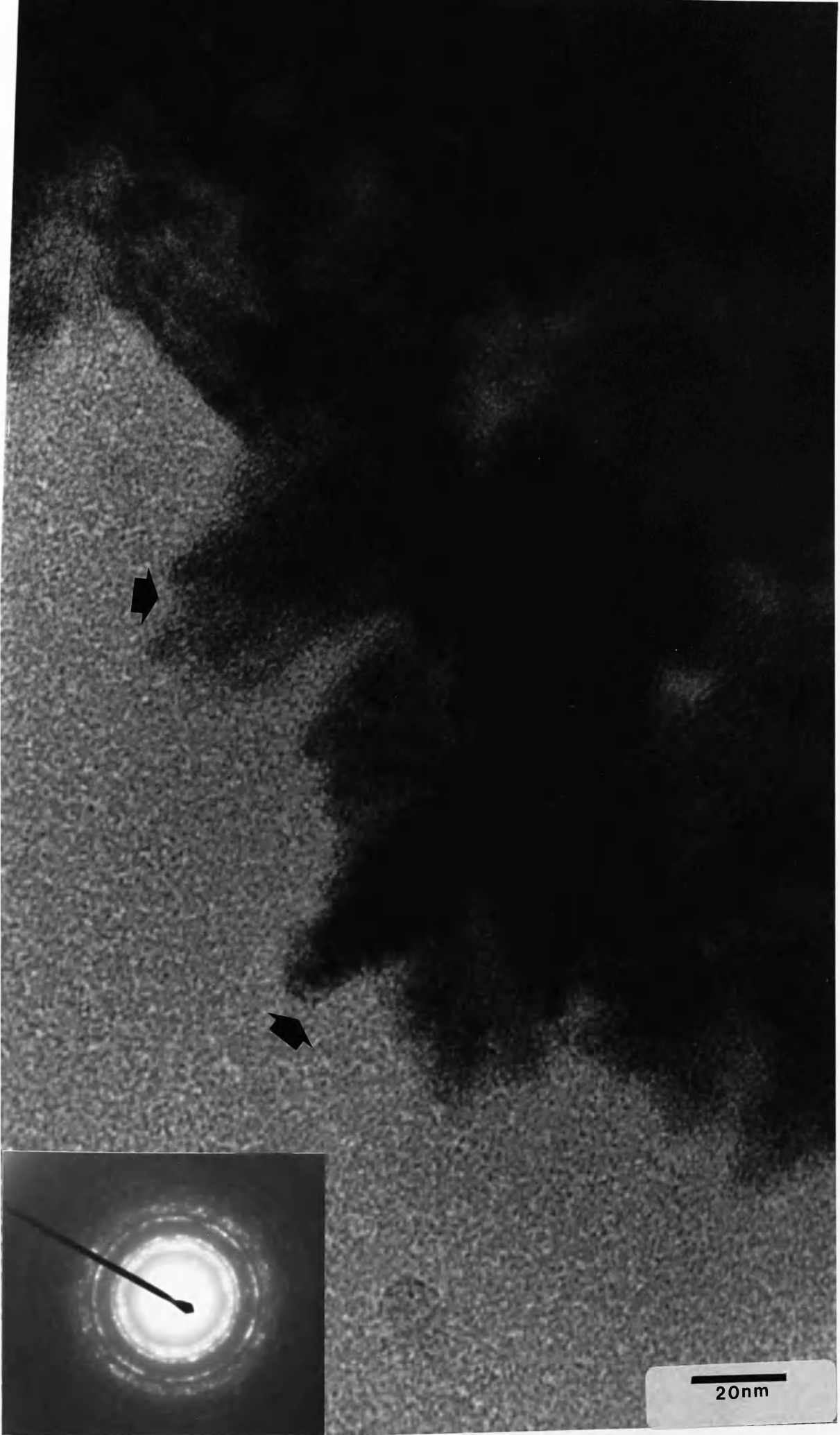
0.496



NEXT PAGE

Figure 5.23: HREM of goethite particles in Sample 404.05. The arrowed particles may be bundles of goethite laths.

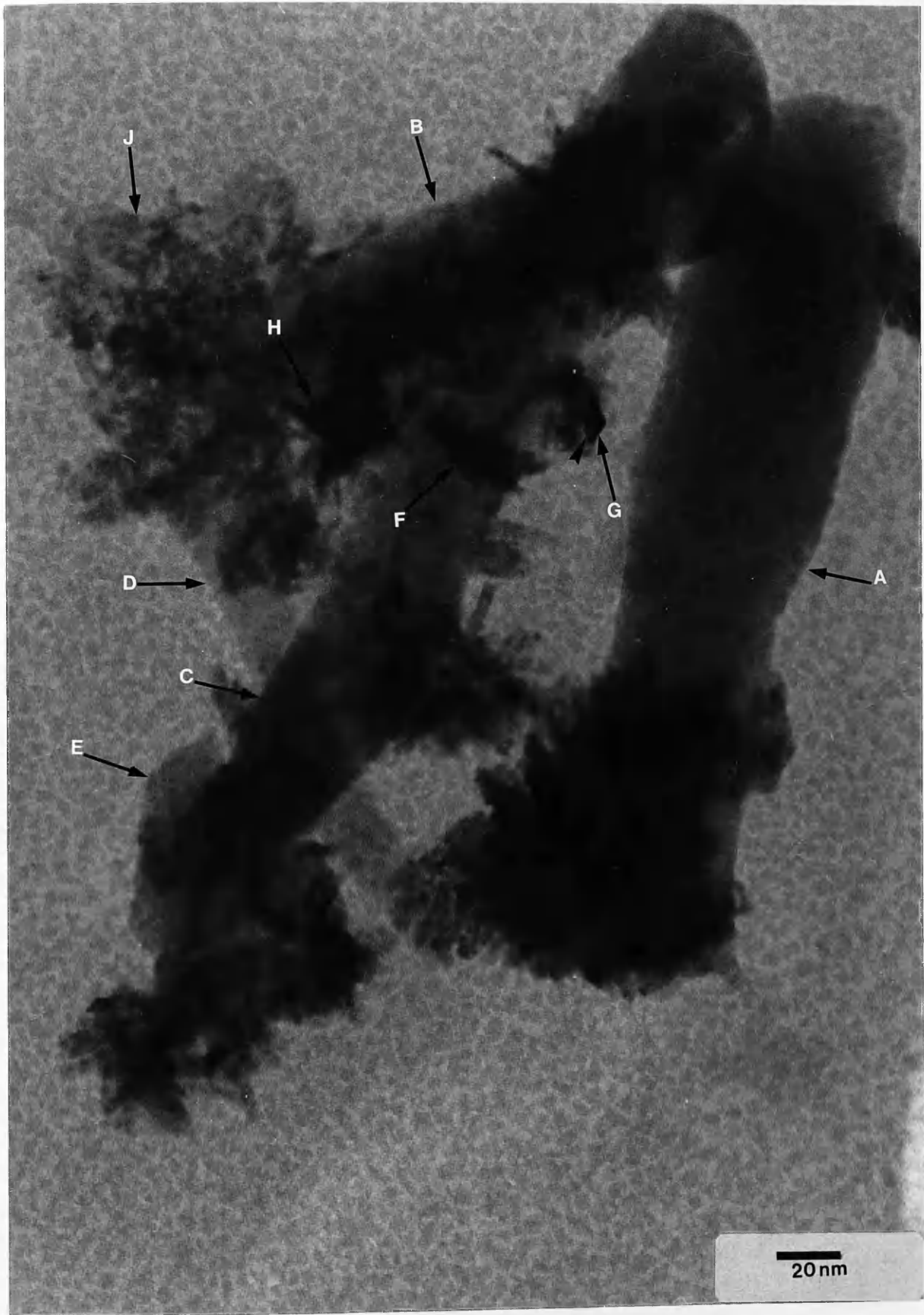




20nm

NEXT PAGE

Figure 5.24: HREM of lath shaped goethite particles and spherical particles (probably ferrihydrite). The particles labelled A, B, C, D and E are likely to be clay particles.



NEXT PAGE

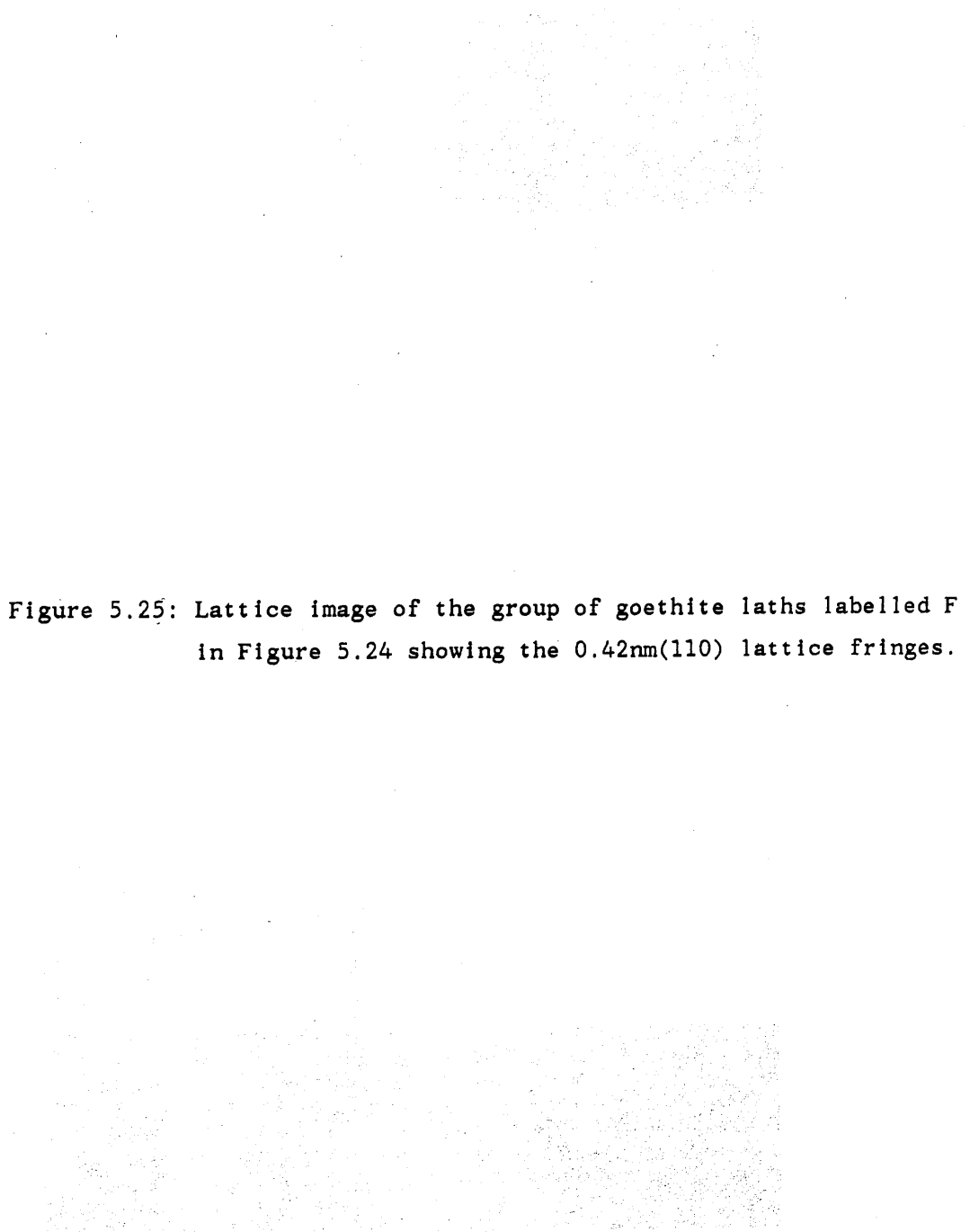
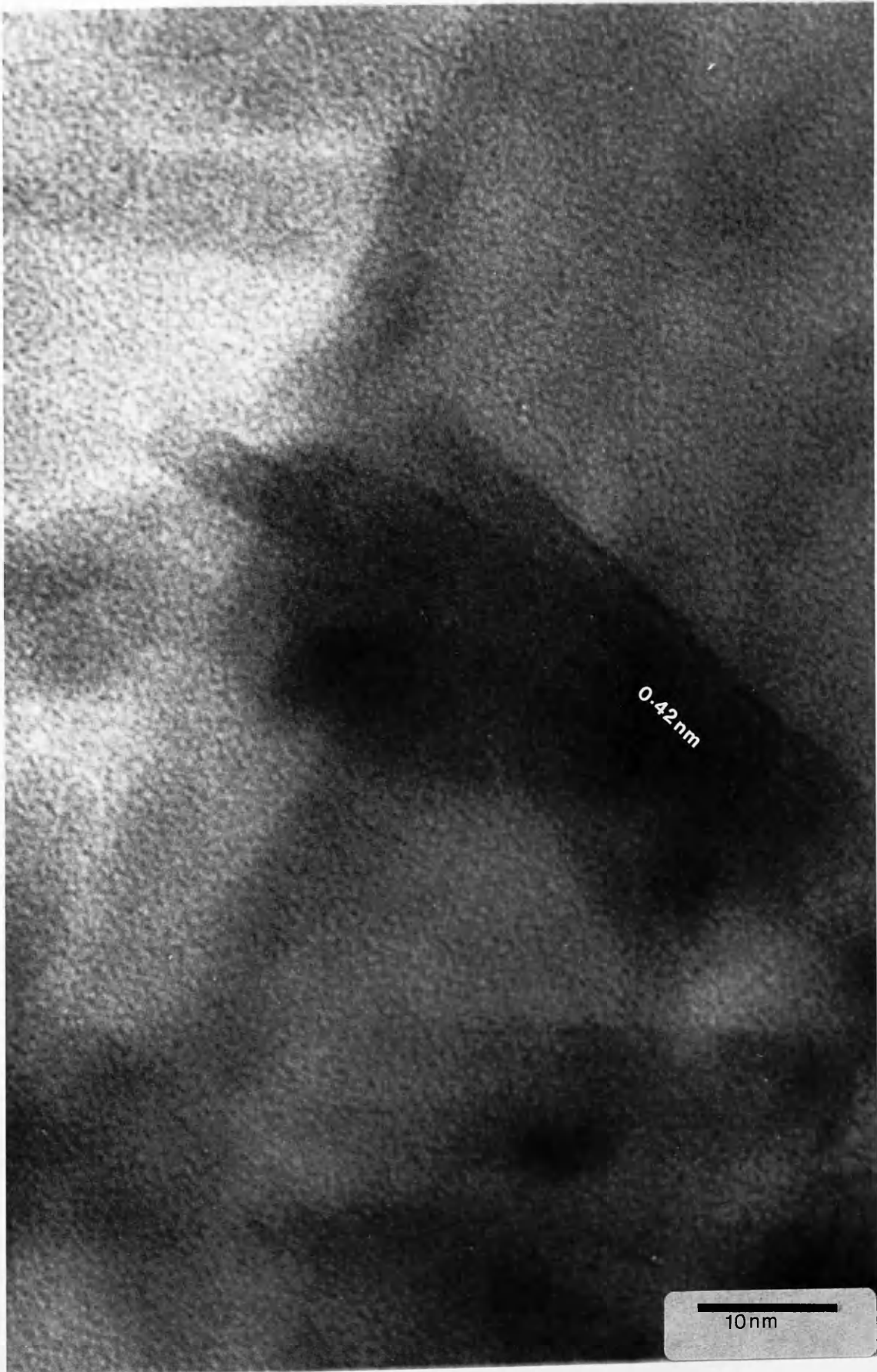


Figure 5.25: Lattice image of the group of goethite laths labelled F in Figure 5.24 showing the 0.42nm(110) lattice fringes.



0.42nm

10nm

NEXT PAGE

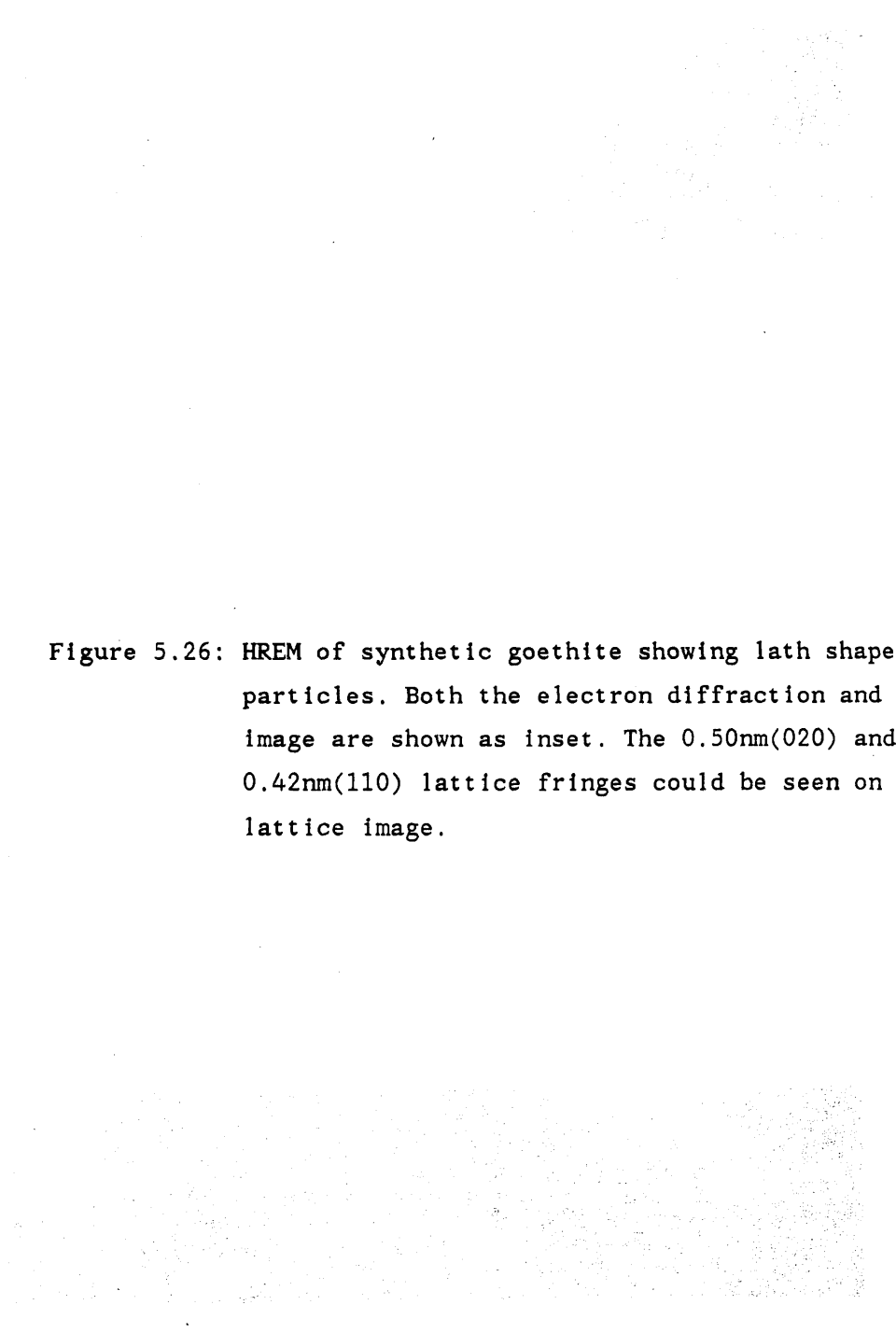
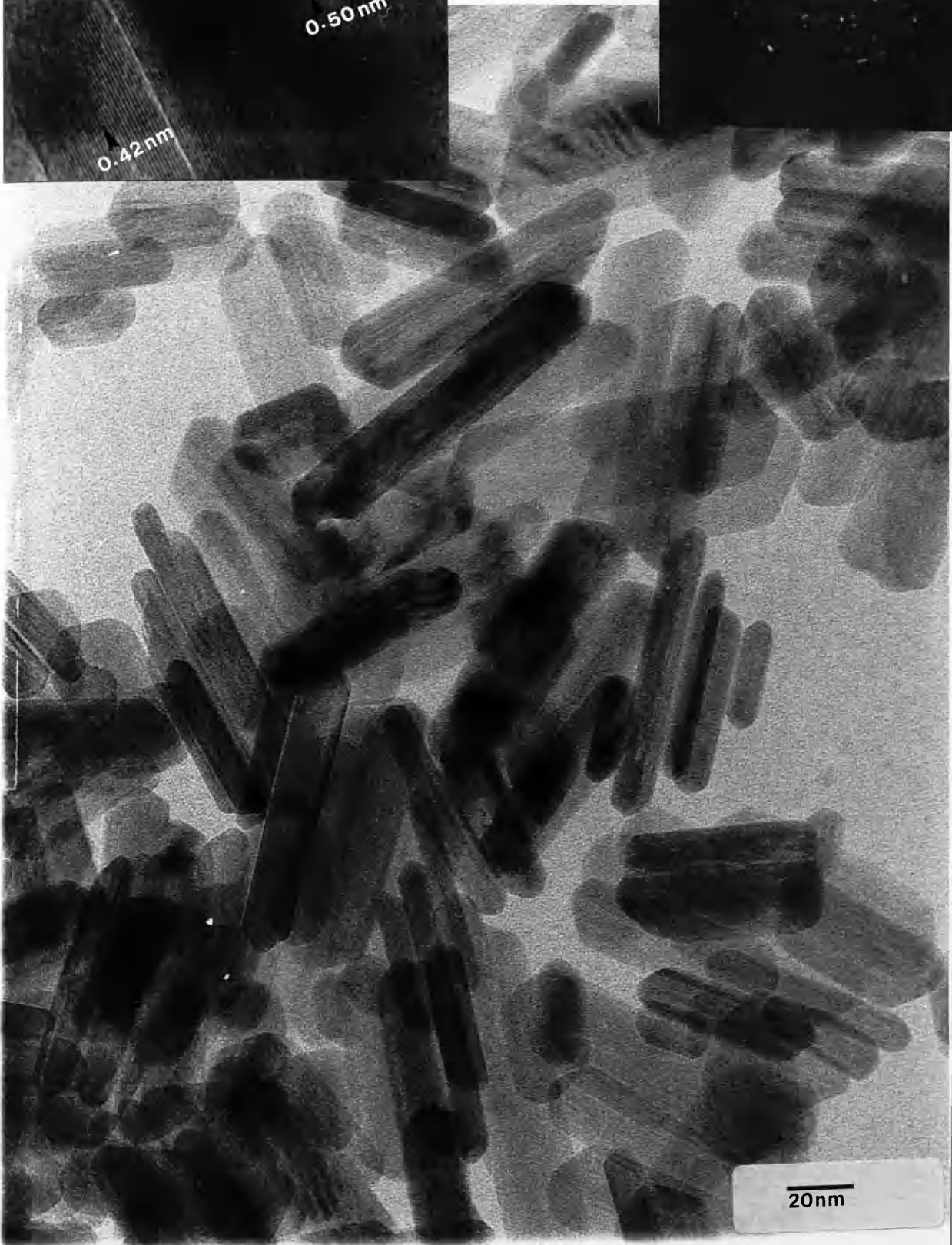
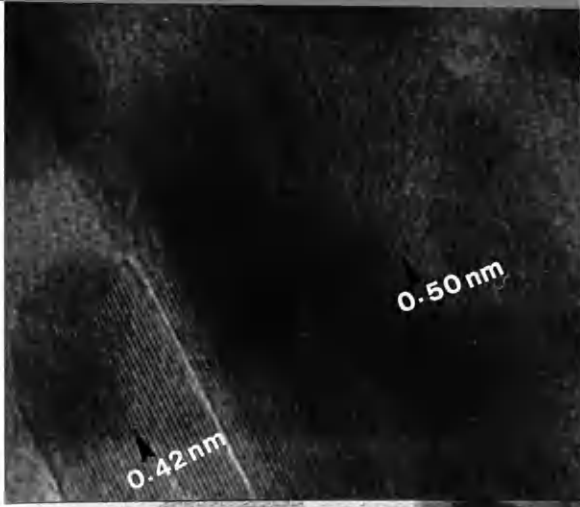


Figure 5.26: HREM of synthetic goethite showing lath shaped particles. Both the electron diffraction and lattice image are shown as inset. The 0.50nm(020) and 0.42nm(110) lattice fringes could be seen on the lattice image.



NEXT PAGE

Figure 5.27: HREM of the goethite particle labelled 'G' in Figure 5.24. The particle is likely to be a goethite crystal showing the (110) face. The lattice fringes of 0.977nm correspond to the cell constant (b_0) of the goethite crystal. The scale bar of Figure 5.28 (below) applies.

Figure 5.29: HREM of the spherical particles labelled 'J' in Figure 5.24.

0.977nm



10nm

NEXT PAGE

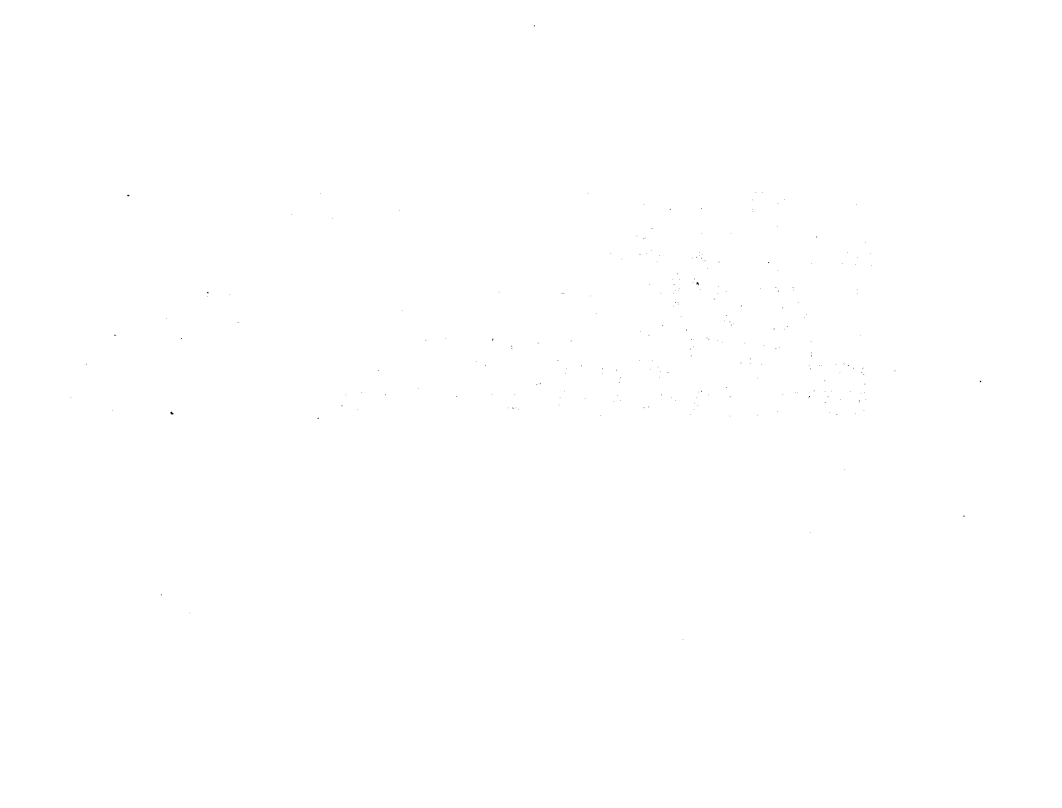


Figure 5.30: HREM of iron oxide and clay particles. The iron oxide particles appear to be attached to the edges and surfaces of the halloysite tubes. Electron diffraction of the iron oxide particles showing goethite reflections is shown as inset.

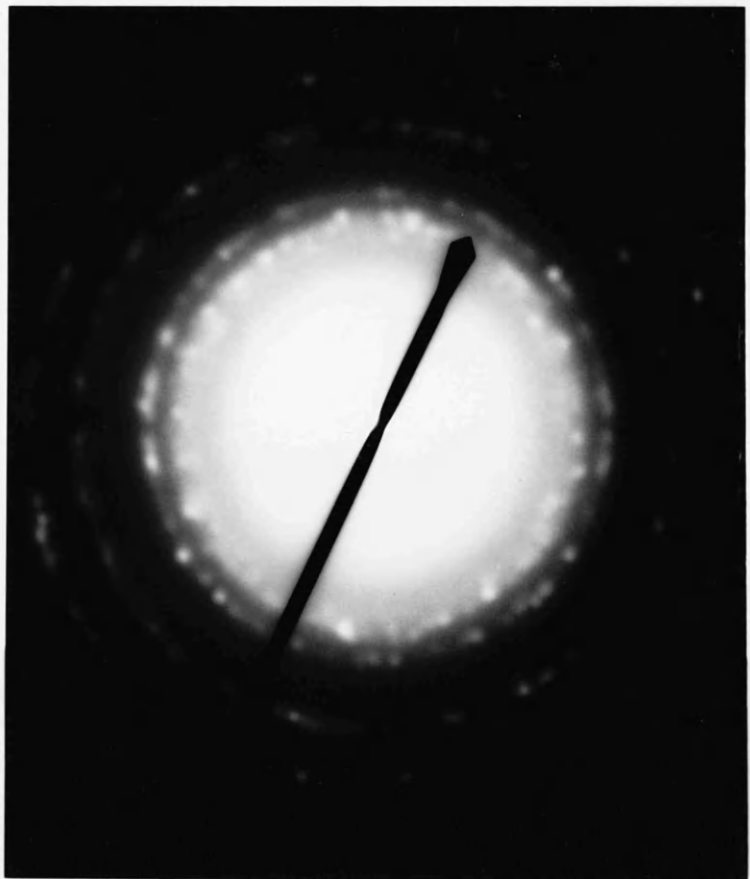


NEXT PAGE

Figure 5.31: TEM of an aggregate of iron oxide particles from the red fraction of Sample 404.06.



Figure 5.32: Electron diffraction of the iron oxide aggregate in Figure 5.31 showing reflections that are typical of goethite.



NEXT PAGE

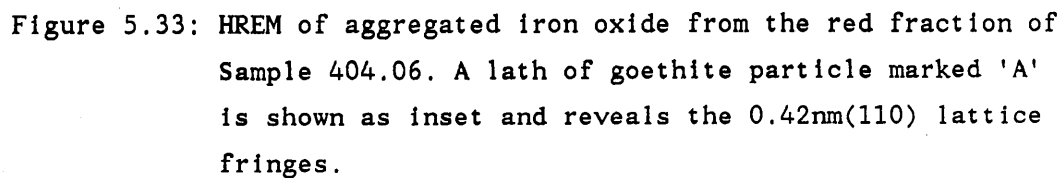
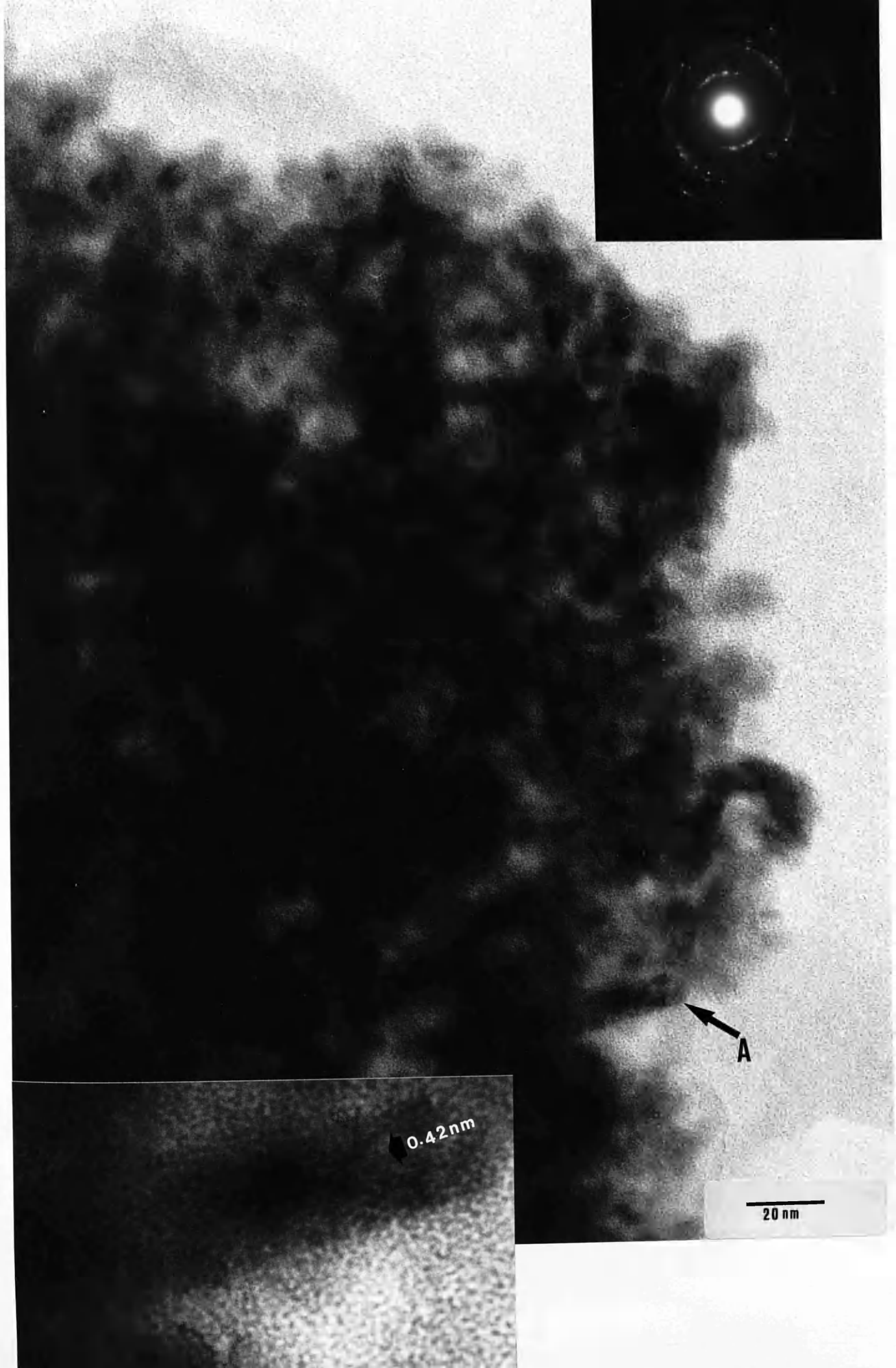
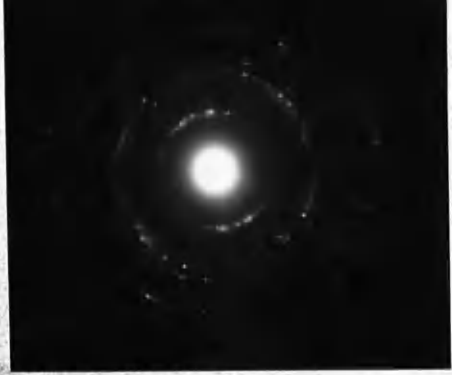


Figure 5.33: HREM of aggregated iron oxide from the red fraction of Sample 404.06. A lath of goethite particle marked 'A' is shown as inset and reveals the 0.42nm(110) lattice fringes.



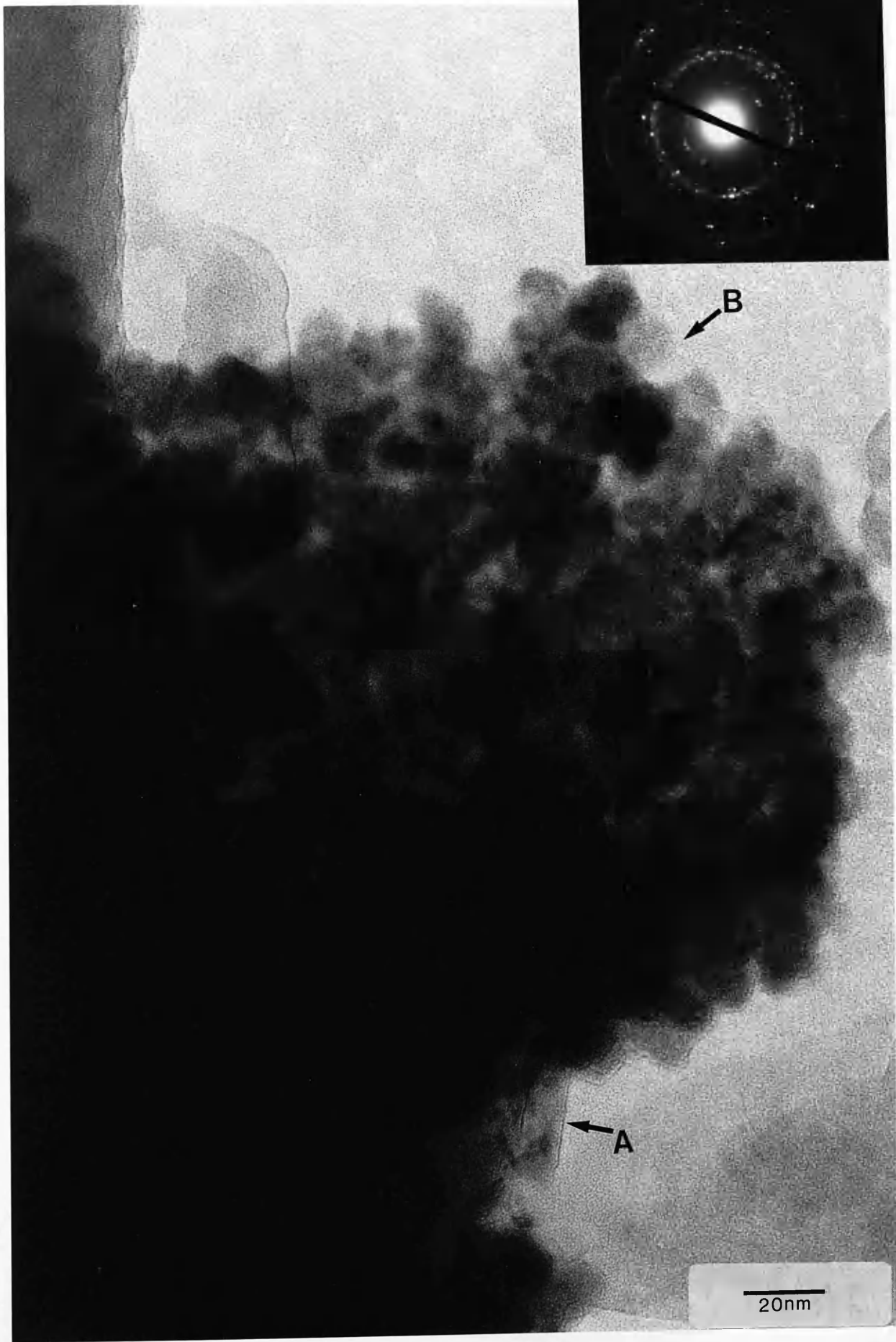
A

0.42 nm

20 nm

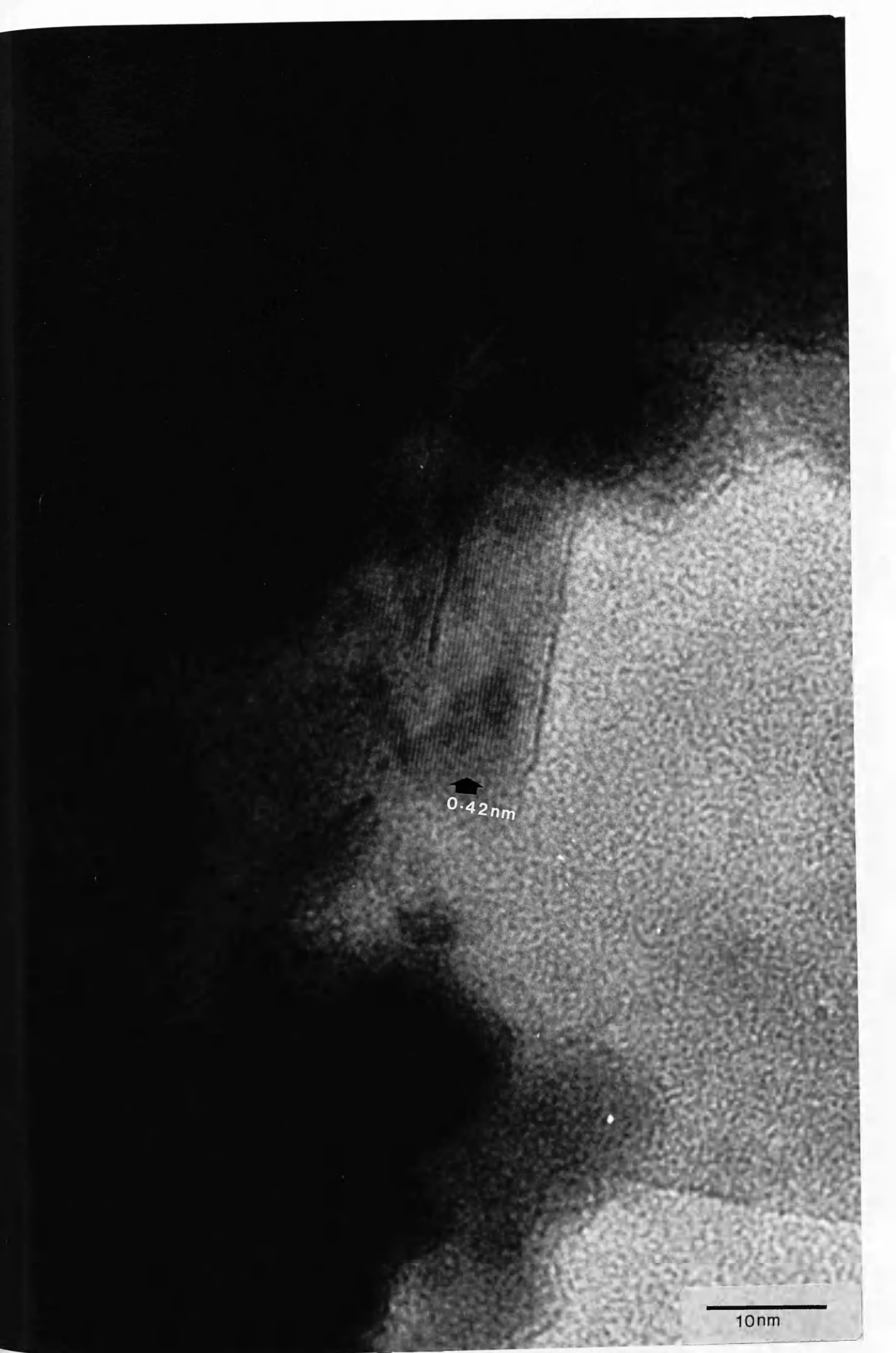
NEXT PAGE

Figure 5.34: HREM of iron oxide particles from the red fraction of Sample 404.06. The electron diffraction pattern showing goethite reflections is shown as inset. The particles labelled 'A' and 'B' are enlarged in Figures 5.35 and 5.36 respectively.



NEXT PAGE

Figure 5.35: Lattice image of a goethite lath labelled 'A' in Figure 5.34. The 0.42nm(110) lattice fringes of goethite are in evidence.

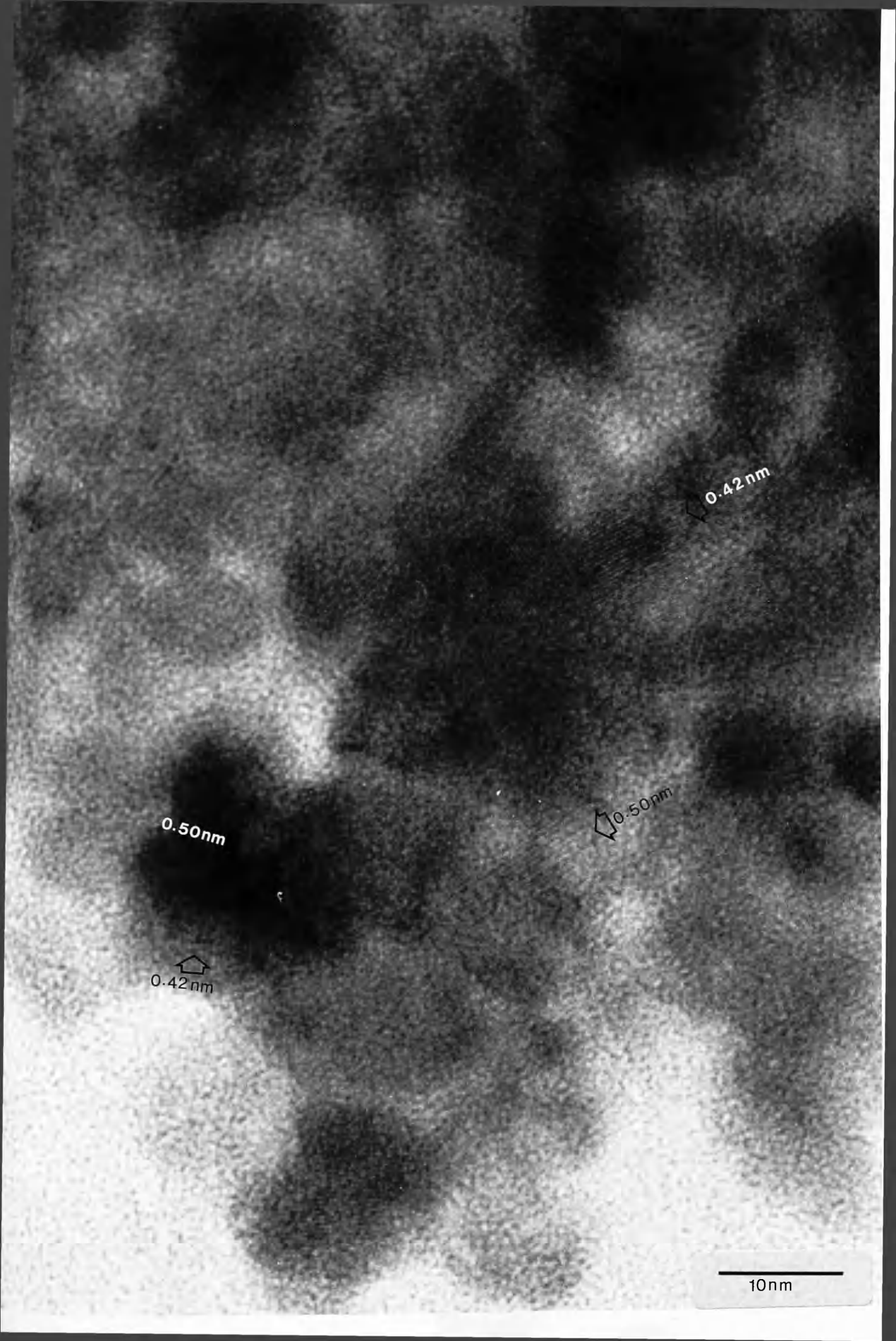


0.42 nm

10 nm

NEXT PAGE

Figure 5.36: HREM of goethite particles labelled 'B' in Figure 5.34 showing particles with 0.50nm(020) and 0.42nm(110) lattice fringes.



0.50nm

0.42nm

0.42nm

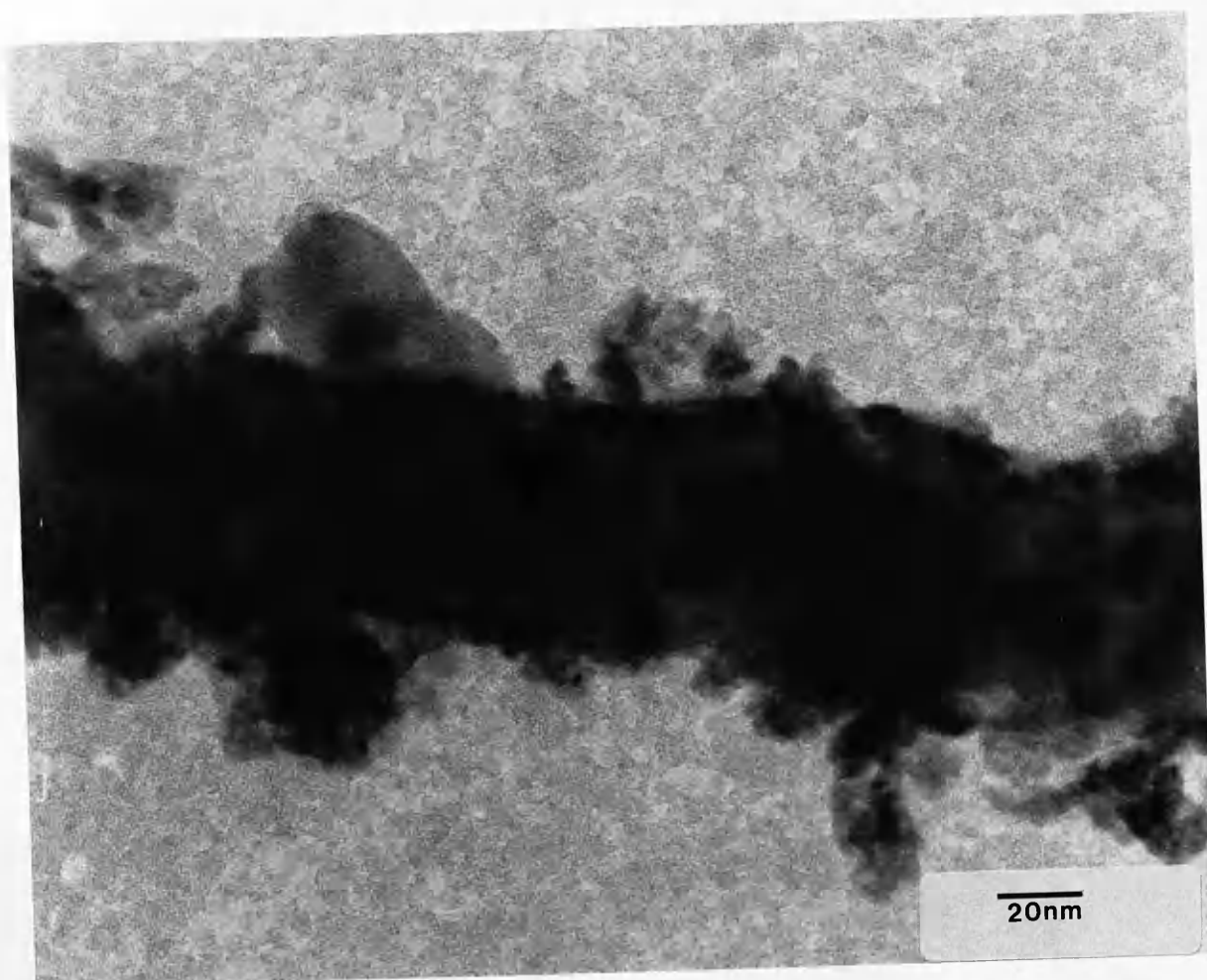
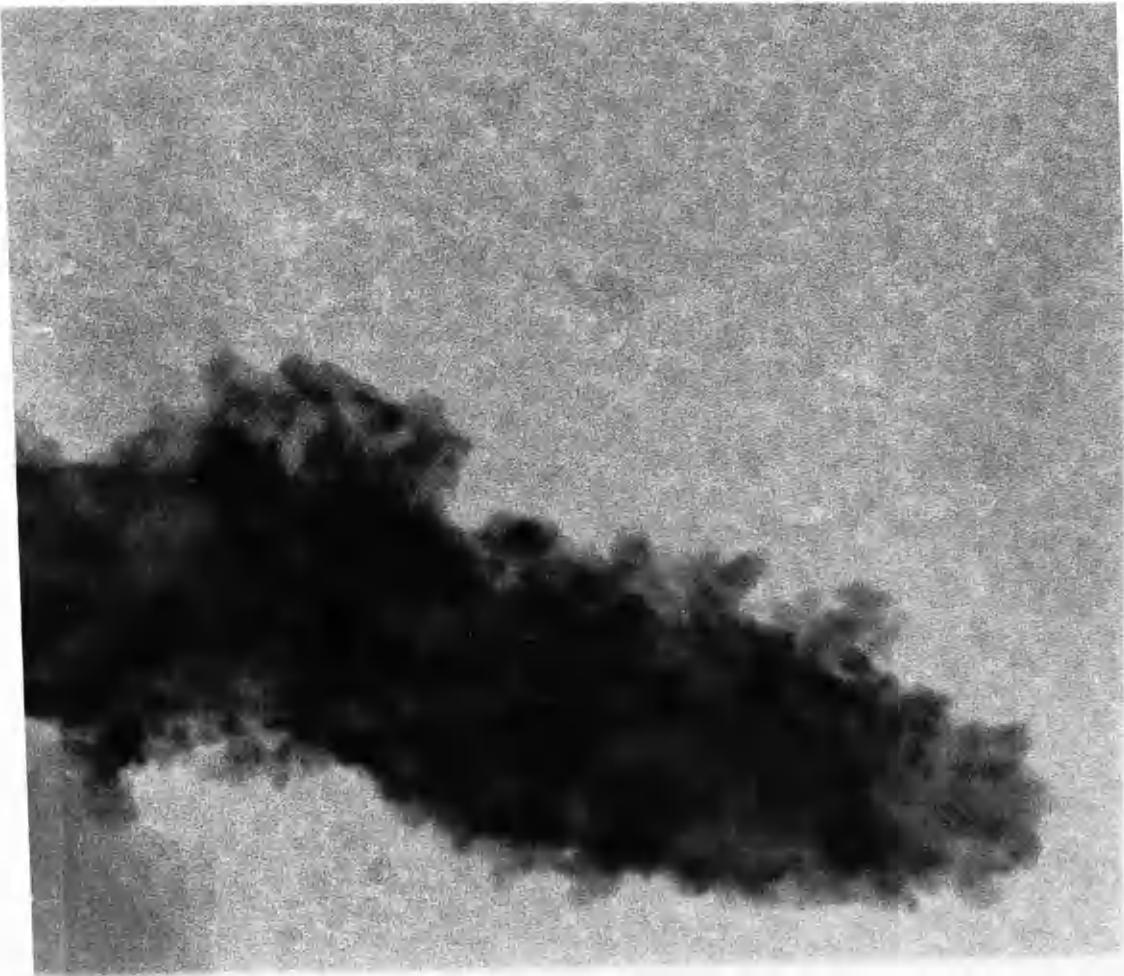
0.50nm

10nm

NEXT PAGE

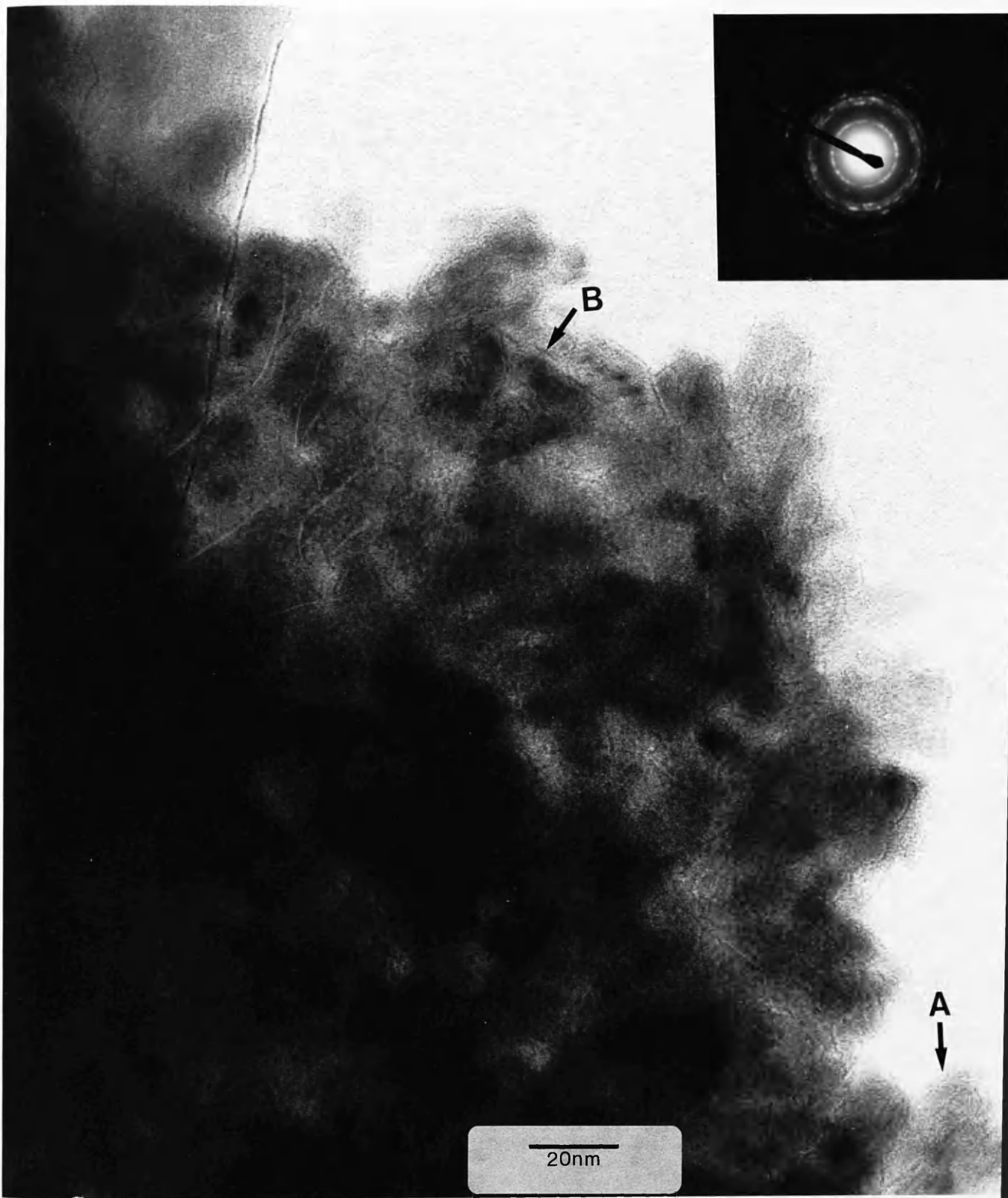
Figure 5.37a: HREM of iron oxide particles stuck to the edges and surfaces of a halloysite particle. The scale bar in Figure 5.37b applies.

Figure 5.37b: Another view of the iron oxide and clay particles in Figure 5.37a.



NEXT PAGE

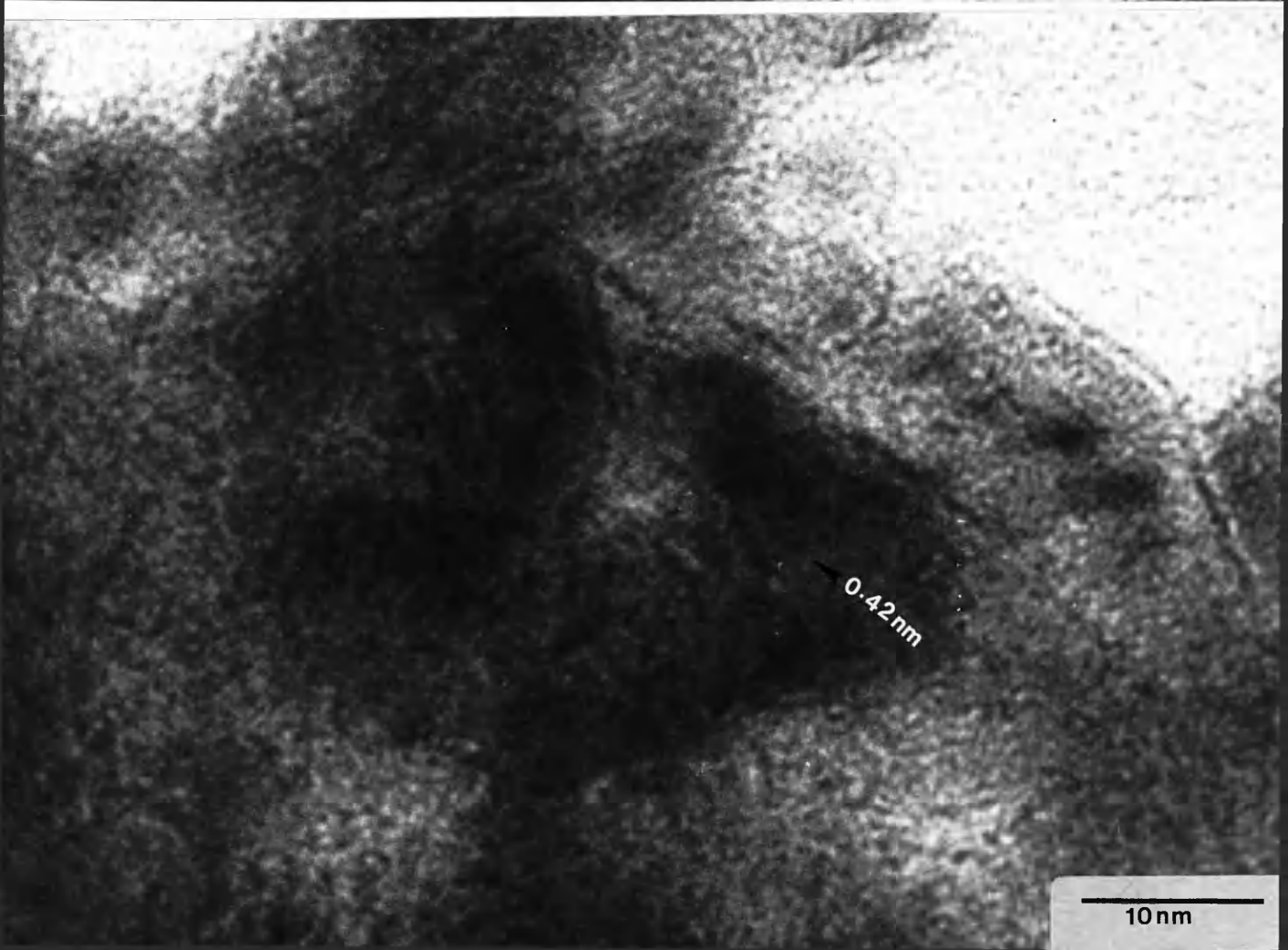
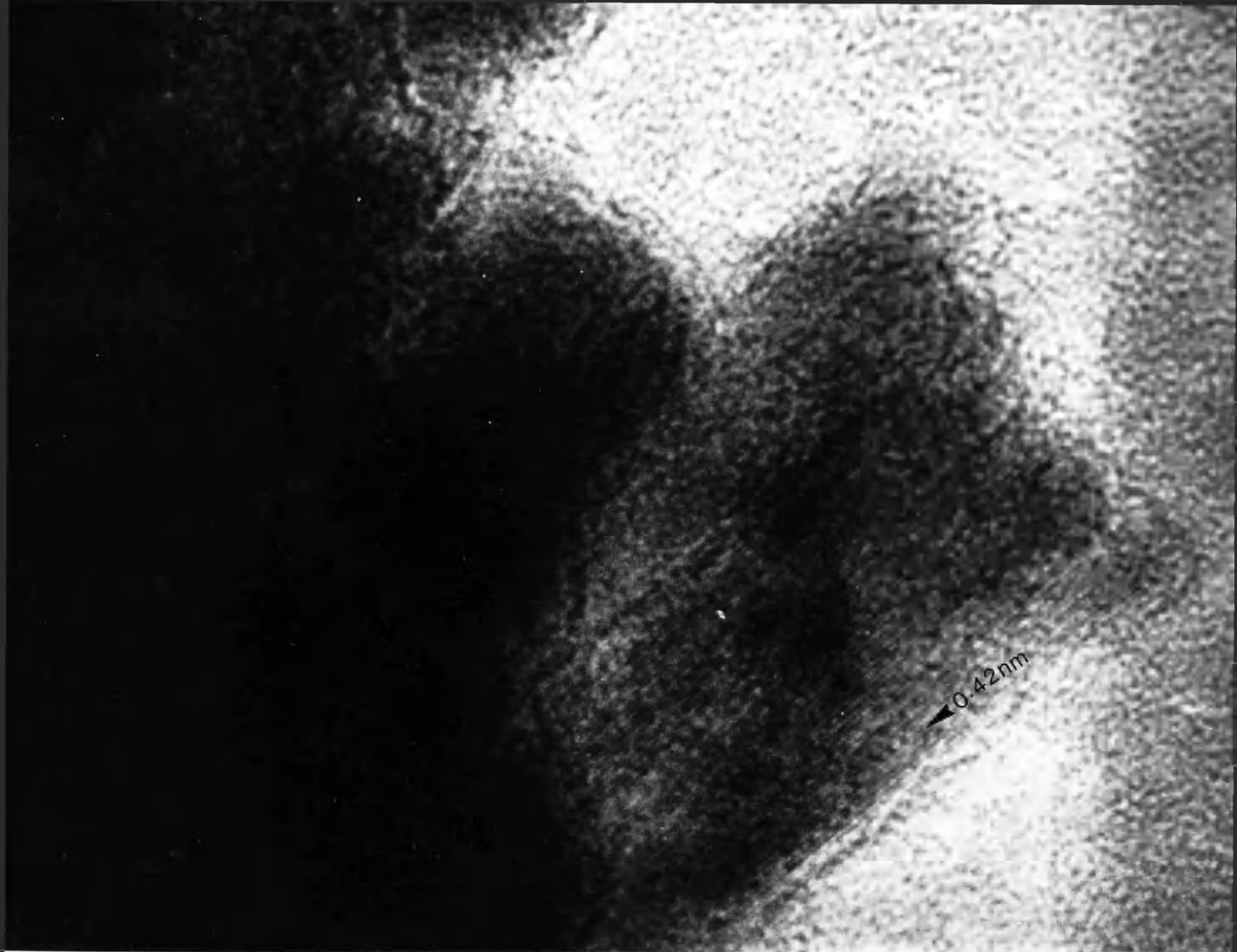
Figure 5.38: HREM of iron oxide particles in the yellow fraction of Sample 404.06 showing lath-like (acicular) particles. The electron diffraction pattern is shown as inset and revealed goethite reflections. The particles labelled 'A' and 'B' are enlarged in Figures 5.39 and 5.40 respectively.



NEXT PAGE

Figure 5.39: Lattice image of a goethite lath labelled 'A' in Figure 5.38. The 0.42nm(110) lattice fringes of goethite are in evidence. The scale bar on Figure 5.40 (below) applies.

Figure 5.40: Lattice image of another goethite lath (marked 'B' in Figure 5.38) showing the 0.42nm(110) lattice fringes.



NEXT PAGE




Figure 5.41: HREM of goethite particles in the yellow fraction of Sample 404.06. The 0.42nm(110) lattice fringes are evident on some of the particles. The particle labelled 'A' is probably a goethite crystal seen on-edge and the 0.455nm and 0.960nm lattice fringes on the particle correspond to the cell constants a_0 and b_0 of the goethite crystal respectively.



0.42nm

0.42nm

A

$0.960\text{nm} = b_0$

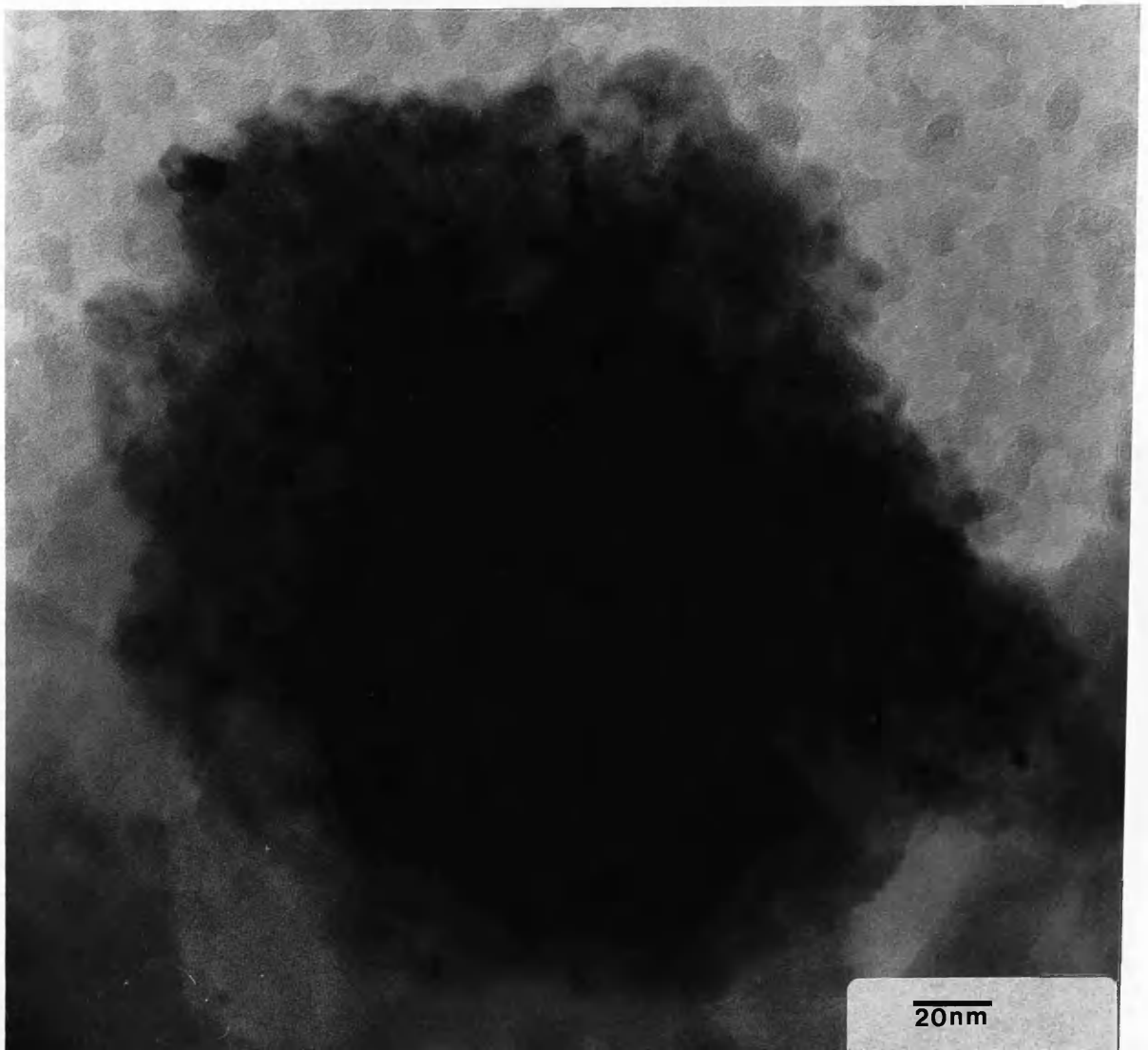
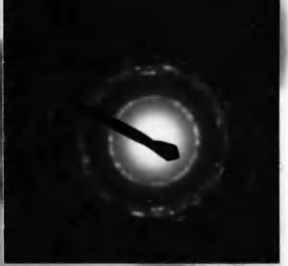
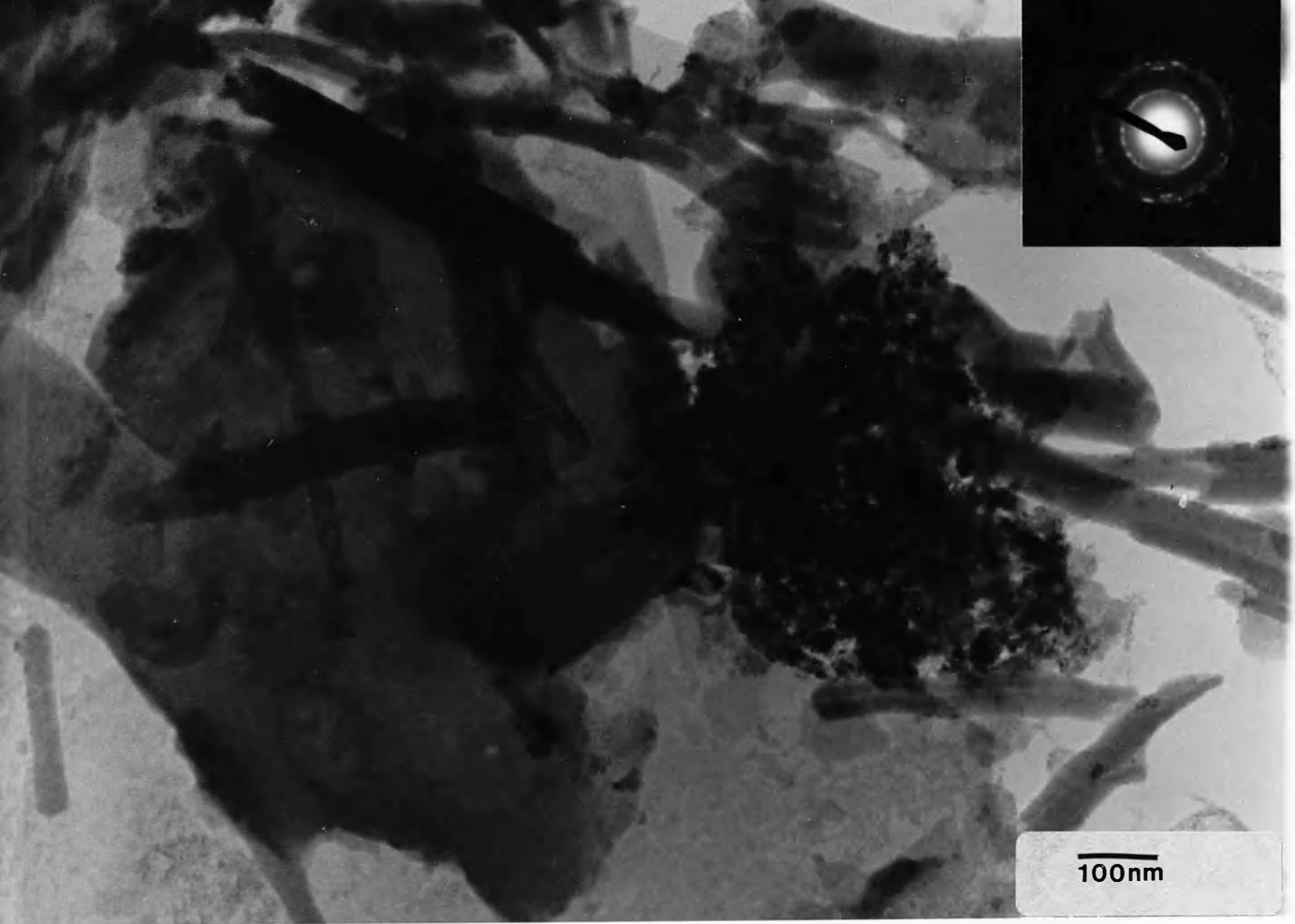
$0.455\text{nm} = a_0$

10nm

NEXT PAGE

Figure 5.42: TEM of iron oxide particles in Sample 404.07. The electron diffraction shown as inset gave reflections that identified the particles as goethite.

Figure 5.43: HREM of aggregated goethite particles in Sample 404.08.



NEXT PAGE


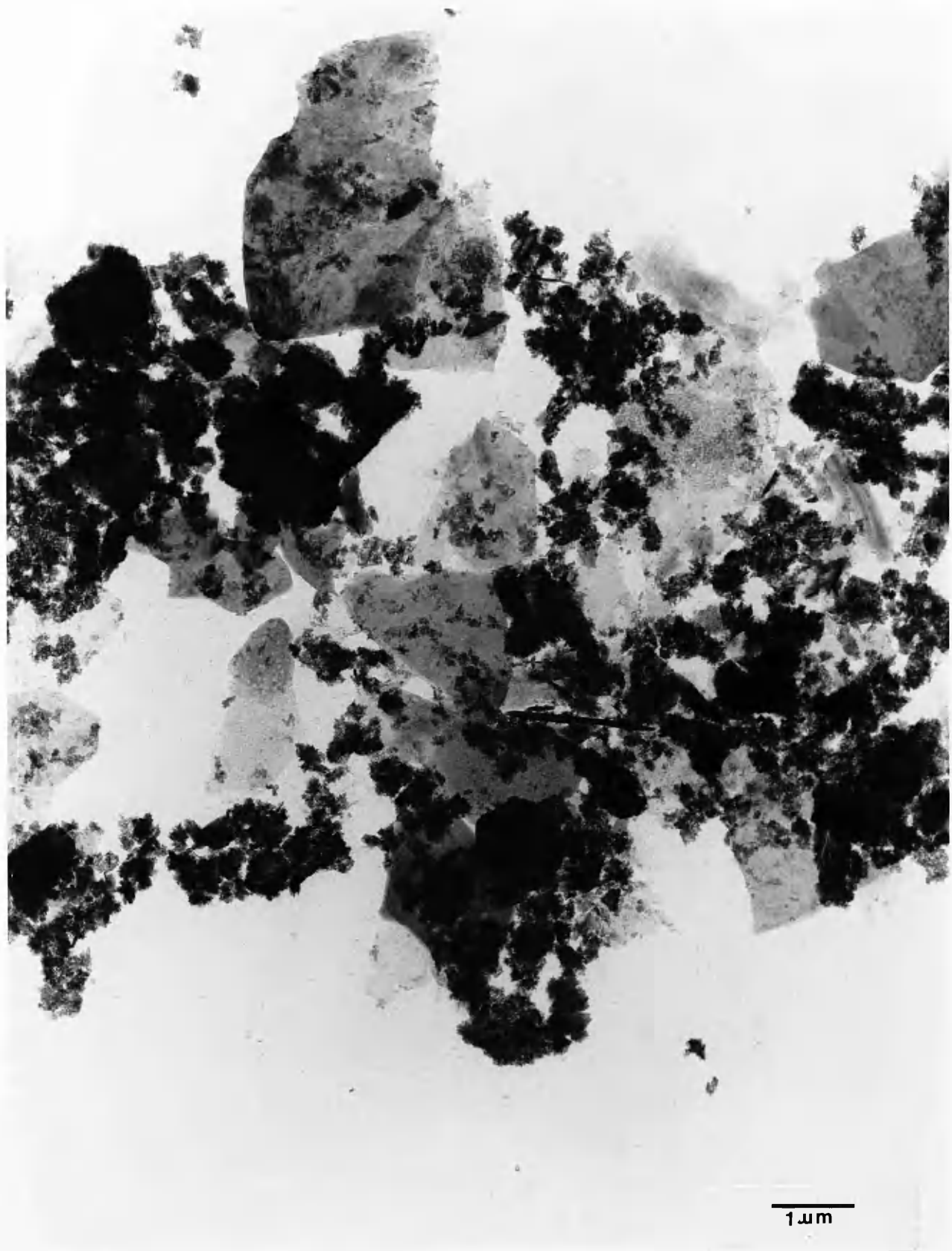


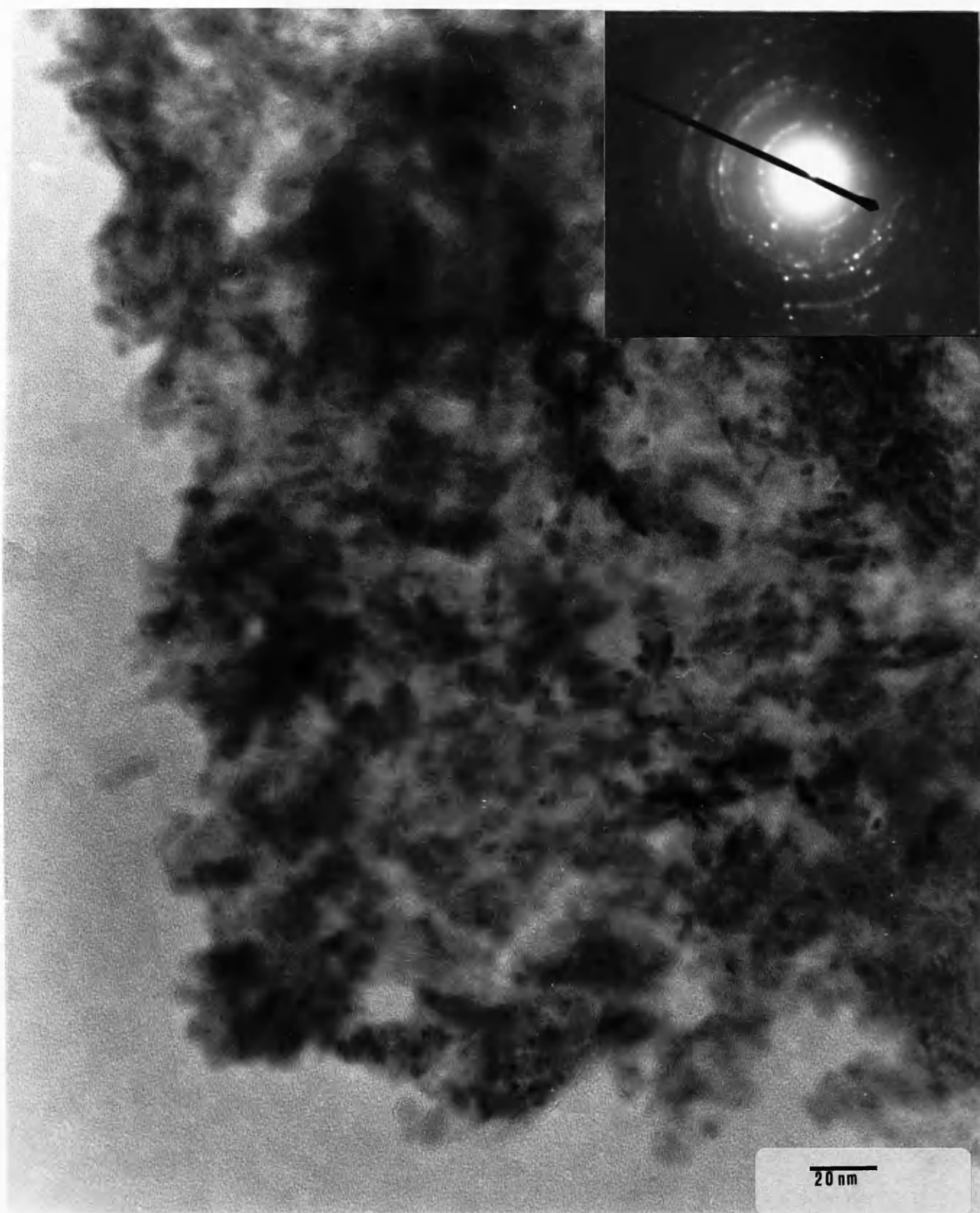
Figure 5.44: TEM of the general section of the NaOH-treated residue of Sample 404.05 showing iron oxide aggregates and clay plates.



1 μm

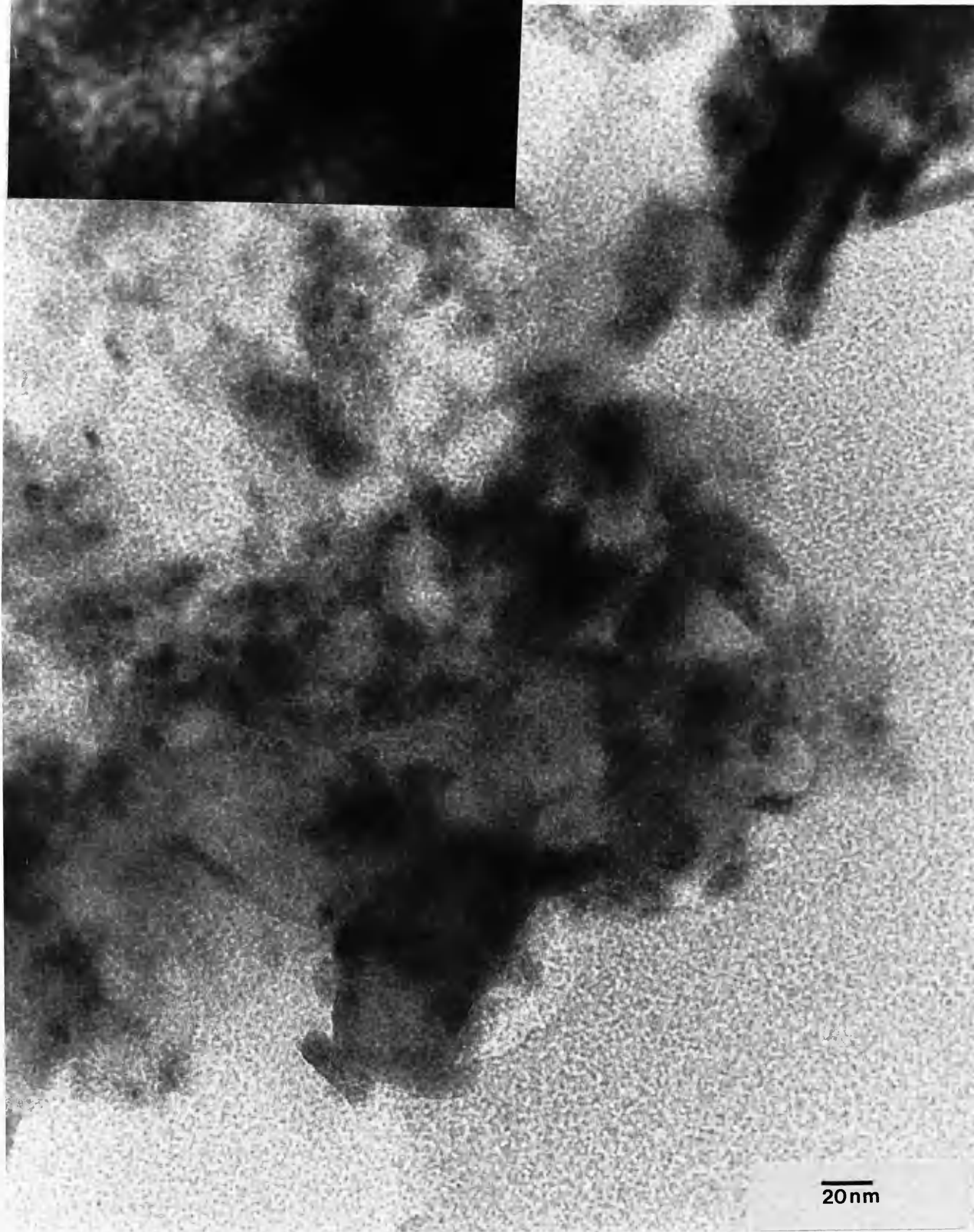
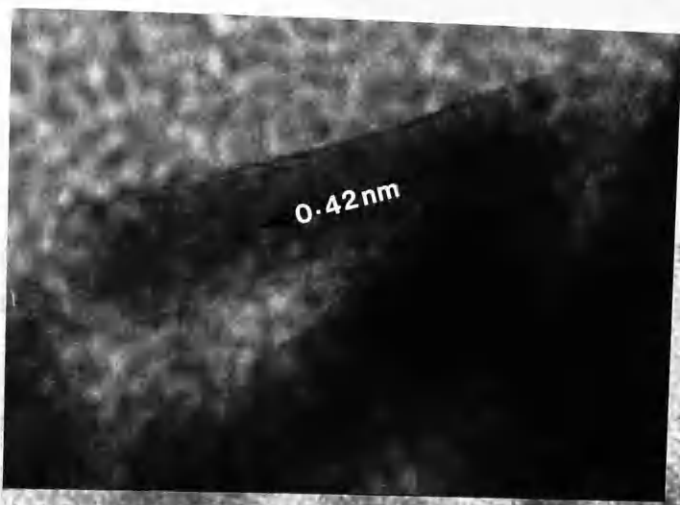
NEXT PAGE

Figure 5.45: HREM of goethite particles in the NaOH-treated residue of Sample 404.05. Electron diffraction is shown as inset.



NEXT PAGE

Figure 5.46: HREM of goethite particles in the NaOH-treated residue of Sample 404.06. Lattice image shown as inset shows a lath of goethite with the 0.42nm(110) lattice fringes in evidence.



NEXT PAGE


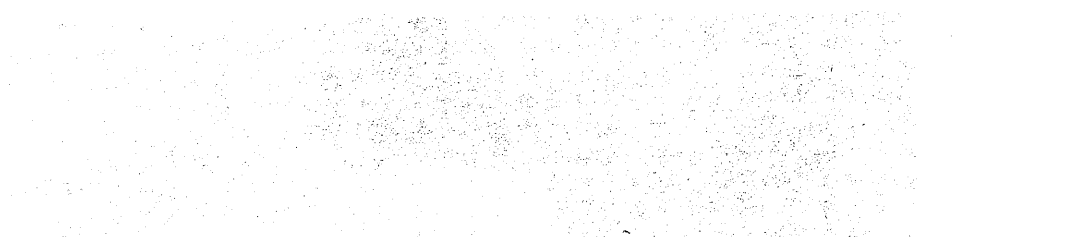


Figure 5.47: HREM of goethite particles in the NaOH-treated residue of Sample 404.07. A more plate-like morphology of the goethite particles, compared to those in the deeper soils, is indicated.





NEXT PAGE

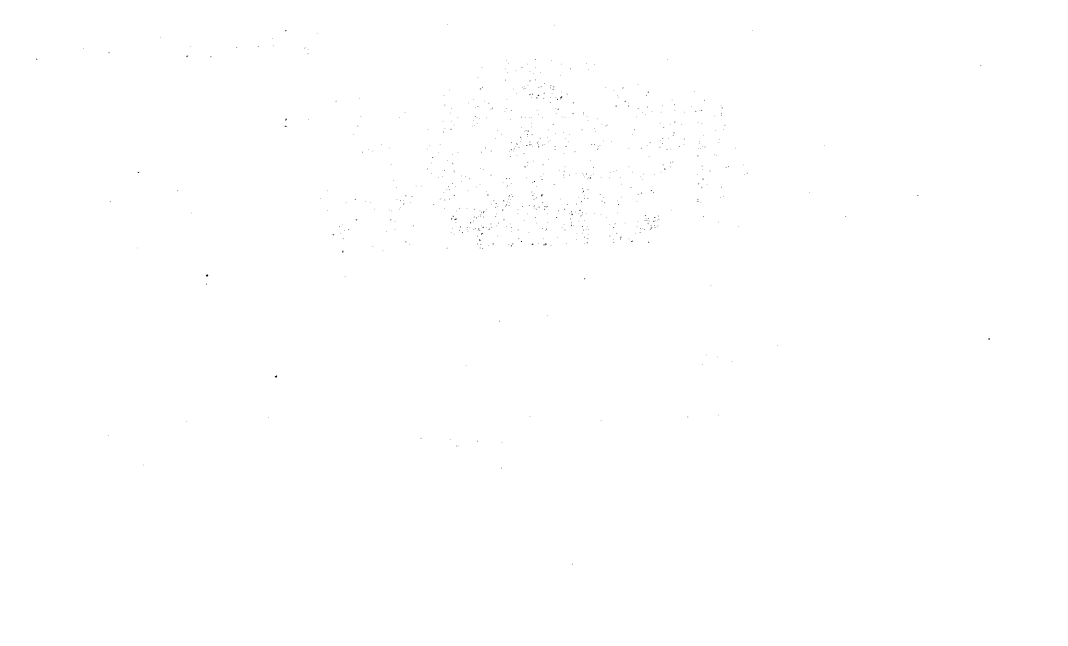
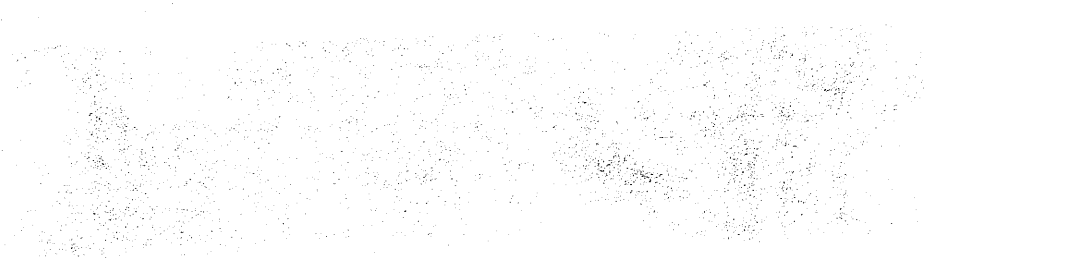
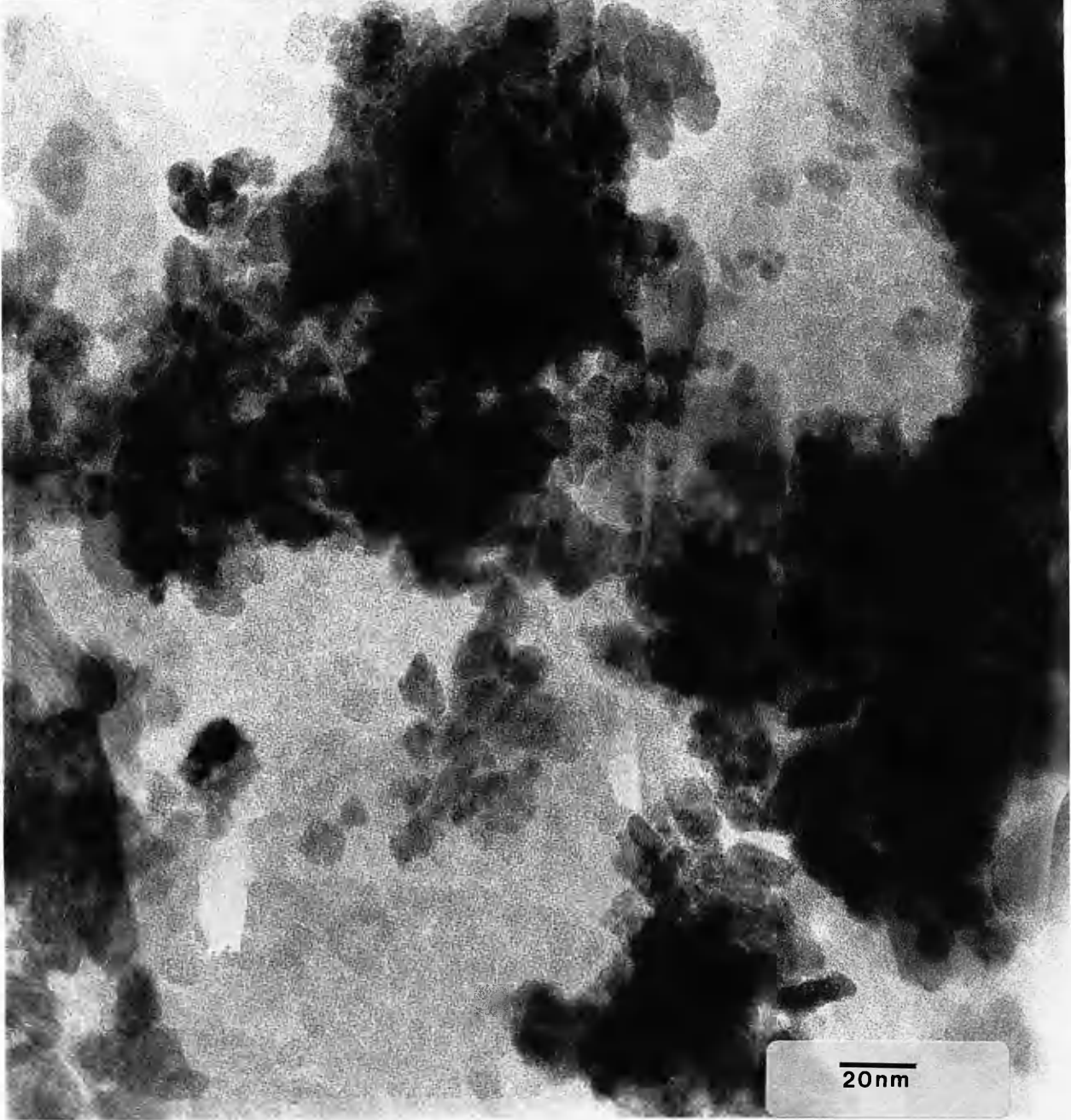


Figure 5.48: HREM of goethite particles in the NaOH-treated residue of Sample 404.08 showing goethite particles with plate-like morphology. Enlarged sections of the micrograph are shown on Figures 5.49 and 5.50.

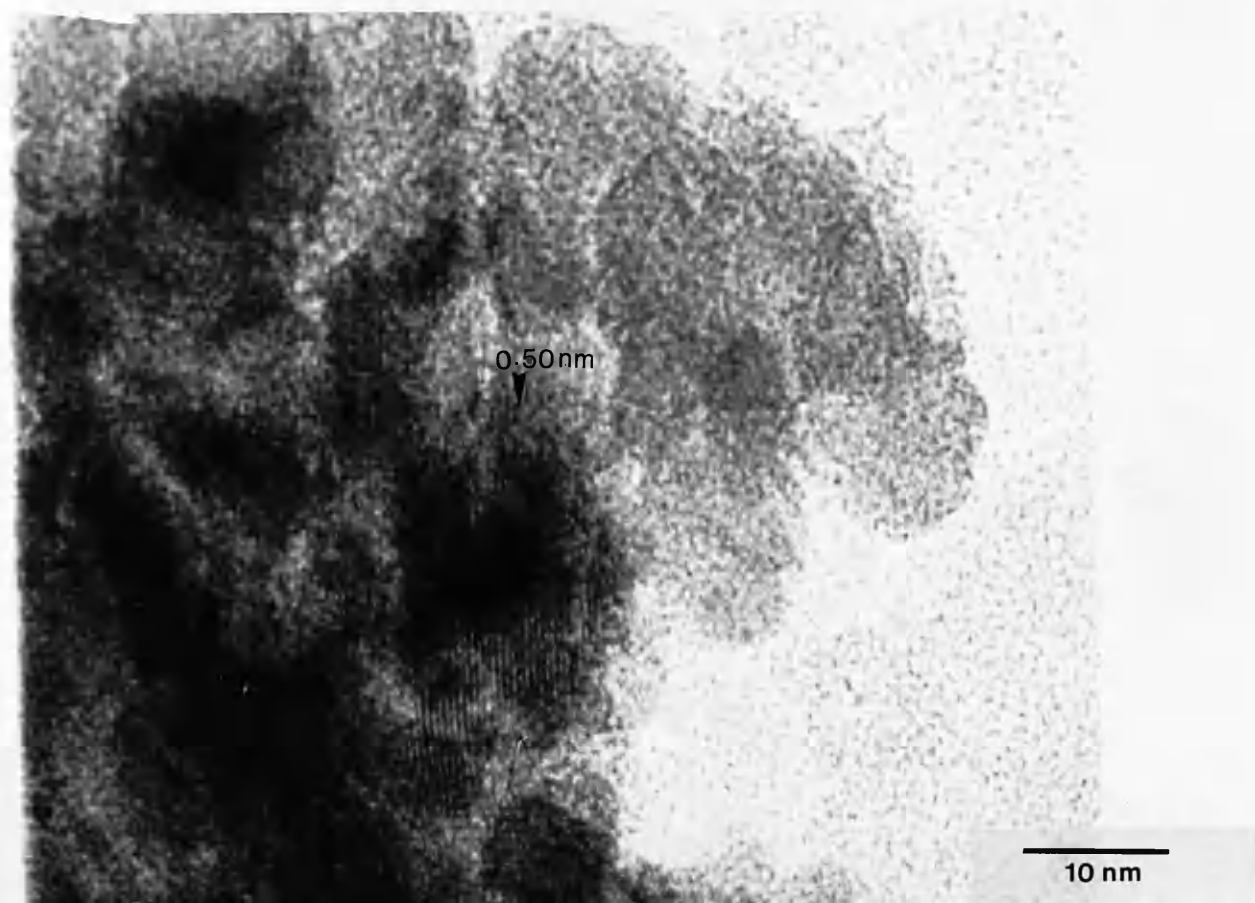
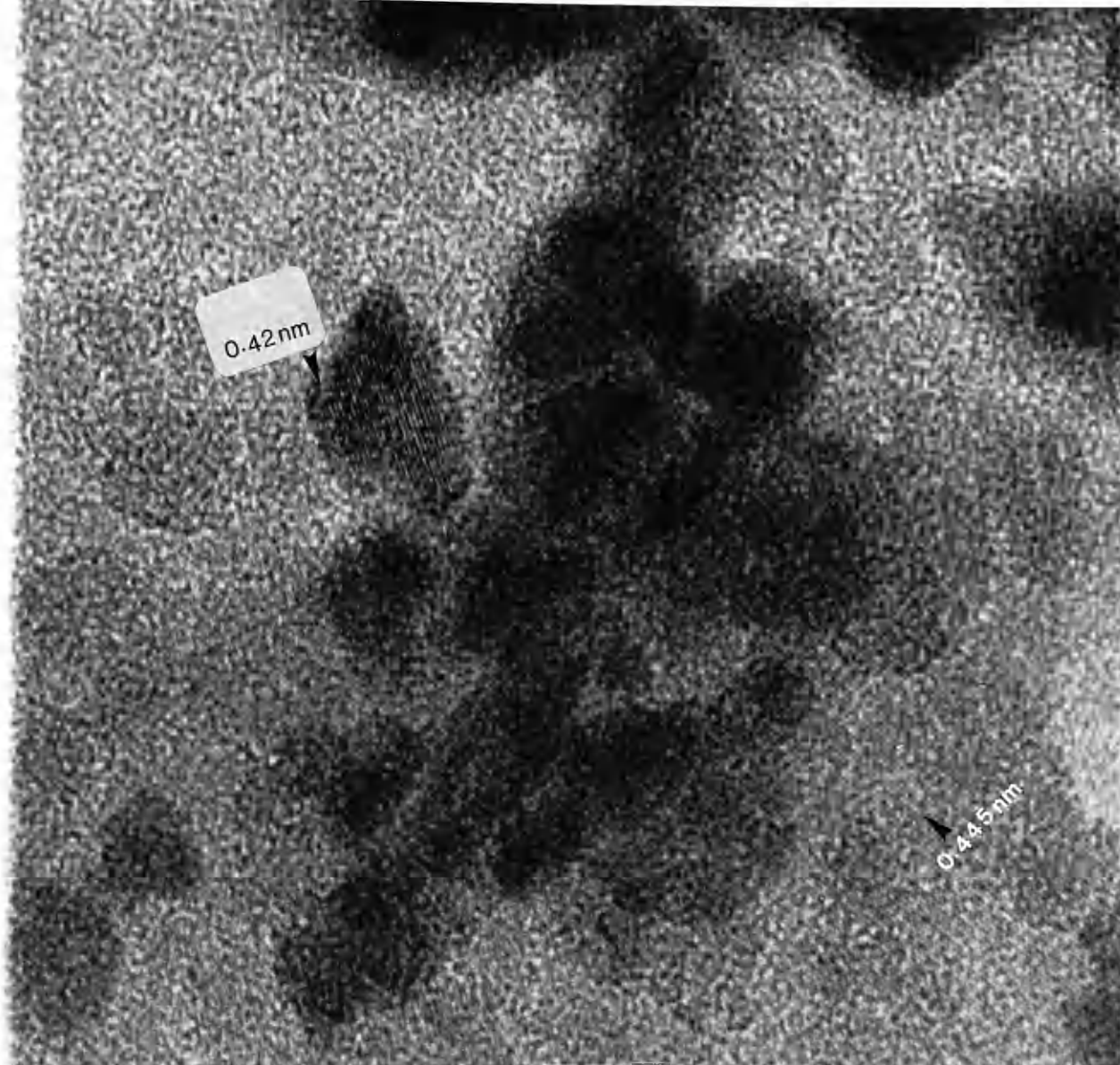




NEXT PAGE

Figure 5.49: Lattice images of some goethite particles shown in Figure 5.48. A plate-like particle with 0.42nm(110) lattice fringes could be seen in the micrograph. The 0.445nm lattice fringes are from a clay particle. The scale bar in Figure 5.50 applies.

Figure 5.50: Lattice image of some goethite particles shown in Figure 5.48 showing particles with the 0.50nm(020) lattice fringes.



NEXT PAGE

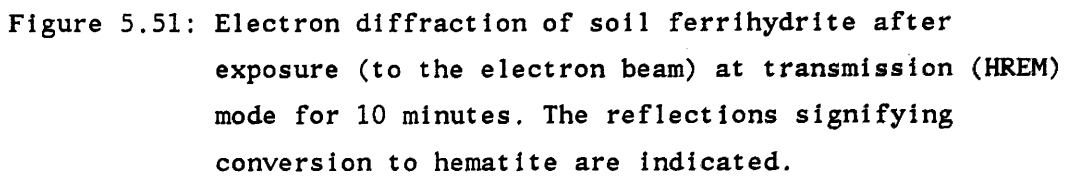
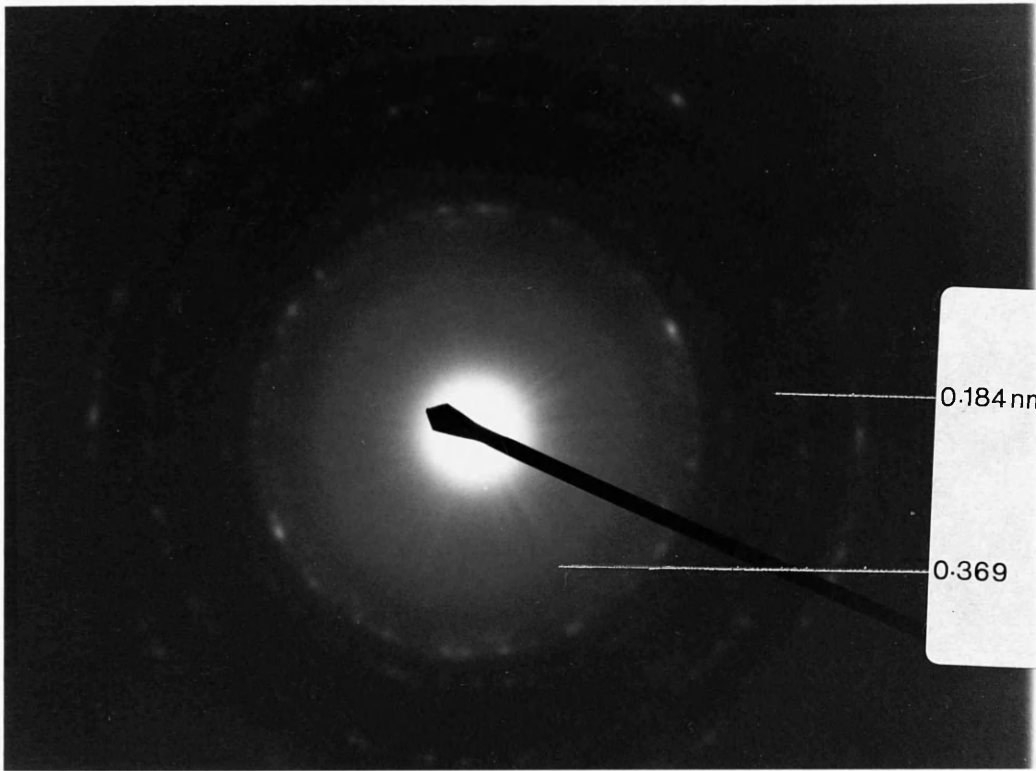


Figure 5.51: Electron diffraction of soil ferrihydrite after exposure (to the electron beam) at transmission (HREM) mode for 10 minutes. The reflections signifying conversion to hematite are indicated.



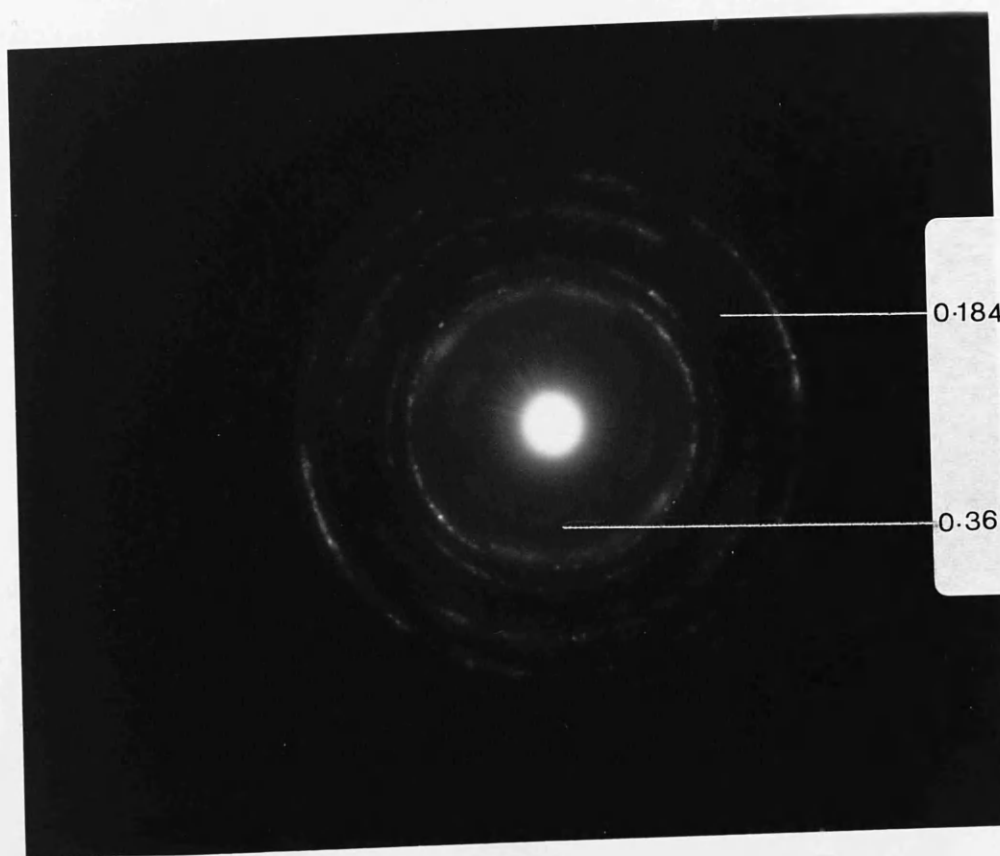
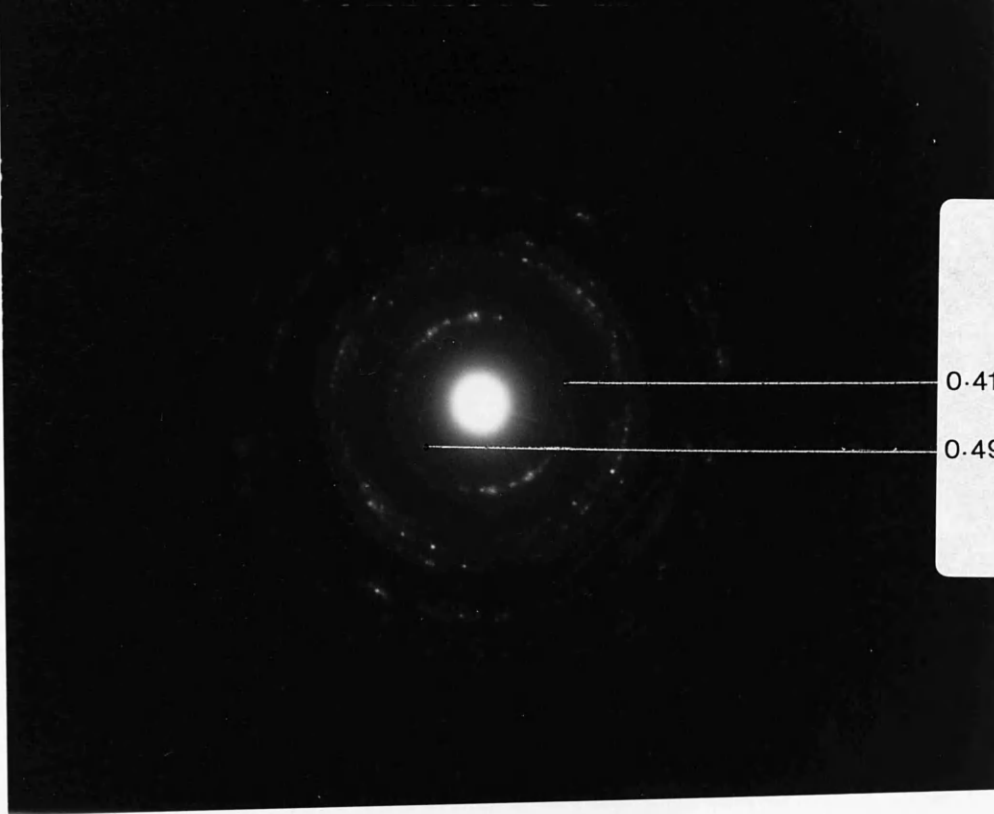
0.184 nm

0.369

NEXT PAGE

Figure 5.52: Typical electron diffraction of soil goethite particles at immediate diffraction (i.e before exposure to the electron beam at transmission mode).

Figure 5.53: Electron diffraction of soil goethite particles after exposure (to the electron beam) at transmission (HREM) mode for 10 minutes. The reflections signifying conversion to hematite are indicated.



CHAPTER 6

X - RAY DIFFRACTION

6.1 INTRODUCTION

X-ray diffraction has been used in this study to determine the mineralogy of the soils and further characterise the iron oxides. In this respect, the technique complements the other techniques such as electron microscopy, infrared spectroscopy, and differential scanning calorimetry used in the investigation. However, the technique has the added advantage that it could be used in the determination of the structure of the iron oxide particles and Al substitution for Fe in the iron oxide structure could be determined.

Sections 6.2 gives a general review of the development of X-ray diffraction, Section 6.3 presents the principles and theory of the technique, Section 6.4 discusses the choice of some diffractometer accessories such as radiations, filters and monochromators for different applications of X-ray diffraction, and Section 6.5 highlights the problems and limitations of the technique in the study of iron oxide mineralogy. The experimental methods employed in the present investigation are given in Section 6.6, and the results of X-ray diffraction on the untreated soil samples and residues from 5 M boiling NaOH and HF concentration methods for iron oxide are presented in Section 6.7. The summary of some of the important findings of X-ray analysis is given in Section 6.8.

6.2 GENERAL

X-ray diffraction is one of the oldest and most widely used techniques for mineralogical studies and its principles and practice have been addressed by various authors such as Buerger (1942), Sproull (1946), Henry et al. (1951), Klug and Alexander (1954, 1974), Clark (1955), Cullity (1956), Whittig (1965), Brown and Brindley (1980) and Wilson (1987) amongst others, and a brief review is included in the next sections. Hadding (1923) and Rinne (1924) were the first to apply X-rays to the study of clay minerals, and Hendricks and Fry (1930) and Kelley et al. (1931) were the first to demonstrate that soil clays contain crystalline mineral components that yield X-ray diffraction patterns. Investigation of the structure, properties, and occurrence of soil clay minerals by X-ray diffraction methods has become a major effort in soil science (Whittig, 1965).

6.3 PRINCIPLES OF X-RAY DIFFRACTION.

Crystalline structures are characterised by a systematic and periodic arrangement of atoms (or ions) in a three-dimensional array. Because crystals are composed of regularly spaced atoms, each crystal contains planes of atoms which are separated by a constant distance. The distances between planes are characteristic of the crystalline species.

X-rays are electromagnetic radiations of short wavelength (of the order of 0.001 to 10nm.). Laue, in 1912, reasoned that if crystals were composed of regularly spaced atoms which might act as centres of scattering for X-rays, and if X-rays were electromagnetic waves of wavelength about equal to the interatomic distances in crystals, then it would be possible to diffract X-rays with crystals. Experiments designed to test his theories were successful, and he established the wave nature of X-rays and the periodicity of the arrangement of

atoms within crystals.

The phenomenon of diffraction involves the scattering of X-rays by atoms of a crystal and the reinforcement of scattered rays in definite directions away from the crystal. Reinforcement of the scattered rays is quantitatively related to the distance of separation of atomic planes as described by Bragg's law,

$$n \lambda = 2 d \sin \theta \quad [6.1]$$

where n is the order of reflection and takes values 1,2,3....., λ is the wavelength of the X-ray radiation, d is the interplanar spacing of atoms within the crystal and θ is the glancing angle of reflection or half the angle between the incident and diffracted beams.

When a collimated beam of monochromatic X-rays of wavelength, λ , strikes a crystal, the rays penetrate and are partially scattered from many successive planes within the crystal (Figure 6.1). For a given interplanar spacing, d , there will be a critical angle, θ , at which rays scattered from successive planes will be in phase along a front as they leave the crystal. A ray following the path BPB', for example, will have travelled some whole number of wavelengths $n\lambda$ further than a ray travelling along the path ADA'. The angle between the normal to the emerging wavefront and the atomic planes will be equal to the angle between the normal to the primary wave front and the atomic planes. Diffraction from a succession of equally spaced lattice planes results in a diffraction maximum which has sufficient intensity to be recorded.

When n is equal to 1, diffraction is of first order. At other angles where n is equal to 2 or 3, or a greater number, diffraction is again possible, giving rise to second, third and higher orders of diffraction. Although d remains the same, d/n values will be different depending on the value of n .

Since no two minerals have exactly the same set of interatomic distances,

the angles at which diffraction occurs will be distinctive for a particular mineral. The interatomic distances within a mineral crystal then result in a unique array of diffraction maxima which serves to identify that mineral.

Diffraction can occur whenever lattice planes become parallel to the incident beam. The wavelength of radiation is characteristic and constant for the particular X-ray tube used. The angle of incidence, θ , of the primary radiation with the crystal planes can be varied, however.

With an X-ray spectrometer, the angle of incidence is varied by rotating the sample in the path of the primary X-ray beam. A Geiger-counter detector, used to intercept and measure the diffracted rays, also moves in such a way as to maintain an angle with the sample which is equal at all positions to the angle of incidence of the primary beam. From the chart of a direct recording X-ray spectrometer, the value of 2θ (with reference to the primary beam) is available directly.

The angle, θ , may be effectively varied by analysis with a stationary sample and recorder, the recorder in this case being a photographic film. Crystals to be analysed are reduced to a very fine powder and placed in the path of a beam of monochromatic X-rays. The particles of the powder are tiny crystals oriented at random with respect of the primary beam. Because of the large number of crystals in the mass of fine powder, there will be sufficient crystals properly oriented so that every set of lattice planes will be capable of diffraction. The mass of powder is equivalent to a single crystal rotated, not about one axis, but about all possible axes. In the event that several crystal species are present in the powder mixture, each component species registers its own diffraction maxima independently. The diffracted rays from a powder mixture may be registered on a photographic film or plate that is geometrically so placed in relation to the sample as to allow determination of the angle of diffraction for each maximum, and subsequent calculation of interatomic spacing.

X-ray diffraction results are often recorded either by using powder cameras or by diffractometer methods (details of these are discussed in various texts including Klug and Alexander, 1974; Brown and Brindley, 1980). The X-ray powder camera produces photographs recorded on photographic films. The reflections are shown in the form of concentric rings similar to those obtained in electron diffraction of polycrystalline samples. The diffraction spacings are then obtained from the measured diameter of the rings. The classical Debye-Scherrer camera is still used but Guinier type focusing cameras with curved crystal monochromators are often preferred because of low background scattering, sharper lines, and greater resolution. Powder photographs show weak reflections with greater certainty than most diffractometer recordings (Brown and Brindley, 1980).

For diffractometer methods reflections are often recorded on charts. Most clay mineral diffraction studies utilize counter diffractometers. Lattice spacings and reflected intensities can be measured quickly and accurately, and line breadths and profiles can be recorded. The reflected intensities are shown as peaks on a calibrated chart from which the value of θ (or 2θ) can be read and used to calculate the diffraction spacing at each peak using the Bragg relationship. Tables have also been produced from which the d -spacing can be read off directly, once the values of θ and λ (or appropriate radiation) are known. For most purposes, a scanning rate of $1^\circ (2\theta)/\text{min.}$ over an angular range of 2° to 65° with filtered Cu $K\alpha$ radiation suffices for routine examination, with 2cm of chart recording for $2^\circ (2\theta)$. With longer wave radiations, correspondingly larger ranges of 2θ will be necessary to cover the same range of spacings and when time is an important factor $2^\circ (2\theta)/\text{min.}$ may be necessary. The output from the diffractometer may be tape-recorded and fed into computers for mineral identification and codifying of results. McCaleb (1966) has described an automated procedure of this kind.

6.4 CHOICE OF RADIATION, FILTERS AND MONOCHROMATORS.

X-ray radiation can be obtained by the use of various anode materials.. The anode materials that are commonly used include Mo, Cu, Co, Fe and Cr. In choosing the most suitable radiation several factors have to be considered that depend on the composition of the specimen and the aim of the investigation. Maximum peak intensity with minimum background is required and the radiation must give adequate dispersion, but with greater dispersion longer times are required to scan a given d-spacing range. The advantages and disadvantages of using the different types of radiation for the studies of clay and related minerals was discussed by Brindley and Brown (1980).

For most X-ray diffraction experiments monochromatic radiation is desirable. Crystal monochromators are necessary to obtain diffraction patterns with little or no appreciable radiation other than the desired $K\alpha$ radiation (possibly with higher harmonics from the general radiation which in powder diffraction are usually unimportant). However the additional cost, experimental complexity, and possible loss of intensity are factors to be taken into consideration. Traditionally a sufficient degree of monochromatization has been achieved by using a filter, usually a thin metal foil, to decrease the intensity of the $K\beta$ component to an acceptable small fraction of that of the $K\alpha$ radiation. The filter also decreases background intensity due to the "white continuum", being especially effective in removing wavelengths just less than the absorption edge of the filter element.

6.5 PROBLEM OF THE STUDY OF IRON OXIDE MINERALOGY OF SOILS USING X-RAY DIFFRACTION

For X-ray diffraction to be used successfully in mineralogical analysis

certain conditions have to be satisfied. For X-ray diffraction of mixtures, each component has to be of enough proportion and crystallinity to allow detection by X-ray diffraction. Since soil iron oxides are often found in mixtures with clays and various other soil minerals, in cases where the oxides are present in relatively small proportions compared with the clays and other components it is often difficult to resolve the iron oxide peaks without prior concentration of the iron oxide minerals. Concentration of the iron oxides in the soil has often been achieved by separation of the soil into different fractions which are then analysed separately. The finer fractions often contain the iron oxide minerals. Also, due to the fact that clay minerals have similar d-spacings with iron oxide minerals the problem of overlapping of clay and iron oxides peaks may lead to difficulty in interpretation of the diffraction results. In such cases separation and concentration of the iron containing phases in the soil may be necessary. Techniques for achieving such separation and concentration of the iron oxides were discussed by Schulze (1987).

Poorly crystalline iron oxide phases such as ferrihydrite can also escape identification by X-ray diffraction, especially when present in mixtures with other iron oxide phases or clay minerals. In recent years, however, improved methods suitable for the detection of ferrihydrite in mixtures with other soil components have been developed. In particular, differential X-ray diffraction (Schulze, 1982), electron diffraction, infrared spectroscopy and Mössbauer spectroscopy have proved successful. Furthermore the small crystal size of most soil iron oxide minerals may lead to broadening of the diffraction peaks (Klug and Alexander, 1974) which makes accurate determination of the d-spacings difficult.

6.6 EXPERIMENTAL METHODS

6.6.1 Instrumentation

X-ray diffraction was performed with a Phillips PW 1130/19, 2KW diffractometer using Co $K\alpha$ radiation and Fe filtration. The instrument was equipped with facilities for varying the scanning voltage and current and both the chart speed and slits could be adjusted. The equipment was operated at a scanning rate of either 2° , 2θ per minute or $1/2^\circ$, 2θ per minute and full scale deflection of 1×10^3 or 4×10^2 counts per second were used depending on the requirements of the sample tested. The equipment settings for the various analysis are shown on the different figures presented.

6.6.2 Sample Preparation

Sample preparation for X-ray analysis was done by two different methods. For the untreated clay samples, where the amount of sample available was large enough, randomly oriented samples were prepared by filling the soil into an Al sample holder and the surface gently pressed with a glass plate without a shearing motion to prevent smoothening of the surface which could induce preferred orientation of the particles. For the ethylene glycol treatment of the clay fraction the sample was sedimented onto a glass slide using distilled water. The slide was then placed on a wire gauze on a beaker containing ethylene glycol and the ethylene glycol evaporated into the sample in an oven at 60°C for 24 hours. Heat treatment was also done by heating the sample sedimented on a glass slide to the desired temperature in an oven for the desired period of time.

For the residues obtained from the various chemical treatments, due to the small size of samples available, a smear of the sample was made on glass slide for X-ray analysis. In order to prevent preferred orientation of the particles which could occur from suspended particles settling down slowly onto the glass

slide, a thick slurry of the soil in distilled water was smeared on a glass slide preheated on a hot plate at 60°C for about 10 minutes and quickly dried down at the same temperature. The sample was made to cover as large area of the glass as would be exposed to the X-ray beam and thick enough to prevent interference from X-ray scattering from glass. Initial tests carried out using these procedures showed them to be satisfactory.

As all the samples examined contained some quartz, this was used as a standard as sample quartz could be used satisfactorily as a standard (Bryant et al; 1983; Campbell and Schwertmann, 1984). Quartz obtained from the sample was washed ultrasonically to remove impurities, crushed and the 20–5µm size obtained by sedimentation and used as both internal and external standard for the estimation of peak positions and instrumental line broadening. In all cases the quartz (100) and (101) reflections were found to occur at 0.4255nm and 0.3335nm respectively while the width at half peak height (WHH) for both lines were found to be $0.150^\circ, 2\theta$. Thus, the preliminary investigations showed sample quartz to be suitable for use as both internal and external standards.

6.7 RESULTS

6.7.1 Clay Fraction

Figures 6.2, 6.3 and 6.4 show the X-ray diffraction traces for the air-dried, heated (at 550°C for 2 hours) and the ethylene glycol treated clay fraction of the soils respectively. For Sample 404.05, the diffraction pattern for the air-dried clay showed major reflections at 1.00nm, 0.74nm, 0.5nm, 0.445nm, 0.424nm, 0.36nm, and 0.334nm. The 1.00, 0.5 and 0.334nm spacings persisted on heat treatment and may thus be attributed to mica (1.00nm, 0.50nm and 0.334nm) and quartz (0.424nm and 0.334nm). The 1.00nm for the clay mica was sharp while the 0.50nm reflection was weak and broad. Both reflections, together with a

sharp peak at 0.334nm (contributions from both mica and quartz) remained unchanged following treatment with ethylene glycol and appeared to suggest a 2M1 type clay mica, i.e. either 2M1 illite or 2M1 muscovite. Since muscovite was indicated in the original granitic rock (observation from optical microscopy) the mica is most probably 2M1 muscovite unweathered from the fresh granite. The 0.74, 0.445, and 0.36nm reflections disappeared on heating but remained unchanged on treatment with ethylene glycol and the spacings may be attributed to kaolin. The kaolin reflections at 0.74nm and 0.36nm were broad with both reflections showing distinct asymmetry towards the low angle side, thus signifying halloysite (7A or metahalloysite) rather than kaolinite (Brindley and Brown, 1980 and Wilson, 1987). The 0.445 (020) reflection for kaolin was more intense than the basal 0.36nm (002), although there might be contribution from muscovite to this reflection, and appeared to indicate a tubular morphology of the halloysite particles (Wilson, 1987). This indication was supported by transmission electron microscopy observations (Chapter 5) which showed the halloysite particles to be in the form of rolled-up tubes.

The traces for the more weathered Sample 404.06 showed similar reflections to those already discussed for Sample 404.05, except for the much smaller amount of muscovite (perhaps due to weathering) indicated by a smaller peak (than 404.05) at 1.00nm, while the 0.50nm peak was absent. Also, the kaolin 001 reflection had shifted slightly to 0.73nm. The characteristics of this reflection and those at 0.445nm and 0.36nm were similar to those described for Sample 404.05 and indicated halloysite (7A) to be the main clay mineral in the soil, as was the case with the previous soil.

For Sample 404.07, a further shift of the kaolin 001 reflection to 0.719nm was indicated and this reflection, together with the 0.36nm (002) reflection were sharper than was the case with Sample 404.05. In addition, the 0.443nm (020) spacing was far less intense than the basal reflections, unlike in previous cases.

The trace for the randomly oriented sample was quite similar to those for disordered kaolinite (Brindley and Brown, 1980 and Wilson, 1987). Clearly, the trace may be interpreted as halloysite (7A) by some investigators (because of the relatively high 001 spacing which is expected at 0.72 to 0.74nm for halloysite) or as disordered kaolinite by others (because of the characteristics of the reflections). In the present investigations, complete identification was aided by transmission electron microscopy observations and electron diffraction (Chapter 5) which showed a mixture of halloysite (rolled-up tubes) and kaolinite (plates) in a ratio approaching 50:50 (estimated from electron micrographs). Hence, there may be a problem of identification of mixtures of halloysite (7A) and kaolinite when X-ray diffraction alone is used for identification purposes. This problem was also highlighted by Brindley et al. (1963) while Miller and Keller (1963) showed that a differentiation can be made by utilising the expansion of all kaolinite group minerals in strong potassium acetate solution or by grinding the clay with potassium acetate added. The wet, K-acetate treated clay expands to about 1.4nm. The potassium acetate is then removed by washing and without allowing the clay to dry, ethylene glycol is added. Kaolinites and dickites return to a basal spacing of about 0.71 to 0.72nm after this treatment, but 7A and 10A halloysites examined by the authors retained an expanded spacing of 1.04nm to 1.09nm. Identification by X-ray diffraction supported by electron microscopy, especially where there is doubt about the exact mineralogy, as was done in the present investigations may however be an easier and surer alternative. A trace of muscovite in this sample was indicated by a very small 1.0nm reflection in the randomly oriented sample and the reflection became sharper in the oriented, heated sample following destruction of the halloysite and kaolinite by heat treatment.

The traces for Sample 404.08 were quite similar to those for Sample 404.07 with the added observation that the 0.719nm (001) and 0.36nm (002)

reflections were sharper than in the traces for Sample 404.07. The traces were also more characteristic of kaolinite than halloysite although transmission electron microscopy and electron diffraction showed a mixture of halloysite (tubes) and kaolinite (plates) with the kaolinite appearing to be in higher proportion than the halloysite in the micrographs. Scanning electron microscopy also showed a similar result for the soil. Muscovite was not indicated in the randomly oriented, untreated clay but its presence was indicated in the oriented, heated specimen by reflections at 1.0nm and 0.5nm. Also, the presence of a very small 1.41nm spacing in the untreated clay which persisted, unchanged in the glycol treated soil indicated the presence of a trace of chlorite in this soil. A small reflection at 0.485nm for the untreated sample also suggested the presence of gibbsite in the soil and appeared to indicate the more advanced stage of weathering of the soil. This result was supported by chemical analysis (Chapter 4) of the clays which showed a higher aluminium content for the soil compared to the other soils.

K-Feldspar was indicated in Samples 404.05, 404.06 and 404.07, by the presence of a 0.324nm peak, and may have got into the clay fractions of the soil through crushing of the softened primary mineral.

From the results of clay mineralogy presented above and summarised in Table 6.1, halloysite (7A) was found to be the main clay mineral in the least weathered soil (Sample 404.05). This trend continued in the slightly more weathered Sample 404.06 and the sample was similar in mineralogy to Sample 404.05. As weathering progressed (Sample 404.07), the soil became dominated by a mixture of halloysite and kaolinite with the proportion of kaolinite increasing relative to halloysite in the most highly weathered residual soil (Sample 404.08). Muscovite and quartz were found as minor minerals in all the soils although the proportion of both minerals decreased with increase in weathering. Chlorite and gibbsite were identified only in the most highly weathered soil (Sample 404.08).

6.7.2 Residues from Iron Oxide Concentration Treatments

As was expected, due to the low concentration of the iron oxide minerals in the clay fraction of the soil, none of the reflections in the X-ray diffraction traces could be safely attributed to any of the iron oxide phases. Since kaolin type clay minerals were present in the soils, the 0.418nm reflection of halloysite and kaolinite would coincide with that for goethite and could not be used for identification of goethite. All other reflections for iron oxides appeared to be absent or too weak and in most cases coincided with reflections for the clay minerals. X-ray diffraction of particles $<1\mu\text{m}$ gave the same problem of interference from kaolinite minerals due to the fact that the kaolinite minerals were in the same size range (as revealed by infrared spectroscopy in Chapter 7). Slow X-ray scanning over the relevant iron oxide peaks was not helpful due to interference from the kaolin reflections.

Because of these problems it was decided to concentrate the iron oxides in the soil by dissolution of the clay minerals in order to make the X-ray diffraction peaks of the iron oxide discernible. The boiling 5M NaOH dissolution method and HF dissolution methods were used to achieve this aim. Details of the procedures and results of chemical analysis on the residues obtained after the treatment on the soil samples are given in Chapter 4. The result of X-ray diffraction on the residues from NaOH and HF treatments are given below:

(a) X-ray Diffraction of Residues from the Boiling 5 M NaOH

Treatment

The possibility of a change to the form, crystal morphology, crystallinity and Al substitution following boiling 5 M NaOH treatment was investigated by Kämpf and Schwertmann (1982). As a check on the experimental procedures used in this study, samples of synthetic ferrihydrite and goethite were used as controls for the experiments on the soil samples. In order to provide the

amount of silicon necessary to prevent changes occurring to these synthetic forms, 50% by weight of poorly crystallised kaolinite was added to each of the synthetic oxides, as recommended by Kämpf and Schwertmann (1982), before the NaOH treatment. The traces for the treated and untreated synthetic samples (Figure 6.5) were similar, signifying no significant changes induced to the iron oxide minerals as a result of the treatment. Since halloysite and kaolinite were the main minerals in the soil samples, it was assumed that these minerals, in addition to the free silica present in the soils, will provide the silicon needed to prevent changes to the iron oxide minerals in the soil samples.

Figure 6.6 shows the X-ray diffraction traces obtained from the residues following treatment with boiling 5 M NaOH. The HF residues gave similar traces. It could be seen that the 0.7nm (001) peak of kaolin had completely disappeared from the traces (compared to Figure 6.2) thus giving an indication that, as expected and in agreement with electron microscopy observations, the kaolin (halloysite and kaolinite) particles were effectively dissolved by the NaOH treatment. In contrast, the 1.0nm (001) and 0.5nm (002) reflections of muscovite and the 0.424nm (100) and 0.334nm (101) reflections of quartz persisted and were more intense due to the increased concentration of the muscovite and quartz particles following dissolution of the kaolinite particles. A similar observation was made for muscovite in electron microscopy (Chapter 5). Feldspar peaks could also be seen in the traces for the residues of the deeper soils, although these peaks decreased progressively up the profile and were barely visible in the traces for Samples 404.07 and 404.08. An indication of the dissolution of gibbsite by NaOH was given by the absence of the 0.485nm (002) reflection in the trace for the residue of Sample 404.08.

The presence of the 0.418nm reflection in all the traces in the absence of kaolinite and other minerals with similar reflections suggested that the reflection could be assigned to the 0.418nm (110) reflection of goethite. In addition the

0.269nm (130), and 0.245nm (111) reflections of goethite were clearly discernible in all the traces for the soils, although the d(120) reflection at 0.338nm coincided with similar reflections for muscovite and quartz in all the samples, and could not be adequately determined. None of the reflections in all the traces could be safely assigned to any of the other iron oxide phases. Figures 6.7 to 6.10 show the sections of traces showing the 0.418 (110), 0.269 (130) and 0.245 (111) goethite reflections. The increased sharpness of the peaks on passing from Sample 404.05 to 404.08 suggested an increase in crystallinity of the goethite particles as weathering increased.

Table 6.2 gives the reflections for pure (unsubstituted) goethite obtained from the Powder Diffraction File and the reflections obtained for the soil goethites following NaOH treatment. A comparison of the diffraction spacings obtained for the soil goethites with those for unsubstituted goethite (Table 6.2) indicated a shift of the soil goethite reflections to lower values in all the samples examined. Perhaps due to this shift there was no severe interference of the 0.426nm reflection of quartz with the 0.418nm reflection of goethite and an accurate determination of the goethite peak was possible. It had been shown by several authors (e.g. Norrish and Taylor, 1961; Thiel, 1963; Jonas and Solymar, 1970; Taylor and Schwertmann, 1978; Schwertmann et al, 1979 and Schulze 1984) that a shift in the X-ray peak positions of goethite from those given for unsubstituted goethite in Table 6.2 is normally due to aluminium substitution for Fe in the goethite structure, and a detailed review of this was given earlier in Section 2.4.3(b). Equations for estimating Al substitution based on the position of d(111) reflection of goethite (Norrish and Taylor, 1961) and based on the c dimension (Schulze, 1984) have been given (Equations 2.8 and 2.6 respectively). These equations have been used to estimate Al substitution in the soil goethites from X-ray diffraction results obtained in this study using the procedure given by Schulze (1984) and outlined below.

The position and width at half peak height (WHH) for the goethite 110 and 111 lines were measured carefully using sample quartz ($20-5\mu\text{m}$) as a standard. The peak positions from which the d - spacings were obtained were determined from the position of a line which divided the upper $1/3$ to $1/2$ of the diffraction peak into two "mirror image" halves. The observed WHHs were corrected for instrumental broadening caused by the goniometer by subtracting the instrumental WHH from the observed WHH (the procedure for correction for instrumental broadening using this method is shown in ^{the} Appendix). If the corrected WHH was greater than $0.6^\circ 2\theta$, then the line positions were corrected for shifts caused by the small particle size effect by adding the values from Table 2.4 to the observed line positions (Schulze, 1984). The c - dimension and aluminium substitution were then calculated from the values of $d(110)$ and $d(111)$ obtained using equations 2.7 and 2.6 respectively. For estimation of Al substitution using only $d(111)$, the value of $d(111)$ obtained above was used in Equation 2.8.

Table 6.3 gives some properties of the goethite particles in the residues obtained from X-ray diffraction. Aluminium substitution in the goethites in the soils could be seen to increase from 9.42 mole % in the least weathered soil (404.05) to 15.72 mole % in the most highly weathered soil (404.08) when the c dimension (Equation 2.6) was used to estimate aluminium substitution. Values of Al substitution obtained using the $d(111)$, equation 2.8, were comparable to those obtained from using the c dimension.

(b) X-ray Diffraction of Residues from HF Treated Soils.

As a control for the experiments on the soils, synthetic ferrihydrite and goethite were added to poorly crystallised Georgia kaolinite and treated with HF. Since the iron oxide content of the clay fractions of the soils were found by X-ray fluorescence to be about 5% (see Table 4.3), in order to represent the

soil conditions as much as possible it was decided to use a mixture of 5% of each of the synthetic oxides to 95% poorly crystallised Georgia kaolinite for control.

No residue was obtained from the mixture of synthetic ferrihydrite and kaolinite following HF treatment signifying a complete dissolution of the ferrihydrite as well as the kaolinite particles by HF. In contrast, the goethite particles were resistant to attack by HF. A comparison of the traces obtained for the untreated and treated samples for goethite showed them to be similar, thus indicating no significant changes to the goethite as a result of HF treatment.

The traces obtained from the residues from the HF treated soils were similar to those of the NaOH residues shown in Figure 6.6. As was the case with the NaOH treatment the HF treatment was very effective in the dissolution of halloysite, kaolinite and gibbsite, but goethite, muscovite, feldspars and quartz were resistant to attack. Again, some of the goethite reflections were quite distinct and the peaks that could be assigned to goethite in the HF residue were similar to those given for goethite in the NaOH residues (Table 6.2) for each soil. The traces of the sections showing the $d(110)$, $d(130)$ and $d(111)$ of goethite obtained from the HF treated residues are also shown in Figures 6.7 to 6.10. The traces gave a similar increase in sharpness of the peaks on passing from sample 404.05 to 404.08 (suggesting an increase in crystallinity of the goethite particles in this direction) as was observed for the NaOH samples. Similarly a shift in the diffraction peaks from those given for unsubstituted goethite in Table 6.2 was indicated and Al substitution was estimated as outlined for the NaOH residues in Section 6.7.2 (a). Table 6.4 gives some properties of the goethite particles in the soils obtained from X-ray diffraction of residues from the HF treatment. Comparison of this table with Table 6.3, for the NaOH treated soil residue showed the goethite in the residues from both treatments to have similar structural properties and aluminium substitution. Except both NaOH

and HF treatments have affected the properties in the same way, this observation would appear to suggest that the NaOH treatment has not adversely affected the c - dimension and Al substitution of the soil goethites.

Synthesis studies (Thiel, 1963; Schulze, 1984) and results of determination of Al substitution of large number of soil goethites from different parts of the world (see Schwertmann, 1987b for a review) have suggested that the range of aluminium substitution in goethites can be between 0 and 33 mole %, i.e; maximally every third Fe atom may be replaced by aluminium. Low substitution prevails in weakly acid soils and in hydromorphic environments, while substitution above 10 to 15 mole % is usually found in goethites from highly weathered soils of tropical and subtropical soils. Fitzpatrick and Schwertmann (1982) reported values of aluminium substitution of between 15 and 30 mole % for goethite in highly weathered strongly acid soils and gibbsitic saprolites in Natal, South Africa while Schwertmann and Kämpf (1985) found values of 33 to 36 mole % for goethite in highly weathered kaolinitic soils from central Brazil. Although the amount of aluminium substitution found for the soils in this investigation (about 10% to 16%) agrees with those found in soils and falls within the range for highly weathered subtropical and tropical soils, no previous determination of aluminium substitution of goethites from young subtropical soils like those in this study appeared to be available. An aluminium substitution of about 10% found for the least weathered soil (404.05), where some of the primary minerals were still intact (see Chapter 3 for description), which increased to about 16% in the most weathered soil appeared to suggest that aluminium substitution in the goethite particles began early in their formation and may be due to the availability of aluminium, to the iron oxides, in the soil system during the early stages of formation. Several studies on synthetic systems (e.g Jonas and Solymar, 1970 and Lewis and Schwertmann, 1979) have shown that this may have an effect on the formation and properties of the soil iron oxides. Lewis and Schwertmann

(1979) synthesised Al-goethites from Al-ferrihydrite system and found, amongst other things, that the rate of conversion of the Al-ferrihydrite to a crystalline product decreased as the Al concentration increased. Since, as stated in Chapter 5, ferrihydrite was found in Sample 404.05 by electron microscopy, and was indicated in Samples 404.06 and 404.07 by acid oxalate treatment (see Chapter 4), it is possible that the presence of Al in the system was partly or wholly responsible for inhibiting the crystallisation of ferrihydrite to other crystalline products in these soils. Due to the small amount of the ferrihydrite in the soils, an analysis of the ferrihydrite for its Al content was not possible for confirmation of this suggestion, and, as mentioned earlier in Chapter 4, the presence of organic carbon in the soils (albeit in very small quantities) and silica (e.g quartz, indicated in X-ray diffraction of the clay fraction of the soils) can also produce the same effect. A combination of all three factors is likely in the present case.

As reported earlier, the Al substitution estimated from the c-dimension and from d(111) gave similar values. Previous studies on the determination of Al substitution from both methods (reviewed in Chapter 2) have however suggested that Al substitution determined from the c-dimension is more reliable. Schulze (1984) reported that the poor dependency of the d(111) line position on Al substitution is due to the variability of the a-dimension which contributes to the d(111) line. The variability in the a-dimension has been explained to be, probably, as a result of structural defects in the goethite crystal (Schulze, 1984). It is possible that the agreement obtained in using both methods in the present investigation is a suggestion that structural defect in the soil goethites was minimal, and so did not have any significant effect on the d(111) line.

The gradual increase in Al substitution from the least weathered soil (404.05) to the most weathered soil (404.08), obtained in this study, is in agreement with earlier works by Fitzpatrick and Schwertmann (1982) and Kämpf and Schwertmann (1985). As was the case with the results of Kämpf and

Schwertmann (1985), the goethite with the highest Al substitution was found in association with gibbsite in Sample 404.08. According to the authors, this does not necessarily mean that gibbsite acts as a source of aluminium for goethite, but more likely indicates that both gibbsite and highly substituted Al-goethite characterise a pedogenic environment of strong desilification where aluminium activity is high and both gibbsite and goethite compete for aluminium. The results obtained in this study appeared to support the suggestion that Al substitution in the iron oxide crystal could serve as an indicator of the weathering state of the soil material (Fitzpatrick and Schwertmann, 1982).

6.8 SUMMARY

Some of the important findings of the study in this chapter are listed below.

6.8.1 Clay Mineralogy

- (1) In line with the results of electron microscopy, X-ray analysis suggested halloysite to be the main mineral in the deeper Samples 404.05 and 404.06. As weathering increased in Samples 404.07 and 404.08, the clay mineralogy became a mixture of halloysite and kaolinite with the proportion of kaolinite increasing progressively until kaolinite became the dominant mineral in the Sample 404.08.
- (2) The difficulty in correctly analysing X-ray diffraction traces of mixtures of halloysite and kaolinite has been highlighted and combination of X-ray analysis and electron microscopy was employed to overcome this problem.

- (3) Muscovite was indicated as a minor constituent of all the soils, with the proportion of muscovite decreasing progressively with increasing weathering.
- (4) Both chlorite and gibbsite were indicated in the most weathered soil (Sample 404.08).

6.8.2 Iron Oxide Mineralogy

- (1) X-ray diffraction analysis showed that both 5M NaOH treatment and HF treatment led to a concentration of iron oxides in the soils by dissolving the halloysite and kaolinite minerals. Both muscovite and chlorite were however resistant to attack by both treatments.
- (2) Goethite was indicated in all the soils. Ferrihydrite was not indicated in any of the soils by X-ray diffraction, most probably due to the small quantity of the mineral in the soils in which it was earlier suggested by selective dissolution (Chapter 4) and electron microscopy (Chapter 5).
- (3) X-ray diffraction suggested an increase in crystallinity of the goethite crystals with increased weathering of the soils.
- (4) A shift in X-ray diffraction peak positions for the soil goethites in all the samples, from standard diffraction peaks for unsubstituted goethites, suggested Al substitution for Fe in the soil goethites.
- (5) Al substitution of 9.42 mole% found for the less weathered, relatively young granitic soil may be considered to be high and appeared to indicate Al

availability to the iron oxides at the early stages of formation which may have promoted the formation of ferrihydrite in the soils. The highest Al substitution of 15.72 mole% found for the goethite particles in the most weathered soil, where gibbsite was earlier identified, is in line with results of previous investigations.

- (6) The fact that similar Al substitutions were obtained from using the c- dimension and d(111) may suggest minimal crystal defects in the goethite crystals.
- (7) The study has supported previous suggestions that Al substitution in soil iron oxide may act as an indicator of the weathering state of the soil material.

Table 6.1 Summary of Mineralogy from X-ray Diffraction

Sample	MINERALS		
	Major	Minor	Trace
404.08	Halloysite/ Kaolinite	Muscovite	Chlorite, Gibbsite Quartz
404.07	Halloysite/ Kaolinite	Muscovite K-Feldspar Quartz	—
404.06	Halloysite	Muscovite K-feldspar Quartz	—
404.05	Halloysite	Muscovite K-feldspar Quartz	—

Table 6.2: Comparison of Diffraction Spacings for Unsubstituted Goethite and Spacings obtained from 5 M Boiling NaOH Treatment Residues.

*Unsubstituted Goethite	SPACINGS (nm)				(hkl)
	404.05	404.06	404.07	404.08	
0.4179	0.41702	0.41685	0.41685	0.41602	110
0.2692	0.26816	0.26829	0.26849	0.26816	130
0.2582	-	-	-	0.25064(?)	021
0.2448	0.24397	0.24370	0.24343	0.24320	111
0.2189	-	-	0.21946	0.21773	140
0.1801	-	-	-	0.17930	211
0.17186	-	-	0.17107	0.17107	221
0.16899	-	-	0.16717	-	240

* Data from Powder Diffraction Pattern

(?) Doubtful spacing

Table 6.3: Properties of Goethite Particles Obtained from X-ray Diffraction of NaOH-Treated Soil Residues

Sample	Spacings (nm)	$^*W_{HH} (2\theta)$	Cell Dimensions (nm)	1Al Substitution (mole %)	2Al Substitution (mole %)
	d(110) d(111)	(110) (111)	c		
404.08	0.41602 0.24320	0.425 0.500	0.2998	15.24	17.10
404.07	0.41685 0.24343	0.500 0.500	0.2999	14.57	15.14
404.06	0.41685 0.24370	0.650 0.575	0.3003	12.28	12.84
404.05	0.41702 0.24397	0.825 0.550	0.3008	9.42	10.55
†Syn. Goe.	0.41885 0.24506	0.750 0.350	0.3025	0	1.27

* Corrected width at half height.

1 Aluminium substitution obtained using the c dimension (Equation 2.6)

2 Aluminium substitution obtained using d(111) (Equation 2.8)

† Unsubstituted synthetic goethite used as control

Table 6.4: Properties of Goethite Particles Obtained from X-ray Diffraction of HF-Treated Soil Residues

Sample	Spacings (nm)		*WHH (2θ)		Cell Dimension (nm) c	¹ Al Substitution (mole %)	² Al Substitution (mole %)
	d(110)	d(111)	(110)	(111)			
404.08	0.41602	0.24316	0.425	0.575	0.2997	15.72	17.43
404.07	0.41685	0.24343	0.550	0.575	0.2999	14.57	15.14
404.06	0.41685	0.24370	0.550	0.505	0.3003	12.28	12.84
404.05	0.41702	0.24397	0.825	0.550	0.3008	9.42	10.55
†Syn. Goe	0.41885	0.24506	0.750	0.350	0.3025	0	1.27

* Corrected width at half height.

1 Aluminium substitution obtained using the c - dimension. (Equation 2.6)

2 Aluminium substitution obtained using d(111) (Equation 2.8)

† Unsubstituted synthetic goethite used as control

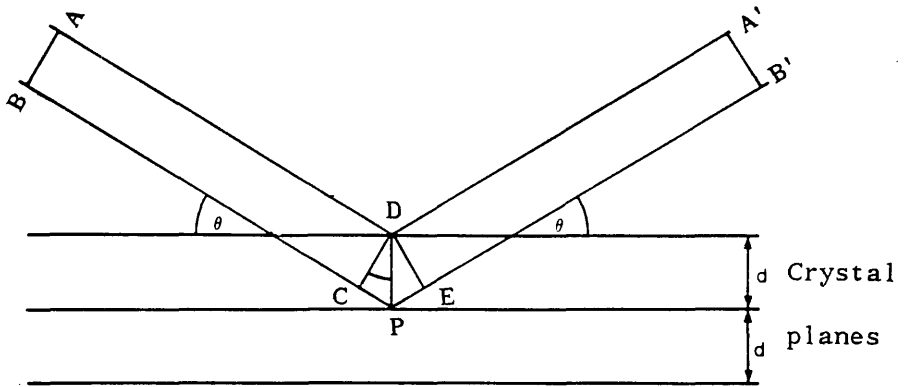


Figure 6.1: X-ray diffraction from crystal planes

Chapter 6: X-ray Diffraction

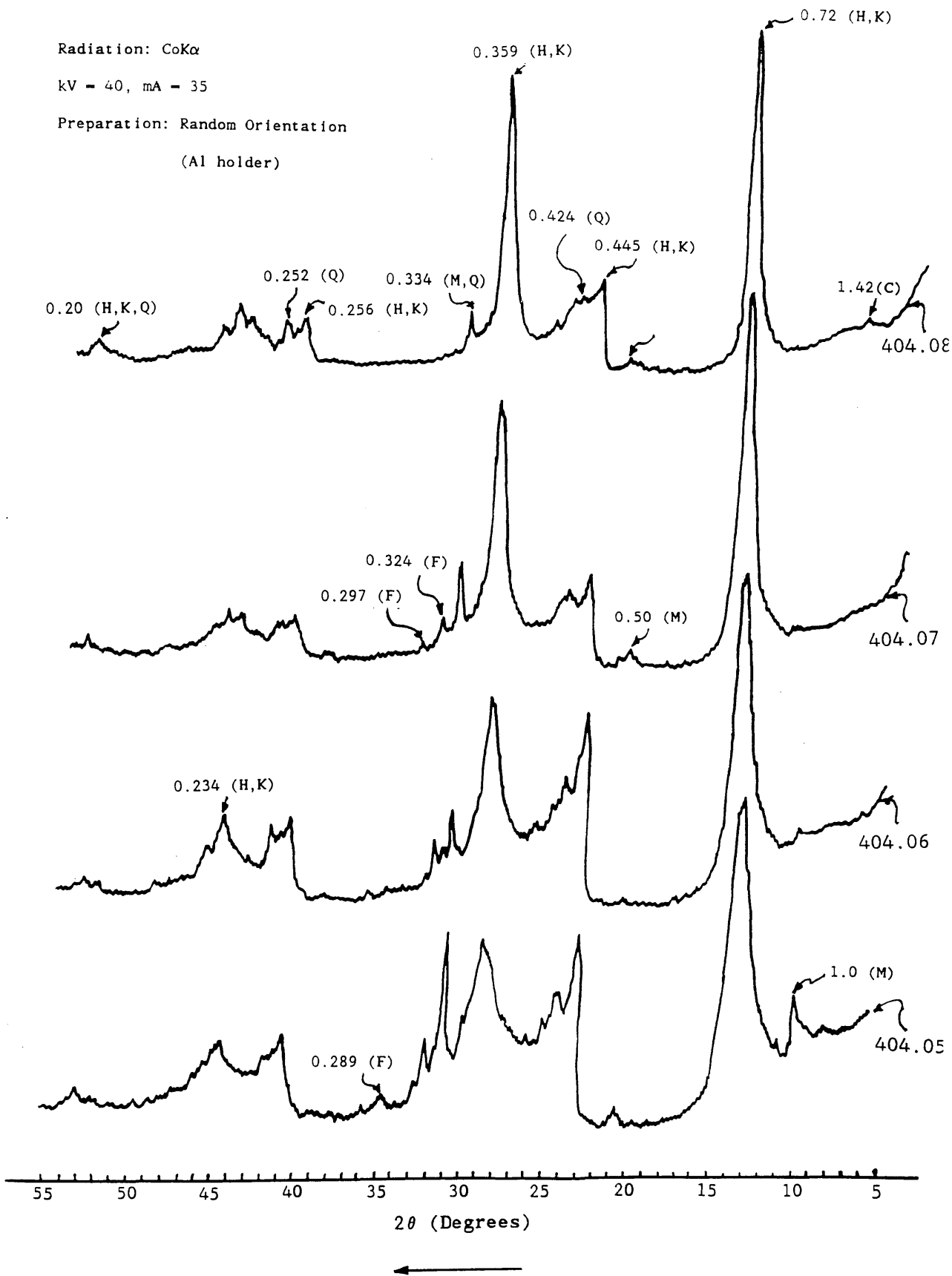


Figure 6.2: X-ray diffraction traces of untreated clay samples

(C = chlorite, M = mica, Gi = gibbsite, H = halloysite,

K = kaolinite, F = feldspar, Q = quartz). Spacings in nm.

Chapter 6: X-ray Diffraction

Radiation: $\text{CoK}\alpha$

kV = 40, mA = 35

Preparation: Sedimented on glass,

Heated to 550°C for 2hrs.

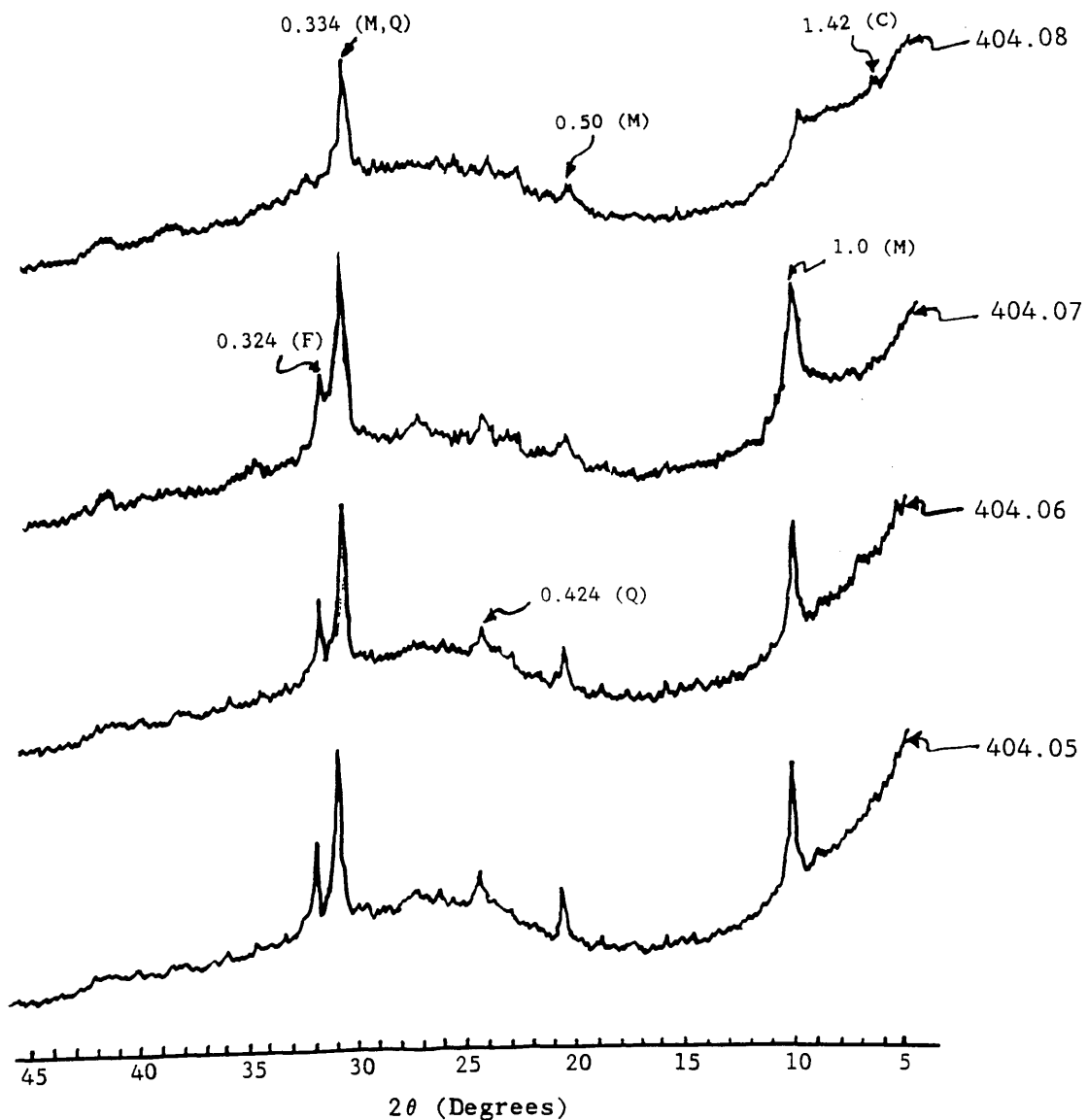


Figure 6.3: X-ray diffraction traces of clay samples heated at 550°C for 2hrs. (C = chlorite, M = mica, F = feldspar, Q = quartz). Spacings in nm.

Chapter 6: X-ray Diffraction

Radiation: $\text{CoK}\alpha$

kV = 40, mA = 35

Preparation: Sedimented on glass,

Ethylene glycol solvated.

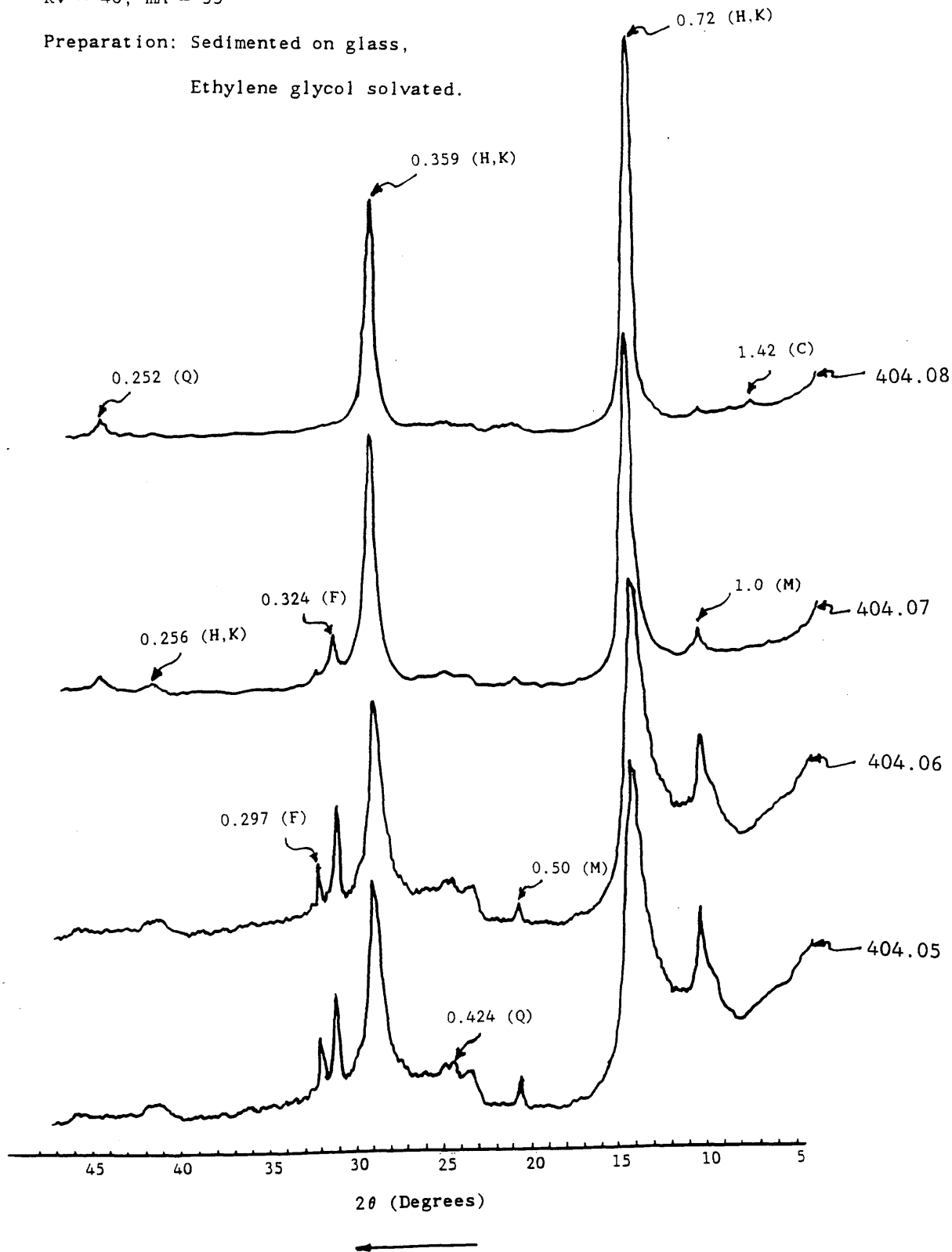


Figure 6.4: X-ray diffraction traces of ethylene glycol saturated clay samples (C = chlorite, M = mica, H = halloysite, K = kaolinite, F = feldspar, Q = quartz). Spacings in nm.

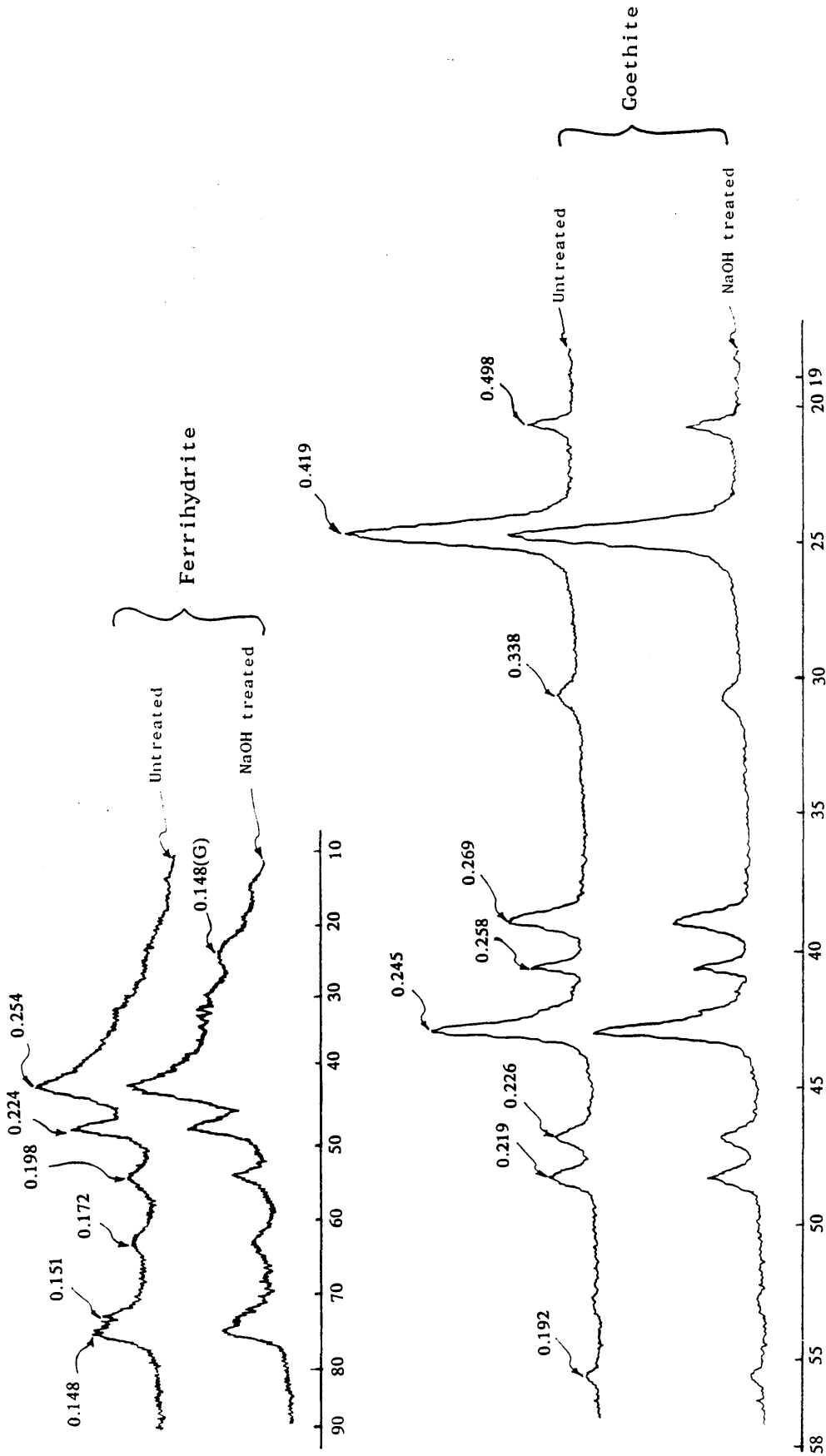


Figure 6.5: X-ray diffraction traces of synthetic ferrihydrite (top) and goethite (bottom) before and after treatment with 5 M NaOH (G = goethite).

Spacings in nm.

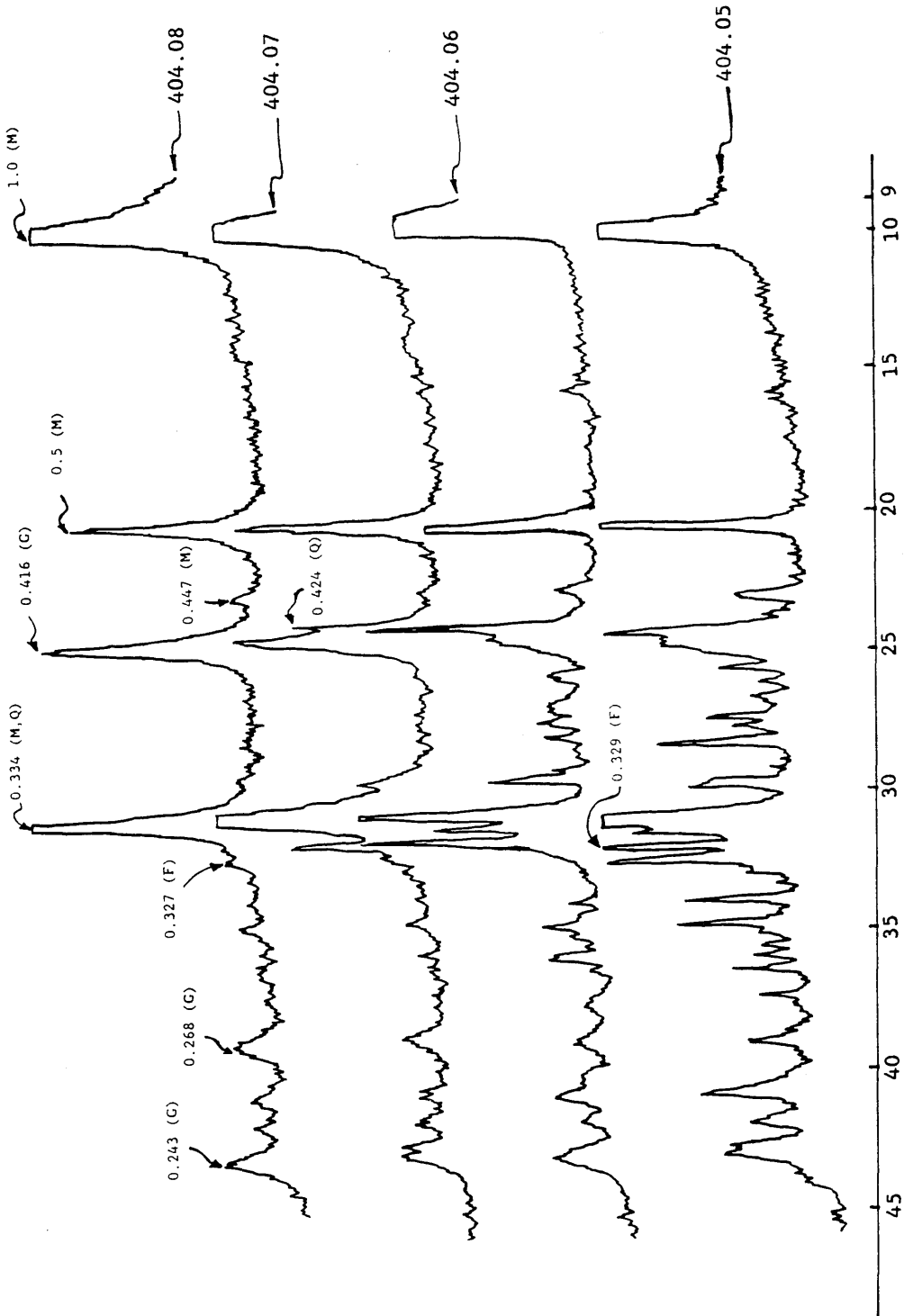


Figure 6.6: X-ray diffraction traces residues from 5 M NaOH treated clay samples

G = goethite, M = mica, F = feldspar, Q = quartz). Peaks not labelled are either feldspar or mica. Spacings in nm.

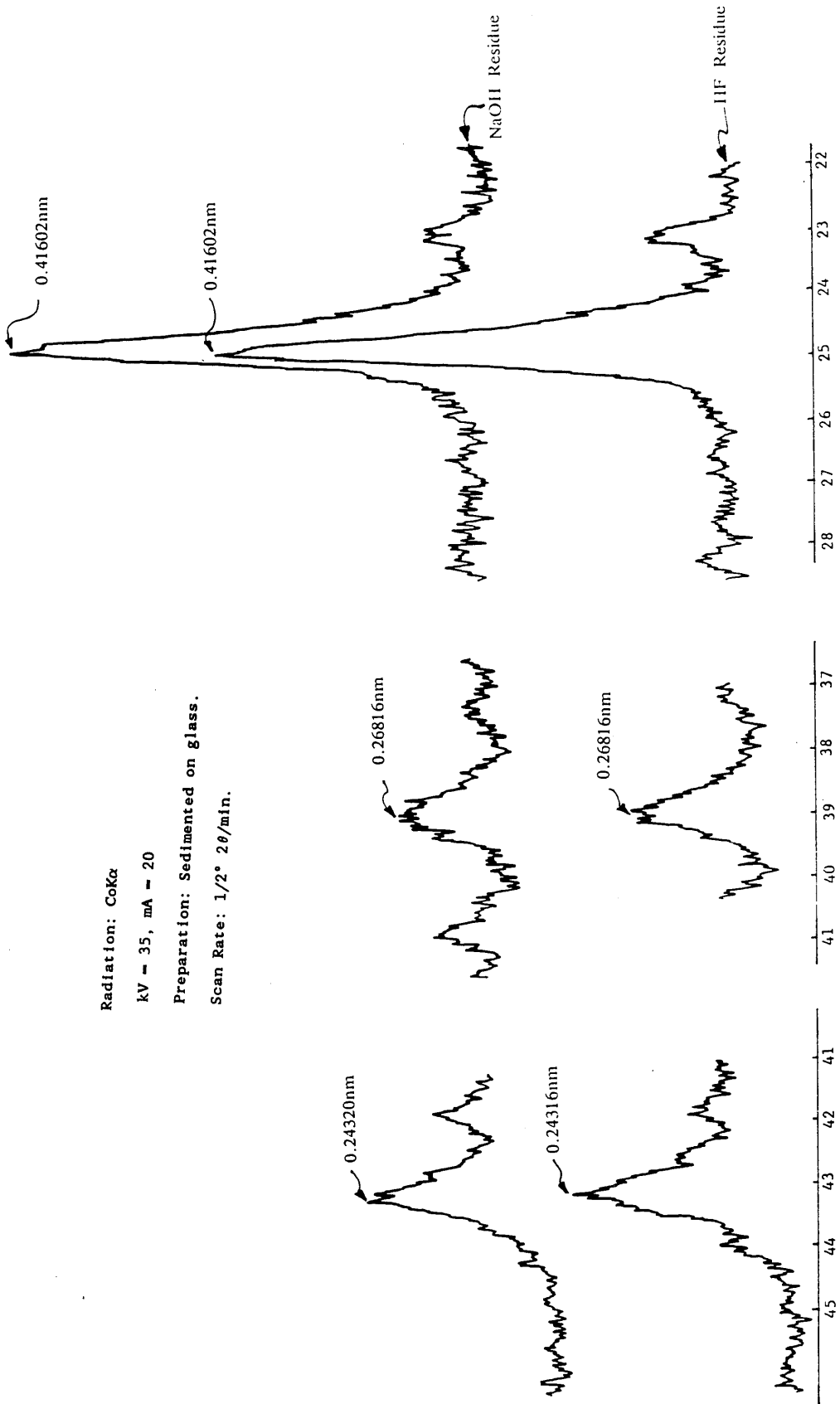


Figure 6.7: X-ray diffraction peaks of goethite in NaOH and HF treated

Sample 404.08.

Chapter 6: X-ray Diffraction

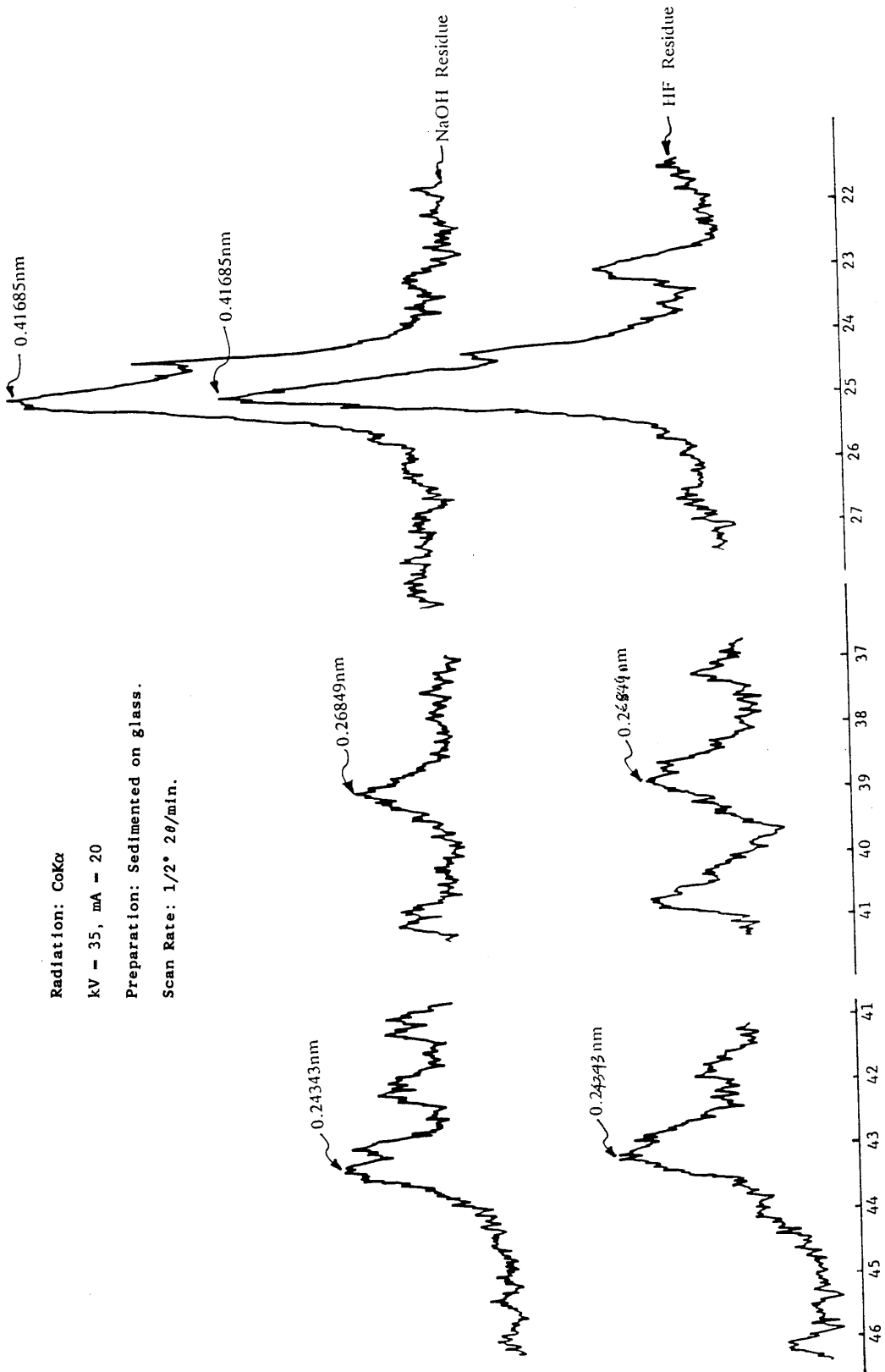


Figure 6.8: X-ray diffraction peaks of goethite in NaOH and HF treated

Sample 404.07.

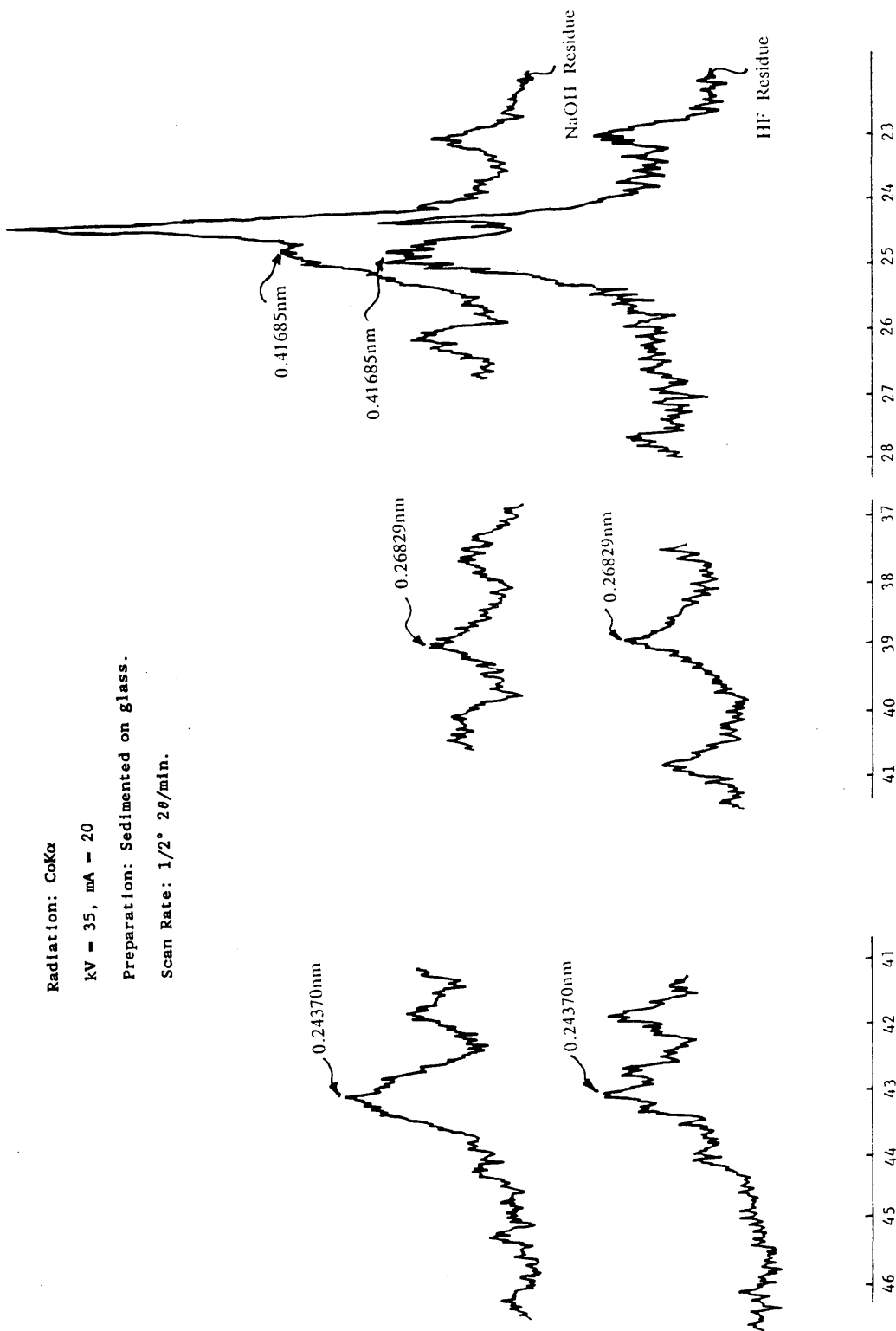


Figure 6.9: X-ray diffraction peaks of goethite in NaOH and HF treated

Sample 404.06.

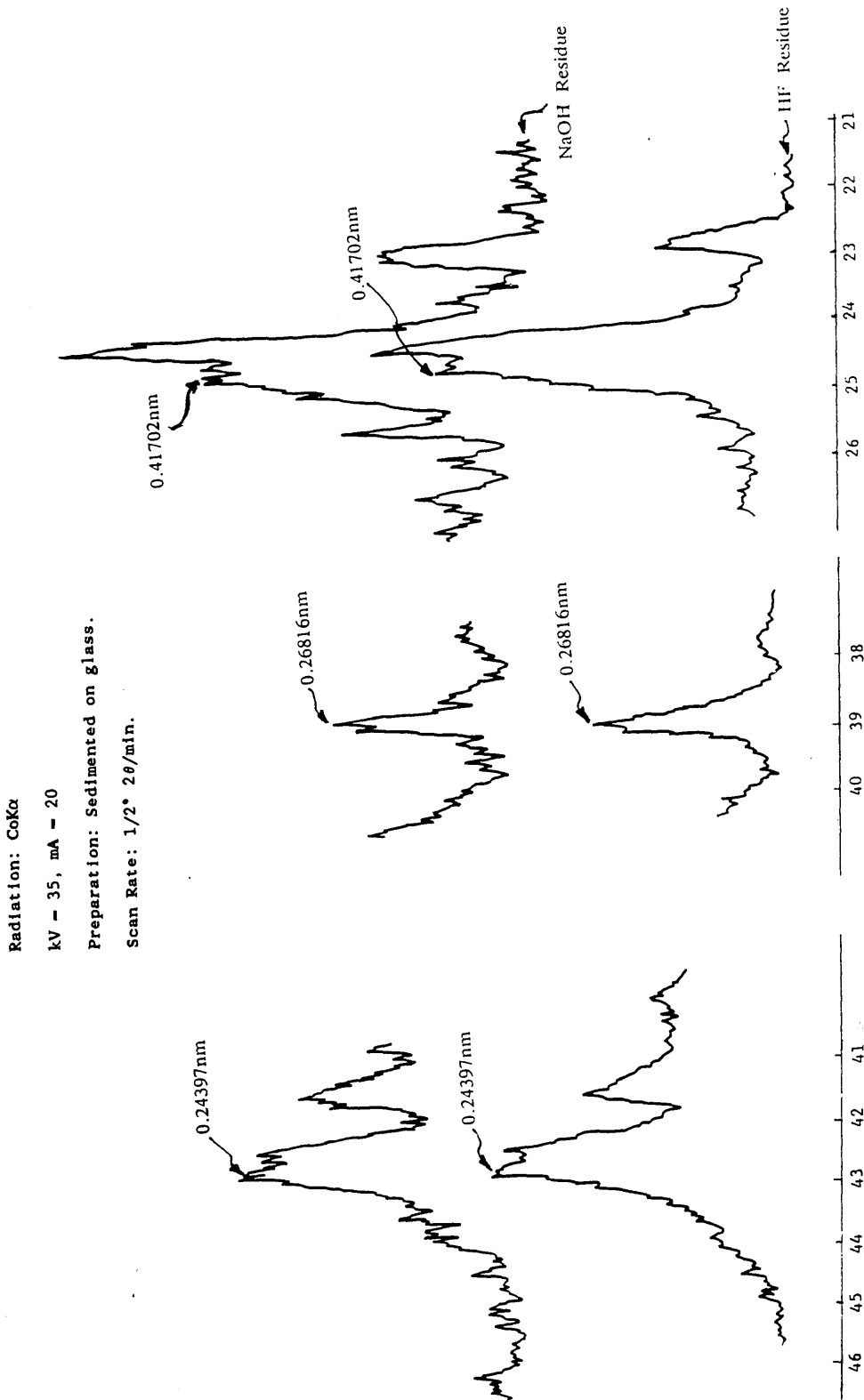


Figure 6.10: X-ray diffraction peaks of goethite in NaOH and HF treated

Sample 404.05.

CHAPTER 7

INFRARED SPECTROSCOPY AND DIFFERENTIAL SCANNING CALORIMETRY

7.1 INTRODUCTION

This chapter presents the infrared spectroscopy and differential scanning calorimetry investigations done on the soils. A brief introduction of the techniques is given in Section 7.2. Section 7.3 presents the experimental methods used, and Section 7.4 presents the results obtained from the investigation.

Infrared spectroscopy (IR) and differential scanning calorimetry have been used in this investigation as techniques for identification and characterisation of the minerals in the soils. Infrared spectroscopy is useful in the identification of poorly crystalline minerals (e.g ferrihydrite) which are often more difficult to identify by X-ray diffraction. Many aspects of the mineralogy of the clays presented in this chapter complement those already presented for electron microscopy (Chapter 5) and X-ray diffraction (Chapter 6) and a detailed treatment is not given here unless necessary.

7.2 GENERAL

Infrared spectroscopy is a useful tool for the solution of problem having to do with molecular structure, molecular behaviour, and the identification of unknown substances and mixtures. Materials absorb infrared radiation, and, given a specific molecular structure, it is possible to calculate the frequencies at which

infrared radiation will be absorbed by the molecule of a material. An infrared spectrum is simply a plot, often obtained automatically, of a function of radiant power (energy) along the ordinate versus frequency or wavelength as abscissa. Commonly one plots transmittance (%T) or absorbance (A) of radiation versus cm^{-1} or μ . The major interest is in those frequencies at which a material absorbs radiation and the amount absorbed. These absorption "peaks" or minima give rise to the uniqueness of the absorption spectra of different materials. For simple identification purposes, the spectra obtained are often compared with standard spectra of known substances.

The theory and applications of infrared spectroscopy were adequately covered by Farmer (1974) and Russell (1987) and the method has been used for the characterisation of different iron oxide minerals (e.g Jonas and Solymar, 1970; Chukhrov et al; 1971, 1972, 1973; Schwertmann and Fischer, 1973; Carlson and Schwertmann, 1980, 1981; Russell, 1979; Wilson et al; 1981, Fey and Dixon, 1981, Fysh and Fredericks, 1983; Goodman et al; 1988, and Carlson and Schwertmann, 1990 amongst many others).

Differential scanning calorimetry (DSC) is a thermoanalytical method, similar to differential thermal analysis (DTA), (the similarities and differences between the two methods were discussed by Mackenzie, 1980). The technique employs the difference in thermal properties between materials to identify and characterise different materials. The physical parameter measured in DSC is the difference in energy inputs into the sample and reference material, when both are subjected to a controlled temperature programme (Mackenzie, 1980; and Paterson and Swaffield, 1987). In the case of the heat-flow method produced by Du Pont and used in this study, there exists a well-defined heat-exchange path between the sample, the reference material and the heat source. Thus any imbalance in the system, caused by the absorption or evolution of heat by the sample, is countered by conductive heat flow through this well-defined path

(Paterson and Swaffield, 1987). Thermoanalytical methods are familiar methods in clay mineralogy and the topic was adequately covered in Mackenzie (1970) and Paterson and Swaffield (1987).

7.3 EXPERIMENTAL METHODS

7.3.1 Infrared Spectroscopy

Infrared spectroscopy was carried out on untreated clay fraction ($<2\mu\text{m}$) of the sample as well as residues obtained from the 5 M NaOH, HF, dithionite citrate bicarbonate (DCB) and acid oxalate treatments of the clay fractions as outlined in Chapter 4.

To reduce particle size, the samples were preground by maintaining them moist with isopropyl alcohol and hand grinding in an agate mortar and pestle for 1–5 minutes. The alcohol was allowed to evaporate completely before proceeding further. 2 mg of the preground material and 170 mg potassium bromide were thoroughly mixed for 2 minutes in a vibrating stainless-steel capsule containing three ball bearings, 2–3.5mm diameter. The mixture was then pressed in an evacuated die to give a 13 mm diameter disc which was used for testing. Infrared spectra were recorded over the range 4000 to 250 cm^{-1} on a Perkin Elmer 580B spectrometer at room temperature and after heating the disc to 150°C for 16 hours (allowed to cool in a dessicator) to remove adsorbed water. The discs were then diluted by a factor of 1 to 8 (equivalent to 0.25mg sample in disc) to show spectra detail of intense silicate absorption near 1000 cm^{-1} .

7.3.2 Differential Scanning Calorimetry

The soil samples were equilibrated at a relative humidity of 56%, using MgOH, for at least 4 days prior to testing. The heat-flux differential scanning

calorimetry (DSC) curves were obtained using a Du Pont 900 Differential Thermal Analyzer equipped with a Du Pont 900 DSC cell. 10 mg samples were used at a heating rate of 10°C per minute, a ΔT sensitivity of 0.5°C per inch and a T axis sensitivity of 100°C per inch. The atmosphere used was nitrogen flowing at 50 cm³ per minute.

7.4 RESULTS

7.4.1 Infrared Spectroscopy

The infrared spectra of the untreated clay fraction (<2 μ m) of the soils are shown in Figure 7.1. The summary of the mineralogical contents of the soils based on the interpretation of the spectra is given in Table 7.1. As was the case with X-ray diffraction and electron microscopy observation of the soils, kaolin type minerals was indicated in the soils by infrared absorption bands at about 3700 and 3620cm⁻¹. These are characteristic OH stretching bands for kaolin minerals. Similarly, the bands at about 938 and 916cm⁻¹ are typical OH deformation bands for the kaolin type minerals (Russell, 1987). Comparison of the positions and character of the OH stretching bands at about 3700 and 3620 cm⁻¹ with standard kaolin charts (e.g see Russell, 1987) indicated the kaolin to be halloysite or kaolinite in the samples rather than any of the rarer kaolin, dickite and nacrite. In most cases, for pure kaolinite the bands are often sharper and the band at 3700cm⁻¹ is often more intense than that at 3620cm⁻¹ whereas for halloysite the opposite is the case. Also, for kaolinite, small absorption bands between 3700 and 3620cm⁻¹ (at 3669 and/or 3653cm⁻¹) may be evident. To distinguish between well crystallised kaolinite and halloysite, the two bands 795 and 758cm⁻¹ could be used. For well crystallised kaolinite the two bands are of equal intensity whereas for halloysite the 795cm⁻¹ band is reduced to a very weak inflection (Russell, 1987). An examination of the bands for Samples 404.05

and 404.06 in Figure 7.1 indicated halloysite to be the predominant mineral in these soils. The presence of a very weak band at about 3669cm^{-1} indicated the presence of a very minor amount of kaolinite in Sample 404.06. In the case of Samples 404.07 and 404.08, the intensity of the 795cm^{-1} band could be seen to increase slightly compared to the previous samples. In addition, for these two soils, the intensity of the band at 3700cm^{-1} increased slightly over that at 3620cm^{-1} and the presence of very small bands at 3669cm^{-1} and 3652cm^{-1} was clearly evident. All these appeared to indicate kaolinite in association with halloysite in these samples. Electron microscopy (Chapter 5) showed a mixture of kaolinite and halloysite for Samples 404.05 in line with infrared spectroscopic observations. The spectra also indicated an increase in the proportion of kaolinite and a decrease in that of halloysite on passing from Sample 404.05 to 404.08 in line with results obtained from electron microscopy and X-ray diffraction. On comparison with standard spectra, the kaolinite looks well crystallised as indicated by the two bands at 3669 and 3653cm^{-1} that is typical for well crystallised kaolinite. A disordered kaolinite will normally have just the band at 3653cm^{-1} (see Russell, 1987). Judging from the shape and position of Si-O bands near 1100cm^{-1} (using spectra from the diluted samples, not shown here) the particle size of the kaolinite is small (less than $1\ \mu\text{m}$) compared with the halloysite (Farmer and Russell; 1964, 1966; and private communication with Russell and Fraser, 1990). According to Farmer and Russell (1964), the position and sharpness of the absorption near 1100cm^{-1} varies with physical state for layer silicates. In the spectra for dickite, nacrite and kaolinite of size $<2\ \mu\text{m}$ this band appears as a broad shoulder near 1080cm^{-1} . The band intensifies, and shifts to higher frequencies in the spectra of smaller crystals until in very finely ground material when the band is close to that found for clay size particles, $<2\ \mu\text{m}$ (Farmer and Russell, 1964). In the present case, for Sample 404.08, where the band was most clear, a very sharp band at 1110cm^{-1} indicated the small size of

the kaolinite. This observation was supported by sedimentation analysis (see Chapter 3) which showed about 80% of the clay to have size less than $1\mu\text{m}$.

The presence of a weak shoulder at about 3630cm^{-1} in the infrared spectra (Figure 7.1) suggested the presence of mica (either 2M1 illite or 2M1 muscovite, but as suggested earlier in Chapter 6 the mica was probably the remnant of the muscovite which was present in the original rock) in all the soils. This band is much more intense in the NaOH and HF treated soils (Figures 7.3 and 7.4 respectively), following dissolution of the kaolin. The band got weaker on passing from 404.05 to 404.08 suggesting a decrease in the proportion of mica in the soils in this direction. Other minerals identified in the samples in minor or trace quantities were chlorite, quartz and feldspar as indicated in Tables 7.1 to 7.3.

As was found by X-ray diffraction (Chapter 6), the presence of gibbsite in sample 404.08 was indicated in infrared spectroscopy by bands at 3460cm^{-1} and 3530cm^{-1} of the infrared spectra of the sample (Fig. 7.1). These bands were absent in the spectra for the other soils and indicated the more advanced weathering of this soil. Since ferrihydrite was indicated in some of the soil samples (see Chapters 4 and 5), the role of organic matter and other ions in inhibiting crystallisation of iron oxides in the soils was of interest. However no indication of organic matter, to any detectable limit, was given by infrared spectroscopy in any of the soils.

Goethite appeared to be the only iron oxide mineral indicated (in minor amounts) in all the untreated samples. Normally, for pure, synthetic goethite, main infrared absorption bands are expected at around 3153cm^{-1} , 893cm^{-1} , 794cm^{-1} , 667cm^{-1} , 633cm^{-1} , 495cm^{-1} , 455cm^{-1} , 409cm^{-1} , 377cm^{-1} , and 276cm^{-1} (See Russell, 1987). In this case, the band at about 3160cm^{-1} wavelength was assigned to the OH stretching (νOH) of goethite, and this was confirmed from difference with the spectra obtained from the dithionite citrate

bicarbonate (DCB) treatment residues (from which iron oxide had been dissolved) shown in Figure 7.2. A comparison of the spectra in Fig. 7.1 with those in Fig. 7.2 showed the bands at about 3160 cm^{-1} to be absent from the spectra in Fig. 7.2 following dissolution of the iron oxide minerals. The usual goethite bands at about 900 cm^{-1} (δOH) and 800 cm^{-1} (γOH), due to OH bending, could not be used for goethite identification and characterisation in this case as they were made obscured by the bands from the clay silicates, and, due to the fact that the goethite was present in minor amounts in the soils, a difference spectra from the untreated and DCB spectra was not helpful. An estimation of the area enclosed by the goethite band at about 3160 cm^{-1} for all the samples showed the amount of goethite in the samples to increase progressively with increased weathering i.e. from sample 404.05 to 404.08. Due to the poor resolution of the OH stretching bands at about 3160 cm^{-1} it was not possible to determine the character of the band in Fig. 7.1.

In order to obtain improved infrared spectra for the iron oxide minerals, infrared spectroscopy was performed on residues obtained from iron oxide concentration treatments using 5 M NaOH and HF outlined in Chapter 3 and discussed in Chapter 4.

Figures 7.3 and 7.4 show the infrared spectra for the residues obtained from the NaOH and HF treatments respectively. The summary of the mineralogy of the residues are given in Tables 7.2 and 7.3 for the NaOH and HF residues respectively. Comparison of Tables 7.2 and 7.3 with Table 7.1 for the untreated samples showed that halloysite and kaolinite were no longer major minerals in the treated samples, having been dissolved by the treatments to concentrate iron oxides. Mica and goethite, on the other hand, were concentrated by both treatments and had become the major minerals in the residues following the treatments. Both 5 M NaOH and HF treatments appeared to have concentrated the same minerals in the soils in agreement with results obtained from X-ray

diffraction.

It could be seen from Figures 7.3 and 7.4 that the absorption bands due to OH stretching (νOH) of goethite (between 3100 and 3200 cm^{-1}) are sharper and larger, due to the increased concentration of goethite in the residues, compared to the untreated samples (Figure 7.1). However the OH bending absorption bands of goethite, usually expected around 800 and around 900 cm^{-1} , were still not clearly discernible due to interference from bands from mica in the same region. Since these bands are very important to the character of the goethite particles especially with regard to aluminium substitution (Jonas and Solymar, 1970; Fysh and Fredericks, 1983, Schulze and Schwertmann, 1984, 1987) attempts were made to make them more discernible by subtracting the DCB spectra (Fig. 7.2) from the spectra in Figures 7.3 and 7.4 (to leave a difference spectra showing, mainly, goethite absorption bands) but these were unsuccessful, perhaps due to poor matching between the DCB spectra and those for the NaOH and HF residues which produced negative bands in the difference spectra around the relevant region.

The band positions for the OH stretching (between 3100 and 3200 cm^{-1}) of goethite are shown in Figures 7.3 and 7.4 for the different soils and tended, in both cases, to indicate a shift to lower values in passing from sample 404.05 to 404.08, although the positions for the 404.06 and 404.07 soils were the same in both cases. Since the mica absorption bands (e.g at 3630 cm^{-1}) which were used as a form of internal standard were not similarly shifted from soil to soil the shifts described above for goethite appeared to be real and represented a difference of as much as 15 cm^{-1} and 34 cm^{-1} between samples 404.05 and 404.06/404.07 and samples 404.05 and 404.08 respectively.

The shift in the OH stretching bands (νOH) described above may be due to differences in structural aspects in the goethite particles between the soils. An increase in absorption frequency in the infrared spectroscopy signifies a decrease

in bond strength and is occasioned by a longer bond length. One major factor that has been reported to lead to shifts in the infrared absorption bands of goethites is aluminium substitution (e.g Jonas and Solymar, 1970; Fey and Dixon, 1981; Fysh and Fredericks, 1983, Schulze and Schwertmann, 1984, 1987). All these authors have reported that the OH bending bands near 900 cm^{-1} (δOH) and 800 cm^{-1} (γOH) exhibited the greatest aluminium dependency which was indicated by a shift in both band positions to higher wave numbers with increasing aluminium substitution for iron in the goethite structure. Such a relationship between aluminium substitution and νOH has not been well established. Schulze and Schwertmann (1984) using synthetic aluminous goethites produced by a variety of procedures reported that the OH stretching band position (νOH) showed a general shift to higher wavenumbers with increasing aluminium substitution but with a correlation coefficient (r) of 0.62, the relationship was not particularly good and even goethites with no Al substitution showed about an 80 cm^{-1} spread in νOH frequency. Mendelovici et al (1979), on the properties of aluminium-bearing soil goethites, also found a shift in νOH to higher wavenumbers with increasing Al substitution which they attributed to a weakening of the hydrogen bond caused by a higher screening effect in Al-O-H groups compared to similar Fe-O-H groups, but Schulze and Schwertmann (1984) are of the opinion that such a weakening of the H-bond by the ionic substitution of Al for Fe is unlikely. Fey and Dixon (1981) reported that νOH became broader but did not change frequency with aluminium substitution. Schulze and Schwertmann (1984) showed that increased structural defects in the goethite particles may shift νOH to higher values in aluminous goethites synthesised at temperatures $25^\circ\text{C} - 70^\circ\text{C}$. They stated that the combined effect of Al substitution and structural defect could lead to an overall weakening of the H-bond and consequent shift of the νOH band to higher values. Results presented by Schulze and Schwertmann (1987) also appeared to show this

combined effect to favour a shift to higher wavenumbers of the νOH band. Schwertmann et al. (1985), using goethites synthesised at varying temperatures between 4°C and 90°C, also reported that the νOH positions of goethites shifted to lower wavenumbers with increase in crystallinity.

In the present case, the shift in νOH observed represented a shift to lower wavenumbers with increasing Al substitution (reported in Chapter 6). Table 7.4 shows Al substitution and νOH values for the soil goethites after NaOH and HF treatments respectively. The decrease of the νOH band position to lower wavenumbers with increasing Al substitution is what can be expected from a comparison between goethite and diaspore (AlOOH), the Al isomorph of goethite. In goethite the $\text{O}_\text{I}-\text{O}_\text{II}$ distance is 0.2757 nm and the angle $\text{O}_\text{I}-\text{O}_\text{II}-\text{H}$ is 11.6° (from data reported by Forsyth et al; 1968 and Sampson, 1969), while in diaspore they are 0.2650 nm and 12.1° (Busing and Levy, 1958). The $\text{O}_\text{II}-\text{H}$ distance is 0.099 nm in each case. The νOH band positions are $\approx 3131\text{ cm}^{-1}$ in goethite and $\approx 2950\text{ cm}^{-1}$ in diaspore (Schwarzmann and Sparr, 1969). The shorter $\text{O}_\text{I}-\text{O}_\text{II}$ distance in diaspore gives rise to a stronger H-bond in diaspore than in goethite, which is indicated by a lower wavenumber of the νOH band. The slightly smaller $\text{O}_\text{II}-\text{O}_\text{II}-\text{H}$ angle in goethite should increase the strength of the H-bond slightly (Schwarzmann and Sparr, 1969) but the increase is not enough to compensate for the change in bond strength caused by the differences in $\text{O}_\text{I}-\text{O}_\text{II}$ distances. For increasing ionic substitution of Al for Fe in the goethite structure one would expect a steady increase in H-bond strength and a corresponding decrease in νOH band position as was observed in this study. Due to the limited number of samples used in the present investigation, it was not possible to establish a definite relationship between Al substitution and νOH , but a trend appeared to have been shown.

Also, since the crystallinity of the goethite particles in this investigation increased in the same direction as aluminium substitution (as revealed by X-ray

diffraction) the combined effect of Al substitution and increasing crystallinity would be a shift of νOH to lower values. The separate effect of increasing crystallinity in causing a shift of νOH to lower values could not be assessed in the present circumstances. In the light of the results of this investigation and those by previous authors, it is possible that several factors may be responsible for the infrared OH stretching band position of goethite, and that the shift of the band position may be dictated by the dominating factors.

A comparison of Figures 7.3 and 7.4 revealed two points. Firstly, the the positions of the goethite νOH band between 3100 cm^{-1} and 3200 cm^{-1} for each soil were about the same in both cases. This may be a support for the results of X-ray diffraction (Chapter 6) which showed the diffraction characteristics of the iron oxides obtained from both methods to be similar, thus reinforcing the observation that the 5 M NaOH treatment may not have altered the properties of the goethite in the soils significantly. Secondly, the size of the peaks in the spectra for the HF treated samples were generally smaller than those for the NaOH treated samples for samples 404.05, 404.06 and 404.07. Values of the ratio goethite:mica showed higher values in NaOH residues compared to those in HF residues (20 to 200% greater) for these soils, but the values for the ratio in residues for sample 404.08 were about the same for both treatments. This observation indicates the presence of poorly crystalline iron oxides in samples 404.05, 404.06 and 404.07. The possibilities are that poorly crystalline goethite in these soils were dissolved by HF treatment, or a poorly crystalline phase, probably ferrihydrite, was converted to goethite by the 5 M NaOH treatment (e.g see Goodman et al; 1987). If the second possibility was the case, other results obtained in the course of the investigation would appear to suggest that the properties of the newly formed goethites did not affect the overall properties of the goethite in the soils.

7.4.2 Differential Scanning Calorimetry

The differential scanning calorimetry (DSC) curves obtained for the untreated clays, and residues from 5 M NaOH treatments are shown in Figures 7.5, and 7.6 respectively. It was not possible to carry out DSC on HF residues due to shortage of samples. For the untreated clays, only one large endothermic peak at about 530°C, belonging to the dehydroxylation of kaolin (halloysite/kaolinite) was obvious in the curves for Samples 404.05, 404.06 and 404.07. In the case of Sample 404.08, an additional, small endothermic peak at about 285°C indicated the presence of gibbsite in the soil. On concentration of the iron oxide minerals with NaOH (Figure 7.6) the DSC curves for each of the soils showed one endothermic peak which could be assigned to the dehydroxylation peak of goethite. A small but consistent shift of this peak to higher temperature could be observed on passing from sample 404.05 to 404.08 in Fig. 7.6. As shown by previous studies by several authors, the dehydroxylation peak of goethite can be influenced by Al substitution (Jonas and Solymar, 1970; Fey and Dixon, 1981, Schulze and Schwertmann, 1984, 1987), particle size, and by structural defects and crystallinity (Mackenzie, 1957 and Mackenzie and Berggren, 1970). Increased Al substitution was found to lead to an increase in the dehydroxylation temperature and this is consistent with the increased thermal stability of goethite as Al substitution increases (Schulze and Schwertmann, 1984). Coarser samples and more crystalline samples also give higher dehydroxylation temperatures (Mackenzie, 1957).

In agreement with previous works, the increase in the dehydroxylation temperature of goethite on passing from sample 404.05 to 404.08 observed in this study may be attributed to the combined effects of increased aluminium substitution, increased particle size and increased crystallinity from Sample 404.05 to 404.08 as was observed by electron microscopy and X-ray diffraction.

7.5 SUMMARY

Some of the important findings of the study in this chapter are listed below.

7.5.1 Clay Mineralogy

- (1) In line with the results of electron microscopy and X-ray analysis infrared spectroscopy and DSC confirmed the main weathering products of the Hong Kong granites to be halloysite in the deeper soils. This was later mixed with kaolinite as weathering progressed with the proportion of kaolinite in the soils increasing with progressive increase in weathering.
- (2) Infrared spectroscopy revealed the kaolinite to be of small particle size (often $<1\mu\text{m}$) in line with observations from particle size analysis.
- (3) Mica (most probably 2M1 muscovite) was indicated in minor quantities in all the soils, with the proportion decreasing progressively with increased weathering of the soils. A minor quantity of chlorite was also indicated in some of the soils.
- (4) Gibbsite was indicated by both IR and DSC in the most weathered soil.

7.5.2 Iron Oxide Mineralogy

- (1) Only goethite was indicated by infrared spectroscopy and DSC in all the samples. The absence of ferrihydrite peaks confirmed the minute quantity of the mineral which

was earlier identified in some of the soils by electron microscopy and acid oxalate dissolution.

- (2) Infrared spectroscopy showed that the amount of goethite in the soils increased progressively with increased weathering.
- (3) A shift of the infrared OH stretching band of the soil goethites to lower wavenumbers was observed. This shift to lower values is contrary to the observation from previous studies but corresponded with the direction of increased Al substitution for Fe in the goethite particles and is what should be expected from comparison with diaspore (the Al isomorph of goethite). Due to the fact that other factors such as variation in crystallinity could lead to similar shifts, it has been concluded that several factors may be responsible for the shift of the infrared OH stretching band to may be caused by several factors and the direction of shift dictated by the dominating factor/s.
- (4) A shift in the DSC dehydroxylation peak positions of goethite to higher values with increased weathering was observed. This increase was attributed to the combined effects of increased Al substitution, increased particle size and increased crystallinity of the soil goethites with increased weathering.

Table 7.1 Summary of the Mineralogy of Untreated Clays

Sample	Major	MINERALS		
		Intermediate	Minor	Trace
404.08	Halloysite/ Kaolinite	-	Goethite Gibbsite	Mica
404.07	Halloysite/ Kaolinite	-	Goethite	-
404.06	Halloysite	-	Goethite	Kaolinite
404.05	Halloysite	-	Goethite	Mica

Goethite: 08 > 07 - 05 > 06
Halloysite: 05 > 06 > 07 > 08
Kaolinite: 08 > 07 > 06 > 05

Table 7.2 Summary of the Mineralogy of 5-M NaOH Treated Clay Residues

Sample	Major	MINERALS		
		Intermediate	Minor	Trace
404.08	Goethite Mica	—		Quartz Kaolinite/ Halloysite Feldspar
404.07	Goethite Mica	—	Quartz Kaolinite Halloysite Feldspar Chlorite	—
404.06	Goethite	Mica Feldspar	Quartz	Chlorite
404.05	Mica	Goethite	Quartz Feldspar	—

Goethite: 08 > 07 = 06 > 05

Mica: 05 > 08 > 07 > 06

Feldspar 06 >> 05 > 07 >> 08

Chlorite 07 > 06

Table 7.3 Summary of the Mineralogy of HF Treated Clay Residues

Sample	MINERALS			
	Major	Intermediate	Minor	Trace
404.08	Goethite	Mica	—	Quartz Feldspar Kaolinite/ Halloysite
404.07	Goethite Mica	—	Quartz Feldspar	Kaolinite/ Halloysite
404.06	Goethite Mica	—	Quartz Feldspar Kaolinite/ Halloysite	—
404.05	Mica	—	Goethite Quartz	Feldspar Kaolinite/ Halloysite

Goethite: 08 > 07 > 06 >> 05

Mica: 05 > 07 > 06 = 08

Table 7.4: OH Stretching Band Position (ν_{OH}) and Aluminium Substitution for 5-M NaOH and HF Treated Clay Residues

Sample	ν_{OH} (cm^{-1})		Al Substitution (mole %)	
	NaOH	HF	NaOH	HF
404.08	3170	3168	15.24	15.72
404.07	3180	3178	14.57	14.57
404.06	3180	3178	12.28	12.28
404.05	3198	3200	9.42	9.42

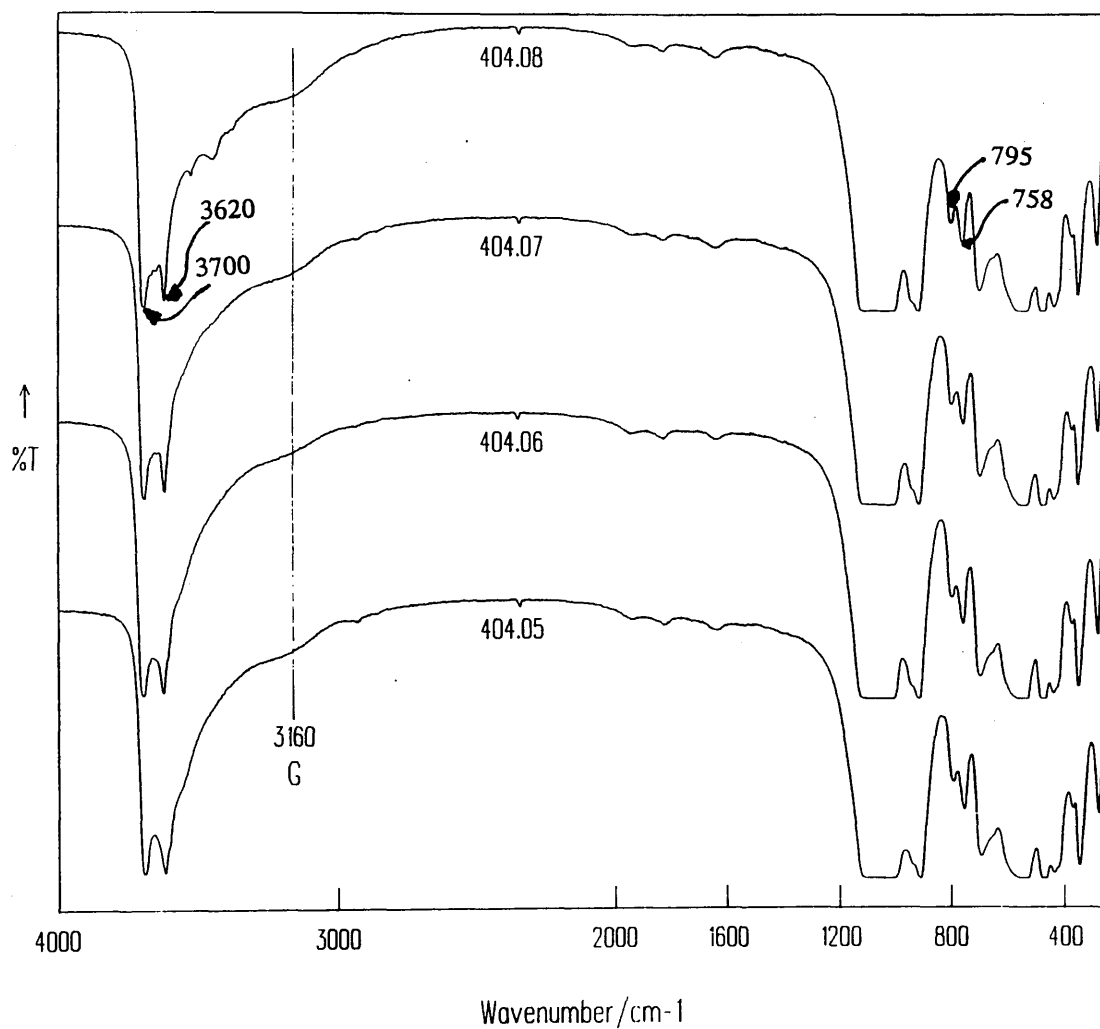


Figure 7.1: Infrared Spectra of Untreated Clays. The Goethite Band at 3160cm^{-1} is indicated (G)

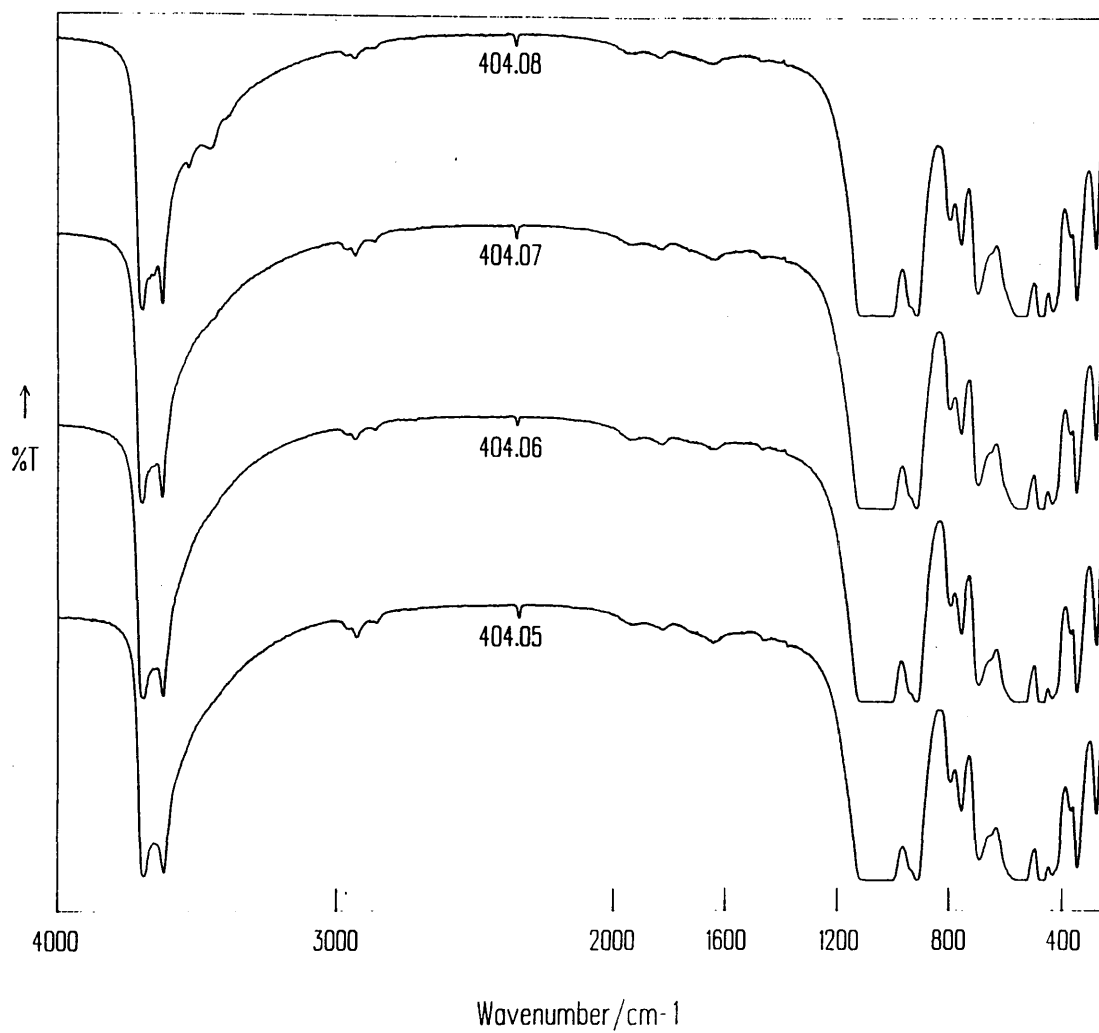


Figure 7.2: Infrared Spectra of Residues from Dithionite Citrate Bicarbonate (DCB) Treated Clays

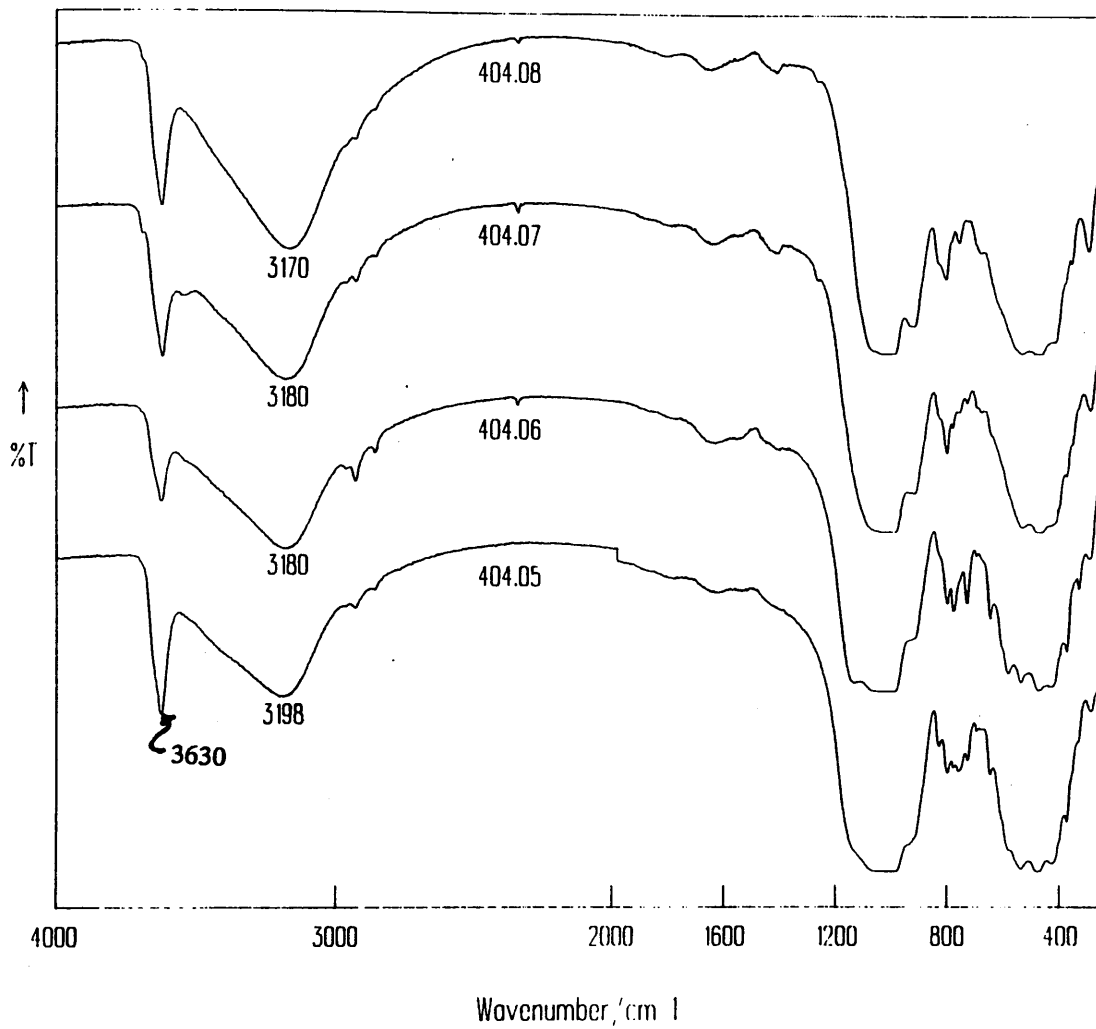


Figure 7.3: Infrared Spectra of Residues from 5 M Boiling NaOH Treated Clays

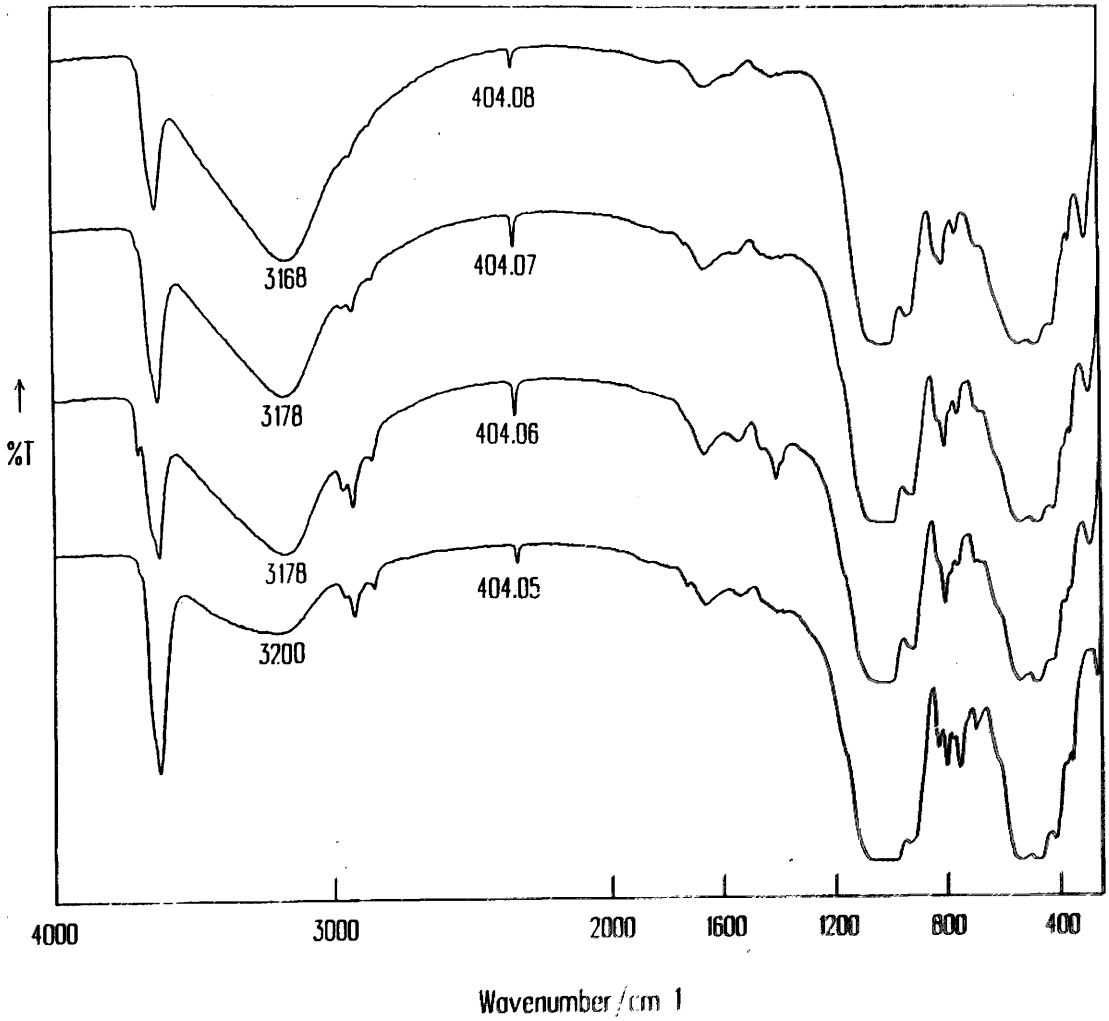


Figure 7.4: Infrared Spectra of Residues from HF Treated Clays

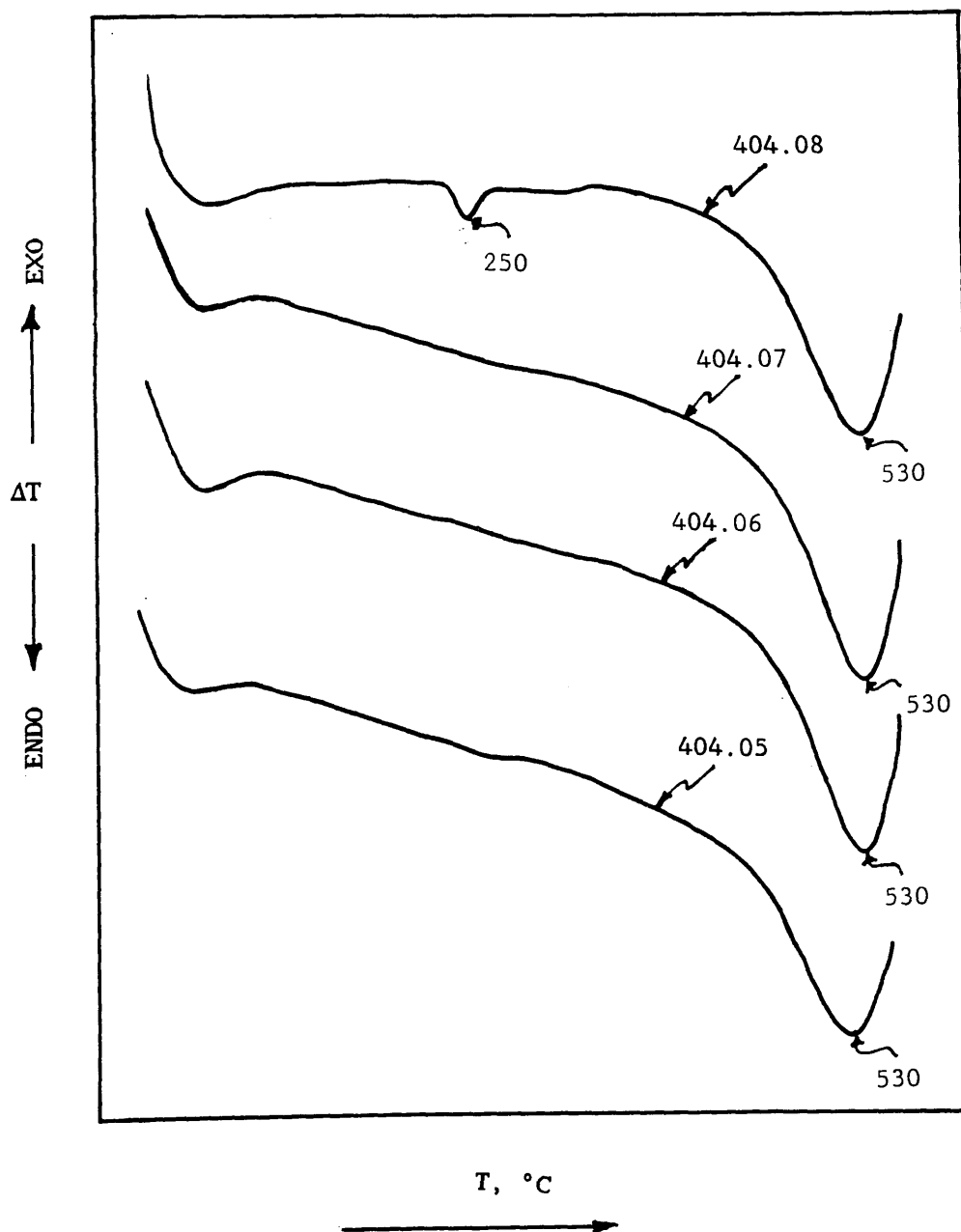


Figure 7.5: DSC Curves of Untreated Clays

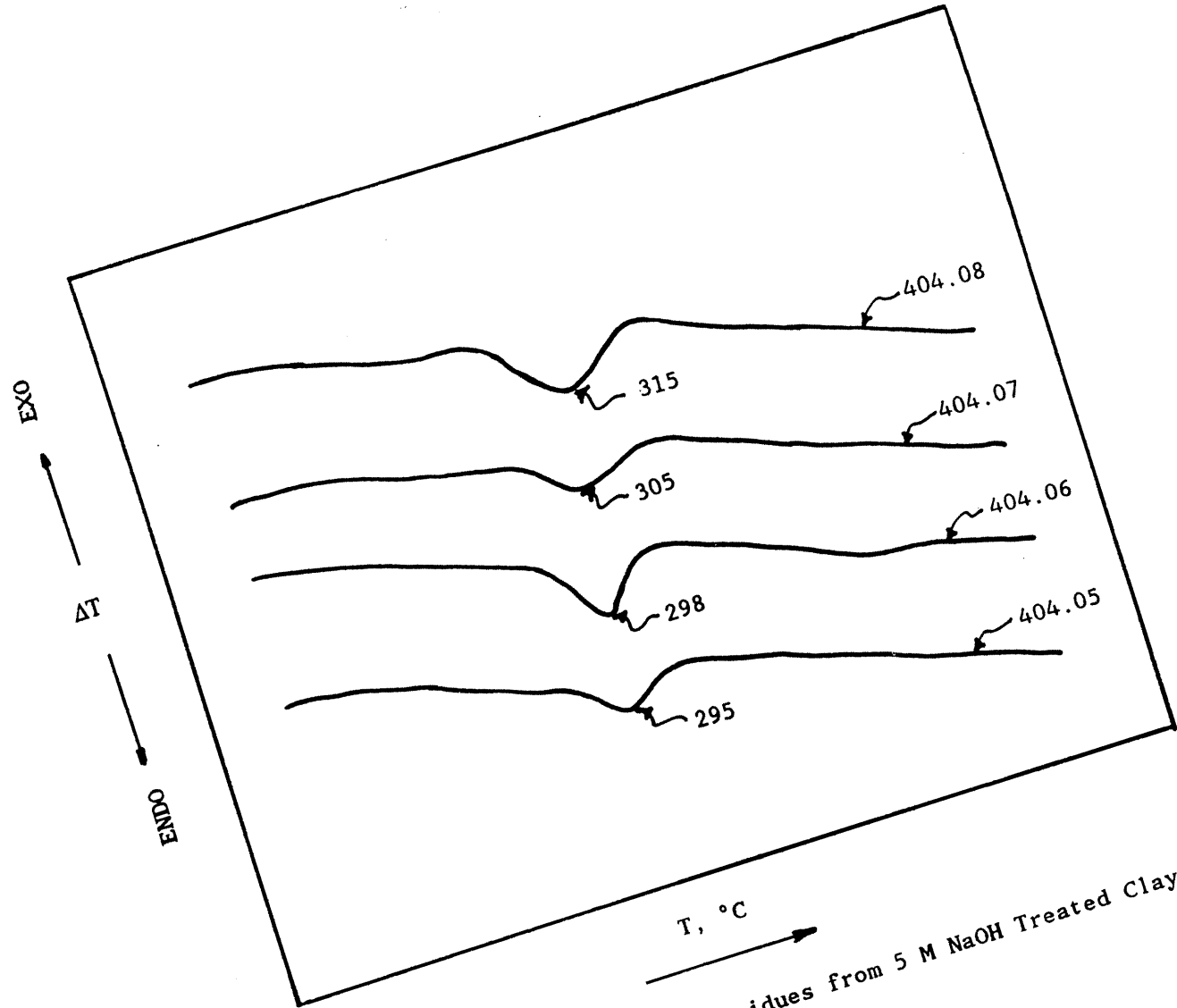


Figure 7.6: DSC Curves of Residues from 5 M NaOH Treated Clays

CHAPTER 8

GENERAL DISCUSSION

8.1 INTRODUCTION

Some specific discussions have already been presented along with the results in the previous chapters. In this chapter these are summarised and a general discussion is given based on the overall findings of the study.

8.2 GENERAL DISCUSSION

8.2.1 Soil Weathering and Clay Mineralogy

The results of chemical analysis by X-ray fluorescence (XRF), scanning electron microscopy (SEM), transmission electron microscopy (TEM) and electron diffraction (ED), X-ray diffraction (XRD), infrared spectroscopy (IR), and differential scanning calorimetry (DSC) reported earlier in the previous chapters have given an insight into the weathering characteristics and clay mineralogy of the weathered granite under investigation.

The depletion of Ca and Na (elements which were contained mainly in the plagioclase feldspars in the soils under investigation) in the least weathered soil, together with the observation of hand specimens and preliminary optical microscopy study indicated that the plagioclase feldspar was the first primary mineral to weather significantly. Significant weathering of K-feldspar and biotite then occurred at later stages while quartz was the most stable of all the minerals and showed minimal dissolution in all the soils although an accumulation of the

mineral in a particular soil relative to another was not indicated. The sequence of weathering of the primary minerals in the soils is in agreement with that reported by Lumb and Lee (1975) for Hong Kong granites and the significant weathering of plagioclase prior to that of K-feldspar agrees with earlier findings that reported K-feldspars to be generally more stable than plagioclase (e.g. Goldich, 1938 and Huang, 1977).

A summary of the mineralogy of the clay fraction of the soils based on the combined findings from using the different techniques is given in Table 8.1. Tubular halloysite (7A) was indicated as the initial weathering product of the granites and dominated the clay mineralogy of the less weathered soils while minor quantities of muscovite, K-feldspar and quartz were also present in these soils. Halloysite was gradually replaced by kaolinite as weathering progressed in the soils. Chlorite was found as a trace mineral in some of the soils while the formation of gibbsite was evident in the most weathered soil. The occurrence of halloysite in the least weathered soil where the plagioclase feldspar was found to be the only primary mineral to be significantly weathered suggested that the halloysite tubes in this soil were formed from the plagioclase. The fact that kaolinite was abundant only in the most advanced stages of weathering, and the increase in the proportion of the mineral at the expense of halloysite as weathering progressed appeared to suggest that the kaolinite may have been formed by alteration of the halloysite. The fact that some of the halloysite tubes appeared to be opening up (e.g. Gilkes et al; 1980) and the similarity in the size of halloysite and kaolinite in the residual soil also support this suggestion. The possibility that at least some of the the kaolinite may have been formed from other minerals such as K-feldspar or biotite cannot however be discounted in the present investigation. The muscovite in the samples was found by X-ray diffraction and infrared spectroscopy to be of the 2M1 polytype. Optical microscopy of unweathered rock fragments showed that the mineral was present as

a primary mineral in very low quantity. The presence of muscovite in all the soils appeared to indicate that the mineral was resistant to weathering under the prevailing conditions although its depletion in the residual soil indicated a possible alteration to other products at this stage. It is possible that the chlorite in the soils was derived from the alteration of biotite. The fact that the identification of chlorite in Sample 404.06 also coincided with the onset of biotite weathering (from observation of hand specimens) which then increased up the profile with increase in the proportion of chlorite appeared to support this suggestion. Gibbsite formation has been reported to occur from either the alteration of primary aluminosilicates or from the secondary clay minerals (Hsu, 1977; Eswaran et al; 1977 and Gilkes et al; 1980). The occurrence of gibbsite only in the most weathered soil in this investigation may be an indication that the gibbsite was formed from one or more of the clay minerals (probably kaolinite and halloysite) after they had been formed from the primary minerals.

TEM and SEM observations showed halloysite tubes of silt and clay sizes. In some cases, for the less weathered soils, the formation of halloysite was at the advanced stages, and although the halloysite tubes could be seen to grow out of a substrate, the main mineral from which they were formed were not recognisable. In other cases, however, the halloysite tubes could be seen to grow out of the surface of the primary mineral (probably plagioclase). In such cases, the halloysite tubes were particularly long with most of the tubes being longer than $5\mu\text{m}$. Such long tubes of halloysite had been identified in soils previously (Eswaran and Bin, 1978a and 1978b) and appear to be typical of granitic weathering in well drained soils of the tropical and subtropical areas. It is possible that these tubes were formed in places within the weathering rock (e.g in etch pits of feldspars) where they were protected from mechanical stresses. Alternatively, the tubes may have been formed from minerals which weathered faster than the other minerals, in which case by the time they were formed, the

fabric of the soil was still mostly intact and protected the tubes from mechanical stresses.

Parham (1969b) also identified halloysite tubes in weathered granites from Hong Kong. According to him, the halloysite was formed as a result of feldspar alteration to allophane from which the halloysite was subsequently formed. The allophane was said to have formed a covering sheet on the feldspar particles. Lumb and Lee (1975) also reported identifying allophane in halloysitic soils formed from granite in Hong Kong and stated a sequence for the alteration of feldspar to kaolinite in which feldspar alters first to allophane from which halloysite crystallises. The halloysite is later transformed to kaolinite as weathering continues. Since no allophane was indicated in the soils studied in this investigation (perhaps due to the advanced stage of formation of the halloysite in the soils) it was not possible to confirm the formation of halloysite from allophane. In the cases where halloysite was observed to be forming from the primary feldspar mineral by SEM, however, no indication of formation from a covering sheet was given. Rather the halloysite tubes were seen to grow out of the surface of the feldspar. It is possible that amorphous intermediates were first formed on the surfaces of the feldspar (not necessarily as covering sheets) and halloysite was subsequently formed from them. This type of formation of halloysite from amorphous materials was reported by Eswaran and Bin (1978b) for halloysites formed from granite in Malaysia. Further investigation is however needed to confirm the mode of formation of halloysites in the present case.

Based on the results of mineralogical analysis of the different weathering grades of soils obtained in this study, a possible weathering path for the primary minerals in the granitic rocks to the residual soil found on site is proposed as shown in Figure 8.1.

8.2.2 Engineering Properties

Various engineering properties of soils are related to their mineralogy, particle size and microfabric (Lumb, 1962, 1965; Yong and Warkentin, 1975, and Jacquet, 1990). The results of mineralogical properties of the soils obtained from using the different techniques already mentioned in Section 8.2.1 above, together with the results of particle size analysis done in the cause of this investigation and those by other authors, and the observation of the soil fabric using SEM could allow a prediction of some of the geotechnical behaviour of these and other similar soils. Mineralogical analysis has shown that either tubular halloysite or platy kaolinite was the main clay mineral in the weathered granite and residual soils with halloysite being dominant in the less weathered soils, but gradually replaced by kaolinite which became slightly dominant in the most highly weathered residual soil. Results of particle size analysis showed that the clay fraction of the soils varied from less than 6% in the least weathered soil to 18% in the most weathered soil (see Table 3.6) thus showing that clay constituted a very small amount of the total soil. Irfan (1986) also found clay fractions of 1 to 9% for eleven samples of Hong Kong granite while Lumb (1962) reported an average of 8% clay content for similar weathered granite from Hong Kong. According to Lumb and Lee (1975), from an engineering point of view, the halloysitic nature of the clay-size fraction and its small amount would suggest that the clay has little influence on performance of these soils, and that the engineering behaviour would be controlled by the coarser silt and sand fractions. This suggestion is in agreement with the observed behaviour of the soils (Lumb, 1962, 1965). Lumb (1962) however reported that considerable variation in grading and voids ratio of the decomposed granite occurred in relatively small volume of soils and that these variations were haphazard and quite unpredictable from the results of a single trial pit or borehole. The results of TEM and SEM (Chapter 5) obtained in this investigation showed silt as well as clay size

halloysite tubes in the soils. It is possible that the silt-size halloysite tubes are fragmented into clay sized tubes during pretreatment for particle size analysis which may include finger or pestle crushing and shaking or ultrasonic vibration of the soils. Hence, the variation in grading noted by Lumb (1962) may be due to differences in pretreatment procedures (e.g amount of shaking or ultrasonic treatment) which do not lead to variation in other soils and are often overlooked. Indeed, particle size determination done on one soil (from the present site) using two different methods (one which involved the use of pestle and mortar without finger crushing of soft feldspars, and another which involved the use of pestle mortar with additional finger crushing of soft feldspars) showed an increase in clay content from 3% to 12% (Irfan, 1986), thus supporting the suggestion that differences in grading may result from differences in pretreatment procedures. The silt size of some of the soils were also found to increase dramatically (up to 14% change) when finger crushing of soft feldspars was done prior to particle size determination (Irfan, 1986). This is probably due to gravel and sand size feldspars being reduced to silt size fractions by finger crushing. Such variation in grading may have serious engineering implications, since grading is an important classification parameter. In addition, the tropical and subtropical areas of the world where these soils appear to be widespread are, currently, areas of intense civil engineering activities. In view of these it would be necessary to adopt a uniform method for particle size analysis in order to be able to relate grading to engineering behaviour and to compare results and experiences from different sites. Previous experience has shown that the relationships which have been successfully developed for transported soils relating the results of soil classification tests and various engineering properties do not seem to hold for some tropical residual soils (Mitchell and Sitar, 1982). According to Irfan (1986), this partly stems from the difficulty of determining the exact grain size of engineering soils formed from the weathering of rocks under mainly tropical conditions. Apart from the

effectiveness of dispersing agents, mechanical treatments given to soils during pretreatments have to be considered. At present, the methods in use for particle size determination are varied. Head (1980) recommended breaking down of particles in a mortar with a rubber pestle, with avoidance of crushing of individual particles. Oven drying of tropical soils was also to be avoided. Ove Arup and Partners (1980) recommended the use of 'soft' methods, i.e dispersion from the natural state by use of sodium hexametaphosphate. No pestle and mortar was recommended. Australian Standard 1289: 1977 also discourages the use of pestle and mortar indicating that, particularly, residual soils of igneous origin suffer severe breakdown when subjected to mechanical stirring. The method currently in use by the Public Works Central Laboratory in Hong Kong involves oven drying at 110°C on occasion followed by breakdown using a porcelain pestle and mortar before dispersion with sodium hexametaphosphate (Irfan, 1986). Irfan (1986) also noted that, for the Hong Kong granites, samples which were oven dried before treatment gave lower clay and silt contents when compared with air dried samples. This observation may be partly due to the mineralogy of the soils as halloysite tubes tend to unroll on drying thus leading to an increase in the size of the particles. Hence it may be more advisable to avoid oven drying of the soils prior to particle size analysis.

Although it may be more appropriate to use 'soft' methods when determining the particle size of decomposed soils for filter design or similar purposes, the particle size determined using 'hard' methods and reagents may be more appropriate for slope design in decomposed soils of clay dominated microfabrics sheared under typical engineering effective stresses. Some crushing of grains, translation as well as shearing through soft grains composed of clay pseudomorphs are likely to occur during shear under static or repeated stresses (Miura and O-hara, 1979). In any case, a statement of the pretreatment procedures appears desirable when reporting results of particle size analysis on

tropical soils.

SEM of fractured surfaces of the soils revealed three main types of voids: (1) A few etch-pits in feldspars (2) Holes with rounded edges (some have cross sections of about $5\mu\text{m}$ diameter) which were fairly common and were often seen going through piles of halloysite tubes. The rounded edges of the holes and the good depth appeared to indicate that they had been formed by infiltrating fluid (3) Channels or 'troughs' between ridges of remnant feldspars from which halloysite particles were growing out. These were the most common. All these macropores, combined to give the soils a generally porous appearance. In addition, the halloysite tubes which were detached from the primary feldspar were often loosely packed and the resultant micropores would allow free passage of fluid to provide a free-draining medium. The porous appearance observed for the soils in this investigation is further supported by the results of void ratio measurement given by Irfan (1986) for soils from the same site. Field void ratio ranging between 0.9 and 1.0 reported by him would give the soils a porosity of between 47 and 50%, using the usual relationship shown below in Equation 9.1.

$$n = \frac{e}{1 + e} \quad [9.1]$$

where n is porosity and e is void ratio.

Irfan (1986) suggested that the high void ratio compared with the low clay content of the soils may be an indication of extensive leaching out of the clay minerals as they were formed during the course of weathering or an extensive etch-pit solution of feldspar without forming clay minerals. Since no evidence of clay translocation was shown by mineralogical analysis, and SEM (as clay mineralogy differed in the least and most weathered soils) weathering and leaching will have to be very rapid in the soil to account for the high void ratio and low clay content. The fact that most of the plagioclase was already weathered in the

least weathered soil (Sample 404.05), as shown by elemental analysis, is a point in support of rapid weathering of the soil, and the good drainage provided by the hilly terrain and the steep slope of the soil mantle and basal rock surfaces of Hong Kong (Lumb and Lee, 1975) would aid leaching. However, the fact that silt size halloysite tubes were also formed from the feldspar should account for part of the low clay content of the soils. From the results of this investigation, a possible explanation for the high void ratio of the soils may be that weathering produced etch-pits in the feldspar with loss of some of the mineral without forming clay minerals. The voids left as a result of this action would provide a good flow of water which would lead to the removal of more material (e.g. amorphous material) during clay formation and leaching of the fine clay minerals which may later be formed. Similar intense and rapid leaching was reported by Eswaran and Bin (1978a) for weathered Malaysian granites.

8.2.3 Iron Oxide Mineralogy of the Weathered Granites

Ferrihydrite and goethite were identified as the iron oxide phases in the weathered granites. Ferrihydrite was identified by electron microscopy only in the red mottles of the least weathered soil (Sample 404.05) but an indication of the mineral was given in Samples 404.05, 404.06 and 404.07 by acid ammonium oxalate extraction although the mineral occurred in minute quantities. Goethite was identified in all the soils by electron microscopy, X-ray diffraction, infrared spectroscopy and differential scanning calorimetry. Hence, it could be summarised that goethite existed together with ferrihydrite in Samples 404.05, 404.06 and 404.07, but goethite occurred as the sole iron oxide mineral in the most weathered Sample 404.08.

Previous identification of ferrihydrite in soils had been confined to the temperate climate regions (e.g. Chukhrov et al; 1972 and Campbell and Schwertmann, 1984). Although on very few occasions, identification of the

mineral in soils from the tropic had been inferred, such identification was in doubt. For example, Eswaran and Bin (1978a) reported the presence of XRD amorphous iron oxides in some weathered granite soils from Malaysia, thus appearing to suggest the presence of ferrihydrite in the soils, but no details of the amorphous iron oxide or the methods of identification were given. Smart (private communication, 1987) also thought the iron oxide particles encountered in a tropical red soil from Nyeri, Kenya (see Smart, 1972, 1973) could be ferrihydrite, but no identification of the oxide was done. The lack of positive identification of ferrihydrite in tropical and subtropical soils to date has led to the popularly held view amongst researchers that the mineral is an indicator of pedogenic environments in cool or temperate, moist climates (Schwertmann, 1985). The positive identification of ferrihydrite in the red mottles of Sample 404.05, by electron microscopy methods, in this investigation represents what appears to be the first of such identification in a tropical or subtropical soil and indicated that ferrihydrite could occur in soils from these climates contrary to the current view. The possible modes of formation of the mineral in the soils are discussed later in Section 8.2.4.

Experiments with synthetic systems have proved that hematite formation requires ferrihydrite as a necessary precursor, and that hematite forms from the dehydration and structural rearrangement of the ferrihydrite particles (Fischer and Schwertmann, 1975; Schwertmann and Taylor, 1977; Schwertmann, 1987b). Similarly, the widespread occurrence of hematite in tropical and subtropical soils is well established (e.g Schwertmann and Taylor, 1977; Kämpf and Schwertmann, 1982; Fitzpatrick, 1987; Herbillon and Nahon, 1987, and Schwertmann, 1987b). It follows that if synthetic systems apply to pedological conditions (although this is not always so) then ferrihydrite must have been formed in tropical hematitic soils, but is likely to be unstable and is rapidly converted to hematite in these soils. Hence the instability, rather than the formation, of ferrihydrite in the tropical

and subtropical soil systems may be responsible for the mineral not being widespread in these soils. Another reason why ferrihydrite may have escaped identification in soils in general derives from its poor crystallinity which makes it difficult to identify by conventional X-ray diffraction methods especially when in mixture with other clay silicates or more crystalline iron oxides (Schwertmann, 1987b). Although improved methods such as differential X-ray diffraction and Mössbauer spectroscopy have proved useful in recent years, electron microscopy on the different iron oxide concentrations in a soil, as done in this investigation, appears desirable for complete identification of all the iron oxide minerals in a soil, especially when some are present in minute quantities.

The occurrence of goethite in the soils was expected due to their yellowish colour (see Tables 2.3 and 3.3). The identification of goethite in soils from the tropical and subtropical areas is well documented (see Schwertmann, 1987b and Fitzpatrick, 1987 for reviews) and this mineral along and hematite, are common minerals in soils from these areas and are often responsible for the yellowish and reddish colours of most tropical soils. Although hematite was expected in the soils, especially in the red mottles, due to the reddish colour and the fact that the soils were of tropical origin, the mineral was not identified in any of the soils. The absence of hematite in the soils is in line with previous observations that hematite has never been detected along with ferrihydrite in a soil. According to Schwertmann, (1987b), this observation would appear to be in discrepancy with the popular concept that hematite is formed in soils by transformation from ferrihydrite and the only plausible explanation is that the rate of transformation of ferrihydrite to hematite is much faster than the neoformation of ferrihydrite. This fast rate of transformation of ferrihydrite to hematite is in agreement with *in vitro* experiments (Schwertmann, 1987b).

8.2.4 Iron Oxide Formation in the Weathered Granites

The formation of iron oxides in synthetic systems as well as in the natural environment was discussed in Chapter 2. The deduction of the possible modes of formation of iron oxides in soils is often done from comparison with results of synthetic systems. However, as stated earlier in Chapter 2, since synthetic systems do not always exactly simulate what actually happens in natural environments, various problems arise from making such comparisons, but the usefulness of results obtained from synthetic systems in explaining the situations in soils increases as the conditions during synthesis approach those in soils. Furthermore, the determination of various chemical properties and composition of the soil as was done in this investigation (Chapter 4) helps to give a clearer picture.

Results of experiments on synthetic systems and deductions from observations of natural systems have shown that the formation of the different iron oxide phases and transformation from one phase to another depend on several factors such as rate of release of Fe from the supplying medium, pH, water activity, temperature and the presence of other compounds and elements such as organic matter and silicates (see Schwertmann, 1987b for a review).

Synthetic ferrihydrite has been prepared by neutralising a ferric salt solution (e.g. Murphy et al; 1976), by dialysing a ferric nitrate solution with distilled water (Towe and Bradley, 1967), and by oxidising a ferrous salt (Schwertmann and Taylor, 1972). Similarly, the formation of ferrihydrite in different natural environments has been discussed by various authors including Spencer et al. (1983), Ottow (1969), Schwertmann and Fischer (1973), Chukhrov et al. (1972), Carlson and Schwertmann (1981, 1987), and Schwertmann et al. (1987) and was summarised by Schwertmann (1987b) who stated that the high degree of disorder and/or extremely small particle size (a few nm) of ferrihydrite as compared to the other Fe oxides indicate that disorder is caused by rapid

formation and/or by hindrance of crystallisation. Both mechanisms are supported by the observation that ferrihydrite forms either when waters containing Fe^{2+} are oxidised very quickly or, more importantly, in the presence of constituents which impede crystal nucleation and growth of other well-ordered forms such as goethite and lepidocrocite. Under favourable conditions and depending on the conditions in the soil environment, hematite or goethite may then be formed from the ferrihydrite. The mechanism for the formation of hematite and goethite from ferrihydrite was summarised by Schwertmann (1985, 1987) and presented in Figure 2.13 in Chapter 2. Based on the results of previous works by other authors and those obtained in this investigation, the presence of ferrihydrite and goethite in the subtropical, Hong Kong weathered granites are discussed here.

For the formation of iron oxides, a source of Fe is essential, and in soils Fe-bearing silicates are often the usual sources. In the present soils, biotite being the main Fe-bearing mineral identified in the soils was likely to be the main source of Fe supply to the soil system. In fact, as stated earlier, most of the red mottles in which ferrihydrite was identified in this study were found around biotite particles and optical microscopy of thin sections of the soils indicated reddish nodules of iron oxides mainly on the biotite particles thus giving an indication that the iron oxides may have been produced from Fe from the biotite. Also, the fact that the ferrihydrite was found in the close vicinity of the biotite particles may suggest a quick oxidation as soon as the Fe was released. The oxidation of Fe in soils were discussed by Escoubes and Karchoud (1977) and Brindley and Lemaitre (1987) while the oxidation of Fe in biotites have been presented by several authors including Farmer et al. (1971), Gilkes et al. (1972a, 1972b), Scott and Amonette (1987) and Brindley and Lemaitre (1987) amongst others. High temperatures such as often occur in the tropical and subtropical areas often lead to a general increase in weathering rate of soils from these areas and may also accelerate Fe release from biotite thereby promoting the formation

of ferrihydrite. Usually, in tropical and subtropical soil conditions, the ferrihydrite is very unstable and is converted to more crystalline iron oxides. The low water activity and high soil temperature which often prevail in these climates usually promote the dehydration of ferrihydrite with consequent formation of hematite. However, in the soils studied in this investigation several factors may be responsible for the relative stability of ferrihydrite. A medium Al substitution of about 9.42 mole% obtained for the goethite in the least weathered Sample 404.05 (see Chapter 6) is an indication that free Al was available in the soil system even at the early stages of weathering. This Al may have been available to the ferrihydrite at the time of formation and led to inhibition to crystallisation of the ferrihydrite to more crystalline minerals. The inhibitory action of Al to the crystallisation of ferrihydrite is well established and was reported by Chukhrov et al. (1972). Some other compounds which appeared to be available in the soil system and may lead to inhibition to crystallisation of ferrihydrite are silica and organic matter. The inhibiting effect of silicon on the crystallisation of ferrihydrite has been demonstrated in laboratory experiments (Chukhrov et al; 1972; Schwertmann and Thalmann, 1976 and Karim, 1984) and has been observed in natural environments by Chukhrov et al. (1972), Henmi et al. (1980), Carlson and Schwertmann (1981) and Childs et al. (1982). For example in a 3.6×10^{-4} M Fe^{2+} solution with 10^{-3} Ca to simulate groundwater, a poorly crystalline lepidocrocite was formed on rapid oxidation at 0 to 4 mg Si per litre, whereas poorly crystalline ferrihydrite was the product at Si concentration between 5 and 12 mg per litre (Schwertmann, 1987b). Likewise a similar inhibiting effect of organic matter on the crystallisation of ferrihydrite is well reported and this was reviewed earlier in Chapter 2. Schwertmann (1987b) reported that on aerial oxidation of a simulated ground water with 3.6×10^{-4} M Fe, ferrihydrite was formed in the presence of organics from a hot-water extract of a soil. Campbell and Schwertmann (1984) also identified ferrihydrite in

soils from podsol B horizons and placic horizons where organic matter was also present and Süsser and Schwertmann (1983) reported ferrihydrite, associated with organic matter, in ochreous deposits from drain pipes or drain ditches. Ferrihydrite was also detected in lake waters containing about 1.5 mg per litre of humics (Tipping et al; 1981). According to Schwertmann (1987b) only a low concentration of these compounds is necessary to impede the crystallisation of ferrihydrite.

Elemental analysis of the whole soil and clay fraction of the weathered granites (see Tables 4.2 and 4.3) showed a generally high quantity of silicon in the Hong Kong soils as would be expected for a granitic material. Although most of the silicon may be bonded in the structures of the alumino-silicates and large quartz grains, the mineralogical analysis of the clay fraction of the soils (see Table 9.1) showed that some quantity of quartz was present in the fine fraction of the soils. Furthermore, although it was not possible to obtain the silicon content of the soil ferrihydrite due to the minute quantity of the mineral, in a system where a high quantity of silicates is present a substantial amount of silicon (from weathering silicates and/or quartz dissolution) would be expected to be available.

The organic matter contents of the whole soil fraction of the Hong Kong granites varied between 0.18% and 0.45% and decreased with increased weathering of the soil samples. A detailed discussion of the role the organics may play in the occurrence of ferrihydrite was given in Section 4.7.5 and pointed to the possibility of the organic matter in the Hong Kong soils inhibiting the crystallisation of ferrihydrite to more crystalline products. The percentage of organic matter in Sample 404.05 is as much as some of those reported by Schwertmann et al. (1987) for samples from some Finnish lakes where ferrihydrite was identified.

The formation of goethite in the soil environment was reviewed earlier in

Section 2.3.2(a). Usually three broad pathways are possible viz: (1) oxidation of Fe^{2+} ions produced from weathering Fe-bearing silicates (2) formation from ferrihydrite and (3) transformation of hematite and other crystalline iron oxides through dissolution and recrystallisation to goethite. In the Hong Kong granites studied in this investigation the first two appear to be possible. The fact that no other crystalline iron oxide apart from goethite was identified in the soils would appear to exclude the third possibility. Goethite usually forms in preference to ferrihydrite in the course of slow oxidation of Fe^{2+} ions (Chukhrov et al; 1972) which is a possibility in most systems. The high stability of goethite compared to other iron oxides also ensures its occurrence in most soils. These factors would account for the formation and occurrence of goethite in the Hong Kong soils. Two observations support the possibility that at least some of the goethite in the soils may have been produced from the ferrihydrite. The first is the fact that electron microscopy observation (Chapter 5) showed that particles of goethite appeared to exist in a mixture with ferrihydrite particles. The possibility that the goethites in the mixture may have been produced by direct oxidation of Fe^{2+} released from the silicates is, however, still valid. Secondly, the fact that only goethite was indicated in the most weathered soil may be an indication that the ferrihydrite in the soils was converted into goethite with time.

Experiments on synthetic systems have shown that the transformation of ferrihydrite to goethite occurs in competition with the formation of hematite from ferrihydrite according to the scheme shown in Figure 2.13 (Schwertmann, 1985, 1987b). The absence of hematite in all the soils studied suggested that the soil conditions were more favourable for goethite formation from ferrihydrite. From Figure 2.13 it could be seen that various factors such as rate of Fe release, organic matter, soil temperature, pH and soil moisture influence the formation of goethite and hematite from ferrihydrite. The effect of the first three factors in iron oxide formation in the Hong Kong soils have already been discussed. In the

case of pH, the measured pH of the soils (Chapter 4) varied between 5.01 and 6.81 in water. This slightly acidic pH range will appear to favour the formation of goethite over hematite from ferrihydrite. Schwertmann and Murad (1983) also found, for a synthetic system, that the proportion of goethite formed from the ferrihydrite increased relative to hematite as the pH of the system dropped from 8 to 4. The effect of soil moisture on the formation of goethite and hematite was discussed by Schwertmann (1985). Firstly, a higher moisture content decreases dehydration and discourages the formation of hematite. Secondly, since goethite has been found to form from crystallisation of Fe^{3+} in solution, a high moisture content should promote the formation of goethite. Due to high temperature and drainage in most tropical soils, the water activity in the soils may drop below 1. The Hong Kong granites tested in this investigation were far from being saturated, and the fact that goethite rather than hematite may have formed from the soil ferrihydrite may be an indication that goethite can form preferentially over hematite even at low soil moisture. The water level of soils in the tropical and subtropical areas could however rise in the raining season and this seasonal rise in moisture content could be beneficial both for the stability of ferrihydrite in the soils and the formation of goethite from the ferrihydrite. The possibility of seasonal flooding in younger soils like those in this study is high due to the fact that, initially, voids are less well developed and drainage may not be rapid. Also the soils may be underlain by unweathered, less permeable rocks that may cause the stagnation of water. In fact it is possible that ferrihydrite may occur more commonly in the deeper seasonally flooded soils of tropical and subtropical areas. In order to resolve this question, it is suggested that samples should be examined while wet and freshly collected, rather than when dry. Based on the preceding discussions, a probable scheme for the formation of iron oxides in the Hong Kong soils is given in Figure 8.2

8.2.5 Properties of the Iron Oxides

Direct observation by electron microscopy suggested a spherical morphology for the soil ferrihydrite particles and the broad, faint electron diffraction patterns indicated a very low crystallinity for the mineral. Both these properties are in line with previous observations for both synthetic and natural samples (Eggleton and Fitzpatrick, 1988). An average diameter of about 5.5nm was obtained for the soil ferrihydrite particles by direct measurement from electron micrographs. Because it has always been difficult to measure the diameter of soil ferrihydrite due to aggregation in electron micrographs very few data are available on direct measurement of ferrihydrite diameter. The diameter obtained here however agrees well with those calculated for natural ferrihydrite particles (about 5.5nm) from Finnish lakes using a measured specific surface area of about $376 \text{ m}^2\text{m}^{-1}$ and an assumed density of 2.8 gcm^{-3} (Carlson and Schwertmann, 1987).

The goethite particles showed variations in morphology, crystallinity and Al substitution from soil to soil. In general an increase in coarseness, crystallinity and Al substitution with increase in soil weathering was indicated. The goethite particles in the least weathered soil were observed by electron microscopy to be acicular and thin (average breadth of particles showing the (100) face was 4.4nm). As weathering progressed in Sample 404.06 acicular particles similar to those in the previous sample were still observed but the particles appeared to be generally larger (average breadth of particles showing the (100) face was 8.2nm). Although it was not possible to measure the particle sizes of individual particles in the micrographs of Sample 404.07 observations of the particles in the micrograph appeared to indicate a more plate-like than lath-like morphology of the particles compared to those encountered in Samples 404.05 and 404.06. In the most weathered Sample 404.08 the goethite particles also had a morphology that was more platy (elongated, plates with irregular edges) than acicular. An average breadth of 12.2nm was found for particles assumed to show the (100) face and

makes them coarser than those encountered in the least weathered Sample 404.05 and of comparable size to those in Sample 404.06. A comparison of the X-ray diffraction intensities (sharpness) of the goethite reflections from the different soils showed a progressive increase from the less weathered sample to the most weathered sample and shows an increase in the crystallinity of the goethite particles in the soils in this direction. This increase in crystallinity was also depicted in the width at half-peak height of the (110) line which decreased steadily from the least weathered to the most weathered soil. The width at half-peak height of the (111) lines did not reflect the increase in crystallinity, thus showing that the (110) line would be better for judgement of crystallinity in this case. In contrast Campbell and Schwertmann (1984) reported that for some soil goethites from Europe, the (111) line was more affected by crystallinity than the (110) line. However, crystallinity effects in synthetic goethites were found to affect the (110) line more than the (111) line (Schulze and Schwertmann, 1984) in line with the findings of this investigation. Further investigations are necessary to clarify these differences.

The differences in crystal morphology and crystallinity of the goethite particles may be due to various factors such as mode of formation (e.g Schwertmann et al; 1985), presence of foreign ions that hinder growth and crystallinity (e.g Quin et al; 1988), Al substitution (e.g Fey and Dixon, 1981) and age. In the Hong Kong soils, it is possible that all these factors have played a part in determining the crystal morphology and crystallinity of the goethite particles. The smaller size and the lower crystallinity of the goethite in the least weathered soil may be due to the presence of foreign substances such as silicon and organic matter which were indicated in the soils as discussed earlier in Section 8.2.4. These substances have a high affinity for the iron oxide surface, and therefore may block the surface of the growing crystal thereby limiting growth and crystallinity. As weathering increased, the proportion of some of the

foreign substances (e.g. organic matter and some cations such as Na and Ca) decreased, with an indication of increase in particle size and crystallinity of the goethite particles (Schwertmann, 1987b and Quinn et al; 1988). The effect of Al substitution on the properties of synthetic goethites has been discussed by Weed et al. (1976), Taylor and Schwertmann (1978), Fey and Dixon (1981), Schulze and Schwertmann (1984) and Schwertmann (1984) amongst others. Fey and Dixon (1981) reported that the lath-shaped (or acicular) morphology of the goethite particles was increasingly disrupted with greater Al substitution with less acicular goethites being produced with increasing Al substitution. Schwertmann (1984) and Schulze and Schwertmann (1984) also reported that with increasing Al substitution, goethite crystals became shorter and narrower, but thicker. An increase in crystallinity with Al substitution was however indicated. Mann et al. (1984) however reported that for the crystals of a goethite with 9 mole % Al substitution were larger than those of unsubstituted goethite and also larger than those with 15.7 mole % Al substitution, thus giving the impression that there may be a maxima in goethite size somewhere in the medium Al substitution range. These authors also reported that at 15.7 mole % Al substitution, acicular as well as plate-like goethites were observed with electron microscopy. Estimation of Al substitution for Fe in the soil goethite structures was obtained from X-ray diffraction traces and showed an increase from about 9.42 mole % in the least weathered soil to about 15.72 mole % in the most highly weathered soil. The results obtained for the Hong Kong soils will appear to indicate an increase in crystallinity of the goethite particles with increased Al substitution, however the effect of the age (which should lead to higher crystallinity of the goethite in the older soils) will also have to be taken into consideration and the increase in crystallinity with increased weathering may be a combination of Al substitution and age. As has been reported for synthetic systems (e.g. Fey and Dixon, 1981; Schulze and Schwertmann, 1984 and Mann et al; 1985) there was also a tendency

towards a platy morphology of the soil goethite particles with increase in Al-substitution.

8.2.6 Interaction of Iron Oxides with Clay Silicates

Presently there are conflicting views on the interaction of iron oxides with clay minerals in soils and this was discussed earlier in Section 2.3.3(c). The results of electron microscopy obtained in this investigation showed some halloysite particles with iron oxide particles attached to their edges and faces and in some cases there appeared to be a real attraction between the iron oxide and the clay particles. Although this may demonstrate the possibility of an attraction between iron oxide and clay minerals under certain conditions, the number of clay particles observed with iron oxide attached to them were too few to make any significant difference to the soil properties. However, such an attraction between clay and iron oxide may be more significant in soils with very high concentration of iron oxides than those studied in this investigation.

Table 8.1 Summary of Clay Mineralogy of Weathered Granite from Hong Kong.

Sample	MINERALS			
	Major	Intermediate	Minor	Trace
404.08	Kaolinite	Halloysite	Muscovite	Chlorite, Gibbsite Quartz
404.07	Halloysite/ Kaolinite	-	Muscovite K-Feldspar Quartz	Chlorite
404.06	Halloysite	-	Muscovite K-feldspar Quartz	Kaolinite Chlorite
404.05	Halloysite	-	Muscovite K-feldspar Quartz	

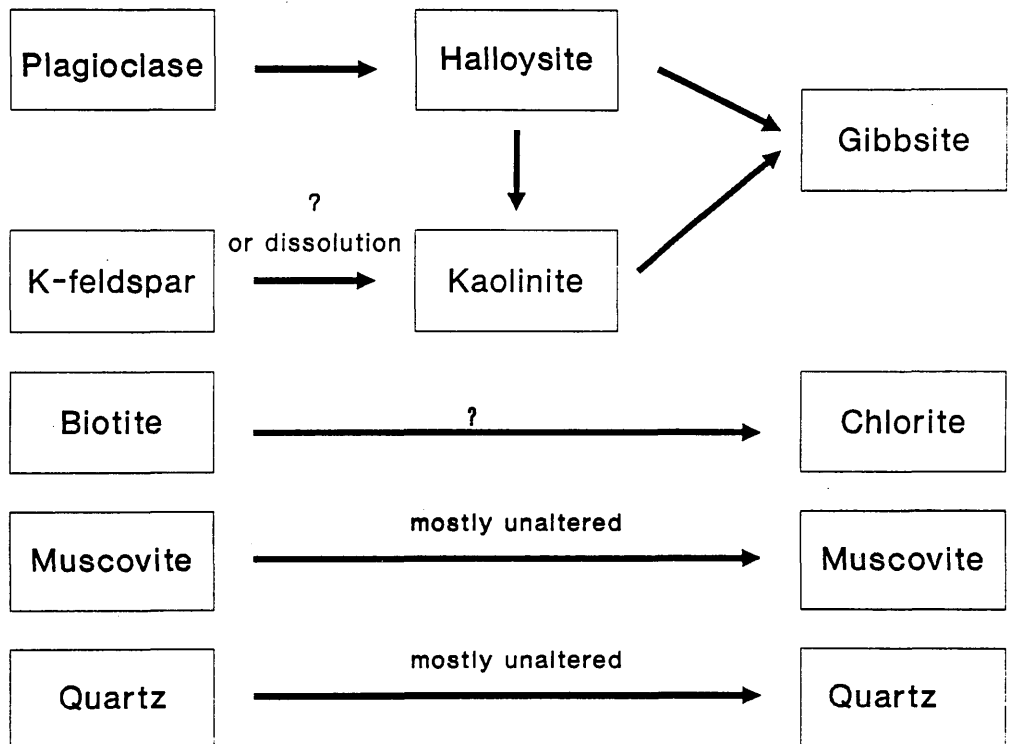


Figure 8.1: Possible weathering path for the primary minerals in the Hong Kong granite

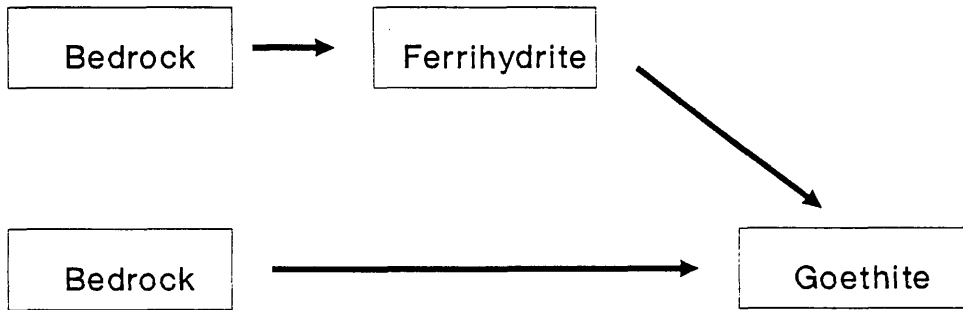


Figure 8.2: Possible path for the formation of iron oxides in the Hong Kong weathered granites.

REFERENCES

- Adams, W. A and Kassim, J. K. (1984). *J. Soil Sci.* **35**, 117–126.
- Adetoye, F. (1970). *Am. Miner.* **55**, 925.
- Agar, A. W. (1960). *Br. J. Appl. Phys*; **11**, 185.
- Ahmed, H. (1971). *Elect. Micros. Anal; Inst. of Physics Conf.*
Ser; No. **10**, 30.
- Allen, P. M. and Stephens, E. A. (1971). "Report on the Geological Survey of Hong Kong", Hong Kong Government Press.
- Allison L.E (1965). "Organic Carbon". In "Methods for Soil Analysis (2)", C.A Black (ed). The American Society of Agronomy, Inc. U.S.A.
- Allison L.E; Bollen, W.B, and Moodie, C.D. (1965). "Total Carbon". In "Methods for Soil Analysis (2)", C.A Black (ed). The American Society of Agronomy, Inc. U.S.A.
- Amelinckx, S. (1964). "The Direct Observation of Dislocations". Solid state physics supplement 6, Advances in research and application. Seitz, F and Turnbull, D (eds). Academic press, New York and London.
- Andrews, K. W; Dyson, D. J. and Keown, S. R. (1971). "Interpretation of Electron Diffraction Patterns", Hilger and Watt; London.
- Ardenne, M; Endell, K. and Hofmann, U. (1940). *Ber. Deut. Keram. Ges.* **21**, 207–227.
- Ardenne, M. von (1944). *Kolloid- Z*; **108**, 195.
- Baird, T; Fryer, J. R. and Galbraith, S. T. (1977). *Inst. Phys. conf. SER.* No. **36**, 211–214.
- Banfield, J. F. (1985). "Mineralogy and Chemistry of Granite Weathering". M.sc. Thesis, Australian National University, Australia.
- Basta, E.Z. (1957). *Mineral. Mag*; **237**, 431.

References

- Batson, P. E; Chen, C. H; Silcox, J. (1976). Proc. 34th. Annu. Meeting. Electr. Microsc. Soc. Am. Baton Rouge, USA.
- Beeston, B. E. P; Horne, R. W. and Markham, R. (1972). In "Practical Methods in Electron Microscopy, Vol 1". Glauert, A. M. (ed). Elsevier, Amsterdam.
- Beeston, B. E. P. (1972). "An Introduction to Electron Diffraction", AEI Scientific Apparatus Ltd; Harlow, Essex.
- Bigham, J. M; Golden, D. C; Bowen, L. H; Buol, S. W. and Weed, S. B. (1978). Soil Sci. Soc. Am. J; 42, 816–825.
- Blackmore, A. V. (1973). Aust. J. Soil. Res. 11, 75–82.
- Blake, R.L; Hessevick, R.E; Zoltai, T. and Finger, L.W. (1966). Am. Mineral; 51, 123–129.
- Blakemore, R. (1975). Science 190, 377–379.
- Bloom, M.C. and Goldbreg, L. (1965). Corros. Sci; 5, 623.
- Borggaard, O. K (1987). In "Iron in Soils and Clay Minerals", Stucki, J.W; Goodman, B.A. and Schwertmann, U. (eds.). NATO ASI Series, D. Reidel, Dordrecht, 83–98.
- Bonifas, M. and Legoux, P. (1957). Bull. Serv. Carte. Geol. Als.–Lorr. 10, 7.
- Borries, B. von and Ruska, E. (1939). Z. Wiss. Mikrosk. Tech; 56, 314.
- Bragg, W.H. and Bragg, W.L. (1918). "X–Rays and Crystal Structure". Third Edition. G. Bell and Sons, London.
- Brady, G. W; Kurkjian, C. R; Lyden, E. F. X; Robin, M. B;
- Brindley, G. W; Santos P. De Souza and Santos H. De Souza (1963). Am. Miner; 48, 897–910.
- Brindley, G. W; and Brown, G. (1980). "Crystal Structures of Clay Minerals and Their X–ray Identification". Mineralogical Society, London.
- Brindley, G. W. and Lemaitre, J. (1987). Thermal Oxidation and Reduction Reactions of Clay Minerals. In Chemistry of Clays and Clay Minerals, Mineralogical Society Monograph, No. 6. Longman Scientific and Technical.
- British Standards Institution (1981). "Code of Practice for Site Investigations". (BS 5930: 1981). British Standards Institution, London.
- Brown, G. (1953). J. Soil Sci. 4, 220–228.

References

- Brown, G. and Brindley, G. W. (1980). In "Crystal Structures of Clay Minerals and Their X-Ray Identification". Brindley G. W. and Brown G. (ed), Mineralogical Society Monograph No. 5, London, 305–359.
- Buerger, M. J. (1942). "X-Ray Crystallography". John Wiley and Sons, Inc; New York.
- Burns, R. G. and Burns, V. M. (1977). In "Marine Manganese Deposit; Glaspy, G. P. (ed.); Elsevier, New York. 186–248.
- Burton, E. F; Hillier, J. and Prebus, A. (1939). Phys. Rev; **56**, 1171.
- Burton, E. F; Sennett, R. S. and Ellis, L. G. (1947). Nature, **160**, 565.
- Busing, W. R. and Levy, H. A. (1958). Acta Cryst; **11**, 798–803.
- Campbell, A. S. and Schwertmann, U. (1984). J. Soil Sci. **35**, 569–582.
- Cardile, C. M. (1988). Clay and Clay Miner; **36**, 537–539.
- Carlson, L. and Schwertmann, U. (1980). Clays Clay Miner; **28**, 272–280.
- Carlson, L. and Schwertmann, U. (1981). Geochim. Cosmochim. Acta **45**, 421–429.
- Childs, C. W. (1985). "Notes on Ferrihydrite", N.Z. Soil Bureau Laboratory Report CM7, DSIR, New Zealand.
- Childs, C. W; Downes, C. J. and Wells, N. (1982). Aust. J. Soil. Res. **20**, 119–129
- Christensen, H. and Christensen, A. N. (1978). Acta Chem. Scand; **A32**, 87–88.
- Chukhrov, F. V; Zuyagin, B. B; Ermilova, L. P. and Gorshov, A. I. (1972). In Proc. Int. Clay Conf; Madrid, 1970, Serratos, J. M. (ed.), 333–341.
- Chukhrov, F. V; Ermilova, L. P; Gorskhov, A. I; Zvyagin, B. B; Shukchlistov, A. P; Sidorenko O. W. and Balashova, V. V. (1973). Chem. Erde, **33**, 109–124.

References

- Chukhrov, F. V; Ermilova, L. P; Zvyagin, B. B. and Gorshkov, A. I. (1975).
Proc. Int. Clay Conf; Mexico City, Mexico. Bailey, S. W. (ed.), 275–286.
Applied Publishing Ltd; Illinois, U.S.A.
- Chukhrov, F. V; Zvyagin, B. B; Gorshkov, A. I; Ermilova, L. P; Korovushkin,
V. V; Rudnitskaya, Ye. S. and Yakubovskaya, N. Yu. (1977). Int. Geol. Rev.
19, 873–890.
- Clark, G.L. (1955). "Applied X–Rays". McGraw–Hill Book Co; Inc; New York.
- Coey, J. M. D. (1987). In "Iron in Soils and Clay Minerals". Stucki, J.W;
Goodman, B.A. and Schwertmann, U. (eds.). NATO ASI Series, 397–466. D.
Reidel, Dordrecht.
- Coleman, J. D; Farrar, D. M. and Marsh, A. D. (1964). Géotechnique 14,
262–276.
- Cornell, R. M. and Schwertmann, U. (1979). Clays Clay Miner; 27, 402–410.
- Cornell, R. M; Schneider, W; and Giovanoli, R. (1989). Clay Miner; 24,
549–553.
- Coventry, R. J; Taylor, R. M. and Fitzpatrick, R. W. (1983). Aust. J. Soil
Res. 21, 219–240.
- Cowley, J. M. and Moodie, A. F. (1957). Acta, Crystallogr; 10, 609.
- Crewe, A. V; Eggenberger, D. N; Wall, J. and Welter, L. M. (1968). Rev. Sci.
Instrum; 39, 576.
- Csencsits, R. and Gronsky, R. (1987). Ultramicroscopy, 23, 421.
- Cullity, B.D. (1956). "Elements of X–Ray Diffraction". Addison–Wesley
Publishing Co; Reading, Mass.
- Dahmen, H; Kim, M. G. and Searcy, A. W. (1987). Ultramicroscopy, 23, 365.
- Davey, B. G; Russell, J. D. and Wilson, M. J. (1975). Geoderma, 14, 125–138.
- Davis, S. G. (1953). "The Geology of Hong Kong". Govt. Printers, Hong Kong.
- Delvigne, J; Bisdorn, E. B. A; Sleeman, J. and Stoops, G. (1979). Pedologie,
29, 247–300

References

- Deshpande, T. L; Greenland, D. J. and Quirk, J. P. (1964). *Nature, Lond.* 201, 107–108.
- Edington, J. W. (1974). "Practical Electron Microscopy in Materials Science". The Macmillan Press Ltd. London.
- Eggleton, R. A. (1984). *Clays Clay Miner*; 32, 1–11.
- Eggleton, R. A. (1987). In "Iron in Soils and Clay Minerals", Stucki, J.W; Goodman, B.A. and Schwertmann, U. (eds.). NATO ASI Series. 165–201. D. Reidel, Dordrecht.
- Eggleton, R.A; Schulze, D.G; and Stucki, J.W. (1987). In "Iron in Soils and Clay Minerals", Stucki, J.W; Goodman, B.A. and Schwertmann, U. (eds.). NATO ASI Series, D. Reidel, Dordrecht.
- Eggleton, R. A. and Fitzpatrick, R. W. (1988). *Clays and Clay Miner*; 36, 111–124.
- English, C. A. and Venebles, J. A. (1971). *Electron Microsc. Anal. 5th. Inst. Phys; Conf; Ser. No. 10, London, 40.*
- English, C. A. and Venebles, J. A. (1972). *Electron Microsc; Proc. 5th. Euro Congr; Inst. Phys; Conf; Ser. No. 14, London, 172.*
- Escoubes M. and Karchoud, M. M. (1977). *Bull. Soc. Fr. Céram*; 114, 43–55.
- Eswaran, H; Stoops, G. and Sys, C. (1977). *J. Soil Sci*; 28, 136–143.
- Eswaran, H. and Bin, W.C (1978a). *Soil Sci. Soc. Am. J*; 42, 149–153.
- Eswaran, H. and Bin, W.C (1978b). *Soil Sci. Soc. Am. J*; 42, 154–157.
- Evans, L. J; Roswell, J. G. and Aspinal, J. D. (1978). *Can. J. Soil Sci.* 58, 391–395.
- Ewing, F. J. (1935a). *J. Chem. Phys*; 3, 420–424.
- Ewing, F. J. (1935b). *J. Chem. Phys*; 3, 203–207.
- Farmer, V. C. and Russell, J.D. (1964). *Spectrochim. Acta.* 20, 1149–1173.
- Farmer, V. C. and Russell, J.D. (1966). *Spectrochim. Acta.* 22, 389–398.

References

- Farmer, V. C; Russell, J. D; McHardy, W. J; Newman, A. C. D;
 Ahlrichs, J. L and Rimsaite, J. Y. H (1971). *Minerog. Mag*; **38**, 121–137.
- Farmer, V. C. (1974), ed. "The Infrared Spectra of Minerals".
 Mineralogical Society, London.
- Fasiska, E.J. (1967). *Corrosion Sci*; **7**, 833–839.
- Feitknecht, W. and Michaelis, W. (1962). *Helv. Chim. Acta* **45(26)**, 212–224.
- Feitknecht, W; Hani, H. and Dvorak, V. (1969). In "Reactivity of Solids".
 Mitchell, J. W; De Vries, R. C; Roberts, R. W. and Cannon, P. (eds.),
 237–245. Wiley, New York.
- Fey, M.V. and Dixon, J. B (1981). *Clays Clay Miner.* **29**, 91–100.
- Fischer, W. R. and Schwertmann, U. (1975). *Clays Clay Miner.* **23**, 33–37.
- Fischer, W. R. (1987). In "Iron in Soils and Clay Minerals", Stucki, J.W;
 Goodman, B.A. and Schwertmann, U. (eds.). *NATO ASI Series*. 715–748.
 D. Reidel, Dordrecht.
- Fitzpatrick, R. W. (1978). "Occurrence and Properties of Iron and Titanium
 Oxides in Soils along the Eastern Seaboard of South Africa". Ph.D. Thesis,
 University of Natal.
- Fitzpatrick, R. W; Taylor, R. M; Schwertmann, U. and Childs, C. W. (1985).
Aust. J. Soil Res; **23**, 543–567.
- Fitzpatrick, R. W. (1987). In "Iron in Soils and Clay Minerals", Stucki, J.W;
 Goodman, B.A. and Schwertmann, U. (eds.). *NATO ASI Series*. 351–396.
 D. Reidel, Dordrecht.
- Forsyth, J. B; Hedley, I.G; and Johnson, C. E. (1968). *J. of Phys. C*
 (Proc. Phys. Soc.) **1**, 179–188.
- Fripiat, J. J. and Gastuche, M. C. (1952). *Nat. Inst. Belg. Congo. Agronomical
 Studies ci. Ser. No. 54*.
- Fryer, J. R. (1978). *Acta Crystallogr*; **A34**, 603.

References

- Fryer, J. R. (1979). "The Chemical Applications of Transmission Electron Microscopy". Academic, London.
- Fryer, J. R; Cleaver, J. R. A. and Smith, D. J. (1980). *Electron Microsc. Anal; Inst. Phys; Conf; Ser. No. 52*, 287.
- Fryer, J. R. (1983). *Mol. Cryst. Liq. Cryst*; **96**, 275.
- Fryer, J. R; and Holland, F. (1984). *Proc. R. Soc*; **A393**, London, 353.
- Fujiyoshi, Y; Kobayashi, T; Ishizuka, K; Uyeda, N; Ishida, Y and Harada, Y. (1980). *Ultramicroscopy*, **5**, 459.
- Fysh, S.A and Fredericks, P. M (1983). *Clays and Clay Miner*; **31**, 377–382.
- Galbraith, S. T; Baird, T. and Fryer, J. R. (1979). *Acta Cryst*; **A35**, 197–200.
- Gallagher, K. J. (1970). *Nature (London)*, **226**, 1225–1228.
- Garrels, R. M. and Mackenzie, F. I. (1971). "Evolution of Sedimentary rocks". W. W. Norton and co; New York.
- GCO (1988). "Guide to Rock and Soil Descriptions", *Geoguide 3*, Geotechnical Control Office, Civil Engineering Services Dept; Government Publications Centre, HongKong.
- Gilkes, R. J; Young, R. C and Quirk, J. P. (1972a). *Clays Clay Miner*; **20**, 303–315.
- Gilkes, R. J; Young, R. C and Quirk, J. P. (1972b). *Nature*, **236**, 89–91.
- Gilkes, R.J; Suddhiprakarn A. and Armitage T.M. (1980). *Clays and Clay Miner*; **28**, 1, 29–34.
- Glemser, O. and Gwinner, E. (1939). *Z. Anorg. Chem.* **240**, 163–171.
- Goldich, S. S. (1938). *J.Geol*; **46**, 17–58.
- Goodman, B.A; Berrow, M.L. and Russell, J.D. (1988). *J. Soil Sci*; **39**, 87–98.
- Gray, H. B. (1971). *Advan. Chem. Ser*; **100**, 365–389.
- Greenland, D. J. and Oades, J. M. (1968). *Trans. 9th Int. Cong. Soil Sci. Adelaide*, **1**, 657–668.

References

- Greenland, D. J; Oades, J. M. and Sherwin, J. W. (1968). *J. Soil. Sci*; 19, 116–122.
- Greenwood, N.N. (1970). "Ionic Crystal; lattice defects nonstoichiometry", 2nd Ed; Butterworth, London.
- Grim, R. E. (1988). *Clays and Clay Miner.* 36, 97–101.
- Haine, M. E. and Cosslett, V. E. (1961). *The Electron Microscope*, Spon, London.
- Hall, C. E. (1966). *Introduction to Electron Microscopy*, 2nd. Edition, McGraw– Hill, London.
- Hannaker, P. and Lie, H. Q. (1984). *Talanta*, 31, 1153–1157.
- Harrison, P. M; Fischbach, F. A; Hoy, T. G. and Haggis, G. M. (1967). *Nature*, 216, 1188–1190.
- Hart, R. G. and Yoshiyama, J. M. (1975). *J. Ultrastruct. Res*; 51, 40.
- Hashimoto, H; Howie, H. and Whelan, M. J. (1960). *Phil. Mag.*[8], 5, 967.
- Haul, R. and Schoon, T. (1939). *Z. Phys. Chem*; 44, 216.
- Head, K. H. (1980). *Manual of Laboratory Testing*. Vol. 1, Pentech Press, London
- Henmi, T. and Wada, K. (1976). *Am. Miner*; 61, 379–390.
- Henmi, T; Wells, N; Childs, C. W. and Parfitt, R. L. (1980). *Geochim. Cosmochim. Acta* 44, 365–372.
- Henry, N. F. M; Lipson, H and Wooster, W. A. (1951). "The Interpretation of X– Ray Diffraction Photographs". Macmillan and Co; Ltd; London.
- Herbillon, A. J. and Nahon, D. (1987). In "Iron in Soils and Clay Minerals", Stucki, J.W; Goodman, B.A. and Schwertmann, U. (eds.). NATO ASI Series, D. Reidel, Dordrecht. 779–795.
- Heuvel Vanden R.C (1965). "Elemental Analysis by X– ray Emission Spectroscopy". In "Methods for Soil Analysis (2)", C.A Black (ed). The American Society of Agronomy, Inc. U.S.A.

References

- Hillier, J. and Vance, A. W. (1941). Proc. Inst. Radio Eng; Aust; 29, 167.
- Hillier, J. and Ramberg, E. G. (1947). J. Appl. Phys; 18, 48.
- Hirsch, P. B; Howie, A; Nicholson, R. B; Pashley, D. W. and Whelan, M. J.
(1965). "Electron Microscopy of Thin Crystals". Butterworth, London.
- Hobbs, L. W. (1979). In "Introduction to Analytical Electron Microscopy"
Hren, J. J. Goldstein, J. I and Joy, D. C. (eds). Plenum Publ; New York.
- Hobbs, L. W. (1984). In "Quantitative Electron Microscopy". Scott. Univ.
Summer School Phys; Edinburgh; Chapman, J. N. and Craven, A. J. (eds).
p399.
- Hobbs, L. W. (1987). Ultramicroscopy, 9, 191.
- Holland, F. (1984). Ph.D thesis, Glasgow Univ.
- Hoppe, W. (1942). Z. Krist. 103, 73–89.
- Howie, A. (1965). In Kay, D. (ed). "Techniques for Electron Microscopy".
Blackwell Scientific Publications, Oxford; 433–477.
- Hsu P.H. (1977). Aluminium Hydroxides and Oxyhydroxides.
In "Minerals in the Soil Environment". J.B Dixon and S.B Weed (eds).
Soil Science Society of America, Madison, Wisconsin USA. 99–143.
- Huang, P.M (1977). Feldspars, Olivines, Pyroxenes and Amphiboles.
In "Minerals in the Soil Environment". J.B Dixon and S.B Weed (eds).
Soil Science Society of America, Madison, Wisconsin USA, 553–601.
- Huggins, F. E; Huffman, G. P; Kosmack, D. A. and Lowenhaupt, D. E.
(1980). Int. J. Coal Geol. 1, 75–81.
- Hughes, J.C. and Brown, G. (1977). Clay Miner; 12, 319–328.
- Humphreys, C. J. (1979). Rep. Prog. Phys; 42. Inst. Phys; p1825.
- IAEG (1981). "Rock and Soil description and Classification for Engineering
Geological Mapping". Report by the IAEG commission on Engineering
Geological Mapping, Bulletin of the International Association of Engineering
Geology, No. 24, 235–274.

References

- Irfan, T. Y. (1986). Special Project Report, SPR 4/86, Geotechnical Control Office, Hong Kong.
- Jackson, M. L. (1958). "Soil Chemical Analysis". Prentice Hall, New Jersey.
- Jacquet, D. (1990). *Engineering Geology*, **28**, 1–25.
- Jeffery, P. G. and Hutchison, D. (1981). "Chemical Methods of Rock Analysis", Third Edition, Pergamon Press, Oxford.
- Jenkins, R. and De Vries, R. L. (1969). "Practical X-ray Spectrometry". 2nd. Edition. Macmillan, London.
- Jette, E. R. and Foote, F. (1933). *J. Chem. Phys*; **1**, 29.
- Johnson, J. H. and Glasby, G. P. (1982). *Marine Chemistry* **11**, 437–448.
- Jonas, K and Solymar, K (1971). *Acta Chim. Acad. Sci. Hung. (Budapest)*, **66**, 383–394 (Chem. Abstr. **74**, 93864).
- Kämpf, N. and Schwertmann, U. (1982). *Geoderma*, **29**, 27–39.
- Kämpf, N. and Schwertmann, U. (1982). *Clays Clay Miner.* **30**, 401–408.
- Karim, Z. (1977). "The Control of Iron Hydrous Oxide Crystallisation by Traces of Inorganic Components in Soil Solution." Ph.D Thesis, University of Reading, U.K.
- Karim, Z. (1984). *Clays Clay Miner*; **32**, 181–184.
- Kassim, J. K; Gafoor, S. N. and Adams W. A. (1984). *Clay Miner.* **19**, 99–106.
- Kassim, M.J.N.M. (1982). "Structural Studies of Iron Corrosion Products in Aqueous Solution at Room Temperature". Ph.D Thesis, University of Glasgow, U.K.
- Kay, D. (ed) (1965). "Techniques for Electron Microscopy". Blackwell Scientific Publications, Oxford.
- Kemper, W. D. (1966). Tech. Bull. No. 1355, US Department of Agriculture.
- Kitagawa, Y. and Moeller, M. R. F. (1979). *Soil Sci. and Plant Nutrition*, **25**, 385–395.

References

- Kittrick, J. A. (1965). In "Methods for Soil Analysis", Black, C. A. (ed).
American Society for Agronomy, Inc; Publisher, Madison, Wisconsin, USA,
632–652.
- Klug, H.P. and Alexander, L.E. (1954): "X-Ray Diffraction Procedures".
John Wiley and Sons, Inc; New York.
- Knight, R. J. and Sylva, R. N. (1974). *J. Inorg. Nucl. Chem.* **36**, 591–597.
- Kuo, I. A. M. and Glaeser, R. M. (1975). *Ultramicroscopy*, **1**, 53.
- Langmyhr, F. J. and Paus, P. E. (1968). *Anal. Chim. Acta*; **43**, 397–408.
- Lewis, G. J. and Goldberg, E. D. (1954). *J. Marine Res.* **13**, 183–197.
- Lindsay, W. L. (1979). "Chemical Equilibria in Soils". Wiley Interscience,
New York.
- Lindsay, W. L. (1987). In "Iron in Soils and Clay Minerals", Stucki, J.W;
Goodman, B.A. and Schwertmann, U. (eds.). NATO ASI Series, D. Reidel,
Dordrecht. 37–60.
- Lindsay, D.H. (1976). In "Short Course Notes", Vol. 3, Oxide Minerals.
Rumble III, D. (ed.) Mineralogical Society of America, Washington, D.C.
- Loewenstam, H. A. (1962). *Geol. Soc. Amer. Bull.* **73**, 435–436.
- Loveland, P. J. (1987). In "Iron in Soils and Clay Minerals", Stucki, J.W;
Goodman, B.A. and Schwertmann, U. (eds.). NATO ASI Series, D. Reidel,
Dordrecht, 99–140.
- Lumb, P. (1962). *Géotechnique*, **12**, 226–243.
- Lumb, P. (1965). *Géotechnique*, **15**, 180–194.
- Lumb, P. and Lee, C. F (1975). In Proceedings of the 4th South East
Conference on Soil Engineering, Malaysia, 41–49.
- Mackay, A. L. (1960). *Mineral. Mag*; **32**, 545–557.
- Mackay, A. L. (1962). *Mineral. Mag*; **33**, 270–280.

References

- Mackenzie, R.C. and Berggren G. (1970). Oxides and Hydroxides of Higher Valency Elements. In "Differential Thermal Analysis", 1, (R.C. Mackenzie; ed.). Academic Press, New York.
- Mackenzie, R.C. (1970). (ed.) "Differential Thermal Analysis", 1, Academic Press, New York.
- Mackenzie, R.C. (1980). *Anal. Proc*; 17, 217–220.
- McKeague, J. A. and Day, J. H. (1965). *Can. J. Soil Sci*; 46, 13–22.
- McKeague, J. A. (1966). *Can. J. Soil Sci*; 47, 95–99.
- Mann, S; Cornell R.M. and Schwertmann, U. (1985). *Clay Miner.* 20, 255–262.
- Massey, J. B; Irfan T. Y and Cipulo, A. (1989). *Proc*; 12th Int. Conf. Soil Mech. and Foundation Engineering, Rio de Janeiro, Vol. 1, 533–542.
- McCaleb, S. B. (1966). *Clays Clay Miner.* 13, 123–130.
- McHardy, W. J. and Birnie, A. C. (1987). In "A Handbook of Determinative Methods in Mineralogy", Wilson, M.J (ed.). Blackie, Glasgow and London.
- McIntosh, P. D; Lee, W. G. and Banks, T, (1983). *Newzealand J. Sci.* 26, 379–401.
- McKinley, W. A. and Feshbach, H. (1948). *Phys. Rev*; 74, 1759.
- Mehra, O. P. and Jackson, M. L. (1960). *Clays Clay Miner. Proc.* 7th. Natl. Conf; Washington, D.C; 1958; Swineford, A. (ed). Pergamon Press, New York.
- Melfi, A.J; Cerri, C.C; Kronberg, B.I; Fyfe W.S and McKinnon B. (1983). *J. of Soil Sci*; 34, 841–851.
- Mendelovici, E; Yariv, SH. and Villalba R. (1979). *Clays Clay Miner.* 27, 368–372.
- Menter, J. W. (1956). *Proc. R. Soc*; A236, London, 119.
- Miller, W.D. and Keller, W.D. (1963). *Clays Clay Miner.* 10, 244–253.
- Misawa, T; Suetaka, W. and Shimodaira, S. (1970). *Zairyo* 19, 537–542.
- Mitchell, J. K. and Sitar, N. (1982). Engineering Properties of Tropical Residual Soils. *Proc. ASCE Speciality Conf. on Engineering and Construction in Tropical and Residual Soils*, Honolulu, 30–57.
- Miura, N. and O-hara, S. (1979). *Soils and Foundations*, 19, No. 3, 1–13.

References

- Morrish, A. H. (1980). In "Crystal Growth, Properties and Applications". 2, 171, H.C. Freyhardt (ed.), Springer-Verlag, Berlin, Heidelberg.
- Murad, E. (1982). N. Jb. Miner. Mh; H. 2, 45-56.
- Murad, E. and Fischer, W. R. (1987). In "Iron in Soils and Clay Minerals", Stucki, J.W; Goodman, B.A. and Schwertmann, U. (eds.). NATO ASI Series, D. Reidel, Dordrecht.
- Murphy, P. J; Posner, A. M; and Quirk, J. P. (1976). J. Colloid Interface Sci; 56, 312-319.
- Murray, J. W. (1979). In "Short Course Notes", Vol. 6, Marine Minerals. Burns, R. G. (ed.) Mineralogical Society of America, Washington, D.C.
- Nadeau, P. H. and Tait, J. M. (1987). In "A Handbook of Determinative Methods in Mineralogy", Wilson, M.J (ed.). Blackie, Glasgow and London.
- Norrish, K. (1968). In Trans. 9th. Int. Congr; Soil Sci; III, Adelaide, 713-723.
- Norrish, K. and Taylor, R. M. (1961). J. Soil Sci; 12, 294-306.
- Oles, A; Szytula, A. and Wanic, A. (1970). Phys. Stat. Sol; 41, 173-177.
- Ottow, J. C. G. (1969). Zbl. Bakt. II 123, 600-615.
- Ove-Arup and Partners (1980). "Mid-Levels Study. Notes on Particle Size Distribution Determination, Ove-Arup and Partners, 9527/RGP/DJGB/vc. (Unpublished).
- Parfitt, R. L; Fraser, A. R. and Farmer, V. C. (1977). J. Soil Sci. 28, 289-296.
- Parfitt, R. L. and Russell, J. D. (1977). J. Soil Sci. 28, 297-305.
- Parham, W. E. (1969a). In Proceedings of the International Clay Conference, Vol. 1; Tokyo. 404-416.
- Parham, W. E. (1969b). Clays Clay Miner. 17, 13-22.
- Paterson, E. and Swaffield, R. (1987). In "A Handbook of Determinative Methods in Mineralogy", Wilson, M.J (ed.). Blackie, Glasgow and London.
- Pauling, L. and Hendricks, S.B. (1925). J. Am. Chem. Soc; 47, 781-790.

References

- Phillips, R. (1960). *Br. J. Appl. Phys*; 11, 504.
- Poole, J. B. le. (1947). *Phillips Tech. Rev*; 9, 33.
- Povitskii, V. A; Makarov, E. F; Murashko, N. V. and Salugin, A. N. (1976).
Phys. Status Solidi (A), 33, 783–787.
- Quin, T. G; Long, G. J; Benson, C. G; Mann, S. and Williams, R. J. P.
(1988). *Clays Clay Miner*; 36, 165–175.
- Reynolds, G. T. (1968). *Adv. Opt. Electron Microsc*, 2, Barer, R and Cosslett,
V. E. (eds.) Academic Press, London.
- Rooksby, H.P. (1972). In "X-ray Identification and Crystal Structure of Clay
Minerals", Brown, G. (ed.), Mineralogical Society, London, 354.
- Ronov, A.B. and Yaroshevsky, A.A. (1971). In "The Earths Crust and
Upper Mantle"; Hart, P. J. (ed.) American Geophysical Union,
Washington, D. C.
- Roth, W.L. (1960). *Acta Cryst*; 13, 140.
- Ruska, E. (1934). *Z. Phys*; 87, 580.
- Russell, J. D. (1979). *Clay Miner*; 14, 109–114.
- Russell, J.D (1987). In "A Handbook of Determinative Methods in Mineralogy",
Wilson, M.J (ed.). Blackie, Glasgow and London.
- Saleh, A. M. and Jones, A. A. (1984). *Clay Miner*; 19, 745–755.
- Sampson, C. F. (1969). *Acta Cryst*, B25, 1963–1985.
- Saltman, P; Spiro, T. and Terzis, A. (1968). *Biochemistry*, 7, 2185–2192.
- Scahabi, S. and Schwertmann, U. (1970). *Z. Pflanzenernahr. Bodenkd.* 125,
193–204.
- Schulze, D.G. (1982). *Ph.D Thesis, Technische Universität, München.*
- Schulze, D. G. (1984). *Clays Clay Miner*; 32, 36–44.
- Schulze, D. G. and Schwertmann U. (1984). *Clay Miner*; 19, 521–539.
- Schulze, D.G and Schwertmann, U. (1987). *Clay Miner*; 22, 83–92.
- Schulze, D. G. (1987). In "Iron in Soils and Clay Minerals", Stucki, J.W;
Goodman, B.A. and Schwertmann, U. (eds.). NATO ASI Series, D. Reidel,
Dordrecht, 63–81.

References

- Schwarzmann, E. and Sparr, H. (1969). *Z. Naturforsch.* **24b**, 8–11.
- Schwertmann, U. (1959a). *Z. Anorg. Allg. Chem.* **298**, 337–348.
- Schwertmann, U. (1959b). *Z. Pflanzenernähr; Dung; Bodenk.* **84**, 194–204.
- Schwertmann, U. and Heinmann, B. (1959). *Neues Jb. Miner. Mh.* **8**, 174–181.
- Schwertmann, U. (1964). *Z. Pflanzenern; Dgg. Bodenk;* **105**, 194–202.
- Schwertmann, U. (1966). *Nature*, **212**, 645–646.
- Schwertmann, U; Fischer, W. R. and Papendorf, H. (1968). 9th. Int. Congr. Soil Sci; Adelaide, Australia, **1**, 645–655.
- Schwertmann, U. (1971). *Nature*, **232**, 624–625.
- Schwertmann, U. and Taylor, R. M. (1972). *Clays Clay Miner;* **20**, 151–158.
- Schwertmann, U. (1973). *Clay Miner.* **10**, 59–63.
- Schwertmann, U. and Fischer, W. R. (1973). *Geoderma* **10**, 237–247.
- Schwertmann, U. and Thalman, H. (1976). *Clay Miner;* **11**, 189–200.
- Schwertmann, U. and Taylor, R. M. (1977). In "Minerals in soil environments". J. B. Dixon et al. (eds); Soil Sci. Soc. of Am; Madison, Wisconsin, U.S.A.
- Schwertmann, U. and Fitzpatrick, R. W. (1977). *Soil Sci. Soc. of Am. J.* **41**; 1013–1018.
- Schwertmann, U; Murad, E. and Schulze, D. G. (1982). *Geoderma* **27**, 209–223.
- Schwertmann, U. and Kämpf, N. (1983). *R. Bras. Ci. Solo* **7**, 251–255.
- Schwertmann, U. and Murad, E. (1983). *Clays and Clay Miner;* **31**, 277–284.
- Schwertmann, U; Carlson, L. and Fechter, H. (1984). *Schweiz. Z. Hydrol;* **46**, 185–191.
- Schwertmann, U. (1985). In "Advances in Soil Science"; **1**, Stewart, B. A. (ed.). Springer-Verlag, New York, 171–200.
- Schwertmann, U. and Kämpf, N. (1985). *Soil Sci;* **139**, 344–350.
- Schwertmann, U; Cambier, P. and Murad, E. (1985). *Clays Clay Miner;* **33**, 369–378.

References

-
- Schwertmann, U; Kodama, H. and Fischer, W. R. (1986). In "Interactions of Soil Minerals with Natural Organics and Microbes". Huang, P. M. (ed). 223–250. Soil Sci. Soc. Am; Madison, WI.
- Schwertmann, U. and Latham, M. (1986). *Geoderma* 39, 105–123.
- Schwertmann, U. (1987a). In "Iron in Soils and Clay Minerals", Stucki, J.W; Goodman, B.A. and Schwertmann, U. (eds.). NATO ASI Series, D. Reidel, Dordrecht, 203–250.
- Schwertmann, U. (1987b). In "Iron in Soils and Clay Minerals", Stucki, J.W; Goodman, B.A. and Schwertmann, U. (eds.). NATO ASI Series, D. Reidel, Dordrecht, 267–308.
- Schwertmann, U; Carlson, L. and Murad, E. (1987). *Clays Clay Miner*; 35, 297–304.
- Scott, A. D and Amonette, J. (1987). In "Iron in Soils and Clay Minerals", Stucki, J.W; Goodman, B.A. and Schwertmann, U. (eds.). NATO ASI Series, D. Reidel, Dordrecht, 537–623.
- Seitz, F. and Koehler, J. S. (1956). *Solid State Phys*; 2, 305.
- Sharma, R; Barry, J. and Eyring, L. (1987). *Ultramicroscopy*, 23, 453.
- Sibley, D. F. and Wilbrand, J. T. (1977). *Geochim. Cosmochim. Acta* 41, 545–554.
- Smart, P. (1972). "Nyeri Red Clay". A dissertation submitted to the Institution of Civil Engineers, U.K.
- Smart, P. (1973). *Q. Jl Engng Geol*; 6, 129–139.
- Smart, P. and Tovey, N. K. (1981). *Electron Microscopy of Soils and Sediments: Examples*. Clarendon Press, Oxford.
- Smart, P. and Tovey, N. K. (1982). *Electron Microscopy of Soils and Sediments: Techniques*. Clarendon Press, Oxford.
- Smith, K. L. and Eggleton, R. A. (1983). *Clays Clay Miner.* 31, 392–396.

References

- Smith, D. J; McCartney, M. R. and Bursill, L. A. (1987). *Ultramicroscopy*, 23, 299.
- Spencer, W. F; Patrick, H. and Ford, H. W. (1983). *Soil Sci. Soc. Am. Proc.* 27, 134–137.
- Sproull, W.T. (1946). "X-Rays in Practice". McGraw–Hill Book Co; Inc; New York.
- Stiers, W. and Schwertmann, U. (1985). *Geochim. Cosmochim. Acta* 49, 1909–1911.
- Susser, P. and Schwertmann, U. (1983). *Z. Kulturtechn. Flurber.* 24, 386–395.
- Szytula, A; Burewicz, A; Dimitrijevic, Z; Krasnicki, S; Rzany, H; Todorovic, J; Wanic, A. and Wolski, W. (1968). *Phys. Stat. Sol;* 26, 429–434.
- Tallman, R.L. and Gulbransen E.A. (1967). *J. of Electrochem. Soc;* 114, 1227.
- Taylor, R. M. and Schwertmann, U. (1974). *Clay Miner.* 10, 289–298.
- Taylor, R. M. (1980). *Clay Miner.* 15, 359–382.
- Taylor, R. M; and McKenzie, R. M. (1980). *Clays Clay Miner;* 28, 179–187
- Taylor, R. M. (1987). In "Chemistry of Clays and Clay Minerals". Newman, A. C. D. (ed.). Mineralogical Society Monograph No. 6. Longman Scientific & Technical; 129–201.
- Tazaki, K; Ferris, F. G; Wiese, R. G. and Fyfe, W. S. (1989). *Proceedings of Abstracts, 9th Int. Clay Conf; Strasbourg, France.*
- Terzaghi, K. (1958). *Design and Performance of the Sasumua Dam.* In *Proceedings of the Institution of Civil Engineers*, 9, 369–394.
- Thiel, R. (1963). *Z. Anorg. Allg. Chem.* 326, 70–78.
- Thiry, M. and Sornein, J. (1983). *Sci. Geol. Mem.* 73, 195–205.
- Tipping, E. (1981). *Geochim. Cosmochim. Acta*, 45, 191–199.
- Tipping, E; Woof, C. and Cooke, D. (1981). *Geochim. Cosmochim. Acta*, 45, 1411–1419.

References

- Torrent, J; Schwertmann, U. and Schulze, D. G. (1980). *Geoderma*, **23**, 191–208.
- Torrent, J; Guzmann, R. and Para, M. A. (1982). *Clays Clay Miner.* **30**, 337–340.
- Towe, K. M. and Bradley, W. F. (1967). *J. Colloid Interface Sci*; **24**, 384–392.
- Towe, K. M. and Moench, T. T. (1981). *Earth Planet. Sci. Letters* **52**, 213–220.
- Turekian, K. K. and Wedepohl, K. H. (1961). *Geol. Soc. of Am. Bull.* **72**, 75–92.
- Uyeda, N; Kubayashi, T; Ishizuka, K and Fujiyoshi, Y. (1980). *Nature*, **285**, 95.
- Van Der Giessen, A. A. (1966). *J. Inorg. Nucl. Chem*; **28**, 2155–2159.
- Van Der Marrel, H. W. (1951). *J. Sediment. Petrol.* **21**, 12–21.
- Van Oosterhout, G. W. (1960). *Acta Crystallogr. Sec. B.* **13**, 932–935.
- Veen, A. W. L. (1973). *Aust. J. Soil. Res.* **11**, 167–184.
- Verwey, E.J.W. (1935). *Z. krist*; **91**, 65.
- Wada, K. (1977). In "Minerals in Soil Environments". Dixon J. B. et al. (eds). *Soil Sci. Soc. Am; Madison, Wisconsin.* 603–633.
- Watson, J. H. L; Cardell, R. R. and Heller, W. (1962). *J. Phys. Chem.* **66**, 1757–1763.
- Wells, A. F. (1962). "Structure Inorganic Chemistry", Oxford University Press, London.
- Wenk, H–R. (ed) (1976). "Electron Microscopy in Mineralogy". Springer–Verlag, Berlin.
- Whittig, L. D. (1965). In "Methods of Soil Analysis (Part 1)". Black C. A. (ed), American Society of Agronomy, Inc; Publisher, Madison, 671–698.
- Williams, R. C. and Fisher, H. W. (1970). *J. Mol. Biol*; **52**, 121.
- Willis, B.T.M. and Rooksby, H.P. (1953). *Acta Cryst*; **6**, 827.
- Wilson, M. J, Russell, J. D, Tait, J. M, Clark, D. R, Fraser, A. R, and Stephen J. (1981). *Clay Miner*, **16**, 261–278.
- Wilson, M. J. and Russell, J. D. (1983). *Min. Mag*; **47**, 85–87.

References

- Wilson, M.J. (1987). (ed.) "A Handbook of Determinative Methods in Mineralogy", Blackie, Glasgow and London.
- Wolf, R. J. and Joy, D. C. (1971). Elect. Micros. Anal; Inst. of Physics Conf. Ser; No. 10, 34.
- Yonezawa, A; Nakagawa, S; and Suzuki, M (1977). Proc. 34th. Annu. Meeting. Electr. Microsc. Soc. Am. Baton Rouge, USA.
- Yong, R.N. and Warkentin, B.P. (1975). "Soil Properties and Behaviour" Elsevier Scientific Publishing Company, Amsterdam.

APPENDIX

EXAMPLE OF THE ESTIMATION OF Al SUBSTITUTION FOR Fe IN GOETHITE

For the illustration of the estimation of Al substitution in goethite the X-ray diffraction lines from unsubstituted synthetic goethite and the goethite X-ray diffraction lines from the HF treated Sample 404.08 would be used. The relevant X-ray reflections for the samples are shown in Figures A1 to A4 and the calculations shown below.

As mentioned earlier in Section 6.6.2 the width at half peak height (WHH) of the (100) and (101) X-ray reflections of sample quartz, which was used as a standard, was found to be $0.150^\circ, 2\theta$.

Unsubstituted synthetic goethite

From Figure A1, d(110) peak at $24.68^\circ, 2\theta$ is 4.1885A,
observed width at half peak height ($WHH_{obs.}$) = $0.9^\circ, 2\theta$.

thus corrected width at half peak height ($WHH_{corr.}$) given by

$$WHH_{obs.} - WHH_{standard} = 0.9 - 0.150 = 0.75^\circ, 2\theta.$$

from Table 2.4 the correction needed to the d(110) spacing is (-0.01)

hence, the corrected spacing is

$$d(110) = 4.1885 - 0.01 = 4.1785A$$

similarly from Figure A2 d(111) peak at $42.85^\circ, 2\theta$ is 2.4506A,

$$WHH_{obs.} = 0.525^\circ, 2\theta$$

Appendix

$$\text{WHH}_{\text{corr.}} = 0.525 - 0.150 = 0.375^\circ, 2\theta$$

from Table 2.4, no correction is needed for this spacing and $d(111) = 2.4506\text{\AA}$.

from Equation [2.7], the c -dimension of goethite was given by

$$c = [(1/d(111))^2 - (1/d(110))^2]^{-1/2}$$

i.e, for the synthetic goethite,

$$\begin{aligned} c &= [(1/2.4506)^2 - (1/4.1785)^2]^{-1/2} \\ &= [0.1665 - 0.0572]^{-1/2} \end{aligned}$$

$$\therefore c = 3.025\text{\AA} = 0.3025\text{nm (see Tables 6.3 and 6.4)}$$

from Equation [2.6]

$$\text{mole \% Al} = 1730 - 572.0 \cdot c$$

\therefore for the synthetic goethite,

$$\begin{aligned} \text{mole \% Al} &= 1730 - 572.0 \times 3.025 \\ &= -0.3 \end{aligned}$$

effectively (0). (see Tables 6.3 and 6.4.)

HF treated Sample 404.08

From Figure A3, $d(110)$ peak at $24.85^\circ, 2\theta$ is 4.1602\AA ,

observed width at half peak height ($\text{WHH}_{\text{Obs.}}$) = $0.575^\circ, 2\theta$.

thus corrected width at half peak height is given by

$$\text{WHH}_{\text{Obs.}} - \text{WHH}_{\text{standard}} = 0.575 - 0.150 = 0.425^\circ, 2\theta.$$

from Table 2.4, no correction is needed to the (110) spacing, and

$$d(110) = 4.1602\text{\AA}.$$

Appendix

Similarly from Figure A4, d(111) peak at $43.2^\circ, 2\theta$ is 2.4316A,

$$WHH_{\text{obs.}} = 0.725^\circ, 2\theta$$

$$\therefore WHH_{\text{corr.}} = 0.725 - 0.150 = 0.575^\circ, 2\theta.$$

from Table 2.4, no correction is needed to the (111) spacing, and

$$d(111) = 2.4316A.$$

Hence c-dimension (using Equation [2.7]) is

$$c = [(1/2.4316)^2 - (1/4.1602)^2]^{-1/2}$$

$$= [0.1691 - 0.0578]^{-1/2}$$

$$\therefore c = 2.998A = 0.2997\text{nm (see Table 6.4)}$$

from Equation [2.6]

$$\text{mole \% Al} = 1730 - 572.0.c$$

\therefore for this soil goethite,

$$\text{mole \% Al} = 1730 - 572.0 \times 2.997$$

$$= 15.72.$$

Hence Al substitution = 15.72 mole % (see Table 6.4)

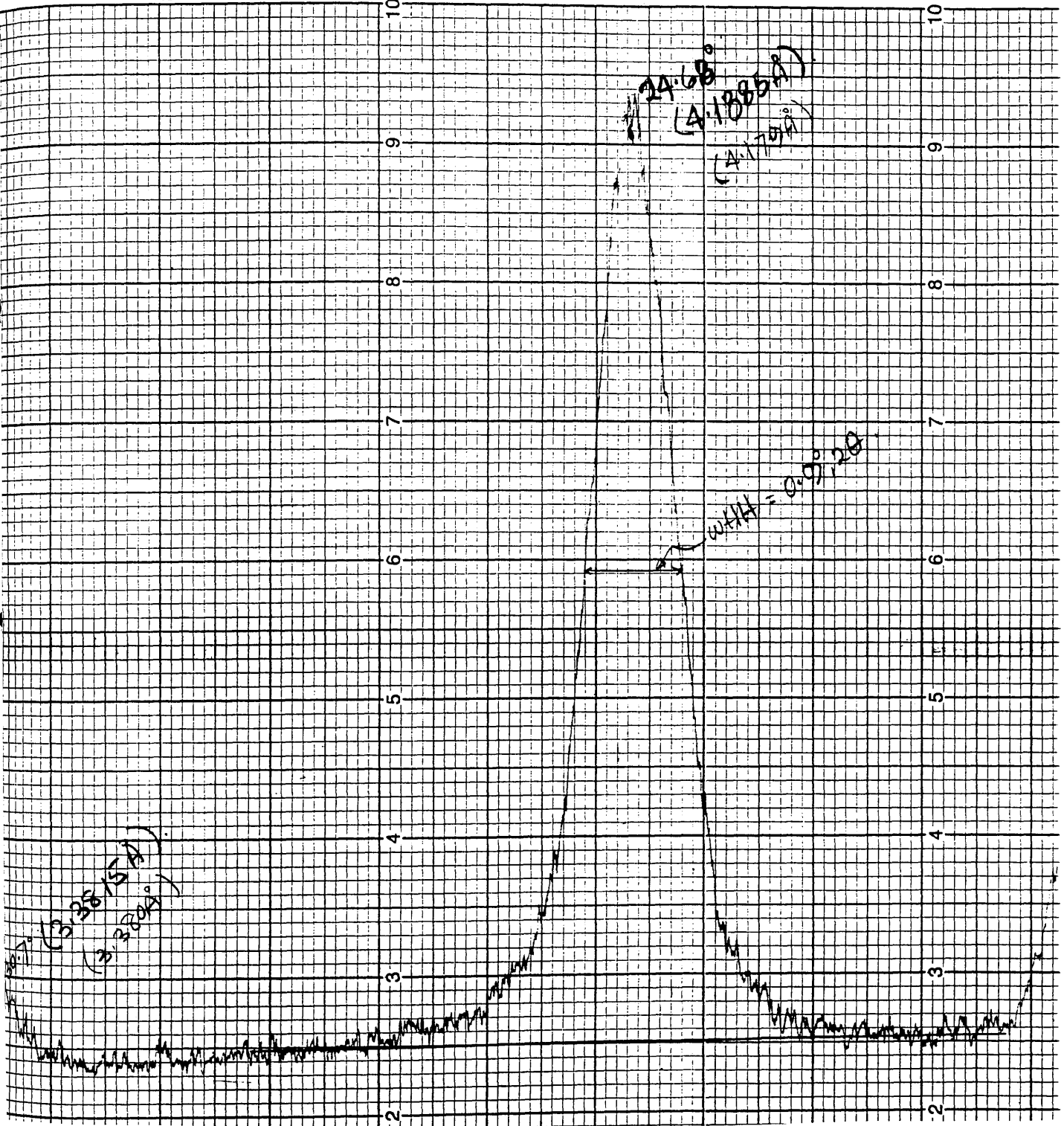
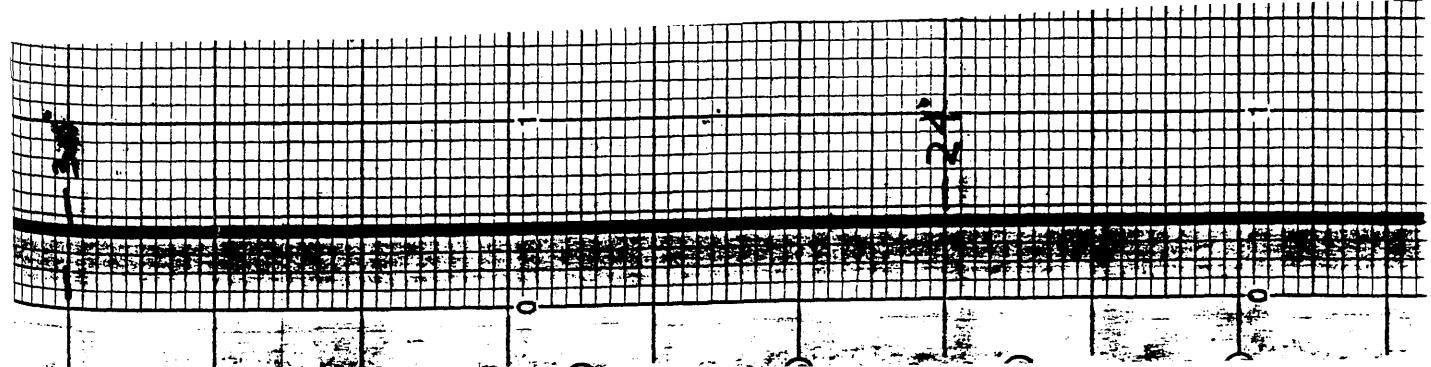


Figure A1: (110) X-ray peak of unsubstituted, synthetic goethite



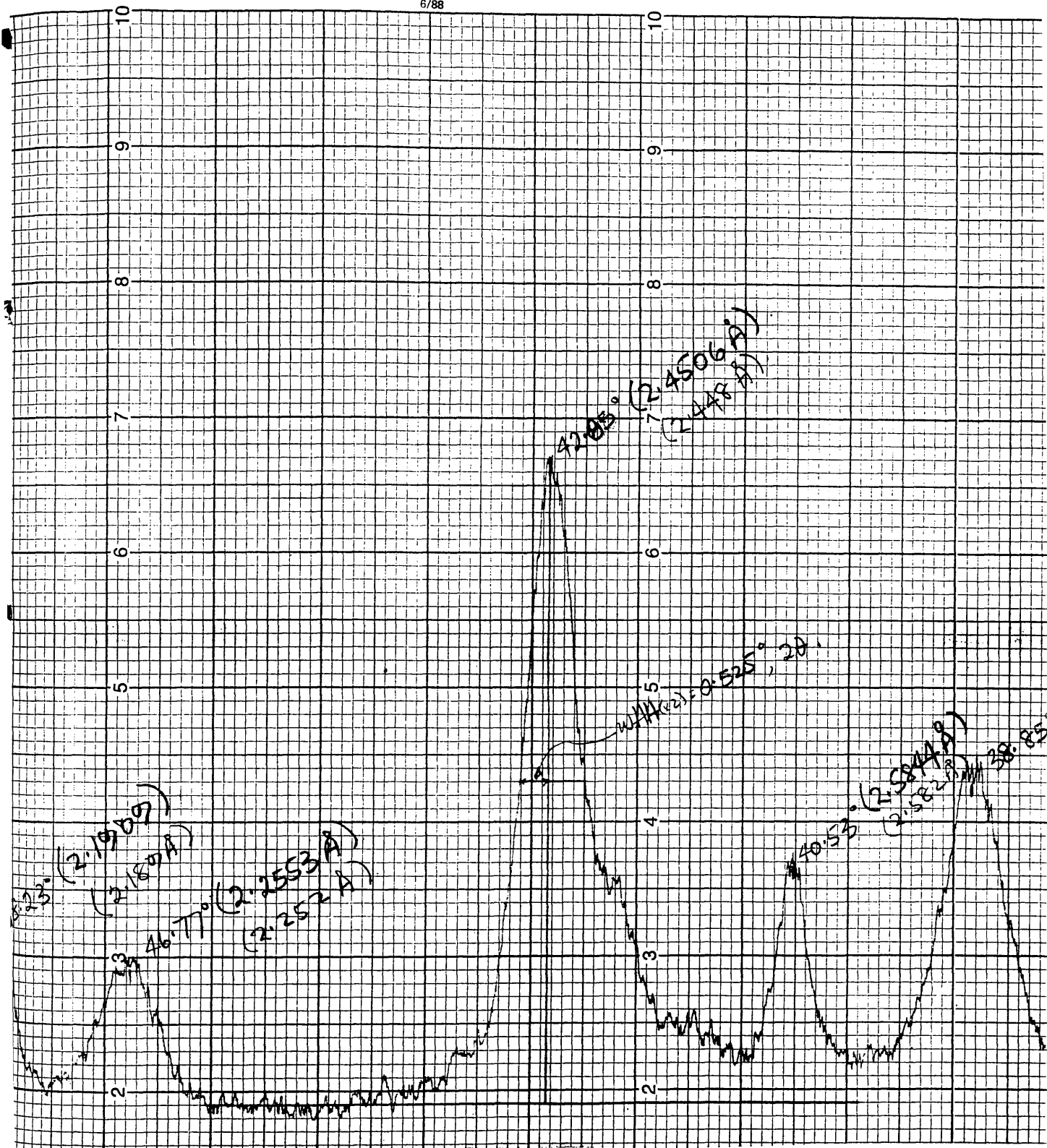


Figure A2: (111) X-ray peak of unsubstituted, synthetic goethite

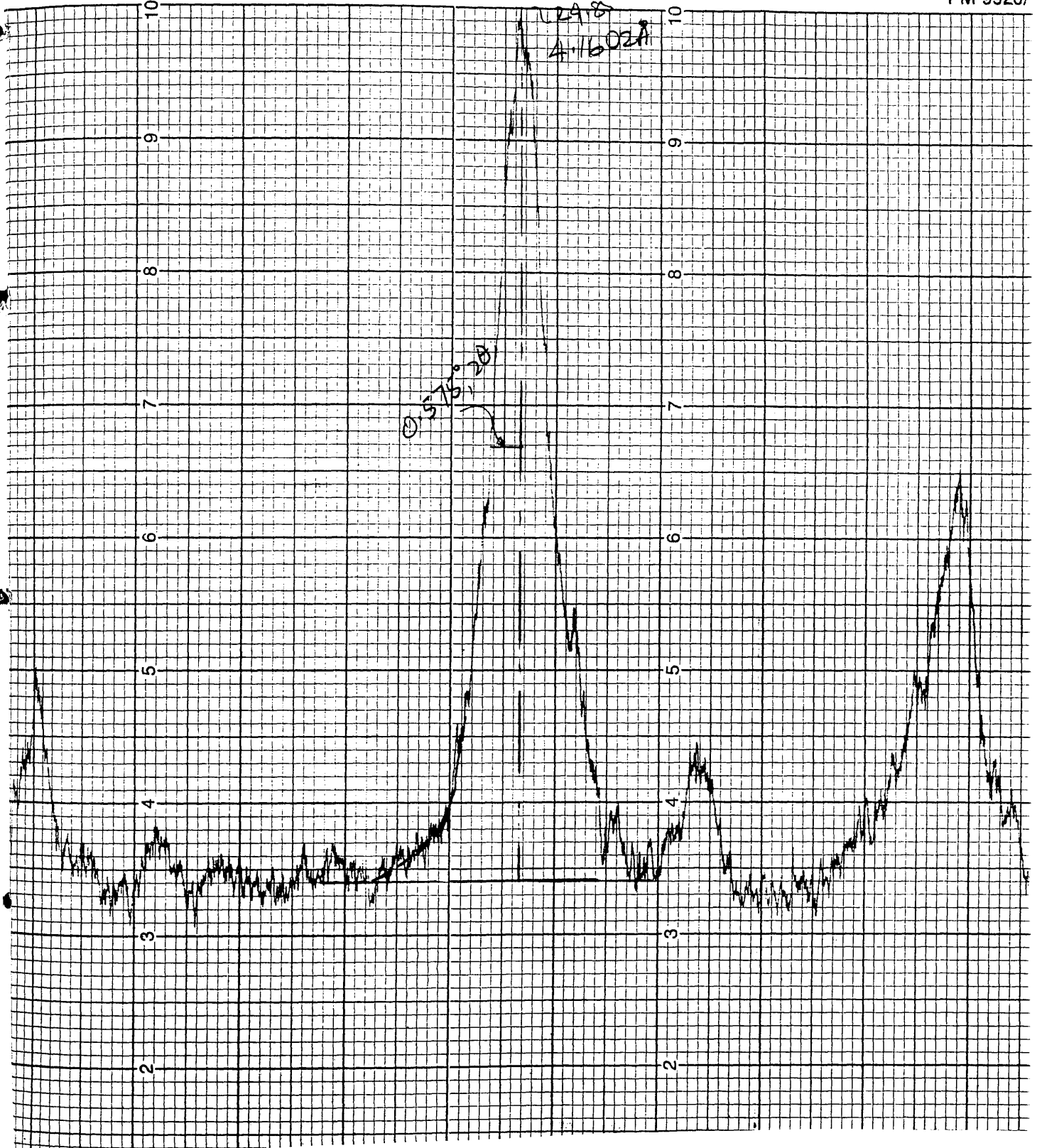
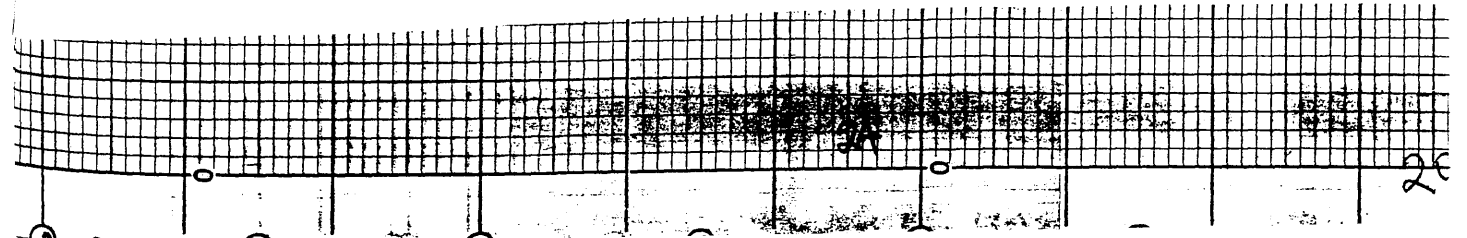


Figure A3: (110) X-ray peak of goethite in HF treated Sample 404.08



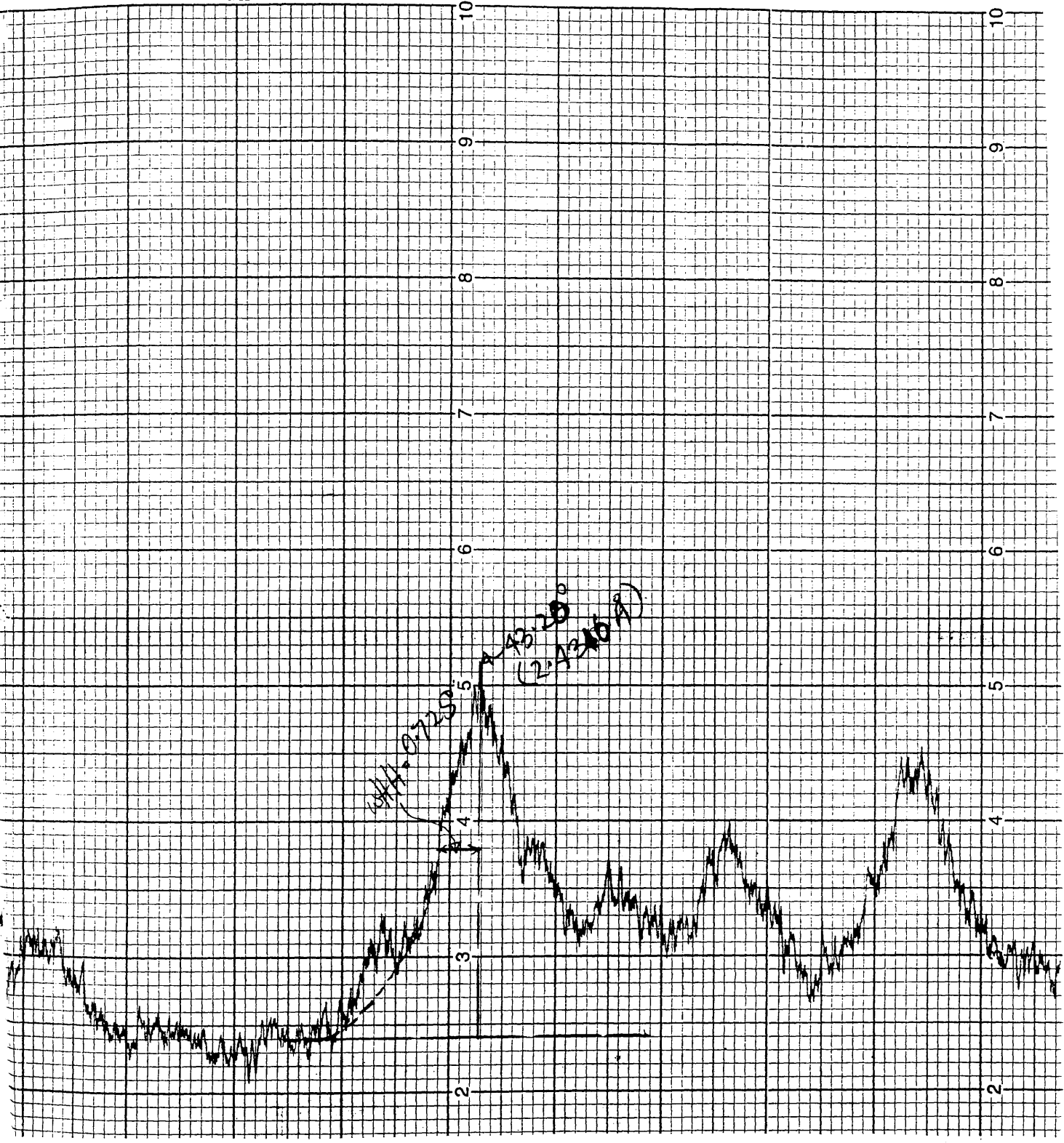


Figure A4: (111) X-ray peak of goethite in HF treated Sample 404.08

